

SimuLase



Version 3.0

May 8, 2019

Contents

1	A Few Basic Guidelines	7
2	Quick Start Guide	9
2.1	Main Tabs	9
2.1.1	Design Structure	9
2.1.2	Advanced Tab	13
2.1.3	Generate Database	13
2.2	Main GUI Components	14
2.3	General Tools	17
2.3.1	PL Analysis Tool	17
2.3.2	Generating Shifted and Broadened Databases	20
2.3.3	Linewidth Enhancement Factor Tool	20
2.4	Tools for Edge-Emitters	22
2.4.1	Current Calculator Tool	22
2.4.2	Gain vs. Current Tool	27
2.5	Tools for Top-Emitters	28
2.5.1	Reflection-Transmission	28
2.5.2	Surface-PL	29
2.5.3	VECSEL LI Curve	30
3	Basic Functionality	33
3.1	Main Menu	33
3.2	Design Structure	39
3.3	Reflection-Transmission	42
3.4	Surface-PL	44
3.5	VECSEL LI Curve	46
3.6	Generate Database	48
3.7	GainDatabase Viewer	55
3.8	PL-Analyzer	57
3.9	Shift and Broaden Database	60
3.10	Current Calculator	61
3.10.1	Threshold Characteristics	63
3.10.2	Input-Output Characteristics	64
3.11	Gain V's Current	65
3.12	Potential and Band Structure Views	66
3.13	Linewidth Enhancement Factor	68
3.13.1	Linewidth Enhancement Factor Carrier Density	68
3.13.2	Linewidth Enhancement Factor Electric Field	69
4	Data Format	71

5	Typical Examples	75
5.1	Edge Emitting Laser	75
5.1.1	STEP 1: Setting Up the Structure	75
5.1.2	STEP 2: Analyzing Experimental PL	77
5.1.3	STEP 3: Setting up a GainDatabase	80
5.1.4	STEP 4: Determining Operating Characteristics	81
5.1.5	STEP 5: How to Further Use the Data	88
5.2	Vertical External Cavity Surface Emitting Laser (VECSEL)	89
5.2.1	STEP 1: Setting Up the Structure	89
5.2.2	STEP 2: Setting up GainDatabases	91
5.2.3	STEP 3: Fine-Tuning the Structure	94
5.2.4	STEP 4: Comparison to the Experiment	96
5.3	Summary	108
6	Important Tips for Optimal Usage	111
6.1	System Requirements	111
6.2	Use of GPUs	113
6.3	Selecting the Number of Subbands, [17s]	114
6.4	Min/Max Energy, Resolution, [17f]	116
6.5	Defining the 'Quantized Region'	117
6.5.1	Use Short Barriers	118
6.5.2	Calculate for Only One Well	118
6.5.3	Fields Across the Quantized Region	119
6.6	Absorption/Gain-Model, [17h]	120
6.7	Model Options	121
6.7.1	Standard Model, [17i]	122
6.7.2	Quick and Dirty 1, [17j]	122
6.7.3	Quick and Dirty 2, [17k]	123
6.7.4	Using the Bulk Barrier Model, [17p]	123
6.8	Including the Poisson Drift-Diffusion Problem	125
6.9	Including the Schrödinger Poisson Problem	125
6.10	Possible Speed-Ups	126
6.10.1	Setting up a Database for PL-Analysis	126
6.10.2	Setting up a Database for Operating Conditions	127
6.10.3	Structures with Very Deep Wells	127
7	Theoretical Background	129
7.1	Implemented Models	130
7.1.1	Bandstructure and Wavefunctions	130
7.1.2	Gain/Absorption, Refractive Index	131
7.1.3	Spontaneous Emission (PL), Radiative Carrier Losses	133
7.1.4	Intraband (Free Carrier) Absorption	134
7.1.5	Inhomogeneous Broadening	134
7.1.6	Auger Losses	135
7.1.7	V(E)CSEL Operating Characteristics	139
7.1.8	Edge Emitter Operating Characteristics	140
7.2	Shortcomings of Simpler Models	141
7.2.1	Absorption/Gain	141
7.2.2	Spontaneous Emission, Radiative Carrier Losses	142
7.2.3	Auger Losses	144

8	Material Parameters	149
8.1	AllnGaAsP-Material Family	149
8.2	AllnGaAsSb-Material Family	151
8.3	Dilute AllnGaAsSbBi-Material Family	152
8.4	AllnGaN-Material Family	152
8.5	Dilute AllnGaNAs-Material Family	153
8.6	Metals	154
8.7	Dielectric Coatings	154
8.8	Air	154
	Bibliography	155

1 A Few Basic Guidelines

Specialized Versions of SimuLase™

SimuLase™ is readily available for some material families like *AlInGaAsP*, *AlInGaAsSb*, or dilute *AlGaInNAs* and we continue working on releasing versions for new material families. The program also includes metallization layers like Gold, Chromium or Titanium and dielectric coatings like *Si₃N₄*, *SiO₂*, or *TiO₂*. If you are interested in other semiconductor materials, metals or coatings please let us know. We also offer specialized solutions on request for particular situations, like different growth-directions, calculations for un-equal electron and hole densities, or reflection calculations requiring more than one GainDatabase since the structure contains different wells, etc..

Please contact us at simulase@nlcstr.com for any inquiries.

Making Entries

All entries that are typed into fields of **SimuLase™** have to be confirmed by hitting the enter key.

Numerical entries have to be in the format *ABCDEF.GHI*, using a decimal point if necessary. Large numbers can be entered using the format *A.BeN* for $A.B \times 10^N$.

Checking for Expected Calculation Time

Setting up a GainDatabase can be CPU-time consuming, requiring several minutes to hours during which your computer might not be available for alternative purposes. Please check the window displaying the estimated CPU-time and memory requirements that will open after the '**Generate Database**' button is clicked and a name and directory for the database has been specified.

Example of an Edge-Emitter

All data required to reproduce the example of an edge-emitting structure discussed in Sec. 5.1 can be downloaded from our website at 'www.nlcstr.com/SimuLaseDemo.htm'. This example can be loaded in to the free demo-version of **SimuLase™** that can also be downloaded at that link. The example includes the structure file, the theoretical gain databases and the experimental PL-data. This data is also included in the DVD on which the full version of **SimuLase™** is shipped. Here, the folder '**demo_ingaasp**' contains the full structure. '**unbroadened_pl**' contains the GainDatabase for the PL-analysis. '**experimental_pl**' contains the experimentally measured PL spectra and '**broadened_gdb**' contains the GainDatabase for the current calculation.

Demo-GainDatabase

You can download a demo-GainDatabase that would take several tens of hours to set up from our website to test all the tools of **SimuLase**TM outside the '**Generate Database**'-tool. There you can also download corresponding experimental PL-spectra for testing the '**PL-Analyzer**'-tool. To download this data go to 'www.nlcstr.com/SimuLaseDemo.htm'.

Demo-Structure

All **SimuLase**TM products come with an example for a more complex structure than the basic default structure. To load this structure go to '**File | Open Structure**' and load the structure-file '`C:/Program Files/NLCSTR/SimuLase/SampleLayeredStructure.sls`'.

In Case of Trouble with the Program

Although this should occur only rarely, if **SimuLase**TM should encounter a problem, it will usually pop up a window stating that a problem has occurred and giving the options to either 'continue' or 'close' the program. Usually the program will be able to recover without problems if the option 'continue' is chosen.

If something unexpected happens during the set-up of a GainDatabase please send us if possible the files 'name.sls' and 'name.slm' that contain the information about the structure and parameters used for your database. 'name' is the name you specified for the Database. You find these files in the directory specified by you for the database. If possible, send us also the files 'sus_control.dat' and 'sus.log'. These are in a temporary working directory that **SimuLase**TM created for intermediate data. Please use the search-option on top of any Windows file manager to locate these files, starting from 'C:\'. Click 'Search hidden files and folders' in the 'More advanced search options'-menu.


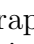
All these files are in ASCII-format. If you are concerned about disclosing proprietary information about your structure do not send the file 'name.sls'. Also search the other files for the section(s) starting with a line containing the string 'working directory' and ending with a line containing the string 'number of z-points' and delete these section(s).

In case of any issues, please contact us at simulase@nlcstr.com.

2 Quick Start Guide

The following is a brief description of the main functionality of **SimuLase™** 's main features. For more details and optimum usage please see the corresponding Sections, 3 and 6 and the description of the underlying models in Sec.7.

In order to test the various tools that **SimuLase™** offers to investigate data you can download a Demo-GainDatabase including various InGaAsP-based wells and radiative and Auger losses from our website at <http://www.nlctr.com/SimuLaseDemo.htm>. There you can also download some experimental spectra that can be compared to the theoretical data using the **PL-Analyzer** tool.

After starting **SimuLase™**, three main tabs appear on top of the graphics display window, 'Design Structure', 'Advanced' and 'Generate Database'. Additional tabs appear when the 'Surface Emitter Mode' or 'Edge Emitter Mode' are selected through the icons  and , respectively. After loading a gain database, a number of tabs appears below the graphics display window which allow to switch between displays of the various data included in the database.

2.1 Main Tabs

2.1.1 Design Structure

The 'Design Structure' tool is the default page that appears when **SimuLase™** is started. Initially the chart displays a basic 3-layer structure. A pre-existing structure layout may be loaded by selecting **File | Open Structure...**

The main chart window displays the currently loaded structure as a series of colored layers stacked horizontally. Superimposed on top of this device representation are plotted one or more graphs showing either the band edges (confinement potential, optionally computed using a classical Poisson-**drift-diffusion** model and/or a microscopic Schrödinger-Poisson model), wavefunctions and associated energy levels or the refractive index profile and the lowest confined mode across the device.

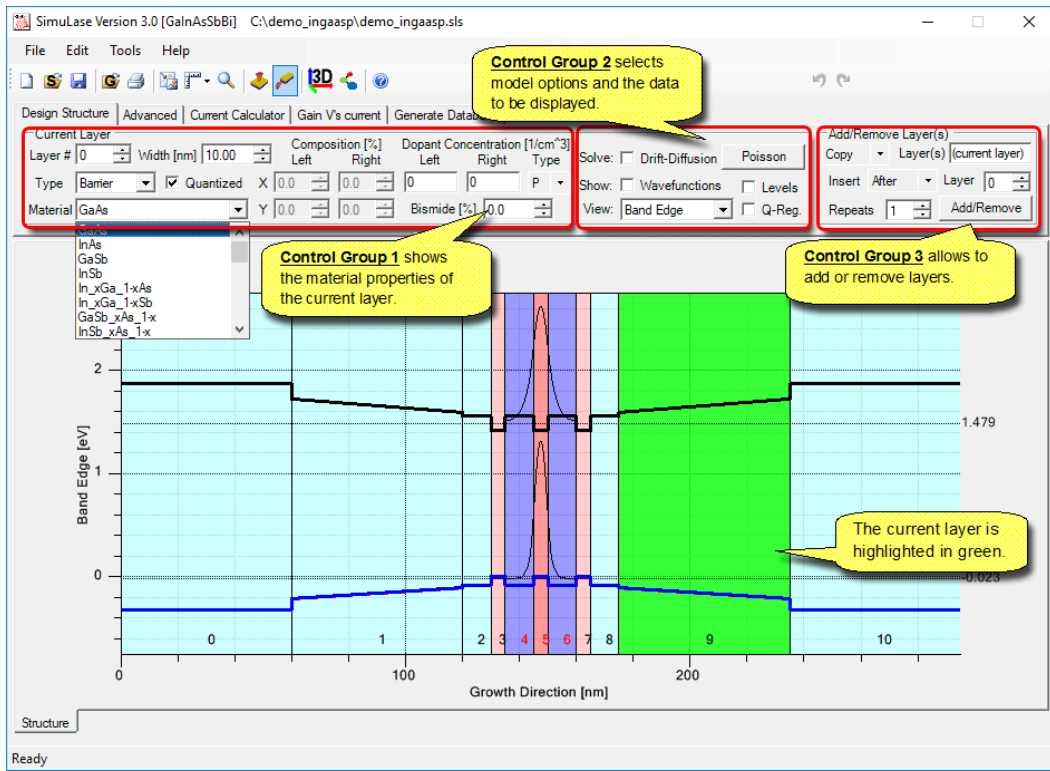
The controls above the main chart enable the user to construct a layered device and dynamically view various aspects of the resulting device. The controls are arranged into three functional groups:

Group 1 allow viewing and editing of the material properties of a single layer;

Group 2 controls the algorithms used to simulate the device and the resulting data view;

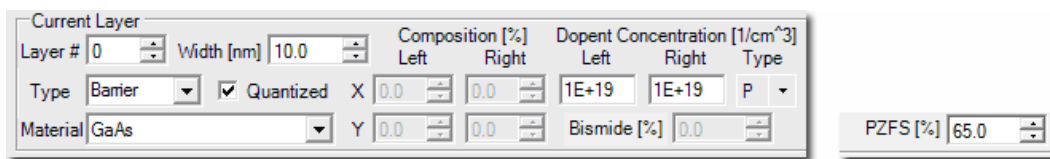
Group 3 enables the addition of new layers or the removal of existing layers.

The individual controls in each of these functional groups are detailed in the following sections.



Group 1: Layer Properties

The various controls in **Control Group 1** detail the physical properties of the current layer. Changing any of the displayed values for the current layer will automatically cause the corresponding plots in the chart to be updated.



Layer # A single layer is selected by changing the number field in this control (or using the mouse wheel or scroll arrows to cycle through layer numbers). Layers are numbered sequentially starting with layer 0. The currently selected layer is highlighted in green

Width [nm] The width the current layer in nanometers.

Type The function of the layer in the device. A layer can be one of three types, 'Barrier', 'Well' or 'Cladding'. The program uses these to determine the number of relevant subbands. It searches the number of bands that are confined in any of the wells, i.e., connected sequence of layers marked as 'Well' within the quantized region. Also, if a GainDatabase is loaded for well or barrier material in the calculation of reflection and transmission spectra, the absorption/gain and carrier induced refractive index changes are added to the background refractive index in all layers marked 'Well' or 'Barrier', correspondingly. No GainDatabase data is associated with layers of the type 'Cladding'.

Quantized Only layers marked as quantized are included in the microscopic calculations of wavefunctions, bandstructures, for solving the Poisson-Schrödinger problem of potential modifications due to local charge inhomogenities and for calculating optical properties like

gain/absorption. Creating a quantized region begins with a single layer of type 'Well' which may then be surrounded by layers of type 'Barrier'. Any structure may contain only a single continuous quantized region. Every quantized region has to include at least one layer of type 'Well'. The actual quantum well can be made of several layers of type 'Well'.

Material Layer material which may be a binary, ternary, quaternary or quinternary material.

Composition[%] This set of four numeric values sets the concentrations X and Y of the material compound at the Left and Right hand edges of the current layer. A linear gradient in concentration is assumed across the layer.

Dopant Concentration This set of two numeric values and a N-type or P-type selector set the dopant type and concentrations at the Left and Right hand edges of the current layer.

Z/Nitrogen/Bismide/PZFS [%] In quinternary materials, this field allows to set the additional composition 'z'. For dilute Nitrogen (GaInNAs) or dilute Bismide (AlInGaAsSbBi) it allows to set the content of the dilute material. In wide bandgap AlInGaN it allows to set the strength of the internal piezoelectric and spontaneous polarization fields. Here, all strain-related internal fields throughout the structure are scaled according to this ratio from the nominal literature value. We found for this parameter a value of 65% to be appropriate in most cases. For quinternary materials and dilute materials the program currently allows only layers with constant 'z' composition across the layer.

Group 2: Algorithm and Data View Selection

The various controls in Control Group 2 specify the computational algorithm used to compute optical properties of the quantized region and dictate which aspects of the computed data should be plotted.

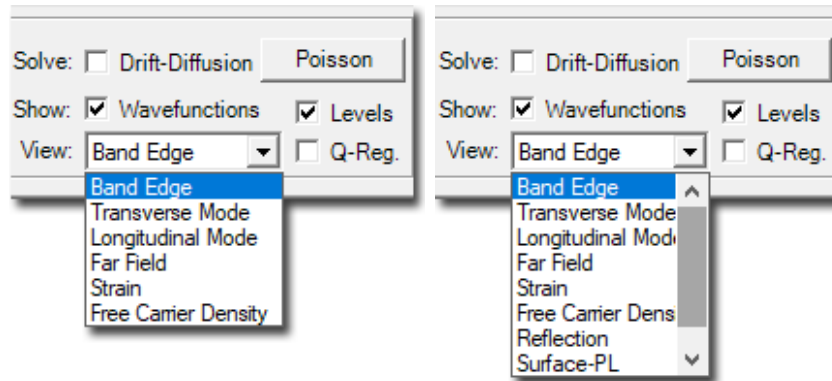


Figure 2.1: Data view options in edge-emitting mode (left) and surface-emitting mode (right).

Drift-Diffusion If this box is checked the Poisson drift diffusion problem describing possible band edge modifications due to local charges from ionized dopants and free carriers is solved.

Poisson Click this button to solve the microscopic Poisson-Schrödinger model for the quantized region. A fully coupled 8x8 kp-model is used in this calculation. The number of subband states that are used in this calculation is set on the '**Advanced**'-panel.

Note: It is assumed that the potential modifications due to charges that are quantized in the wells are small as compared to the global potentials due to ionized dopants and/or externally applied Voltages. Thus, we do not use a self consistency loop that couples the classical Poisson drift diffusion problem to the quantized Poisson-Schrödinger problem.

Wavefunctions If checked, in addition to the confinement potentials the wavefunctions are shown. The number of wavefunctions to be shown is set on the '**Advanced**'-panel.

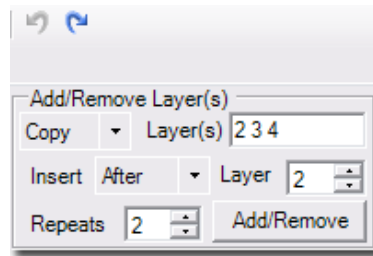
Levels Show energy levels associated with the wavefunctions in addition to band edges.

View This field allows to switch from displaying the confinement potential and wavefunctions ('Band Edge' view) to displaying the transverse or longitudinal optical mode together with the corresponding optical confinement factor and refractive index profile, the far field for transverse modes, the strain or the free carrier density due to ionized dopants. In the 'Surface Emitter Mode' (select by clicking the icon: 📌 in the top menu) it also allows to show the reflection/transmission spectrum, the surface-PL spectrum and the LI-characteristic.

Q-Reg Provides a "zoomed-in" view of the 'Quantized Region', i.e., the region of the device containing layers marked as quantized that are used in the microscopic calculations.

Group 3: Add/Remove Layers

The various controls in Control Group 3 enable the addition or removal of one or more layers to or form the layered structure. The '**Add/Remove**' button performs an operation on the



structure according to the values of all active controls contained in the group. For example with the setting shown in the figure above, clicking **Add/Remove** will “**Copy layers 2, 3, 4 and insert them After layer 2, Repeating this operation 2 times**”. Using the drop-down arrows the user can select either a **Copy**, **Clone** or **Delete** operation and similarly may select **After** or **Before** to specify the insertion location.

The **Repeats** numeric value may be used to construct periodic arrangements of layers. For example a Bragg mirror can be created by first defining two layers that define the unit cell for the mirror and then cloning those two layers N times by setting the **Repeats** numeric value to N. The designer first creates a substructure composed of the cloned layers and then inserts that substructure at the appropriate location specified in the Insert (**After** | **Before**) numeric box. While the attributes 'well/barrier' will be transferred to the clones or copies, the new layers will not be part of the 'quantized region' unless they are manually marked to be part of it.

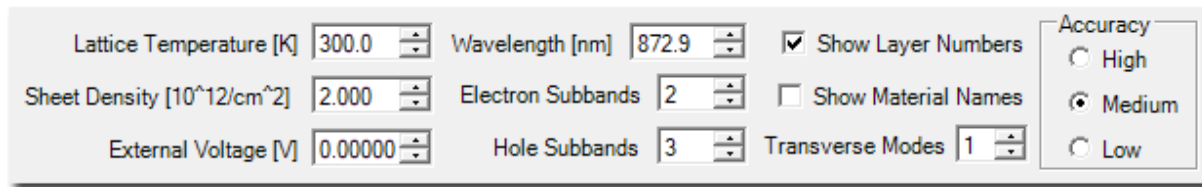
The **Clone** operation differs from the **Copy** operation in that cloned layers share the same material properties. Changing any property of a cloned layer like width, dopant concentration etc., will cause the same change in all clones of that layer. The **Clone** operation is most commonly used (with **Repeats** set to a value greater than 1) to construct periodic arrangements, such as Bragg mirrors, where layers share common properties.

The **Delete** operation permanently removes all layers listed in the Layer(s) numeric box. If a layer is part of a series of clones, all corresponding layers in the clones will also be deleted.

The **undo** and **redo** buttons, 🔄, allow to undo or redo changes made with the controls of this group.

2.1.2 Advanced Tab

The various controls contained under the Advanced tab are used to specify parameters related to the whole structure such as Lattice Temperature operating wavelength etc.. These are used only while setting up the structure. Corresponding parameters - if relevant - have to be set separately for the generation of GainDatabases.



Lattice Temperature The temperature of the device. This temperature is assumed to be also the carrier temperature.

Sheet Density The sheet carrier density in the quantized region as used for the quantized Poisson-Schrödinger problem. Equal electron and hole densities are assumed. This is the density related to external optical or electrical pumping. Intrinsic, dopant related carrier densities are assumed to be negligible in the Poisson-Schrödinger calculation. This density is also used if absorption/gain is included in the calculation of the longitudinal mode and reflection and transmission spectra.

External Voltage A possible external voltage applied across the device.

Wavelength The wavelength at which the device is assumed to operate. This is used in the calculation of the mode profiles and optical confinement factors as well as the calculation of reflection and transmission spectra. See Sec.7.1.2 for a discussion of the confinement factor calculation.

Electron/Hole Subbands Specifies the number of confinement wavefunctions and subband levels which are displayed in the chart. Also specifies the number of subbands that are used to solve the Poisson-Schrödinger problem for the structure display. The numbers are not used for the GainDatabase calculation and have to be reset there.

Accuracy Allows to change the number of grid-points used for the calculation of the wavefunctions and levels. The calculation-time increases with the accuracy level which can become noticeable especially if the Poisson-Schrödinger problem shall be calculated.

Show Layer Numbers Labels each layer on the chart with its associated layer number.

Show Material Names Labels each layer on the chart with the type of material used in the layer.

Transverse Modes Specifies the number of transverse modes and corresponding far fields that shall be displayed.

2.1.3 Generate Database

The details of the various selections that can be made on this panel are explained in Sec.3.6.

In order to get a feeling for how **SimuLaseTM** generates GainDatabases, follow the steps as indicated in Fig.2.1.3 and leave all other options in their default setting. With these settings the model is reduced to a two-band model without any Coulomb effects. The calculations should only take a few tens of seconds for each density/temperature-combination. You can then load the created database into the other tools of **SimuLaseTM** to view the absorption, PL, etc. by using **'File | Open Gain Database** and opening the file

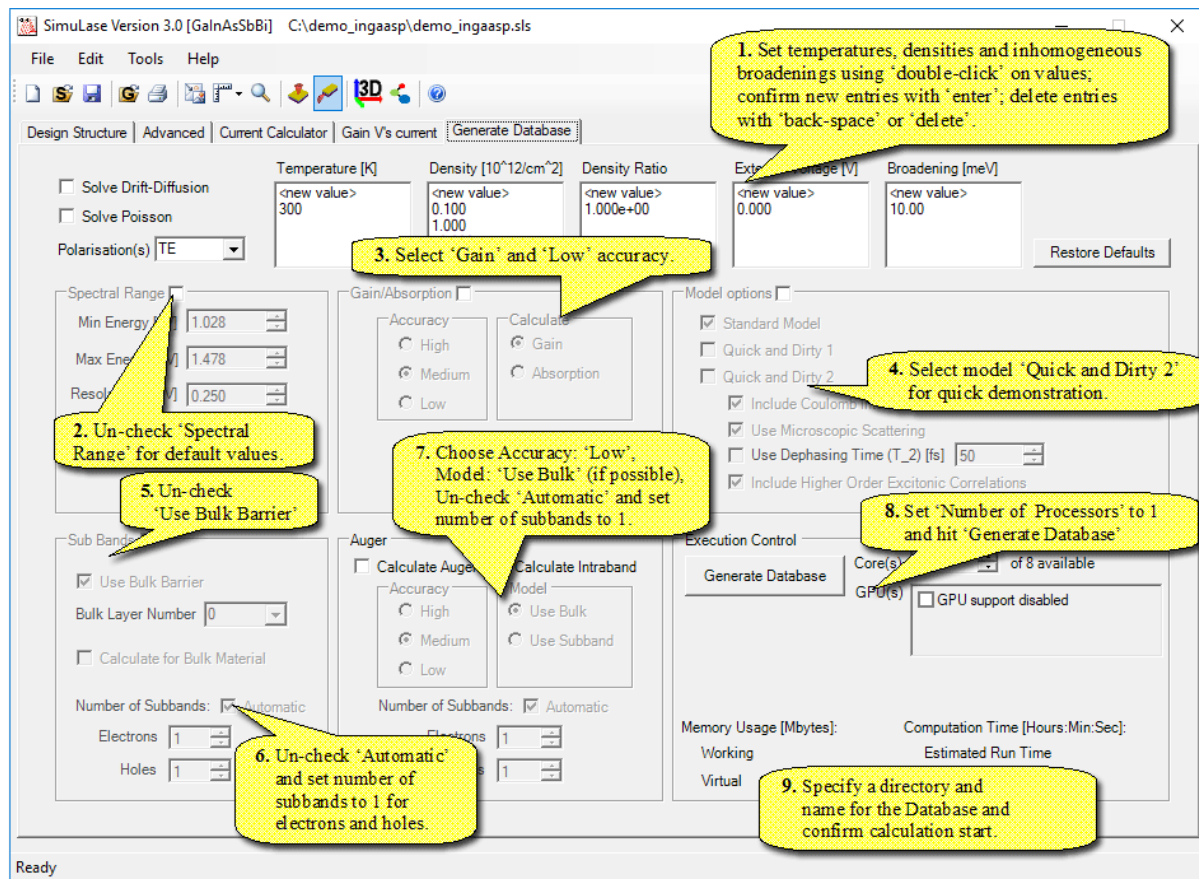



Figure 2.2: Overview of the 'Generate Database' panel with instructions for a very quick demonstration run.

that starts with the 'Name' you have chosen for the database followed by the extension '.gdb'. For setting up realistic GainDatabases one should always use the 'Standard Model' which includes Coulomb effects like excitonic resonances, Coulomb enhancement of the absorption or density dependent bandgap renormalization as well as electron-electron and electron-phonon scattering that describe the broadening of the spectra and higher excitonic resonances as source terms for the spontaneous emission. All of these effects are essential to obtain the quantitatively predictive quality for the results that separates **SimuLaseTM** from any other available software tool.

2.2 Main GUI Components

The main GUI components are shown below. To load a GainDatabase select 'File | Open Gain Database' or click the 'G' Folder' symbol, .

By clicking on one of the tabs below the plot window, 'Spontaneous Emission', 'Refractive Index', 'Absorption', or 'Losses', ..., the respective data are shown for the selected parameters (Polarization(s), Electric Field(s), Temperature(s), Shift(s), (inhomogeneous) Broadening(s) and Carrier Densities(s)). At least one entry has to be selected for each of these parameters to display data. To hide all data de-select all entries for at least one of the parameters. To de-select an entry press the 'control' key and click on the entry.

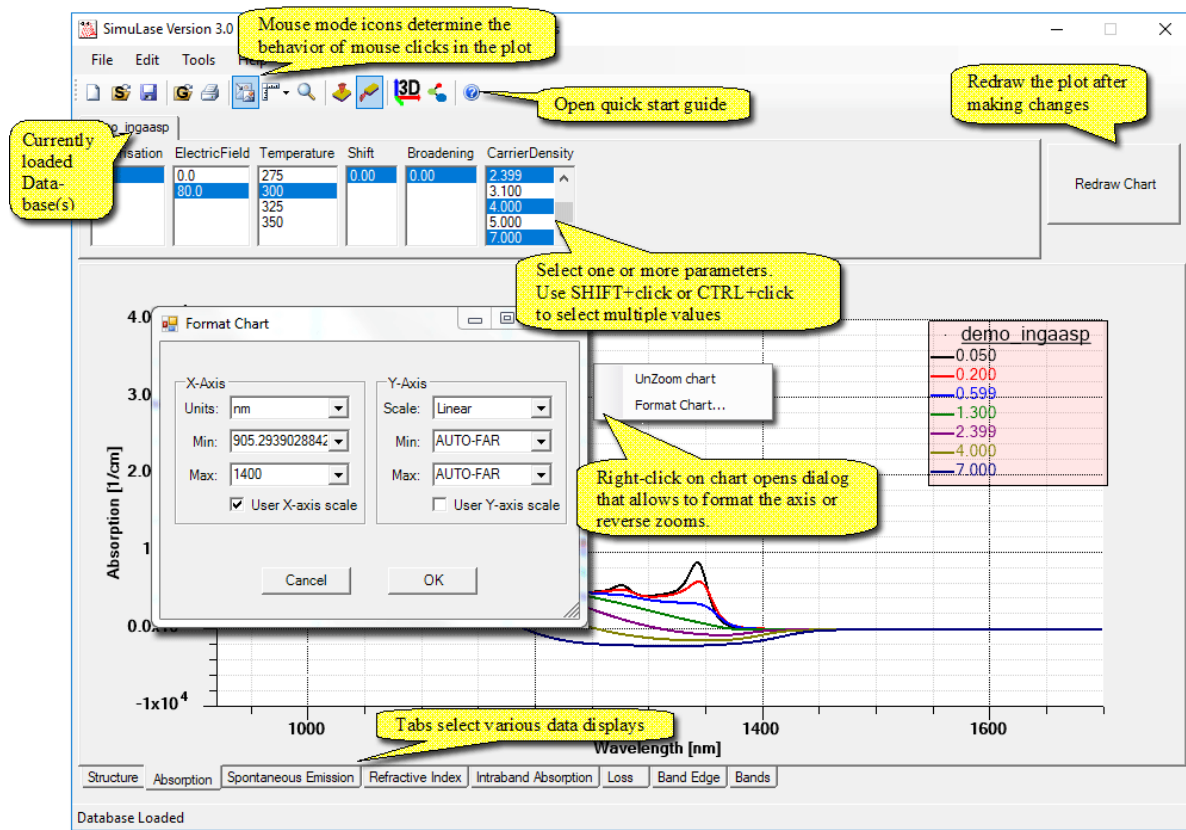


Figure 2.3: Overview of the main GUI plotting panel.

The tabs 'Band Edge' and 'Subbands' display the confinement potential and subbands for the structure for which the database has been created. One or more energy levels and/or wave functions may be superimposed on the confinement potential by choosing the desired number and activating 'Show Wavefunctions' and/or 'Show Levels'.

Formatting the Axes

The layout of the chart may be formatted by 'right-clicking' the mouse to display a pop-up menu. Selecting the 'Format Chart' option displays the dialog box shown as an insert in Fig.2.3. Use this dialog to format the X-axis units (electron Volts or nanometers), the Y-axis scale (Linear or Logarithmic) and the physical extents of each axis. **When changing numeral entries these have to be confirmed by hitting the 'enter' key.**

By default a chart will auto-scale the X and Y-axes so as to include all data points within the chart area and also present well-rounded major and minor tick mark spacing of the chart axes. Three auto-scale modes are provided:

'AUTO-EXACT' sets the Max and Min value of the axis to the **exact** Max and Min values in the displayed data sets.

'AUTO-NEAR' sets the Max and Min value of the axis to the next minor tick mark that encompassed displayed data sets.

'AUTO-FAR' sets the Max and Min value of the axis to the next major tick mark that encompassed displayed data sets.

The user may override the default auto-scale settings (AUTO-EXACT for the X-axis and AUTO-

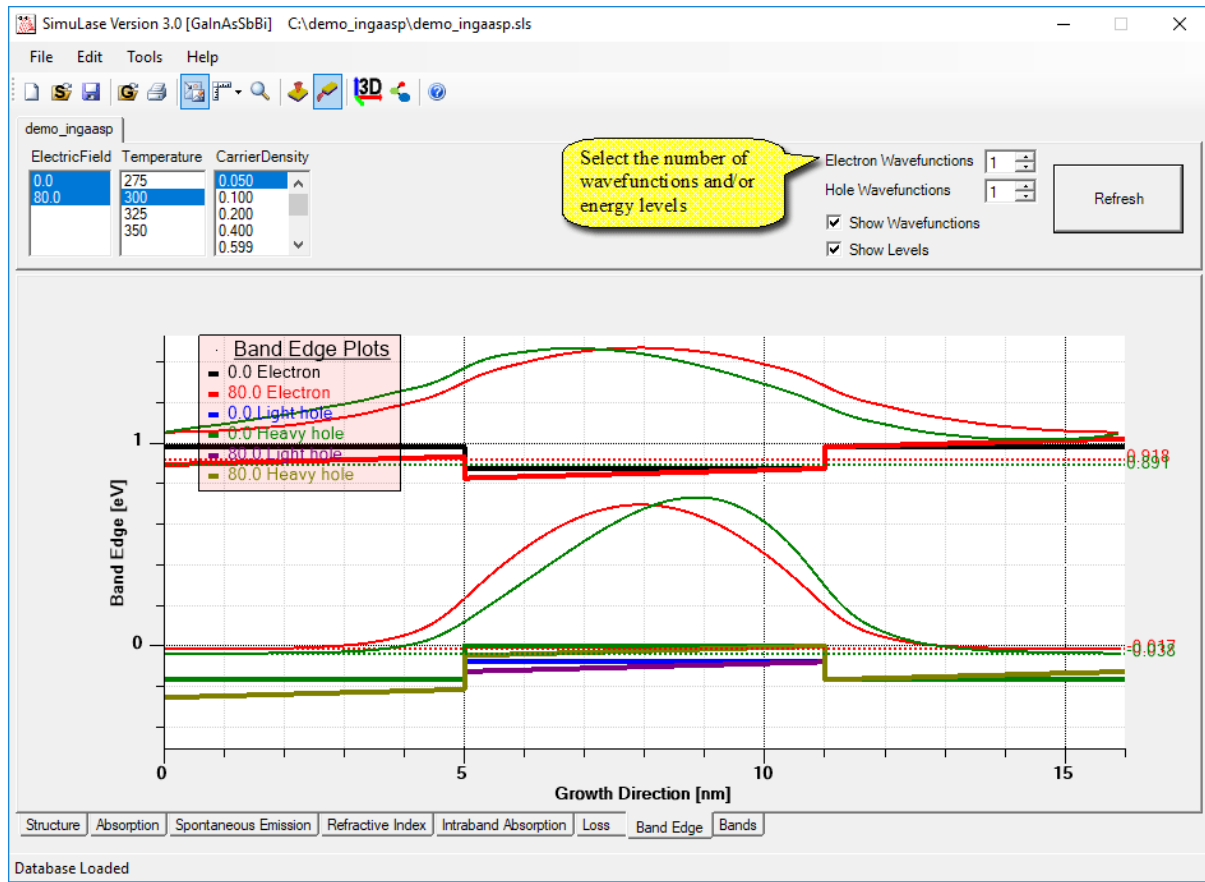



Figure 2.4: 'Band Edge' plot window.

FAR for the Y-axis) by clicking the **User (X or Y)-axis scale** check box. A user defined numeric value for either Max or Min (or both) may be entered.

Chart legends may be repositioned by clicking the  icon on the main toolbar and using the left button mouse to select and move the legend to a new location.

Save/Reload/Export a Structural Layout

The structural layout can be saved and reloaded using '**File | Save Structure**' and '**Open Structure**' from the main menu. The structural information is saved in xlm-format in an *.sls file which can be read externally using, e.g., Microsoft Excel.

Exporting a GainDatabases

GainDatabases can be exported into a format that allows to import the data contained in them into other software products for further evaluation using '**File | Export Database as**' from the main menu. Currently, this option allows to export a database in a format that can be imported into Crosslight Inc.'s Lastip software. It also allows to produce reduced GainDatabases containing just subsets of the original database. For more info on this feature see Sec.3.1.

RegionName	LayerMaterialName	LayerActive	Width	CloneOfLayer	ConcentrationXLeft	ConcentrationXRight	ConcentrationYLeft	ConcentrationYRight	ConcentrationNitride	ConcentrationNPdopantLeft	ConcentrationNPdopantRight	Dopant
Barrier	InP	INACTIVE	200	-1	0	0	0	0	0	2E+18	2E+18	P_TYP
Barrier	In_xGa_1-xAs_yP_1-y	INACTIVE	35	-1	0.863	0.863	0.3	0.3	0	0	0	P_TYP
Barrier	In_xGa_1-xAs_yP_1-y	INACTIVE	5	-1	0.863	0.863	0.3	0.3	0	0	0	P_TYP
Well	In_xGa_1-xAs_yP_1-y	INACTIVE	6	-1	0.9	0.9	0.53	0.53	0	0	0	P_TYP
Barrier	In_xGa_1-xAs_yP_1-y	INACTIVE	5	-1	0.863	0.863	0.3	0.3	0	0	0	P_TYP
Barrier	In_xGa_1-xAs_yP_1-y	ACTIVE	5	-1	0.863	0.863	0.3	0.3	0	0	0	P_TYP
Well	In_xGa_1-xAs_yP_1-y	ACTIVE	6	-1	0.9	0.9	0.53	0.53	0	0	0	P_TYP
Barrier	In_xGa_1-xAs_yP_1-y	ACTIVE	5	-1	0.863	0.863	0.3	0.3	0	0	0	P_TYP
Barrier	In_xGa_1-xAs_yP_1-y	INACTIVE	5	-1	0.863	0.863	0.3	0.3	0	0	0	P_TYP
Well	In_xGa_1-xAs_yP_1-y	INACTIVE	6	-1	0.9	0.9	0.53	0.53	0	0	0	P_TYP
Barrier	In_xGa_1-xAs_yP_1-y	INACTIVE	5	-1	0.863	0.863	0.3	0.3	0	0	0	P_TYP
Barrier	In_xGa_1-xAs_yP_1-y	INACTIVE	35	-1	0.863	0.863	0.3	0.3	0	0	0	P_TYP
Barrier	InP	INACTIVE	50	-1	0	0	0	0	0	5E+17	5E+17	N_TYP
Barrier	InP	INACTIVE	200	-1	0	0	0	0	0	5E+17	5E+17	N_TYP

Figure 2.5: Structure file, *.sls, in Windows Excel.

Saving/Printing Chart Images

An image of the current chart (in *.BMP, *.JPG, *.GIF, *.TIFF or *.PNG format) may be stored in a file by selecting 'File | Save as Image' from the main menu.

High resolution printouts are available by selecting 'File | Print' from the main menu.

Exporting Displayed Data

The currently displayed data can be exported into ASCII-format data files by selecting 'File | Export Data' from the main menu.

2.3 General Tools

Some analysis tools that are independent of the device geometry (edge- or surface emitting) can be found under the tab 'Tools' of the main menu.

2.3.1 PL Analysis Tool

The PL Analyzer tool allows to compare theoretical material PL-spectra to measured data in order to obtain information about the inhomogeneous broadening and spectral mismatches between nominal and actual structure. The results provide direct insight into device growth quality. In contrast to the 'Surface-PL' panel, here the PL is assumed to be the pure material PL that is not disturbed by cavity effects. This is usually the case in edge-emitting devices or for PL that has been measured from the edge of the device.

The tool may be activated by selecting 'Tools | Analyze Experimental PL' from the menu bar. Performing a PL analysis requires the following steps:

- 1) Select a gain database that matches the material system of the experimental PL spectra to be analyzed. Click on 'Gain Database' and select a pre-computed gain database.
- 2) Select the parameters, like polarization and temperature, that most closely match the experimental conditions. The corresponding theoretical PL spectra from the database are plotted.

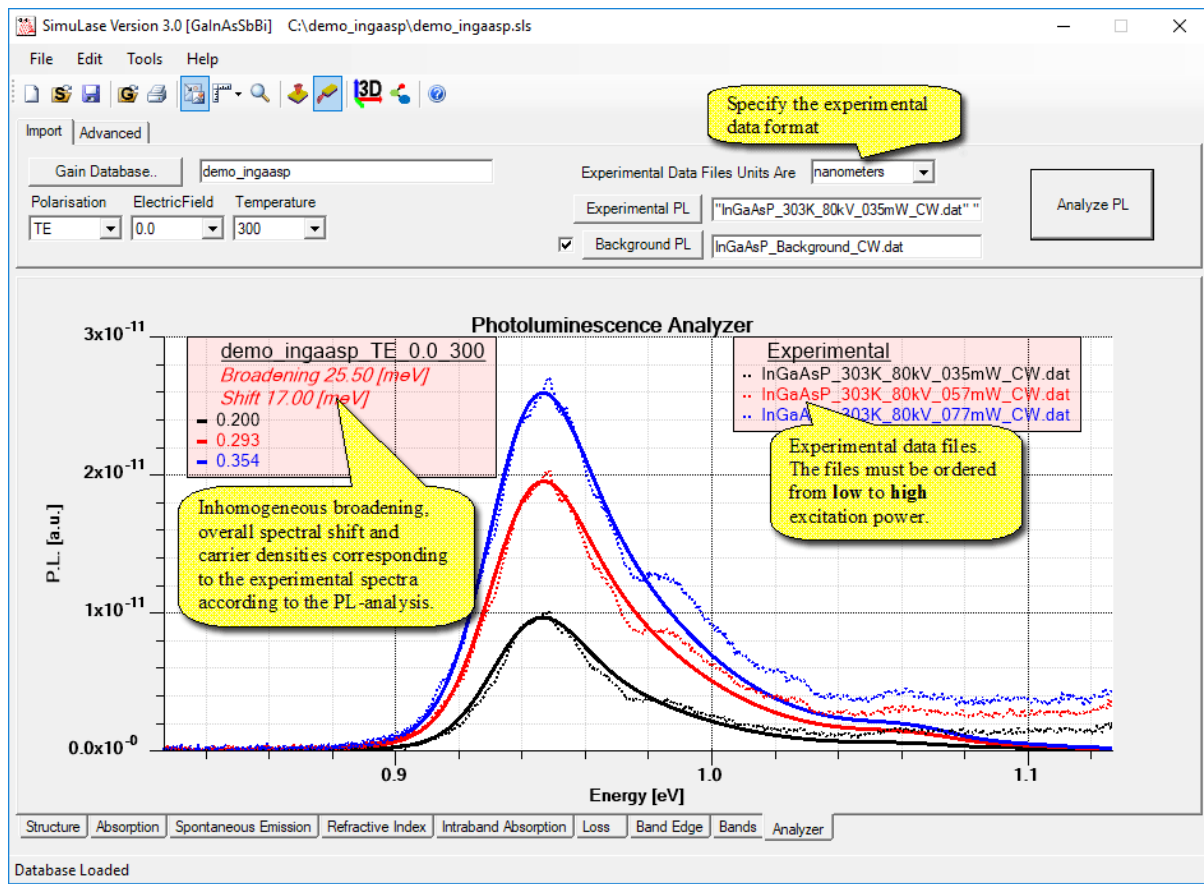


Figure 2.6: Main PL-Analysis panel.

- 3) Import the experimental PL data (in order of increasing excitation power) by clicking the '**Experimental PL**' tab and importing the data. In the current version of **SimuLase™** the experimental data has to be in two-column ASCII format. The first column containing the transition energy in [eV] or the wavelength in [nm]. The second column containing the PL data. Specify the data format using the '**Experimental data file units**' selector box.
- 4) If available, load an experimental background noise spectrum data file using the '**background**' tab. This background will be subtracted from all experimental spectra.
- 5) Click the '**Analyze PL**' button to perform an analysis).
- 6) Analysis results may be improved by "clipping" noisy tails from the experimental data and selecting suitable control points on the '**Advanced**' tab.

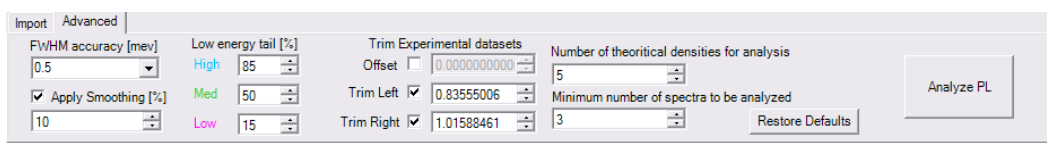


Figure 2.7: Advanced PL-Analysis panel.

On the '**Advanced**' tab, details of the analysis can be influenced by choosing low-energy matching points, high energy cut-off, the desired accuracy ('**FWHM accuracy**' tab), as well as the number of theoretical spectra used for the analysis.

The '**Offset**' can be used to subtract a constant background value from the experimental spectra - similarly to subtracting a background-noise spectrum.

'**Trim Left**' and '**Trim Right**' allow to exclude low- and high-energy tails in the experimental spectra from the analysis. Low energy tails are often covered by noise where the ideal spectra fall off below the bandgap. On the high energy side experimental spectra often show enhancements of the PL beyond the ideal theoretical PL. This is usually due to non-thermal carriers in the experiment which arise in particular when using CW-excitation. These carriers have not relaxed toward the bottom of the wells - occupying higher subbands - and lead to an enhancement beyond the ideal thermal equilibrium situation assumed in the theory (see e.g. the features at 0.98 eV in Fig.2.6. These parts should be excluded from the analysis.

The Analysis should focus on the spectral region around the main peak that gives the best information about the inhomogeneous broadening and spectral shifts - starting where the PL reaches about 20% of the maximum to where the PL falls off again to about 50% of the peak value.

The theoretical spectra to the lowest carrier densities are used since experimental data usually is taken under low excitation conditions. The '**Number of theoretical densities for analysis**' should be increased if no good match is found when considering only the lowest densities.

If one has a very large experimental database loaded, one might want to save computation time and/or to focus on the qualitatively best spectra one can choose a subset of spectra to be analyzed by specifying the '**Minimum number of spectra to be analyzed**'. The analysis tool internally selects then a subset of experimental spectra of that size that matches closest average criteria. The final results are displayed only for these spectra.

In case of noisy experimental spectra one can apply a smoothing algorithm by choosing '**Apply Smoothing**' in order to eliminate artificial local peaks in the spectra which might obscure the true spectral location of the PL maximum. The percentage value chosen for smoothing is given as the percentage of the estimated inhomogeneous broadening present in the experimental data.

After choosing the desired settings, click the '**Analyze PL**' tab. After a short calculation, the best matching theoretical curves appear on the screen superimposed to the experimental data. In order to obtain the agreement, usually it is necessary to inhomogeneously broaden the ideal theoretical spectra (to take into account the experimentally unavoidable local composition and/or well width fluctuations) and to apply a spectral shift. Physically, this shift often appears as a consequence of deviations between nominal and actual composition and/or quantum-well width. The computed broadening and shift can be read from the legend in the display window. This legend also shows the theoretical densities chosen for the best agreement with the experimental data.

The analyzer requires that the experimental datasets be imported in order of increasing excitation power. Internally, the analyzer arranges the imported data files by sorting the file names in alphabetical order. The resulting ordering of the data files is visible in the '**Experimental**' legend that appears on the plot window next to the experimental data plots. If, after clicking the '**Analyze PL**', button the analyzer determines that the experimental data files are NOT in correct order the following dialog is displayed.

The order of data files may be rearranged by selecting a file name and using the '**Move up**' or '**Move down**' buttons. Once all file have been correctly reordered from low (on top) to high excitation power (at the bottom) click OK, the experimental PL data will be redisplayed in the plot window and the PL analysis may be reapplied by clicking the '**Analyze PL**' button.

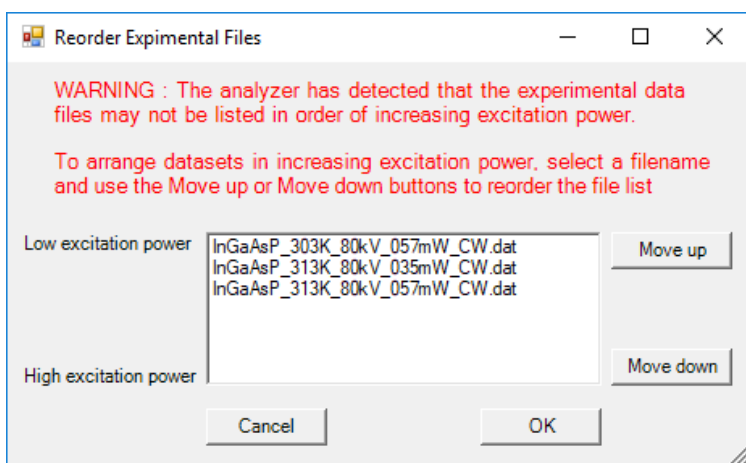


Figure 2.8: Re-arrange experimental PL panel.

2.3.2 Generating Shifted and Broadened Databases

Shifted and inhomogeneously broadened copies of existing GainDatabases may be generated by selecting **Tools | Shift and Broaden Database** from the main menu bar. The dialog Fig.2.9 will be displayed. Select an existing GainDatabase using the **'Gain Database'** button, enter the desired shift and broadening, select a directory into which the new database shall be stored and click OK. A new database will be generated in the destination directory with all spectra shifted and broadened by the requested amount. All other data unaffected by the shift and broaden operations, like wavefunctions and band structure etc., will be copied to the destination directory. The new database that may be loaded into the viewer, like any other Gain Database, using the **'File | Open Gain Database'** from the main menu bar.

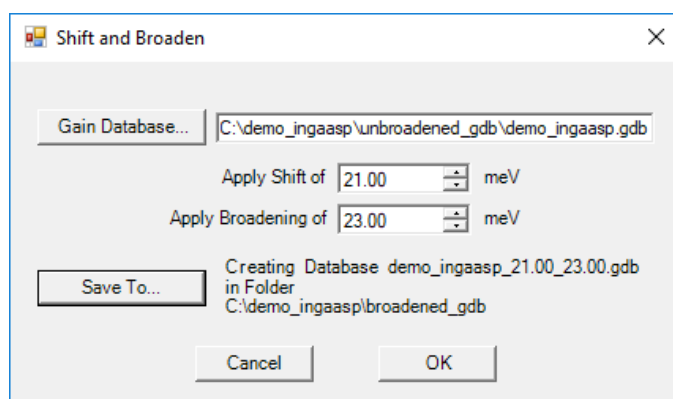


Figure 2.9: Dialog to create shifted and/or broadened copies of existing GainDatabases.

2.3.3 Linewidth Enhancement Factor Tool

The linewidth enhancement factor tool may be activated by selecting **Tools | Linewidth Enhancement Factor** from the menu bar.

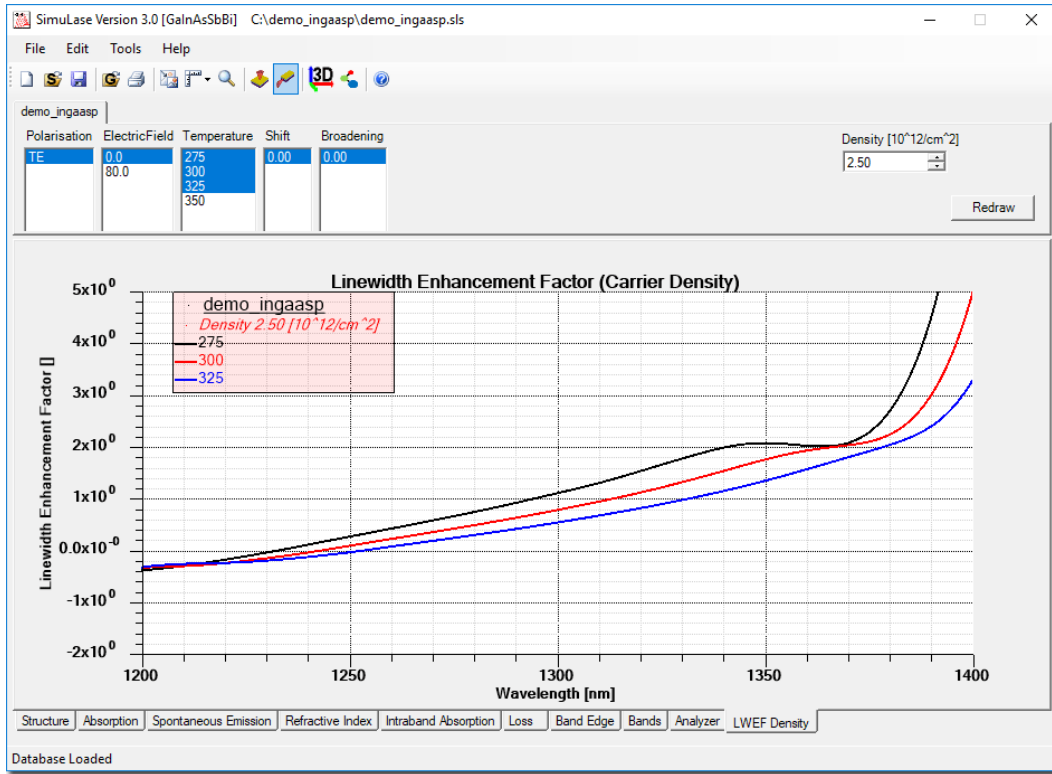


Figure 2.10: Linewidth Enhancement Factor tool for the calculation of the LWEF for a given carrier density.

Linewidth Enhancement Factor | Carrier Density

This tool calculates the linewidth enhancement factor spectrum ($\alpha(\omega)$) for a specified carrier density (N) using:

$$\alpha(\omega, N) = \frac{n(\omega, N + \Delta_N) - n(\omega, N)}{a(\omega, N + \Delta_N) - a(\omega, N)}, \quad (2.1)$$

where n is the refractive index in the units as displayed in the 'Refractive Index'-window, a is the material absorption and Δ_N is an infinitesimal density change.

Since the linewidth enhancement factor is given by the ratio of two differentials, it can vary dramatically when viewed on an extended energy/spectral-range. One usually has to zoom into the relevant region of the spectra.

Linewidth Enhancement Factor | Electric Field

This tool calculates the linewidth enhancement factor spectrum ($\alpha(\omega)$) for a change in electric field/applied Voltage (F) using:

$$\alpha(\omega, F_0, F_1) = \frac{n(\omega, F_0) - n(\omega, F_1)}{a(\omega, F_0) - a(\omega, F_1)}, \quad (2.2)$$

where n is the refractive index in the units as displayed in the 'Refractive Index'-window, a is the material absorption and F_0, F_1 are two electric field values from the list of fields for which

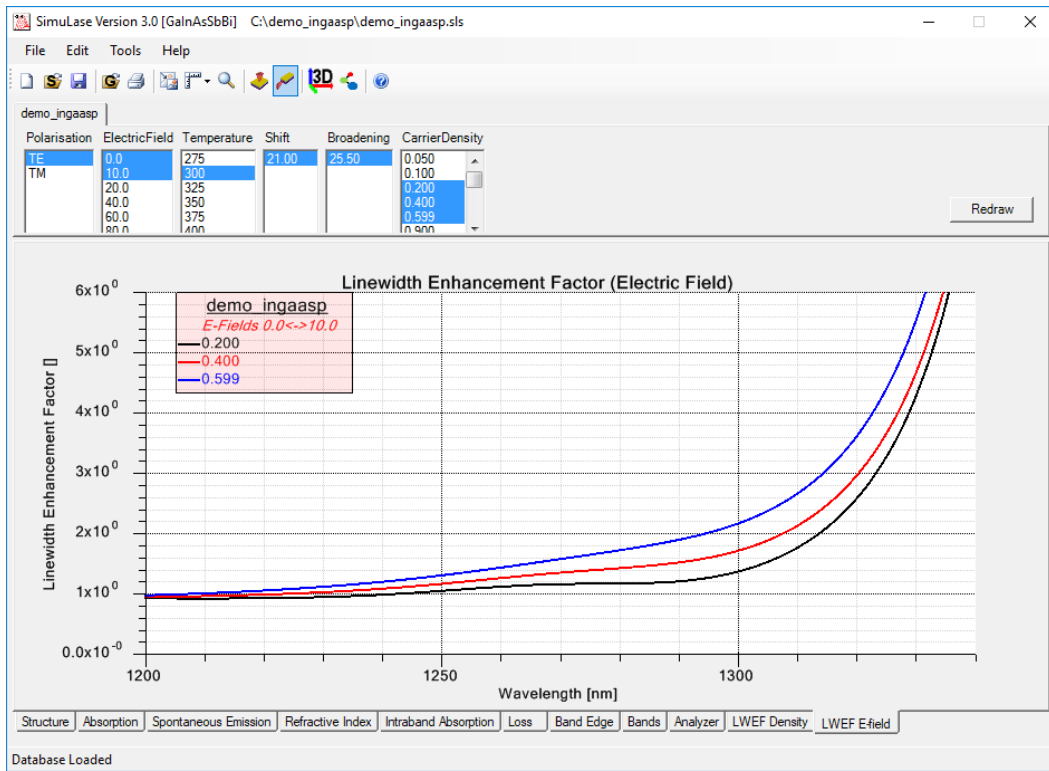



Figure 2.11: Linewidth Enhancement Factor tool for the calculation of the LWEF for a change in the electric field across the active region.

the database has been set up. This definition of the linewidth enhancement factor follows the one given in Ref. [1].

2.4 Tools for Edge-Emitters

SimuLaseTM offers some tools that are most useful for analyzing edge emitting structures. They can be accessed by clicking on the icon  in the top panel or by selecting 'Tools | Edge Emitter Mode'.

2.4.1 Current Calculator Tool

Once the edge-emitting mode has been selected, the 'Current Calculator' tool appears as a tab above the plot panel.

While **SimuLase**TM does not model the electrical pump injection problem that is crucial for a quantitative analysis of the operating characteristics of electrically pumped devices, this tool allows to determine basic characteristics like the threshold current or internal quantum efficiency for somewhat idealized cases and allows to study their dependence on various parameters like the number of wells or the absorption loss. It also allows to calculate the input-output characteristics using a model that is accurate for the case of optical pump injection and can be used to study dependencies in the case of electrical pumping.

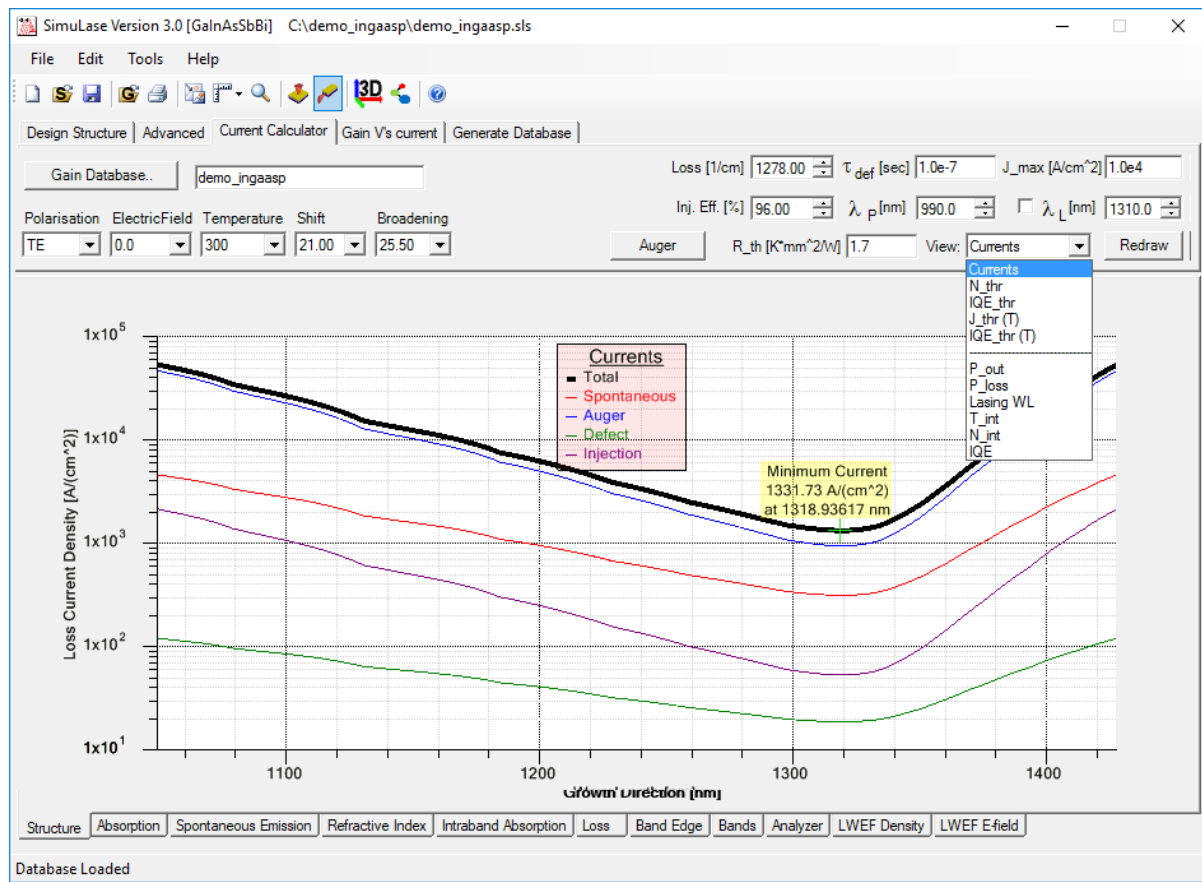


Figure 2.12: Current Calculator tool displaying threshold characteristics.

The tool requires a gain database and the corresponding structure should be loaded in the 'Design Structure' window. The 'quantized region' for which the database has been set up should be marked correctly in the structure. Then the program automatically determines the number of wells in the structure (identical copies of the quantized region) and scales the data in the database accordingly. This is important for the case where - as typically suggested - the database has been set up for only one well of a multi-well structure.

The tool has two operating modes:

- (1) One determines the threshold characteristics like threshold current, lasing wavelength and IQE, for the fixed temperatures for which the database has been set up. Here, internal heating is neglected.
- (2) One calculates the input-output characteristics taking into account heating due to non-radiative losses.

Mode (1) requires only very limited and usually rather well known input. Assuming that internal heating is not too relevant at threshold, it gives correct results that are independent of the way of pumping.

Mode (2), while more powerful than mode (1), requires to know more input parameters, like the thermal impedance. It is a complete model for the case of optical pumping. However, it does not consider heating mechanisms that occur in electrical pumping like Joule heating and Thomson-Peltier heating. The influence of these can only be roughly approximated within this model. Thus, the absolute accuracy is questionable for electrically pumped cases. However, the

model should allow to determine general trends of the operating characteristics correctly also for this pump mode.

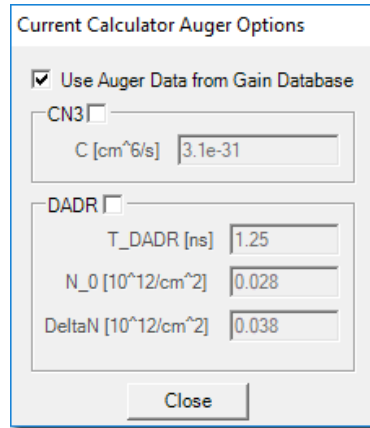


Figure 2.13: Panel allowing to choose between different Auger models.

Three different models for the Auger losses can be chosen. When selecting 'Use Auger Data from Database,' the microscopically calculated Auger losses from the database are used. If the database was not set up including Auger losses, they are assumed to be zero. When selecting the 'CN3' model the classical CN^3 cubical density dependence is assumed. The density-activated defect recombination model, 'DADR', was found to be appropriate for AlInGaN materials. Details of the Auger models can be found in Sec.7.1.6.

Threshold Characteristics

As mentioned above, the calculations require a gain database and the corresponding structure has to be loaded in the 'Design Structure' window. The structure is used to determine the number of wells, i.e. the number of repeats of the quantized region for which the gain database has been set up within the full structure. Thus, the number of wells can be varied by adjusting the structure accordingly.

For these calculations internal heating is neglected. The temperature for which the calculations are done is selected from the ones available in the database. The user has to specify the total material absorption loss in the field '**Loss**'. This is usually given by the sum of the out-coupling loss plus the internal absorption loss. If this is known as a modal loss for the full structure, it has to be divided by the optical confinement factor for the structure. The confinement factor can be calculated using the 'View | Transverse Mode' option from the 'Design Structure' panel. It is calculated for the temperature and wavelength as specified in the 'Advanced' options panel. One also has to specify the defect recombination time in the field ' τ_{def} ', and the injection efficiency in the field '**Inj. Eff.**'. The latter accounts for pump injected carriers that are not captured into the wells.

The tool looks up from the database what carrier density is required to yield enough gain to overcome the absorption losses. Then the loss currents due spontaneous emission (radiative loss) and Auger losses (according to the selected Auger model) are calculated from the database data for this density. If the database contains data for TE and TM polarization, the corresponding spontaneous emission losses are combined assuming that one third of the spontaneous emission goes into TM-modes and two thirds go into TE-modes. The defect recombination loss is calculated using the specified recombination time.

This evaluation is done for all wavelengths for which optical gain is found in the absorption/gain spectrum that is specified in the database selection fields. The resulting currents are plotted as function of the wavelength.

In a free running device, the threshold lasing wavelength and current is given by the point of minimum total current. For wavelength selective devices, like edge emitters with surface gratings, the fixed lasing wavelength can be set by checking the box next to the field ' λ_L ' and specifying the value there. All calculations will then be done for this fixed wavelength.

The tool also allows to display the corresponding intrinsic carrier densities, N_{thr} and internal quantum efficiencies, ' IQE_{thr} ' (spontaneous emission loss current divided by total loss current). It also calculates the threshold current and internal quantum efficiency for all temperatures within the database if it contains data for more than one temperature. The data is determined at each temperature from the wavelength of minimum total current or the specified lasing wavelength. The results are displayed by selecting ' J_{thr} (T)' and ' IQE_{thr} (T)'. Exponential fits according to characteristic temperatures (T_0) and (T_1), respectively, are shown in these plots.

Input-Output Characteristics

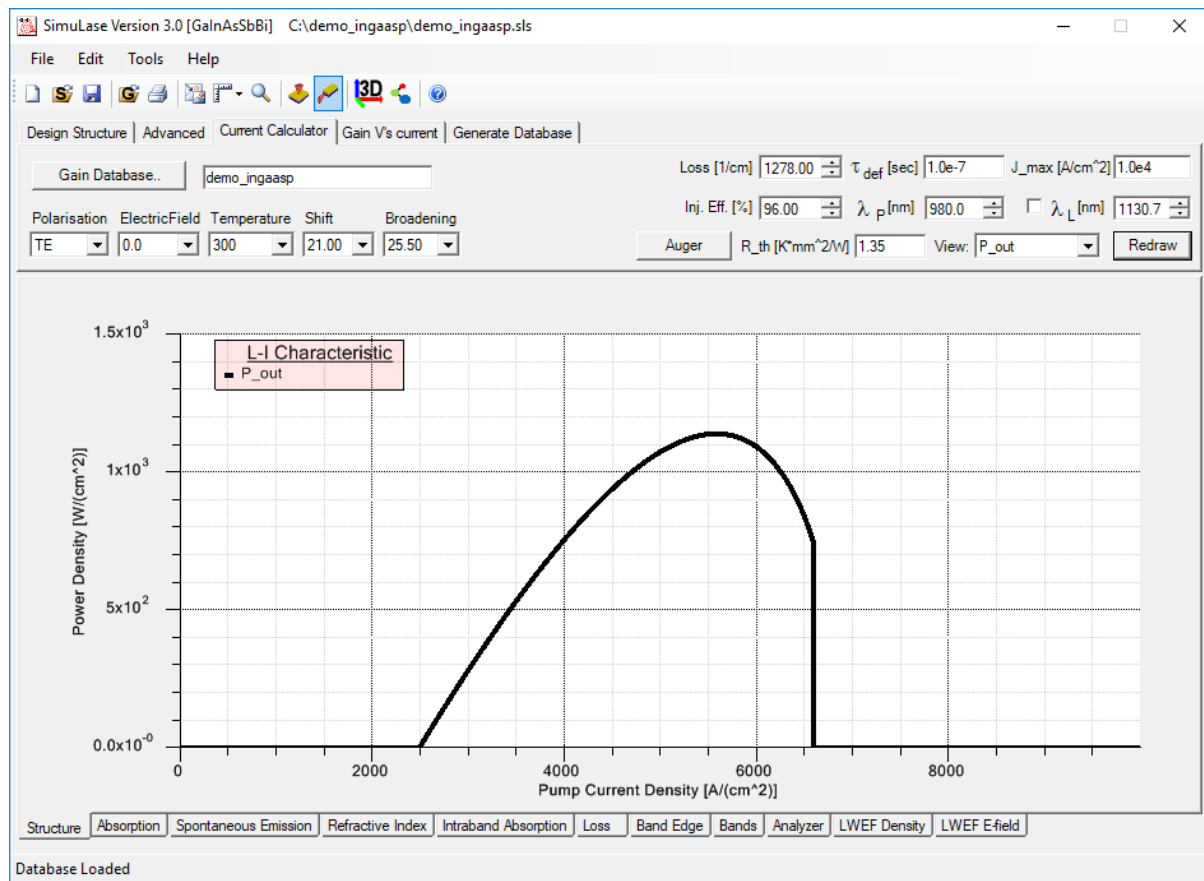


Figure 2.14: Current Calculator tool displaying input-output characteristics.

Besides the input required also for the threshold calculations described above - database, structure, optical loss, defect recombination time and injection efficiency (η_{inj}), the calculations of the input-output characteristics require some additional input to model the internal heating.

Here, the heat sink temperature is given by the temperature set on the 'Advanced' panel. A maximum pump current for which the data shall be calculated has to set in the field ' \mathbf{J}_{max} '. The thermal impedance of the device has to be specified in the field ' \mathbf{R}_{th} '. A pump wavelength has to be set in the field ' λ_p '.

The operating characteristics are determined directly from the balance of powers, $P_{\text{pump}} = P_{\text{out}} + P_{\text{heat}} + P_{\text{rest}}$, where P_{heat} is the amount of pump power that is converted to heat and P_{rest} is power lost to spontaneous emission that leaves the device without contributing to heating. For each temperature in the database the intrinsic carrier density at lasing is determined by looking for the density for which the gain is high enough to lead to enough gain to compensate for the optical losses as specified in 'Loss'. If a fixed lasing wavelength has been specified in the field λ_L , the gain has to be high enough at this wavelength. Otherwise, the gain maximum selects the lasing wavelength.

Then, the spontaneous emission, Auger and defect losses are calculated for this density. It is assumed that all these losses contribute to heating except for a fraction of the spontaneous emission that escapes the device. The results usually do not depend significantly on this fraction. We currently assume that 50% of the spontaneous emission escapes in all cases.

For each pump power, P_{pump} , additional heating losses are given by the amount of carriers that are not captured in the well, $P_{\text{pump}}(1 - \eta_{inj})$, and the quantum defect, P_{qd} , i.e. the difference between pump energy and lasing energy.

The intrinsic temperature increase due to this heating power, ΔT_{heat} is calculated using:

$$\Delta T_{\text{heat}} = P_{\text{heat}} R_{\text{th}}. \quad (2.3)$$

Finally, the operating point is determined by interpolating between the data for the fixed temperatures of the database in order to look up the temperature, T for which the heating losses lead to a temperature increase satisfying $T = T_{\text{HS}} + \Delta T_{\text{heat}}$. Here T_{HS} is the heat sink temperature. If such a temperature exists for a given pump power the device will lase with non-zero output power.

This model works for optically pumped devices. In electrically pumped devices there is of course no well defined pump wavelength. Carriers will also lose part of their energy to relaxation from the barrier into the wells, but the total energy loss depends on the positions of the Fermi levels, dopant levels and overall band bending due to space charges and applied Voltages - all of which are pump current dependent. Joule heating and Thomson-Peltier heating are not taken into account. Thus, this model is not an exact tool for this situation. It should merely be seen as a help to estimate overall trends in the performance like their variation with optical losses, number of wells or heating as varied with the parameter λ_L .

The following data can be displayed through the '**View**' pull-down menu:

P_out: Input-output characteristic.

P_loss: Various power losses:

P_SE: Spontaneous emission loss

P_aug: Auger loss

P_def: Defect recombination loss

P_qd: Quantum defect

P_inj: Injection loss

Lasing WL: Lasing wavelength

T_int: Internal temperature

N_{int}: Internal carrier density
IQE: Internal quantum efficiency

2.4.2 Gain vs. Current Tool

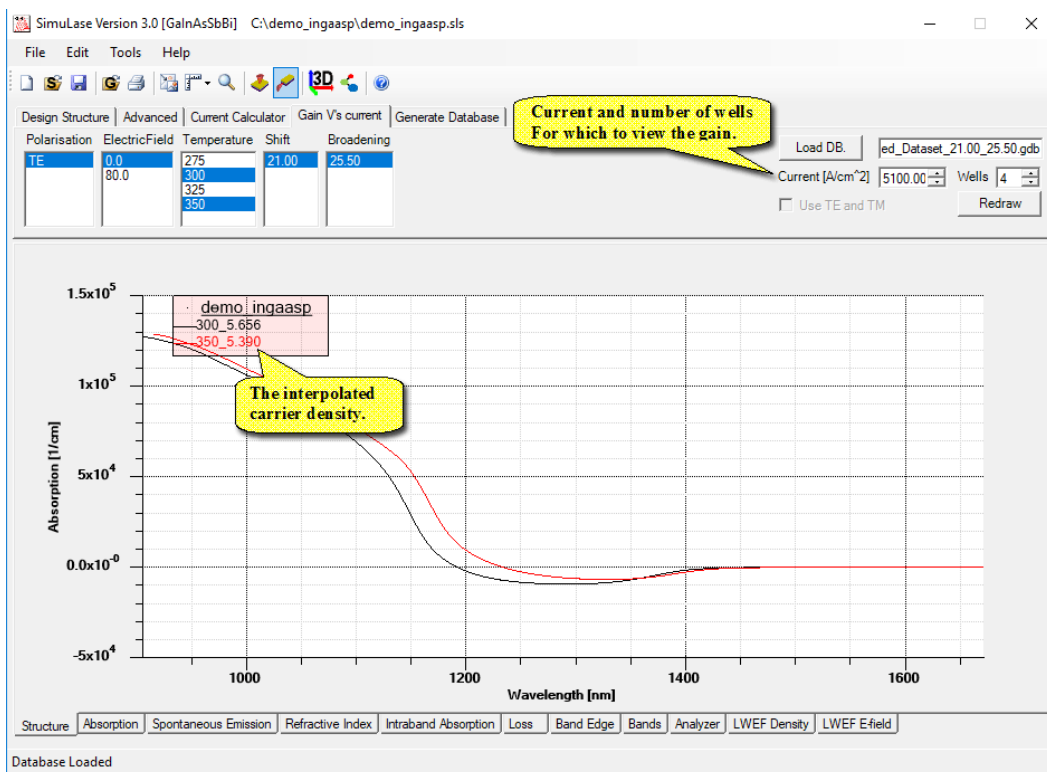



Figure 2.15: Gain vs. Current tool.

The '**Gain vs. Current**' tool allows to investigate the absorption/gain for a specific current. This tool helps e.g. to see how the gain for a fixed pump-current changes with temperature.

Databases are loaded using '**Load DB**' the gain vs. current tool may be activated by selecting '**Tools | Gain V's Current**' from the menu bar. After selecting a parameter set the user may view plots of the gain (absorption) as function of the loss current and the number of wells.

The '**Current**' is the assumed intrinsic loss current density solely due to radiative and Auger losses as included in the Gain Database and the 'Auger' panel, respectively. The corresponding currents are shown in the Current Calculator tool described above. As in that tool, the '**Number of Wells**' is the number of repeats of the active structure for which the Gain Database has been set up. The '**Current**' is divided by this number in order to obtain the current density corresponding to the loss values as included in the Gain Database. The displayed spectra are the ones as interpolated from the Gain Database, properly rescaled according to this number of repeats - assuming that the optical confinement factor scales linearly with the number of repeats. If the box '**Combine TE TM losses**' is checked, the radiative loss current is calculated by combining the TE and TM loss currents using $J_{rad} = 2/3 J_{TE,rad} + 1/3 J_{TM,rad}$. Otherwise, $J_{rad} = J_{TE,rad}$ and/or $J_{rad} = J_{TM,rad}$ is used depending on which polarization(s) has been chosen through the selector field '**Polarization**'.

2.5 Tools for Top-Emitters

SimuLase™ offers some tools that are most useful for analyzing top emitting structures. They can be accessed by clicking on the icon  in the top panel.

2.5.1 Reflection-Transmission

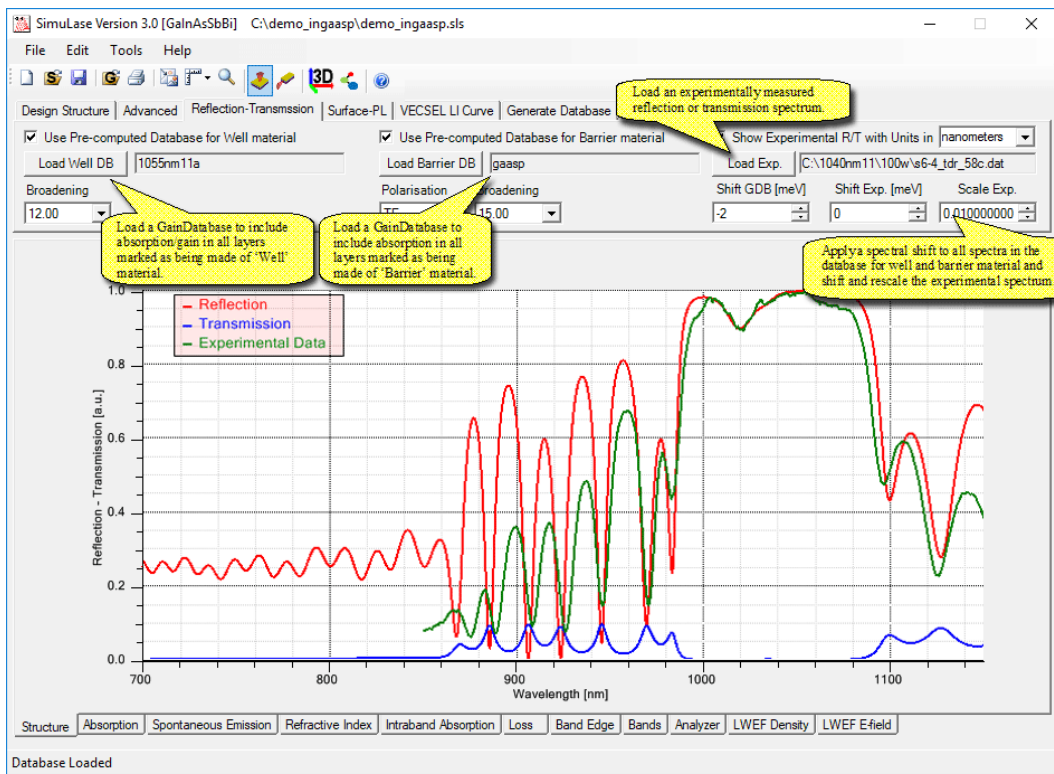


Figure 2.16: 'Reflection-Transmission' panel for an example of a VECSEL operating at 1040 nm . The structure has a thin metallization layer on the back which reduces the transmission to a low level.

The 'Reflection-Transmission'-tool allows to import GainDatabase data for the absorption/gain and carrier induced refractive index change for the calculation of the longitudinal (propagating) mode as well as the reflection and transmission spectra. It also allows to import experimentally measured reflection or transmission spectra and compare them to the theoretical results. This tool is particularly helpful for designing vertically emitting devices like VECSELs (see Sec.5.2 for a detailed example).

If a database is loaded for the wells or barriers, absorption/gain is added as imaginary part to the refractive index of the corresponding layers which are identified by selecting the corresponding option 'Type' on the 'Design Structure' panel. The carrier induced refractive index changes are added to the real part of the refractive index. For the absorption/gain in the well layers the carrier density and temperature are set on the 'Advanced'-options panel. Since the barrier layers are usually much wider than the wells, the corresponding carrier densities are usually very small. Thus, for the barrier layers the absorption for the lowest carrier density in the corresponding

GainDatabase is used. For this density the carrier induced refractive index change is assumed to be zero.

The tool also allows to shift all spectra in the GainDatabase by a certain amount. This allows to quickly account for small deviations between the nominal structural layout that has been assumed when setting up the well-GainDatabase and actually grown structures without having to re-calculate the database. The experimentally measured data can be rescaled and shifted in order to find a fit to the theory.

2.5.2 Surface-PL

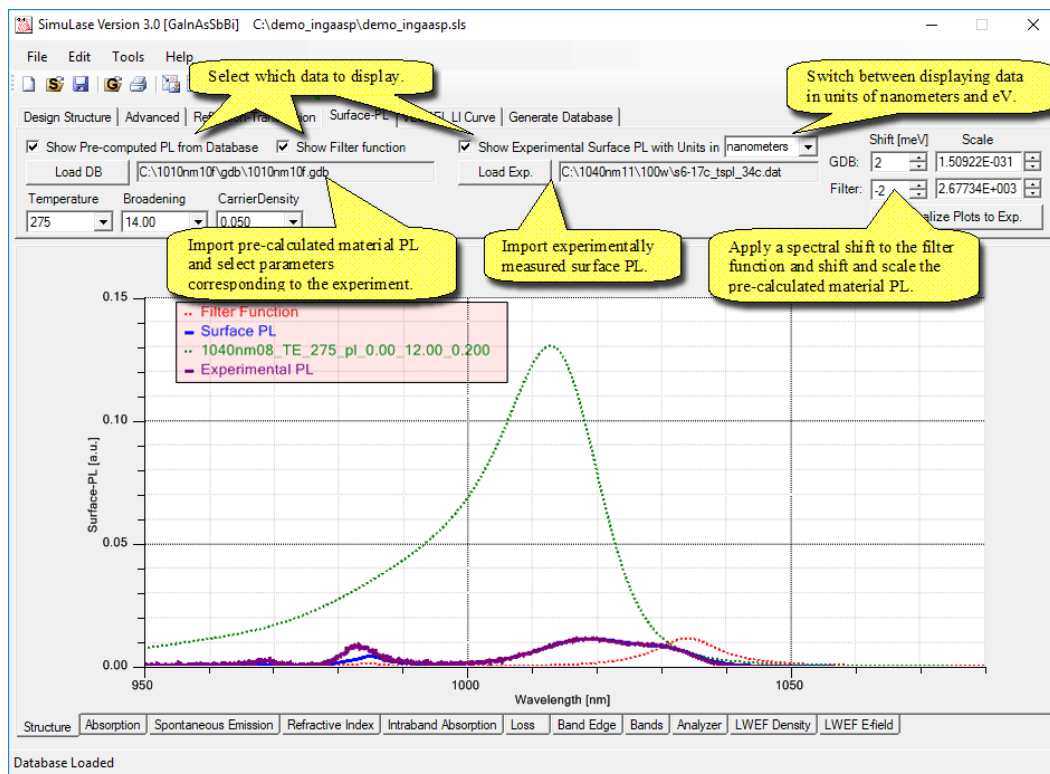


Figure 2.17: 'Surface-PL' panel for an example of a VECSEL operating at 1040 nm.

The 'Surface-PL'-tool allows to calculate the PL that is emitted vertically from the surface of a structure and to compare it to experimentally measured data. The surface-PL is calculated using the filter function approach where it is given by the product of the pure material PL as it is contained in the GainDatabases and a filter function that describes the modifications of the PL on its way from the well(s) to the surface due to reflections and interferences at the layer interfaces. Especially in V(E)CSELs, these modifications can be very significant and lead to significant changes from the pure material PL that would be measured in the absence of the interfaces or from the edge of the device.

The filter function is calculated for the structure that is currently set up in the 'Design Structure' tool and is updated whenever changes are made to the structure. It is calculated for the temperature and carrier density as specified on the 'Advanced' panel. The experimental PL has to be provided in two column ASCII data files where the first column gives the transition energy in [eV] or the wavelength in [nm] and the second column is the measured PL in arbitrary units.

The material PL from the GainDatabase and the filter function can be shifted and the material PL can be rescaled in order to find a best fit between theory and experiment.

2.5.3 VECSEL LI Curve

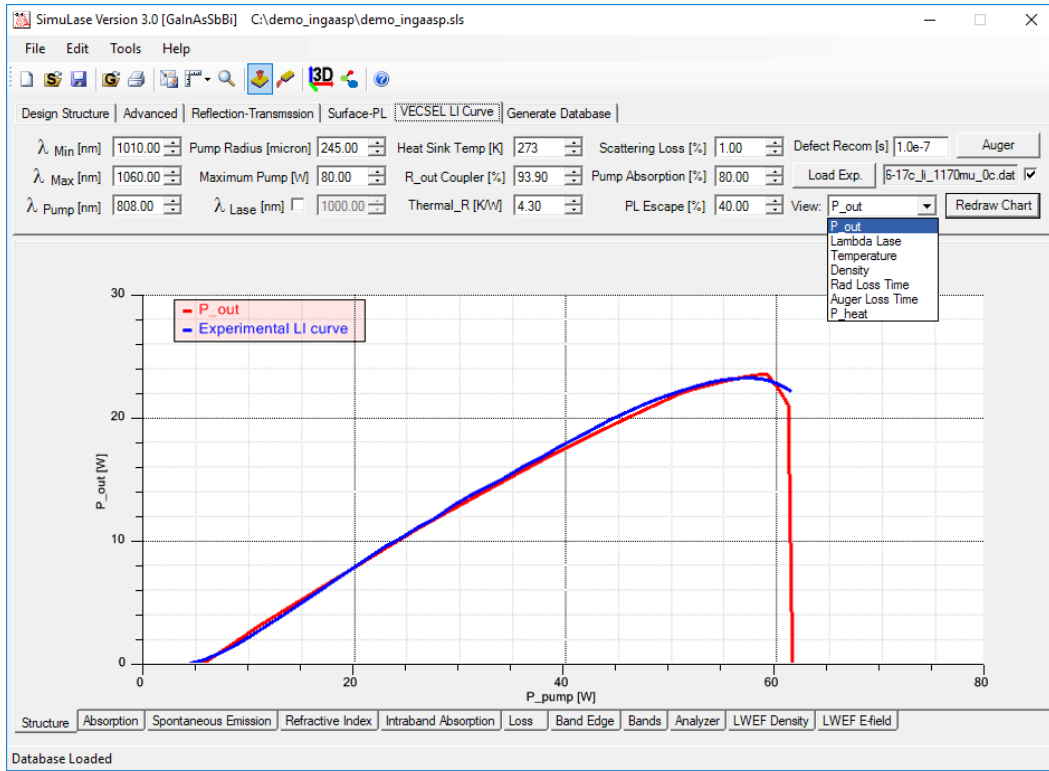


Figure 2.18: Overview of the 'VECSEL LI Curve' panel with a set up for the example of an VECSEL for 1040nm that is discussed in Sec.5.2.

The 'VECSEL LI Curve'-tool allows to calculate the operating characteristics of V(E)CSELs. Based on a one-dimensional rate equation model it calculates the input-output power characteristics and other essential characteristics like lasing wavelengths and intrinsic temperatures.

The calculations are done for the structure currently present in the 'Design Structure' window. They require a GainDatabase for the quantum wells of the structure. This has to be loaded through the corresponding option on the 'Reflection-Transmission'-panel. The database for the barriers is not taken into account even if one is loaded through the same panel. The choices for the polarization, inhomogeneous broadening and the shift of the database ('Shift GDB') are also taken over from the Reflection-Transmission panel.

Although the calculation time is only a few seconds, it can be reduced further by changing the values for $\lambda_{Min,Max}$ from their default settings in order to reduce the spectral range that is taken into account in the calculation. The lasing wavelength can be fixed using the option λ_{Lase} in order to simulate devices in which the lasing wavelength is kept pump-independent using, e.g., an etalon in the external cavity.

Heating is simulated using a thermal conductivity ('Thermal_R'). Incomplete pump absorption is taken into account through the variable 'Pump Absorption' that specifies what fraction of the

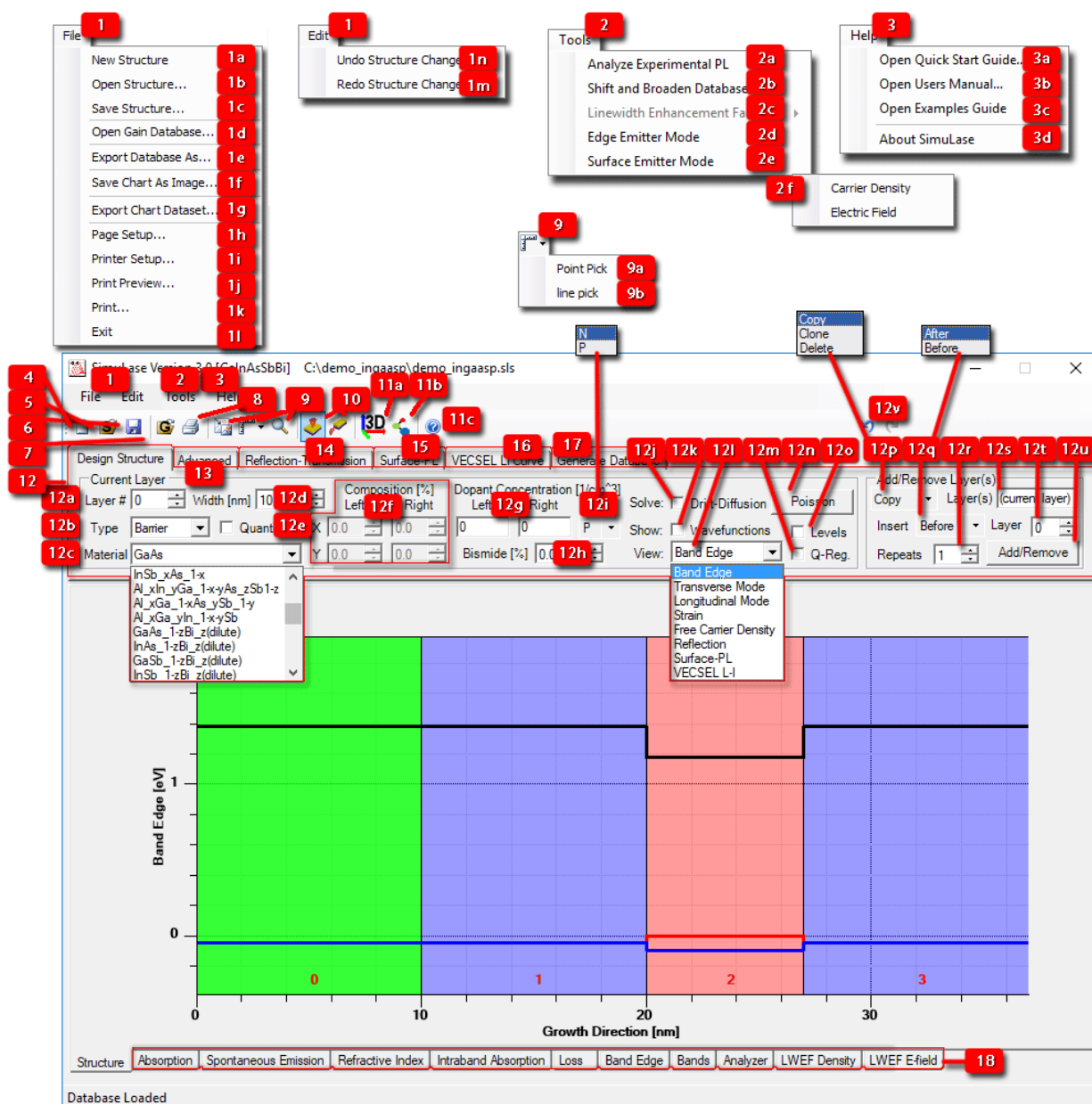
pump is absorbed in the active region. It is assumed that the rest of the pump energy goes into heating of the device. The variable 'PL Escape' specifies the percentage of spontaneous emission emitted from the active region that is not absorbed in un-pumped regions outside the pump spot but escapes the device. It is assumed that the fraction of the spontaneous emission that does not escape is re-absorbed and contributes to heating. In general, the correct value for this parameter has to be calculated using ray-tracing software or a comparable model. However, the results are typically not very sensitive to this parameter. The maximum output power changes about 10% when varying this parameter between zero and 100%. The influence on the threshold or slope efficiency is even less.

Experimental data can be imported into the plots. The data has to be in two column ASCII format with the first column giving the net pump power in [W] and the second one giving e.g. the output power in [W] or lasing wavelength in [nm].

3 Basic Functionality

This chapter gives an overview over the basic functionality of **SimuLase™**. It describes the various panels, charts and options it offers.


3.1 Main Menu




The main menu, [1-11], can be reached from all points of **SimuLase™**. It allows to load GainDatabases (*.gdb-files), export GainDatabases in a format that can be imported by other

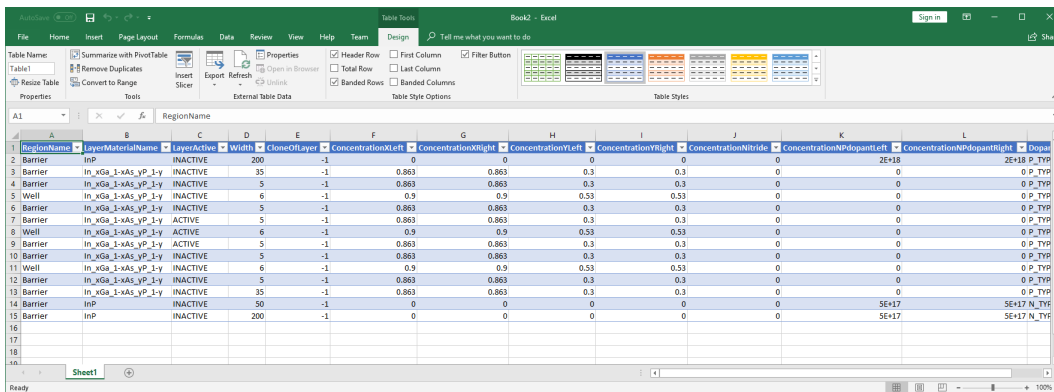
software, open and save structures (*.sls-files), save or print chart-windows, export data, start various tools and access help manuals.

[1] File and Edit Menus

[1a] New Structure: opens the **Design Structure**-window in the default setting to create a new structure. **[4]** (icon: ) provides a shortcut for this.

[1b] Open Structure: opens a File Manager to load an existing structure.

[1c] Save Structure: opens a File Manager to save all information about a structure. **[6]** (icon: ) provides a shortcut for this.) The structural information is saved in xlm-format in an *.sls file which can be read externally using, e.g., Microsoft Excel.

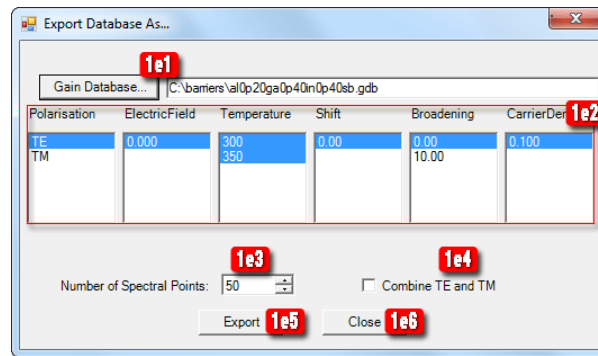


RegionName	LayerMaterialName	LayerActive	Width	CloseOffLayer	ConcentrationXLeft	ConcentrationXRight	ConcentrationYLeft	ConcentrationYRight	ConcentrationNitride	ConcentrationNpDopantLeft	ConcentrationNpDopantRight	Dopant
2	IMP	INACTIVE	200	-1	0	0	0	0	0	2E+18	2E+18	P_TYP
3	Barrier	IN_xGa_1-xAs_vp_1-y	35	-1	0.863	0.863	0.3	0.3	0	0	0	0 P_TYP
4	Barrier	IN_xGa_1-xAs_vp_1-y	5	-1	0.863	0.863	0.3	0.3	0	0	0	0 P_TYP
5	Well	IN_xGa_1-xAs_vp_1-y	6	-1	0.9	0.9	0.53	0.53	0	0	0	0 P_TYP
6	Barrier	IN_xGa_1-xAs_vp_1-y	5	-1	0.863	0.863	0.3	0.3	0	0	0	0 P_TYP
7	Barrier	IN_xGa_1-xAs_vp_1-y	5	-1	0.863	0.863	0.3	0.3	0	0	0	0 P_TYP
8	Well	IN_xGa_1-xAs_vp_1-y	6	-1	0.9	0.9	0.53	0.53	0	0	0	0 P_TYP
9	Barrier	IN_xGa_1-xAs_vp_1-y	5	-1	0.863	0.863	0.3	0.3	0	0	0	0 P_TYP
10	Barrier	IN_xGa_1-xAs_vp_1-y	5	-1	0.863	0.863	0.3	0.3	0	0	0	0 P_TYP
11	Well	IN_xGa_1-xAs_vp_1-y	6	-1	0.9	0.9	0.53	0.53	0	0	0	0 P_TYP
12	Barrier	IN_xGa_1-xAs_vp_1-y	5	-1	0.863	0.863	0.3	0.3	0	0	0	0 P_TYP
13	Barrier	IN_xGa_1-xAs_vp_1-y	35	-1	0.863	0.863	0.3	0.3	0	0	0	0 P_TYP
14	Barrier	IMP	50	-1	0	0	0	0	0	5E+17	5E+17	N_TYP
15	Barrier	IMP	200	-1	0	0	0	0	0	5E+17	5E+17	N_TYP

Figure 3.1: Structure file, *.sls, in Windows Excel.

[1d] Open Gain Database: opens a File Manager to open a GainDatabase (*.gdb) file. **[5]** (icon: ) provides a shortcut for this.






[1e] Export Database as: currently allows to create a reduced version of an existing GainDatabase or to export the GainDatabase in a format that allows to import the data into Crosslight Inc.'s simulation software **Lastip™**.















[1e1] Gain Database: opens a File Manager to load the GainDatabase that shall be exported. Select the corresponding *.gdb-file.

[1e2] Polarization...: select the subset of the GainDatabase data that shall be exported by highlighting the entries of the displayed contents. If a reduced GainDatabase is created only exactly those entries will constitute the new database. If the data is exported into Crosslight's data format, the data for the highest and lowest density and temperature are exported and data for as many equally spaced

densities and temperatures between them as contained in the original database are created by linear interpolation between the original data and exported.

- [1e3] **Number of Spectral Points:** allows to specify the number of spectral points that shall be used in the exported dataset for all spectral data. The data is calculated using linear interpolation. This can be used to reduce the memory size of the exported dataset.
- [1e4] **Combine TE and TM:** if this option is checked the carrier losses due to spontaneous emission into TE and TM modes are combined to an overall loss according to Eq.(7.9). Otherwise only the loss time due to the polarization as selected in [1e2] is used in the exported database.
- [1e5] **Export:** opens a File Manager that allows to select a name and destination for the exported database. The option '**Save as type**' in this file manager allows to specify whether the database is going to be a reduced SimuLase-style GainDatabase or for use in Crosslight's software.
- [1e6] **Close:** abandons the export process.
- [1f] **Save Chart As Image:** opens a File Manager to save the currently displayed plot in various picture formats (*.bnp, *.png, *.gif, etc.). Type in the file name with the extension for the desired format. If no extension is added, the default format, *.bnp, will be used.
- [1g] **Export Chart Dataset:** opens a dialog that allows to export currently displayed data into ASCII-formatted files.
- [1h] **Page Setup:** opens a dialog to set the page format and margins for a print of the currently displayed plot and select a printer.
- [1i] **Printer Setup:** opens a dialog to setup your printer.
- [1j] **Print Preview:** opens a preview of a print of the current plot.
- [1k] **Print:** sends the current plot to the printer. [7] (icon: ) provides a shortcut for this.
- [1l] **Exit:** Closes SimuLase™ .
- [1m] **Undo Structure Change:** like [12v], , un-does a change to the structure done with one of the options from the 'Add/Remove Layer(s)' panel, [12p]-[12u].
- [1n] **Redo Structure Change:** like [12v], , re-does a change to the structure done with one of the options from the 'Add/Remove Layer(s)' panel, [12p]-[12u].
- [2] **Tools Menu**
 - [2a] **Analyze Experimental PL:** opens the **PL Analyzer** tool that makes automated comparisons between theoretical and experimental PL spectra to determine spectral mismatches and inhomogeneous broadenings.
 - [2b] **Shift and Broaden Database:** opens a dialog to create a copy of a GainDatabase that is inhomogeneously broadened and/or spectrally shifted.
 - [2c] **Linewidth Enhancement Factor:** a tool that calculates and displays the linewidth enhancement factor for a given carrier density or a change in the electric field across the active region.
 - [2d] **Edge Emitter Mode:** opens a set of tools that are particularly useful for edge-emitting devices. The tools will appear as additional tabs on top of the plot window. This can also be accessed by clicking the icon .
 - [2e] **Surface Emitter Mode:** opens a set of tools that are particularly useful for top-(surface-) emitting devices. The tools will appear as additional tabs on top of the plot window. This can also be accessed by clicking the icon .

- [2f] **Linewidth Enhancement Factor:** a tool that calculates and displays the linewidth enhancement factor for a given carrier density or a change in the electric field across the active region.
- [3] **Help Menu**
- [3a] **Open Quick Start Guide:** opens a pdf-file with a short description of the basic functionality of **SimuLase™**. [11] (icon: ) provides a shortcut for this.
- [3b] **Open Users Manual** opens this Users Manual as a pdf-file.
- [3c] **Open Examples Guide** opens a pdf-file that describes typical examples for the use of **SimuLase™**.
- [3d] **About SimuLase 1.0:** displays information about the Version of the program.
- [4] , **Create New Structure:** like [1a]; opens the **Design Structure**-window in the default setting to create a new structure
- [5] , **Open Current Structure:** opens a File Manager to load all information about a structure from a '.sls'-file.
- [6] , **Save Current Structure:** opens a File Manager to save all information about a structure in a '.sls'-file.
- [7] , **Open Gain Database:** opens a File Manager to load an existing GainDatabase.
- [8] , **Print Current Chart:** like [1j]; sends the current plot window to the printer.
- [9] **Chart Manipulation Tools:**
- , **Edit Chart Elements:** activates the option to move plot legend boxes by left-clicking on them and holding the mouse button down.
- , **Pick Info Mode:** allows to determine exact data values from plots using either:
- [9a] **Point Pick:** after selecting this option left-clicking on the plot will display the nearest x- and y-data value(s).
- [9b] **Line Pick:** after selecting this option left-clicking on the plot will display a vertical line through the data at the respective x-point and all y-data values along this line.
- , **Chart Zoom:** activates the option to zoom into the plot by right clicking and holding the mouse bottom down to select a rectangular area that will fill the plot window after releasing the mouse button. Right clicking on the plot and selecting **UnZoom Chart** reverses this and/or consecutive zooms.
- [10] **Top/Edge Emitting Mode:** selecting either of this activates additional tools that are particular relevant for evaluating data for top- (surface-) emitting and edge-emitting devices, respectively.
- , opens a set of tools that are particularly useful for surface- (top-) emitting devices. The tools will appear as additional tabs on top of the plot window. This can also be accessed through the **Tools Menu** [2e].
- , opens a set of tools that are particularly useful for edge-emitting devices. The tools will appear as additional tabs on top of the plot window. This can also be accessed through the **Tools Menu**, [2d].
- [11a] , **3D Plotting:** opens and closes the GUI that allows to display database content using 3D surface plotting.
- [11aa] **Export Chart Image:** opens a dialog that allows to export the current surface plot as a image of various formats and sizes.
- [11ab] **Print, Page Setup** open dialogs that allow to print the current plot in various formats.
- [11ac] **Nudge, Zoom, Rotate,...** enable various ways to manipulate the plots.

- [11ad] **Data Selection:** determines which data shall be plotted. The y-axis is selected by choosing two or more entries from any field that has two or more entries.
- [11ae] **Load GainDB:** opens a file browser that allows to import a gain database by selecting the corresponding *.sls file.
- [11af] **Plot Surface:** allows to select between displaying the (material) 'Absorption', the (carrier induced) 'Refractive Index' (change), or the 'Photo-luminescence'.
- [11ag] **Plot Cross Section:** allows to make cuts through the surface along various directions. The cut can be moved by dragging the blue points with the mouse. The data along the crosssection is plotted as a 2D-plot on the bottom of the plotting area [11ak].
- [11ah] **Use Log Scale:** allows to switch between a linear and a logarithmic z-axis.
- [11ai] **Use eV Scale:** allows to switch between [eV] and [nm] units for the x-axis.
- [11aj] **Redraw:** refreshes the plot.
- [11ak] **Cross Section:** Displays the cross section data as a 2D plot.

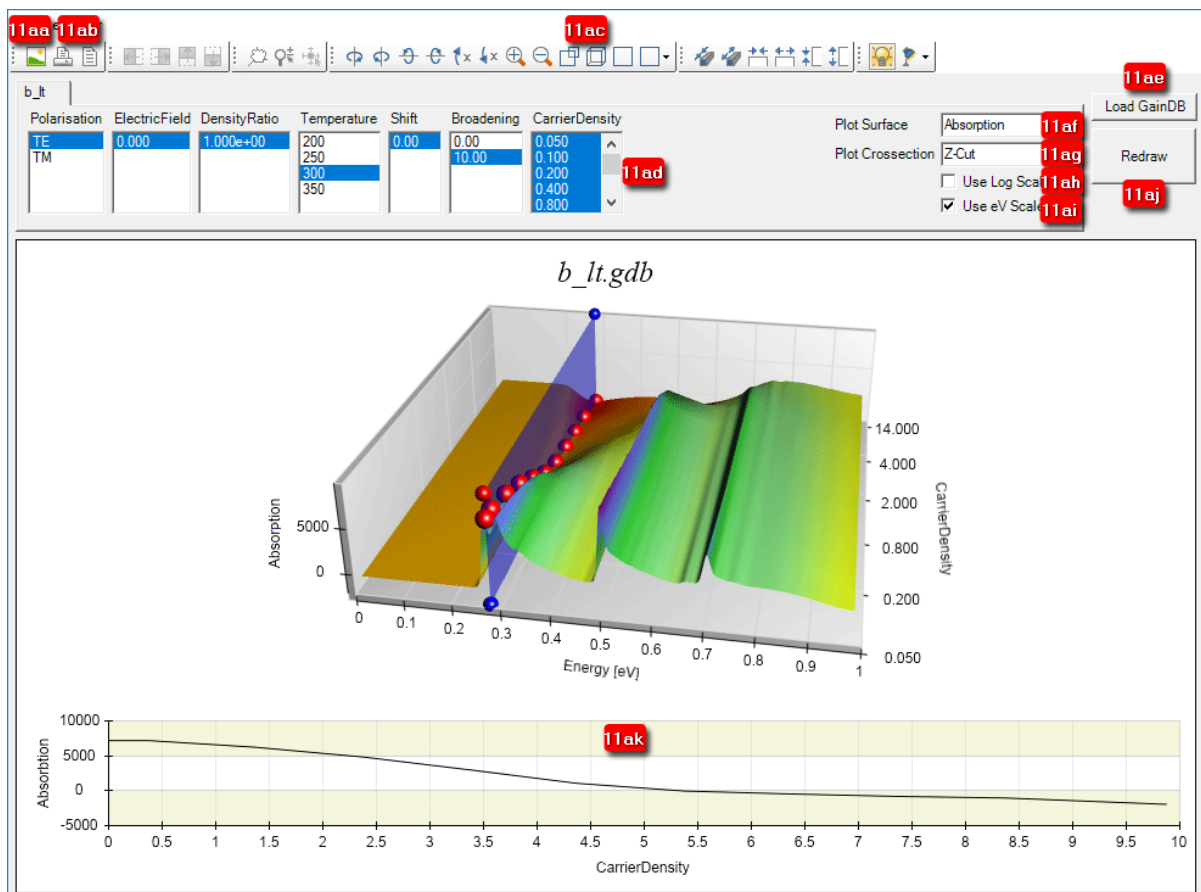



Figure 3.2: 3D database plotting tool.

- [11b]  **POSCAR Viewer:** opens and closes a GUI that allows to display the atom configuration of the supercell used in DFT calculations with the commercial software VASP. This is only included for special versions of **SimuLase™** that allow calculations based on DFT calculated energies and wavefunctions as calculated with VASP. This tool is only available in special versions of **SimuLase™** that allow to run its microscopic many-body calculations directly on the output of VASP DFT calculations.

- [11ba] **Export Chart Image:** opens a dialog that allows to export the current plot as a image of various formats and sizes.
- [11bb] **Print, Page Setup** open dialogs that allow to print the current plot in various formats.
- [11bc] **Nudge, Zoom, Rotate,...** enable various ways to manipulate the plot.
- [11bd] **Load POSCAR:** opens a file manager to select the POSCAR file containing the information about the atom configuration of the supercell used in the DFT calculation.
- [11be] **Show Bonds From:** allows to select the types of atoms for which atom-bonds shall be displayed.
- [11bf] **Bond Range [A]:** allows to set the maximum atom distance in Angstrom for which atomic bonds will be drawn.
- [11bg] **Atom scale [%]:** allows to vary the size of the symbols used for the atoms.

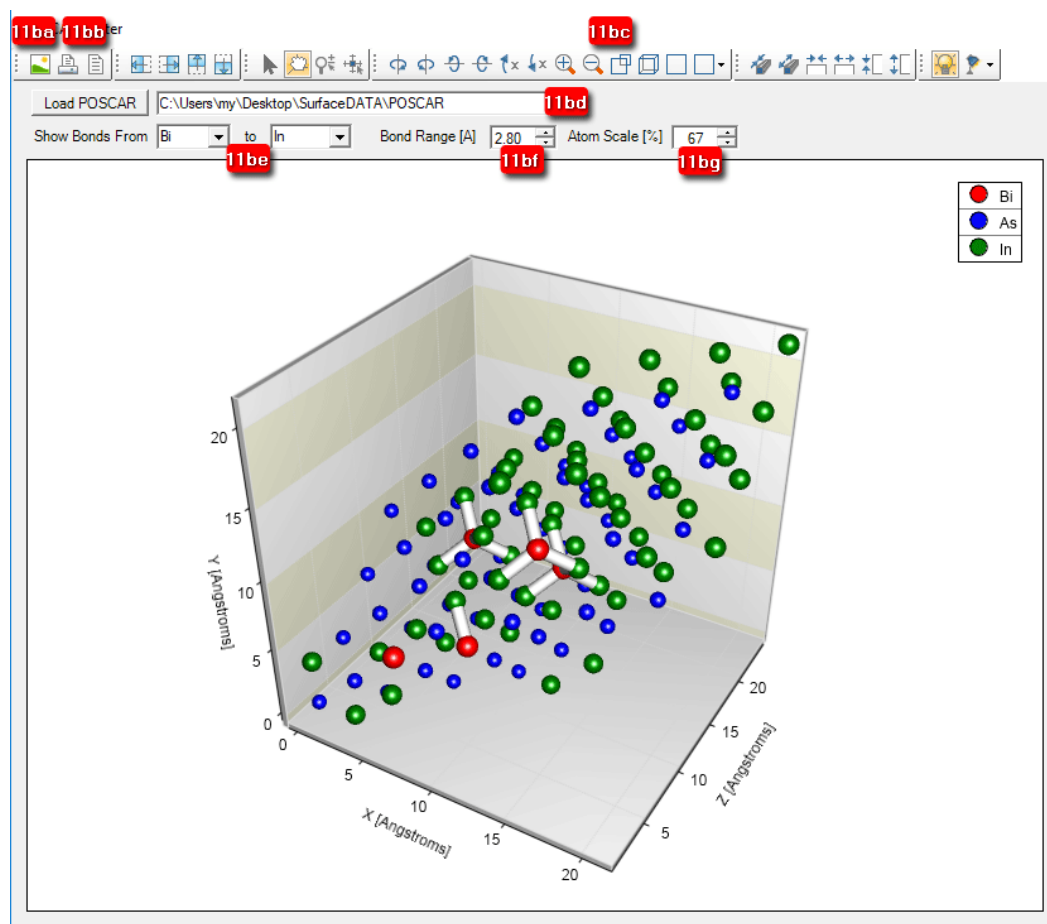


Figure 3.3: Tool that allows to plot the supercell used in DFT calculations with VASP software.

- [11c]  **Help:** like [3a]; opens the 'Quick Start Guide' pdf-file that explains the basic functionality of SimuLase™.

3.2 Design Structure

This Panel is used to set up the structure for which **SimuLaseTM** will calculate.

A '**Valid Structure**' must contain one - and only one - '**Quantized Region**' which is used for the microscopic calculation. Other layers may surround this region and will be used to calculate the optical mode and confinement factor and to solve the classical drift-diffusion problem for electrical potentials due to ionized dopants. The '**Quantized Region**' has to consist of consecutive layers which are marked as part of this region by the checkbox '**Quantized**', [12e]. This region has to contain at least one layer that is marked as a '**Well**'-layer through field [12b]. The region can contain quantum wells that are made of several '**Well**'-layers and can contain more than one well.

To modify numbers in any of the fields [12*] you can either use the scroll arrows or click on the field and use the wheel of the mouse or type in directly. Numbers typed into fields have to be confirmed by hitting the 'return' key.

For large numbers, like usually necessary for '**Dopant Concentration**', [12g], use the scientific notation '*A.AeB*' for ' $A.A \times 10^B$ '.

[12] Design Structure Window

[12a] **Layer #:** specifies the layer you are editing. The currently selected layer is highlighted in green in the plot window. Layer numbers can be displayed in the plot window by selecting option [13g] from the **Advanced** menu.

[12b] **Type:** specifies the functionality the layer serves within the structure. This information is required to determine the number of relevant subbands. It is also used for the calculation of reflection and transmission spectra. If a GainDatabase is loaded for wells or barriers through the 'Reflection-Transmission'-panel, the absorption/gain and carrier induced refractive index data is added to the background refractive index in all layers marked correspondingly as 'Well' or 'Barrier'.

Well: If the '**Automatic**' option is selected for the number of subbands used for the microscopic calculations ([17r]), the number of subbands is determined by searching the layer(s) in the '**Quantized Region**' marked '**Well**' for confined states. If a GainDatabase is loaded for the well material for the calculation of reflection and transmission spectra its data is added to the background refractive index in all layers marked 'Well'.

Barrier: If a GainDatabase is loaded for the barrier material for the calculation of reflection and transmission spectra its data is added to the background refractive index in all layers marked 'Barrier'.

Cladding: Marks layers for which no GainDatabase data shall be taken into account in the calculation of the reflection and transmission, like e.g. non-absorbing *AlAs*-layers of a DBR in a VECSEL.

[12c] **Material:** selects the type of material for the currently selected layer. The material names can be displayed in the plot window by selecting option [13h] from the **Advanced** menu.

[12d] **Width [nm]:** sets the width (in nanometers) of the currently selected layer.

[12e] **Quantized:** if checked, the current layer will be included in the '**Quantized Region**' for which the microscopic calculation of wavefunctions, spectra, etc., is performed. A valid structure, for which the microscopic calculation can be performed, must contain at least one layer marked '**Quantized**'. A valid '**Quantized Region**' must contain at least one layer marked '**Well**' through field [12b]. A structure can contain only one '**Quantized Region**', i.e. all layers marked as '**Quantized**' must

be next to each other.

- [12f] Composition [%]:** material compositions x and y , in percent, for the current layer. Compositions can be selected as different at the left and right end of a layer to create a linearly varying potential.
- [12g] Dopant Concentration [$1/\text{cm}^3$]:** dopant concentration at the start and end of the layer in units of $1/\text{cm}^3$. A linearly varying dopant profile can be set by using different values on the left and right end of the layer. Use the scientific notation ' $A.AeB$ ' for ' $A.A \times 10^B$ '.
- [12h] Z/Nitrogen/Bismide/PZFS [%]:** For quinary materials a field allowing to set the additional composition ' z '. For dilute Nitrides like ' GaN_xAs_{1-x} (dilute)' or dilute Bismide materials like ' $InAs_{1-x}Bi_x$ (dilute)', a field to set the dilute material content. For wide bandgap Nitrides (AlInGaN), a field to scale all strain related internal fields (piezoelectric and spontaneous polarization) from their nominal literature values.
- [12i] Type:** sets the type of dopants in the current layer. Select '**N**' or '**P**' for donors or acceptors, respectively.
- [12j] Solve: Drift-Diffusion:** if checked, the classical carrier Poisson drift-diffusion problem is solved to determine potentials due to dopant related local charges. This is updated automatically whenever the structure is changed as long as the box remains checked. This usually only takes fractions of a second. If the solver cannot find a converging solution it returns an error window after a few tens of seconds of attempts.
- [12k] Show: Wavefunctions:** if checked, the quantum mechanical single particle Schrödinger equation is solved and the resulting confinement wavefunctions are displayed. The number of wavefunctions to be displayed can be set on the '**Advanced**' menu, field **[13e]**.
- [12l] View:**
- Band Edge:** if selected, the electron and hole confinement potentials and, if checked, wavefunctions and levels are displayed.
- Transverse Mode:** if selected, the transverse (confined) optical mode and confinement factor are calculated. Plot screen then switches from displaying the confinement potentials to a plot of the refractive index profile and the mode. The confinement factor is then displayed in a box on the graph. The '**Wavelength**' and '**Temperature**' for which the mode calculation is performed, as well as the number of '**Transverse Modes**' that shall be displayed has to be set on the '**Advanced**' panel, **[13d]**. If no confined mode is found a corresponding message will be displayed in the legend box and no mode is displayed.
- Longitudinal Mode:** if selected, the longitudinal (propagating) optical mode and confinement factor are calculated and displayed. The '**Wavelength**' and '**Temperature**' for which the mode calculation is performed has to be set on the '**Advanced**' panel.
- Far Field:** if selected, the far field for each transverse mode is displayed as a function of the angle. The full width at $1/e^2$ of the maximum amplitude is listed in the legend for each mode.
- Reflection:** if selected, the transmission and reflection spectra are displayed for the '**Temperature**' as set on the '**Advanced**' panel. Absorption/gain and refractive index changes can be taken into account for the calculation through the '**Reflection-Transmission**'-panel. Then, the data is added to the background refractive index assuming a carrier density in the wells as specified through the field '**Sheet Density**' on the '**Advanced**' panel.
- Surface-PL:** if selected, the PL as emitted to the surface of the device is displayed.

In structures with strong cavity effects, like V(E)CSELs, this can be significantly different than the pure material PL due to reflections and interferences of the PL at the layer interfaces on its way from the well(s) to the surface. If no GainDatabase containing the material PL for the structure has been imported through the '**Surface-PL**' panel, only the filter function that describes the modifications of the material PL due to cavity effects is calculated and displayed. The '**Surface-PL**' panel allows to import pre-calculated PL as well as experimental PL for comparison. The filter function and resulting surface-PL is calculated for the temperature as set on the '**Advanced**' panel and updated whenever the structure is modified.

[12m] View: **Q-Reg**: if checked, the plot window zooms from displaying the whole structure to displaying only the quantized region, i.e., layers marked as '**Quantized**' through field **[12e]**. After un-checking, the whole structure is displayed again.

[12n] Solve: **Poisson**: if clicked, the quantum mechanical Schrödinger-Poisson problem is solved for the '**Quantized Region**' to determine modifications of the confinement potential due to local charge inhomogeneities caused by free carriers in the quantized states. This can take a few seconds. The carrier density in the quantized region can be set through the field '**Sheet Density**', **[13b]**, on the '**Advanced**' panel .

[12o] Show: **Levels**: if checked, the energy levels of the lowest confined subbands are plotted. The number of levels to be displayed can be set on the '**Advanced**' panel, field **[13e]**.

[12p] Add/Remove Layer(s):

Copy: select this to copy one or more layers and insert them somewhere else as addition to the current structure. While the attributes 'well/barrier' will be transferred to the copies, the copies will not be part of the 'quantized region' unless they are manually marked to be part of it.

Clone: select this option to copy one or more layers and insert them as addition somewhere else. Unlike for option '**Copy**', all properties of the new layers are linked to the ones of the original layers. When modifying properties of the cloned layers, the corresponding properties of the original layers will be changed the same way, and vice versa. This is a helpful option when dealing with periodic structures like DBRs. While the attributes 'well/barrier' will be transferred to the clones, the clones will not be part of the 'quantized region' unless they are manually marked to be part of it.

Delete: select this option to delete one or more layers from the structure.

[12q] Insert: **After/Before**: select this option to insert copies or clones of the layers as specified by field **[12s]** **after/before** the layer as specified by field **[12t]**.

[12r] **Repeats**: specifies how many copies/clones of the layers as specified through field **[12s]** are to be inserted.

[12s] **Layer(s)**: specifies which layers to be copied, cloned or deleted. Replace the default text '**(current layer)**' by the number of the layer you wish to copy, clone or delete. For multiple layers insert the numbers of the layers separated by space ' ' or semicolons ','.

[12t] **Layer**: specifies the number of the layer after/before which new layers are to be inserted.

[12u] **Add/Remove**: hit this button to insert or delete layers. If a cloned layer is removed all other clones of the layer are removed as well.

[12v] **Undo/Redo**, : allow to undo or redo additions or removals of layers.

[13] **Advanced**: panel that allows to specify some parameters that influence the results as displayed in the '**Structure Layout**' window. The options/parameters as set on this

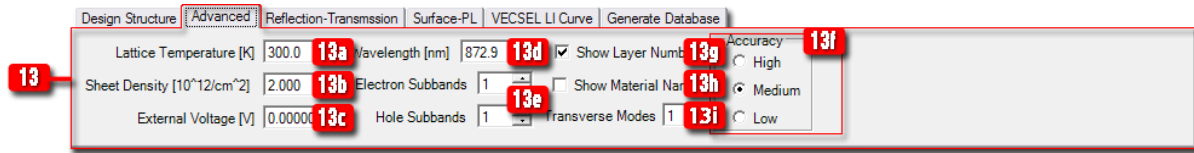


Figure 3.4: 'Advanced'-options panel of the 'Design Structure'-window.

panel are not used for the generation of Gain Databases. Vice versa, controls of panel 'Generate Database', [17*], are not used for the results displayed in the 'Structure Layout' window.

- [13a] **Lattice Temperature [K]:** temperature, in Kelvin, for which the confinement potentials, wavefunctions, etc., as displayed in the plot window are calculated. The same temperature is assumed to calculate the Fermi-distributions for carriers when solving the Schrödinger-Poisson problem ([12n]) and for the calculation of the modes, reflection and transmission spectra and the filter function for the surface-PL.
- [13b] **Sheet Density [$10^{12}/\text{cm}^2$]:** sheet carrier density, in units of [$10^{12}/\text{cm}^2$], that is assumed when solving the Schrödinger-Poisson problem ([12n]) or if a GainDatabase is included in the calculation of the longitudinal mode and reflection and transmission spectra. It is assumed that the carrier densities are the same for electrons and holes.
- [13c] **External Voltage [V]:** externally applied voltage in units of [Volts].
- [13d] **Wavelength [nm]:** operating wavelength, in nanometers, for which the optical modes and confinement factors are calculated. By default, reflection/transmission and surface-PL data is calculated for a spectral range of 100nm centered around this wavelength. To change the spectral range, right-click on the corresponding plots and select 'Format Chart'. The maximum value for this wavelength is limited by the minimum possible transition energy as determined from the confinement potentials. See Sec.7.1.2 for a discussion of the confinement factor calculation and how to set this wavelength.
- [13e] **Electron/Hole Subbands:** sets the number of electron and hole subband levels and wavefunctions that will be displayed in the plot window and that are used to solve the Schrödinger-Poisson problem ([12n]).
- [13f] **Accuracy:** allows to change the number of grid-points used for the calculation of the wavefunctions and levels. The calculation-time increases with the accuracy level which can become noticeable especially if the Poisson-Schrödinger problem shall be calculated. ([12n]).
- [13g] **Show Layer Numbers:** if checked, the layer numbers are plotted with the confinement potential.
- [13h] **Show Material Names:** if checked, for each layer the material type as specified through [12c] is plotted with the confinement potential.
- [13i] **Transverse Modes:** sets the number of transverse modes and corresponding far fields that shall be displayed. The maximum number is given by the number of confined modes in the specific structure.

3.3 Reflection-Transmission

To activate this panel the 'Surface Emitter Mode' has to be selected through the icon  from the main menu or through the 'Tools' menu.

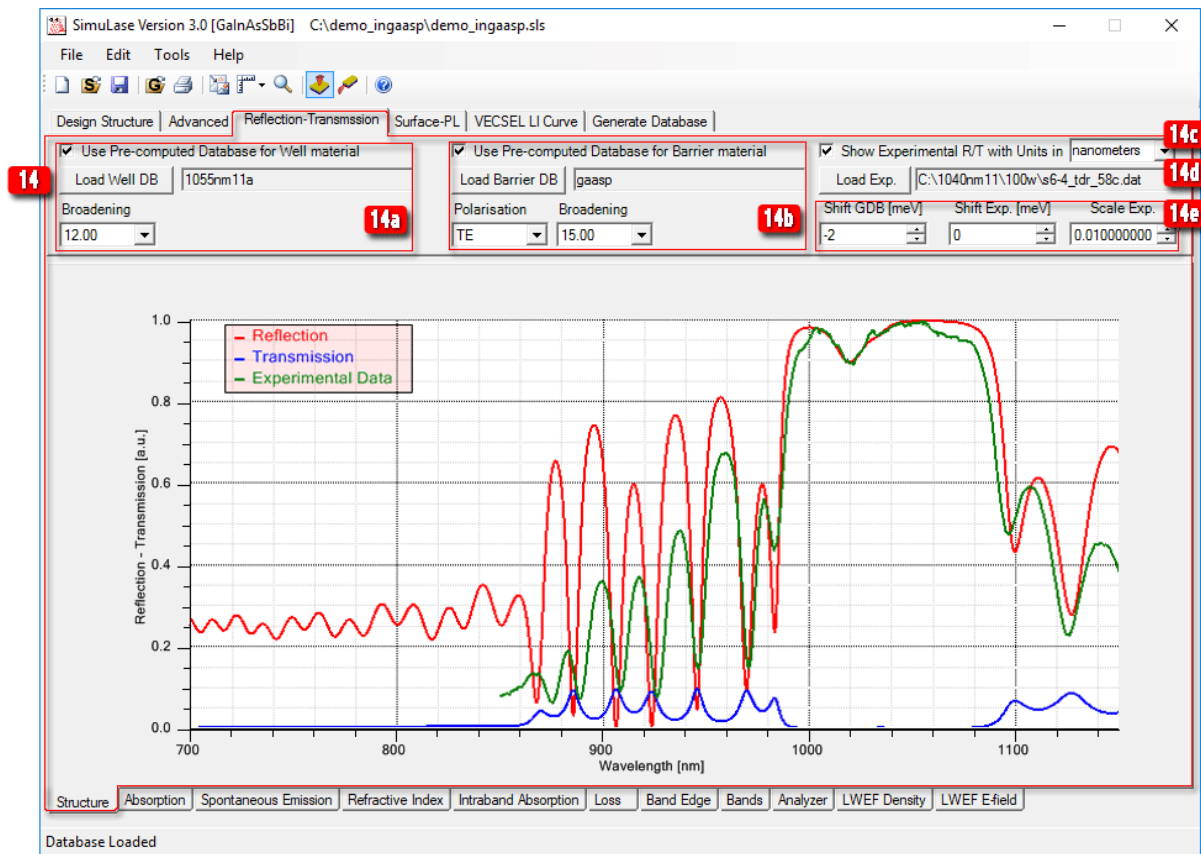


Figure 3.5: 'Reflection-Transmission'-panel for the example of the VECSEL that is discussed in Sec.5.2.

This panel allows to calculate the reflection and transmission spectrum for the structure as set up on the 'Design Structure' window, [12]. The temperature and carrier density assumed in the calculations are set through the fields 'Temperature' and 'Sheet Density', [13a] and [13b], also on the 'Advanced'-panel.

By default, reflection/transmission spectra are calculated for a spectral range of 100nm centered around the operating wavelength as specified on the 'Advanced'-panel[13d]. To change the spectral range, right-click on the corresponding plots and select 'Format Chart'.

This tool is most useful for VCSEL and OPSL devices. Sec.5.2 demonstrates a typical application for a VECSEL.

[14] Reflection-Transmission Window

[14a] Use Pre-Computed Database for Well Material: Allows to load a pre-computed GainDatabase for the quantum well layers. The absorption/gain for the temperature and carrier density as specified through the corresponding options on the 'Advanced'-panel, [13a] and [13b], is then added as imaginary part to the refractive index in all layers that are marked as being a 'Well' through the option 'Type', [12b] on the 'Design Structure' window. The carrier induced refractive index changes are added to the real part of the refractive index. If the database contains data for various polarizations and/or inhomogeneous broadenings, the relevant ones can be selected. The data for the specific temperature and density and wavelength is obtained through

linear interpolation from the data within the database. After loading the database, the absorption/gain is taken into account in the calculations as long as the checkbox is checked.

- [14b] Use Pre-Computed Database for Barrier Material:** Allows to load a pre-computed GainDatabase for the barrier layers. The absorption for the temperature and wavelength as specified through the corresponding option on the 'Advanced'-panel, [13a], is then added as imaginary part to the refractive index in all layers that are marked as being a 'Barrier' through the option 'Type', [12b] on the 'Design Structure' window. If the database contains data for various polarizations and/or inhomogeneous broadenings, the relevant ones can be selected. Assuming that the carrier densities in the barrier layers is very small, the absorption to the lowest carrier density in the database is used. The carrier induced refractive index change for this density is assumed to be zero. The data for the specific temperature and wavelength is obtained through linear interpolation from the data within the database. After loading the database, the absorption is taken into account in the calculations as long as the checkbox is checked.
- [14c] Show Experimental R/T with units in:** The checkbox on the left of this line allows to show or hide the experimental reflectivity. The x-axis for the experimental data can be changed from nanometers to eV using the selection tab at the right of this line.
- [14d] Load Exp.:** Opens a File-dialog to import experimentally measured reflection or transmission spectra. The data has to be in two-column ASCII files where the first column gives the transition energy in eV or the wavelength in nanometers and the second gives the spectrum.
- [14e] Shift GDB:** Allows to specify an energy by which all data in GainDatabases that have been loaded for well and/or barrier material through fields [14a] and [14b] is shifted and to shift and scale the experimental data in order to find a good fit.

3.4 Surface-PL

To activate this panel the 'Surface Emitter Mode' has to be selected through the icon  from the main menu or through the 'Tools' menu.

This panel allows to calculate the surface-PL for the structure as set up through the 'Design Structure' window, [12] and to compare the result to experimentally measured data. In structures with strong cavity effects, like V(E)CSEs, the PL emitted through the surface differs strongly from the pure material PL as it is calculated for the GainDatabases due to reflections at the layer interfaces on its way from the quantum wells to the surface.

In SimuLase™ the surface-PL is calculated using the 'Filter-Function-Approach' [2]. Here the surface-PL is given by the product of the pure material PL and the 'filter function' which describes the modifications due to cavity effects. The theoretical material PL has to be loaded from an existing GainDatabase. The filter function is calculated for the structure that is currently in the 'Design Structure' panel and updated whenever the structure is modified. The temperature assumed in the calculation of the filter function is set through the field 'Temperature' ([13a]) on the 'Advanced'-panel.

To display the surface-PL one has to select 'View: Surface-PL' on the 'Design Structure' panel ([12]). If no material PL or experimentally measured PL has been imported on the 'Surface-PL' panel, the panel displays only the filter function.

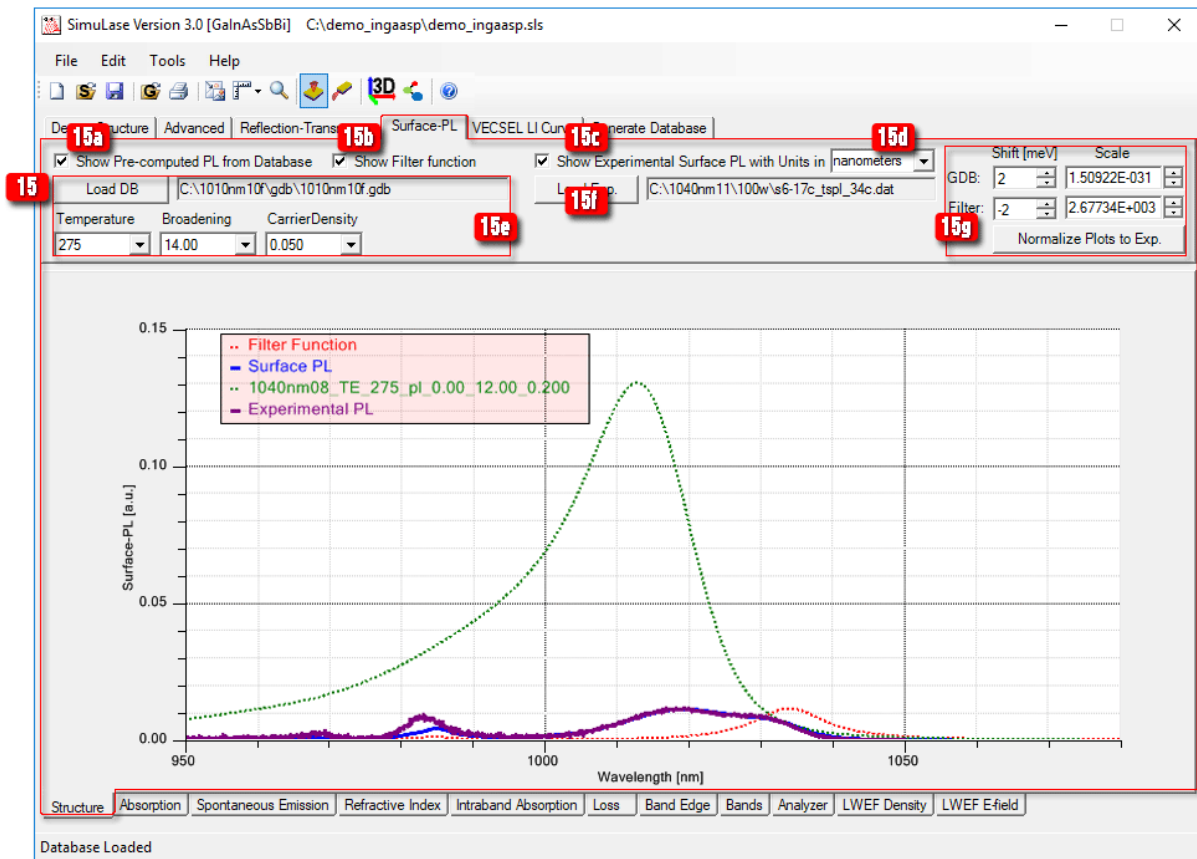


Figure 3.6: 'Surface-PL'-panel for the example of the VECSEL that is discussed in Sec.5.2.

By default, surface-PL spectra are calculated for a spectral range of 100nm centered around the operating wavelength as specified on the 'Advanced'-panel[13d]. To change the spectral range, right-click on the corresponding plots and select 'Format Chart'.

This tool is most useful for determining deviations between nominal design and actual growth of VCSEL and OPSL structures. Sec.5.2 demonstrates a typical application for a VECSEL.

[15] Surface-PL Window

[15a] **Show Pre-Computed PL from Database:** Checking this option shows or hides the pre-calculated material PL.

[15b] **Show Filter Function:** Checking this option shows or hides the filter function.

[15c] **Show Experimental Surface PL:** Checking this option shows or hides the experimental spectra.

[15d] **with Units in:** Allows to switch the units that are assumed for the experimental data from 'nanometers' to 'eV'.

[15e] **Load DB:** Allows to load a pre-calculated GainDatabase and select the parameters (Polarization, Temperature,...) for which the surface-PL shall be calculated.

[15f] **Load Exp.:** Opens a File-dialog to import experimentally measured surface-PL spectra. The data has to be in two-column ASCII files where the first column gives the transition energy in eV or the wavelength in nanometers and the second gives the spectrum in arbitrary units.

[15g] Shift/Scale GDB/Filter: Allows to specify energies by which the material PL and filter function are shifted and scalings to possibly improve the agreement between experiment and theory. This is a quick alternative to modifying the layer thicknesses of the structure in the 'Design Structure' window or to adjust the material PL for temperatures that are not contained in the GainDatabase.

Normalize all plots: Normalizes the maximum of the filter function, the theoretical surface PL and the experimental PL to one for easier comparisons. The scalings in the 'Scale'-boxes are adjusted accordingly. Please note that the pre-computed material PL cannot be scaled independently from the filter function and surface PL.

3.5 VECSEL LI Curve

To activate this panel the 'Surface Emitter Mode' has to be selected through the icon 

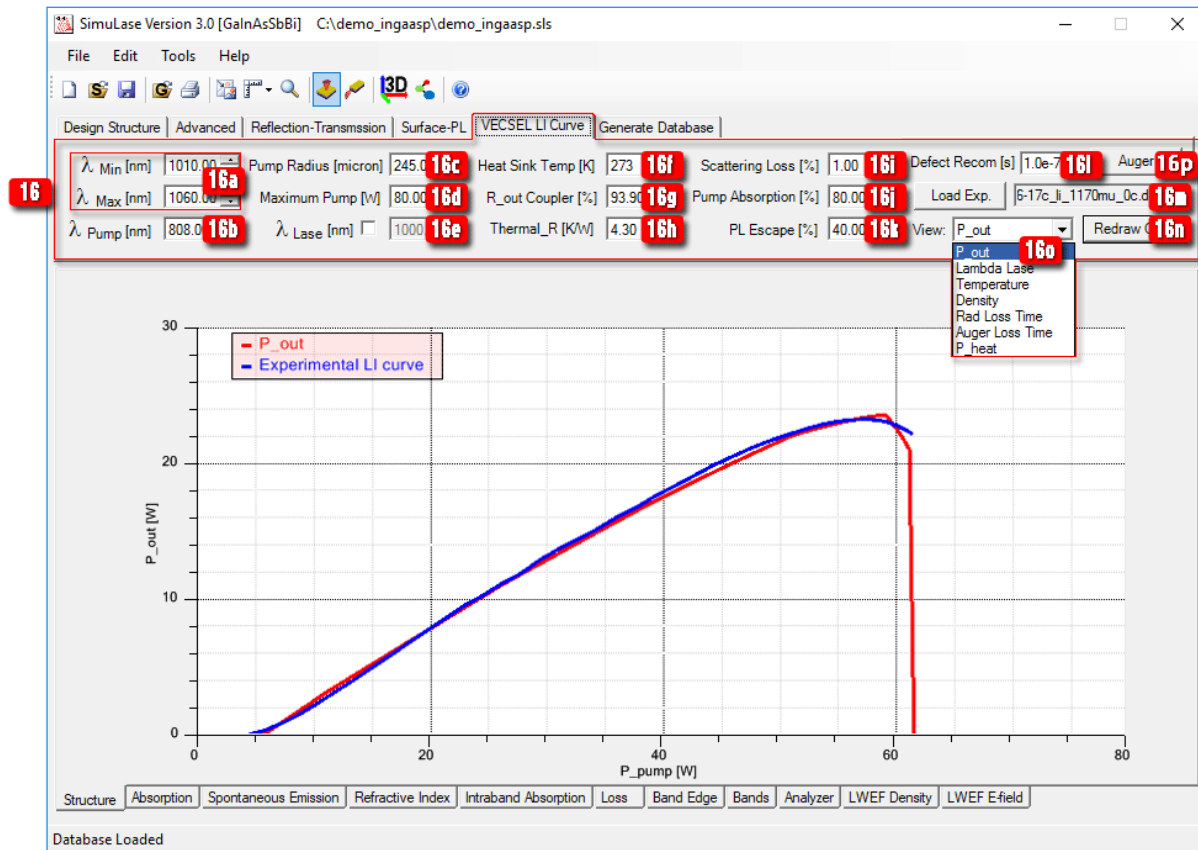


Figure 3.7: 'VECSEL LI Curve'-panel for the example of the VECSEL that is discussed in Sec.5.2.

from the main menu or through the 'Tools' menu.

This panel allows to calculate the operating characteristics for optically pumped VECSELs as discussed for a typical example in Sec.5.2. The calculations are done for the structure as currently set up in the 'Design Structure' window, [12]. The calculations require a GainDatabase for the quantum wells. This has to be loaded through the 'Load Well DB'-option on the 'Reflection-Transmission' panel, [14a]. The calculations are done for the same parameters, 'Polarization'

and 'Broadening' as set in [14a]. Also, the GainDatabase data is shifted as specified on that panel through option 'Shift GDB', [14e]. The GainDatabase for the barriers, [14b], is not taken into account in the calculations.

It is assumed that the GainDatabase is set up for one well, i.e., that the quantized region for which the GainDatabase was set up included only one of the layers marked as 'Well' through the option field 'Type' on the 'Design Structure' window, [12b]. The absorption/gain, refractive index changes and carrier losses from the GainDatabase are then applied to the imaginary and real part of the refractive index of all layers marked as 'Well'.

All results are plotted versus the net pump power in [W]. The 'net pump power' is the fraction of the total pump power that is not reflected at the air-interface and actually enters the device.

[16] VECSEL LI Curve Window

- [16a] λ_{Min} , λ_{Max} : Can be changed from their default values to speed up the calculation. They are the minimum and maximum of the wavelength range in which the lasing solution is looked for. If the actual lasing wavelength is outside this range no correct solution will be found. By default, these wavelengths are determined by the range covered within the GainDatabase. Reducing the range typically speeds up the calculation by about a factor of two.
- [16b] λ_{Pump} : Wavelength at which the device is pumped.
- [16c] **Pump Radius [micron]**: Radius of the pump spot in micron. A circular pump spot is assumed in the calculation.
- [16d] **Maximum Pump [W]**: Upper limit of the pump power for which the characteristics are calculated. The calculation time does not depend significantly on the range of pump powers.
- [16e] λ_{Lase} : Allows to set a fixed lasing wavelength for the case where the lasing wavelength is determined, e.g., by a wavelength selective intra-cavity etalon. If the checkbox is not checked, the lasing wavelength-variation with pump power is fully resolved.
- [16f] **Heat Sink Temp.:** Heat sink temperature in [K].
- [16g] **R.out Coupler:** Reflectivity of the external out-coupling mirror in [%].
- [16h] **Thermal_R:** Thermal impedance of the device in [K/W].
- [16i] **Scattering Loss:** Scattering loss in the external cavity due to surface scattering or losses due to intra-cavity elements like etalons or frequency doubling crystals (in [%]).
- [16j] **Pump Absorption:** Fraction of pump power, in [%], that is absorbed in the active region of the device. It is assumed that the rest of the pump power is absorbed somewhere else (e.g. the DBR) and contributes to heating.
- [16k] **PL Escape:** Percentage of spontaneous emission emitted from the pumped area that is not re-absorbed outside the pump area but escapes the device. It is assumed that the fraction of PL that is re-absorbed contributes to heating. This fraction can be calculated using ray-tracing software. An error in this number leads usually only to minor changes in the maximum output power of up to about 5-10%. Typically this number is about 40-50%.
- [16l] **Defect Recomb.:** Carrier recombination time for defect recombination processes in [sec].
- [16m] **Load Exp.:** Opens a File-dialog to import experimentally measured data. The data has to be in two-column ASCII files where the first column gives the net pump power in [W] and the second gives the data that shall be plotted against the theoretical data, like output-power [W] or lasing wavelength in [nm]. If the checkbox is un-checked the experimental data is not displayed.

- [16n] Redraw Chart:** Starts the calculation.
- [16o] View:** allows to select the data that shall be displayed.
- P_{out}:** output power [W].
- Lambda Lase:** lasing wavelength [nm].
- Temperature:** internal temperature of the active region [K].
- Density:** sheet carrier density in the wells [$10^{12}/\text{cm}^2$].
- Lambda Lase:** lasing wavelength [nm].
- Rad Loss Time:** carrier loss time due to spontaneous radiative recombination processes [ns].
- Auger Loss Time:** carrier loss time due to Auger recombination processes [ns].
- P_{heat}:** the amount of power that is converted to heat [W].
- [16p] Auger:** Opens/closes a sub-panel that allows to select between different Auger models and set the corresponding parameters. See Sec.7.1.6 for details on the models.

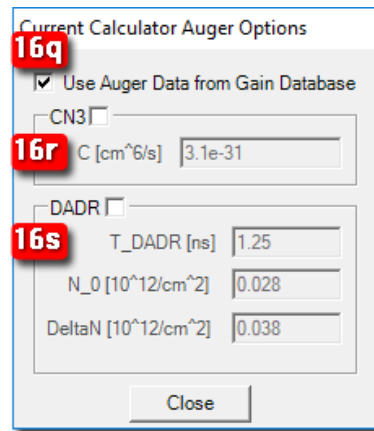


Figure 3.8: Sub-panel to switch between different models for Auger losses.

- [16q] Use Auger Data from Database:** If selected, microscopically calculated Auger losses included in the database are used.
- [16r] CN3:** If selected, the CN^3 model is used for Auger losses. The Auger coefficient, C has to be specified in [cm^6/s].
- [16s] DADR:** If selected, the density-activated defect recombination model is used. A DADR lifetime in [ns], a threshold density, N_0 , in [$10^{12}/\text{cm}^2$], and a density broadening, Δ_N , in [$10^{12}/\text{cm}^2$] have to be provided. .

3.6 Generate Database

This panel is used to create GainDatabases for the structure as set up through the 'Design Structure' window, [12]. The GainDatabase is created for the 'Quantized Region' of that structure, i.e. all layers marked 'Quantized' (see the introduction to Sec.3.2 for more details on the 'Quantized Region'). Layers that are not marked 'Quantized' are only taken into account to determine the strain in the quantized region, to correctly take into account external Voltages as specified through panel [17d] and to take into account dopant related electric fields across the quantized region if the 'Poisson Drift Diffusion'-problem is included by checking [17a].

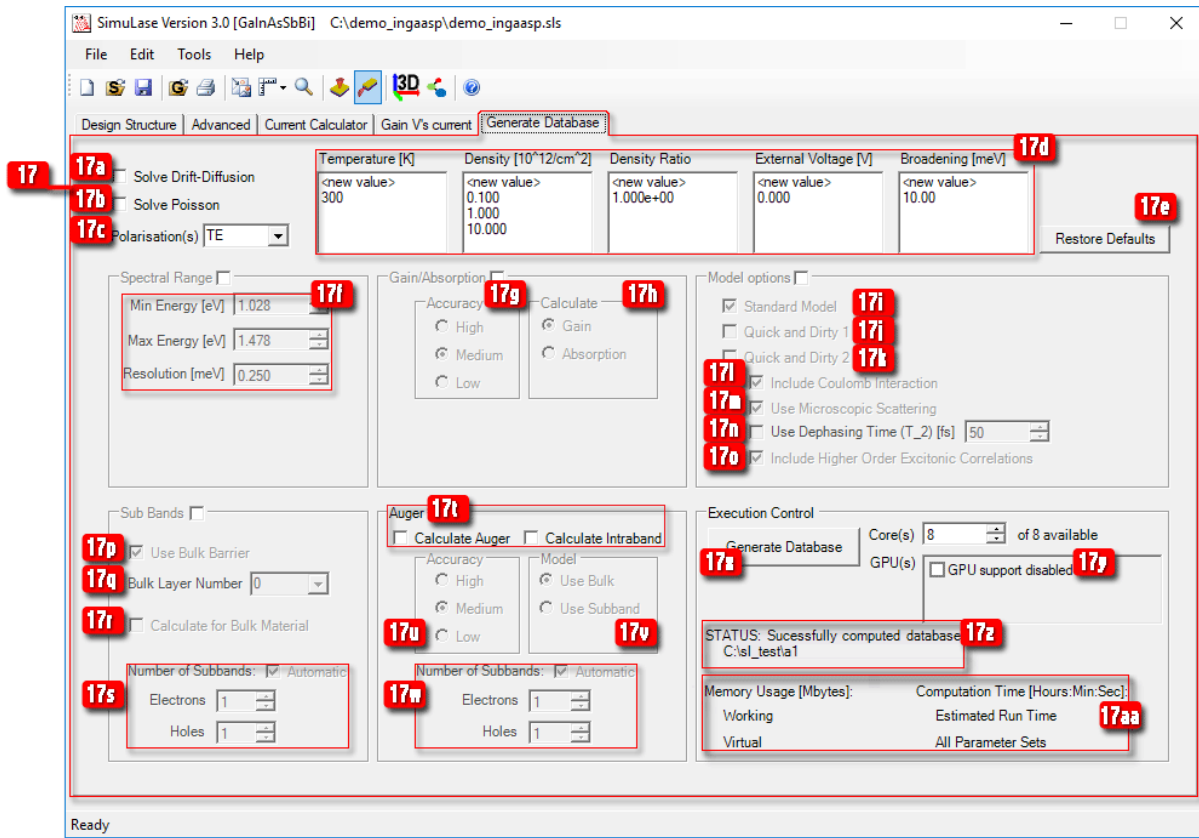


Figure 3.9: 'Generate Database'-panel.

Only those parameters/options from the 'Design Structure' panel, [12] that define the structure are carried over. Other options, set on that panel, like 'Solve Drift-Diffusion', or options set on the 'Advanced' panel, [13], are not used here. If relevant, these have to be specified through the corresponding fields, [17*], here.

In the current configuration of **SimuLase™** some of the parameters are limited to certain ranges. E.g., only temperatures between 100 K and 600 K are allowed. For calculations outside these ranges special optimization of the program has to be done. Please contact NLCSTR if you are interested in specialized versions of **SimuLase™**.

To modify numbers in any of the fields you can either use the scroll arrows or click on the field and use the wheel of the mouse or type in directly. **Numbers typed in by hand have to be confirmed by hitting the 'return' key of the key board.** To eliminate an entry from the range of temperatures, densities, external Voltages or broadenings on has to double click on them, delete the entry using the back-space or delet key and confirm by hitting the return key.

[17] Generate Database Window

[17a] Solve Drift-Diffusion: if checked, the classical Poisson drift-diffusion problem is solved to determine potentials due to dopant related local charges. This should be done if the characteristics like PL are calculated for a doped structure that is not electrically pumped. This is usually the case if PL is measured on un-processed devices and/or at an on-wafer stage. Under operating conditions of a laser the dopant related fields are usually compensated by the pump current. When calculating for that situation or for undoped optically pumped structures like VECSELs, this box should be un-checked. See Sec.7.1.1 for further discussion on this topic.

- [17b] Solve Poisson:** if checked, the quantum mechanical Schrödinger-Poisson problem is solved for the '**Quantized Region**' to determine modifications of the confinement potential due to local charge inhomogenities caused by free carriers in the quantized states. This option should be checked if asymmetric structures are investigated or a dopant related or external field is taken into account. Under operating conditions in typical single quantum well structures (i.e. here: one well in the '**Quantized region**' or all wells are identical), this is usually unnecessary. Using this option leads to significantly longer calculation times (up to several times slower) and requires more CPU-memory.
- [17c] Polarization(s):** sets the light-polarization (**TE or TM**) for which the spectra shall be calculated. If '**TE&TM**' is selected data for both polarizations will be calculated. The calculation time is independent of the choice of polarization and doubles if the calculation is run for both polarizations.
- [17d]** These fields allow to determine for which situations the characteristics of the structure shall be calculated. To enter a value to the list double-click on '<new value>', replace the string by a number and hit return to confirm. To delete an entry double-click on it, hit the 'backspace' or 'delete' button and then 'return' to confirm. Data will be calculated for all possible combinations of temperatures, densities and inhomogeneous broadenings. The calculation time and amount of produced data scales with the number of entries in the '**Temperature**'-field times the number of entries in the '**Density**'-field times the number of entries in the '**Density Ratio**'-field times the number of entries in the '**External Voltage**'-field. The number of broadenings has virtually no influence on the calculation time. However, the amount of produced data increases about linearly with it significantly which might have to be considered if very large GainDatabases are to be created.
- Temperature [K]:** sets up a list of temperatures in Kelvin for which the database shall be created. The temperature as entered here is used as lattice and carrier temperature. Calculation effort increases with decreasing temperature.
- Density [$10^{12}/\text{cm}^2$]:** sets up a list of electron sheet carrier densities in units of [$10^{12}/\text{cm}^2$]. It is assumed that the carriers are in thermal equilibrium.
- Density Ratio[1]:** sets up a list of ratios between hole densities and electron densities. For each electron density in the '**Density**'-list calculations are done for hole densities that are the electron density times the list of density ratios.
- External Voltage [V]:** sets up a list of externally applied voltages in units of [*Volts*]. Positive and negative values are allowed. If this list contains a non-zero entry the option '**Use Bulk Barrier**', **[17p]**, cannot be used which can dramatically increase the calculation effort. See Sec.7.1.1 for further discussion on this topic.
- Broadening [meV]:** Sets up a list of inhomogeneous broadenings in units of [*meV*] (FWHM). Besides the spectra that include only the homogeneous broadening due to electron-electron and electron-phonon scattering, inhomogeneously broadened copies of the spectra will be generated. Inhomogeneously broadened copies of spectra can also be created after the GainDatabase is set up by using the '**Shift and Broaden Database**'-tool, **[2b]**.
- [17e] Restore Defaults:** restores all fields on the '**Generate Database**' panel to it's default settings. It does not influence the settings on any other panel like the structure setup as defined on the '**Design Structure**'-panel, **[12]**.
- [17f] Spectral Range:** sets the spectral range for which spectra shall be calculated. By default these values are set to a 'reasonable' estimate according to the minimum and maximum electron-hole confinement potential separation (bandgap) within the '**Quantized Region**'.

- Min Energy [eV]:** lowest transition energy, in electron Volts, for which spectra shall be calculated. By default, this is set to be 0.15 eV lower than the lowest bandgap transition at any point in the '**Quantized Region**'.
- Max Energy [eV]:** highest transition energy, in electron Volts, for which spectra shall be calculated. By default, this is set to be 0.25 eV higher than the highest bandgap transition at any point in the '**Quantized Region**'.
- Resolution [meV]:** spectral resolution, in meV . By default this is set to 0.25 meV . For spectra with sharp features this could be reduced. This has no significant influence on calculations time, but some influence on required storage for the produced data and time for post-processing with the '**Shift and Broadening**'-option, [2b].
- [17g] **Accuracy: High/Medium/Low** determines the number of grid points and, thus, the accuracy of the calculations. The calculation time and CPU-memory requirement scale strongly with the accuracy level. Typical, the calculation time increases by about a factor of five when going to a higher accuracy level. By default the accuracy-level is set to 'Medium' which we recommend for calculations.
- [17h] **Calculate: Gain/Absorption** switches between two different algorithms used for the calculations (see Secs.6.6 and 7.1.2 for details). The '**Gain**'-model is fast and recommended for use for materials for wavelengths longer than about $800\text{ nm} - 900\text{ nm}$. While the in-band absorption and optical gain are generally calculated with sufficient accuracy, this model tends to lead to an error of a few tens per centimeter in the absorption below the bandgap. If e.g. absorption for electro-optical modulators shall be calculated with high accuracy and for materials at shorter wavelengths we recommend using the '**Absorption**'-model. This model should also be used for materials operating at wavelengths shorter than about 800 nm . For the same accuracy level, the calculation time is usually about a factor of three longer when using the '**Absorption**' model than when using the '**Gain**' model.
- [17i] **Standard Model:** by checking this option, the fully microscopic model NLCSTR suggest for calculating reliable GainDatabases is selected. This is the most extensive model available, including all Coulomb effects and microscopically calculated electron-electron and electron-phonon scatterings that are required for correct lineshapes and amplitudes.
- [17j] **Quick and Dirty 1:** by checking this option the GainDatabase is set up using a model that includes everything the '**Standard Model**', [17i], takes into account except for microscopic scatterings and higher order excitonic correlations which are source terms for the PL. Since the scatterings are not used to describe the dephasing of the optical polarization, a dephasing time T_2 has to be used ([17n]). Calculation times within this model are much shorter than when using the the '**Standard Model**' (see Sec.6.1). However, the resulting lineshapes, spectral positions and amplitudes will have significant errors. The calculations loose their quantitatively predictive quality that the '**Standard Model**' provides. The resulting radiative carrier lifetimes are typically wrong by a factor of two or more.
- [17k] **Quick and Dirty 2:** by checking this option the simplest model **SimuLase**TM offers for calculating GainDatabases will be used. In addition to the simplifications used by option '**Quick and Dirty 1**', this model also neglects all Coulomb effects. It requires to specify a dephasing time T_2 using [17n]. With these simplifications the calculation time for one carrier density and one temperature usually reduces to a few tens of seconds and is essentially given by the time needed to calculate the single particle wavefunctions and subbands. Thus, it can be further reduced by adjusting controls [17g,h,p,q,s]. This option can be used to quickly get some rough estimates.

- [17l] **Include Coulomb Interaction:** if un-checked, all Coulomb effects are neglected, including all microscopic scatterings and higher order excitonic correlations. Un-checking reduces the model to the level of '**Quick and Dirty 2**' described under [17k]. If un-checked, a dephasing time T_2 has to be specified using [17n].
- [17m] **Use Microscopic Scattering:** if un-checked, the dephasing of the optical polarization will be described by a dephasing time, T_2 , [17n], rather than by calculating the underlying electron-electron and electron-phonon scattering processes.
- [17n] **Use Dephasing Time T_2 [fs]:** if checked, the specified dephasing time will be used for the dephasing of the optical polarizations. This usually leads to significant errors in the lineshapes, amplitudes and spectral positions. Even if microscopic scatterings are taken into account ([17m] is checked), this dephasing time is added into the description of the dephasing of the polarizations unless this field is un-checked or deactivated.
- [17o] **Include Higher Order Excitonic Correlations:** if checked, these correlations will be included as source terms for the PL. Without them, the radiative carrier lifetime and PL amplitude are usually wrong by a factor of two or more.
- [17p] **Use Bulk Barrier:** if checked, the barrier states are described as bulk material. Then, only the states that are confined in the well, i.e., states that have confinement energies below the bandedge of the barrier material, are treated in terms of subbands and confinement wavefunctions. The bulk barrier contribution is additive to the contributions of the confined states, with no interaction between the two. Carriers are filled in all states, the confined ones and the barrier ones. This option cannot be used if the barrier layers are graded (have different compositions on the left side than on the right side), or when an electric field is applied ([17d]), or if the '**Drift-Diffusion**' problem is to be solved ([17a]), which usually also results in an electric field across the active region. This option should be used for barriers wider than about 10 nm where many subbands would be required to describe the barrier material which would result in extremely long calculation times and high CPU-memory requirements. In these cases it drastically reduces the calculation effort.
- [17q] **Bulk Layer Number:** specifies the layer within the '**Quantized Region**' whose material is to be used as bulk barrier material.
- [17r] **Calculate for Bulk Material:** if selected, a strict bulk-calculation is performed for the material as specified by [17r]. All confinement effects and other layers are neglected.
- [17s] **Number of Subbands:** specifies the number of subbands that shall be taken into account. If '**Automatic**' is selected these numbers are determined internally according to the number of subbands that are confined in the '**Well**' layer(s) (have energies below the bandedge of the '**Barrier**' layer(s)). If '**Use Bulk Barrier**', [17p], is selected, only these subbands are taken into account and the barrier is added as bulk material, otherwise three more subbands are used to describe the barrier material. The calculation time and CPU-memory rise with the third and fourth power of the number of subbands, respectively.
- [17t] **Calculate Auger/ Calculate Intraband:** if checked, Auger losses and/or intraband absorption spectra are calculated for the structure will be calculated together with the gain/absorption, etc.. Details of these models and calculations are described in Secs.7.1.6 and 7.1.4
- [17u] **Accuracy: Low/Medium/High :** determines the numerical accuracy with which the Auger losses and intraband absorption are to be calculated. The numerical uncertainty for Auger losses is typically around 30% – 50% for 'Low', 10% – 20% for

'Medium' and less than 10% for 'High' accuracy. The calculation time is about five times longer for 'Medium' than for 'Low' and about five times longer for 'High' than for 'Medium'. We recommend to use 'Medium' accuracy. For typical structures the calculation time for the Auger losses and intraband absorption are shorter than the one for calculating gain/absorption, etc.. For 'High' accuracy the calculation times for Auger and intraband absorption can exceed the one for absorption/gain, etc..

[17v] Model: determines what model is used to describe the final states of the Auger and intraband absorption processes. For Auger losses, these are the states high above the bandgap into which the carriers are scattered which took on the excess energy of the recombined electron-hole pair. This is similar to the choice of the model used to describe the barrier material in the gain/absorption calculations (**[17p]**). The selection of these models for the Auger/intraband absorption calculation is independent from the one for the gain calculation.

Use Bulk: in this model the final states are described by bulk material. The material which is used for the bulk barrier is specified by field **[17q]**. This is the model we suggest as default model. In most cases this is the most realistic model - especially for cases with wide barriers. As for the use of the 'Bulk Barrier Model' for the gain/absorption calculation, this model cannot be used if electric fields are present. I.e., if a non-zero external voltage (**[17d]**) is applied or fields due to ionized dopants are present as it is usually the case if the drift-diffusion problem (**[17a]**) is taken into account.

Use Subbands: in this model the final states are described by subbands. This model has to be chosen if electric fields are present in the active region. When using this model the results will show a dependence on the barrier width (see Sec.7.1.6). This model should be used for structures with narrow (total) barrier width (typically: $< 20\text{ nm}$). For very wide barriers a high number of subbands is required. Then, this model can be significantly slower than the 'Bulk-Model'. For structures with barrier widths less than usually about 30 nm the 'Bulk-Model' and the 'Subband-Model' take similar calculation times and require similar amounts of CPU-memory.

[17w] Number of Subbands: determines the number of subbands that shall be included as initial states for the Auger and intraband absorption processes. I.e. the number of subbands which are close to the bandgap and occupied with carriers. We suggest to choose the 'Automatic' option in which case the program determines internally the number of required subbands. In the case that the program determines an extraordinarily high number of required subbands this option allows to reduce the number of subbands in order to make the calculation time and CPU-requirements reasonable. Of course, this will introduce an error in the results. The numbers of subbands as set here are independent from the ones as set through **[17s]** for the gain/absorption calculation.

[17x] Generate Database: starts the calculation of the GainDatabase. After this button is clicked a file manager window opens that allows to specify a name for the database and the directory into which it shall be written. Then, a dialog (**[17ab]**) is opened that shows the expected system requirements and numbers of subbands and $k_{parallel}$ points that will be used. Before clicking the 'continue'-option **one should check in particular the expected computation time.** It can take several hours to complete all calculations for a database. In case of computations that require significant CPU memory your computer will be mostly unusable for other purposes. **Using the computer for other purposes while a database is created can cause problems to the calculation.** On a multi-processor machine one should leave one processor open for alternative work. **SimuLaseTM** allows to stop the calculation

at an arbitrary stage through dialog [17ac], but it can take several minutes before this takes effect since the system has to clean up used resources before terminating the process.

[17y] Using # Processors: defines the number of processors that will be used for the calculations. Creating the data for each temperature-density combination is done in an individual calculation and these calculations are distributed over the number of processors as defined here. If this number is set to be higher than the number of processors available on your computer, multiple calculations will be started on individual processors at the same time. This will slow the individual calculations down and leads to increased memory required on the processors.

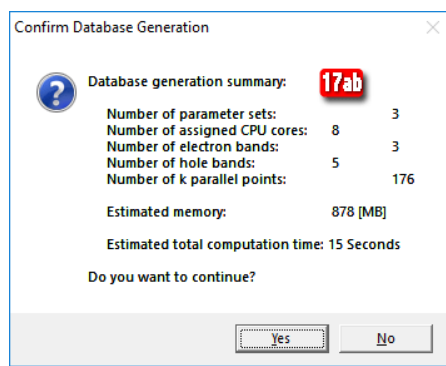
The option 'Using # GPUs' is currently not used. We are working on a GPU-implementation of the gain database calculation. Please check with us for updates on this.

[17z] Status: in this field information about the success or failure of creating the database is displayed. Upon successful creation the directory and name of the database are displayed.

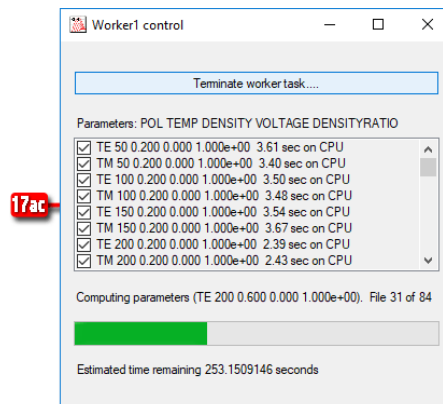
[17aa] System Report: gives you an overview about the current system requirements once the calculation is started. At the end of the calculation the peak values during the calculation are displayed.

Memory Usage [Mbytes]: (Peak) Paged/Virtual/Working: CPU-memory, in megabytes, that is accessed during the calculation.

Computation Time [Hours : Min : Sec] CPU-time used during the calculation. 'Estimated Run time' is the time SimuLase™ estimates for the creation of the complete database if the computer is not used for other purposes during this time. This estimate can be off by up to a factor of about two, depending on the problem size, processor speed and alternative usage. Especially for very small problems this time can be somewhat in-accurate. During the creation of a database this field also displays the time it has been working on it so far. After completion the total run time and the average time it spend on one density-temperature combination are displayed.




[17ab] Confirm Database Generation: window that is opened before the actual calculation is started and displays the involved numbers of subbands, in-plane momentum grid points and estimates about the resulting calculation time and memory requirements. Since setting up GainDatabases can take significant calculation time during which other functions of your computer may become unavailable, **especially the expected calculation time should be checked before actually launching the calculation.**



[17ac] Worker# Control: window that is opened once the calculation is started and displays the progress of the calculation. One of these windows will be opened for each used processor. These windows disappear once the calculations that are scheduled for the respective processors are finished. The button '**Terminate Worker Task...**' can be used to end the calculation prematurely. It can take a couple of minutes for the system to properly terminate the calculation - be patient. Once this is done, the window will close and the system control returns to the **SimuLaseTM** main program. The 'Solving for Parameters'-panel shows the combinations of carrier densities and temperatures that are scheduled for this processor. Once a calculation for one density-temperature combination is finished a green check-mark appears next to that entry and the CPU-time it took for that calculation is displayed. Once the calculation for the first density-temperature pair is finished the progress-bar shows how long it will probably take to finish all the calculations scheduled for this processor. The respective time is displayed at the bottom of the window.

[18] Absorption,...: switches to other tools and displays of GainDatabase data.

3.7 GainDatabase Viewer

These charts are used to display the data contained in GainDatabases. After loading a GainDatabase through the '**File | Open GainDatabase**' option on the main menu, **[1d]**, or the  icon, you can access plots of the '**Absorption**', '**Spontaneous Emission**' (i.e. PL), '**Refractive Index**', and the carrier '**Loss**' due to radiative and, if available, Auger loss processes, the '**Band Edges**' and '**Subbands**' by selecting the respective tabs on the bottom of the chart, **[24]**.

[19a] GainDatabase Information Panel: displays the data that is contained in the selected GainDatabase. To display data select at least one choice from each selection field and hit the '**Redraw**' button, **[19b]**. Use the 'Shift' and 'Control' keys on your keyboard to (un-)select one or more choices.

[19b] Redraw Chart: hit to refresh the plot window **[20]**.

[20] GainDatabase Chart: plot window displaying selected data. The chart contents can be switched, e.g., from '**Absorption**' to '**Spontaneous Emission**' (i.e. PL), using the tabs on the bottom, **[24]**.

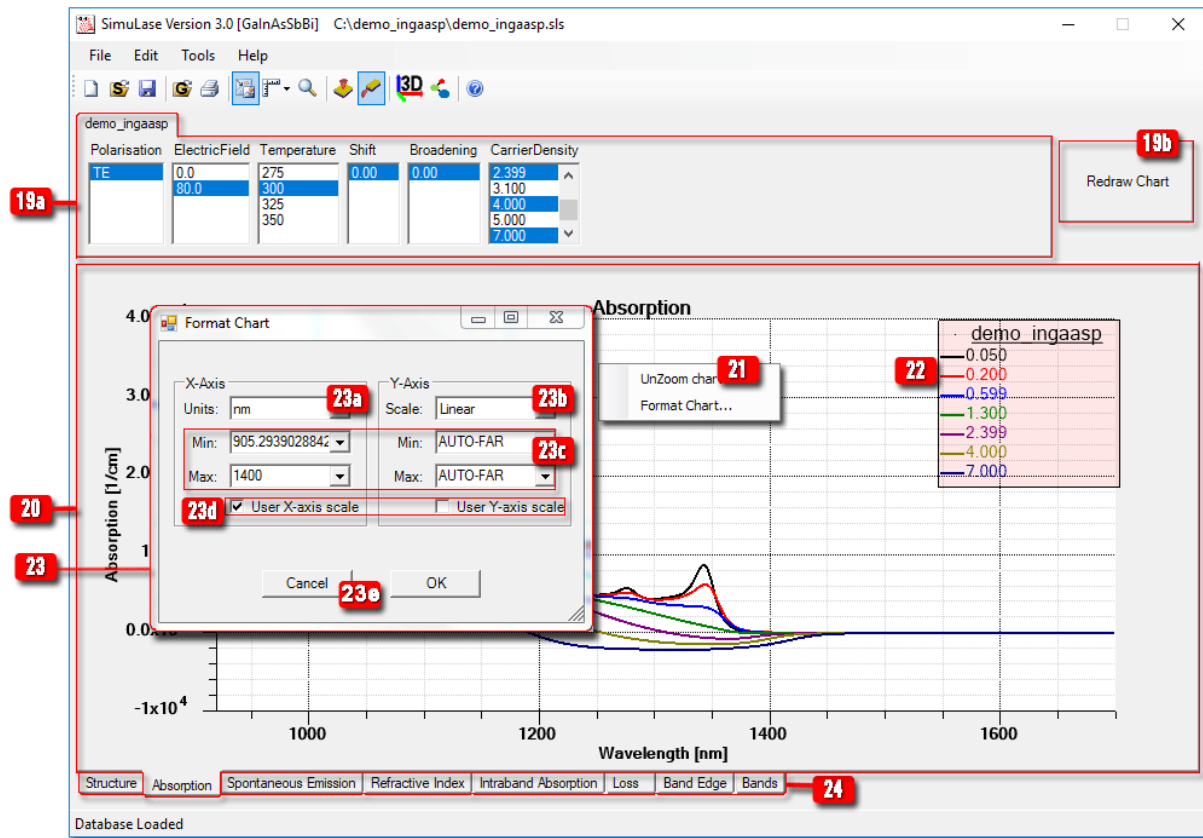




Figure 3.10: Plot panel displaying various gain database data.

- [21] **UnZoom Chart, Format Chart:** dialog opened by right-clicking on the chart.
UnZoom Chart: reverses zooms done using the zoom option [10] (icon ). Each click on this option reverses one zoom from the history.
Format Chart: opens the dialog [23], which allows to set chart boundaries and switch scales.
- [22] **Legends:** give information about the currently displayed data. These can be moved with the 'Edit Chart Element' option [8] (icon .
- [23] **Format Chart Dialog:** opened by right-clicking on the chart and selecting 'Format Chart...'.
 [23a] **X-Axis Units:** allows to switch between an x-axis wavelength scale in units of nanometers to an energy scale in units of electron Volts.
 [23b] **Y-Axis Scale:** switch between linear and logarithmic y-axis scaling.
 [23c] **Min, Max:** select upper and lower bounds for the axis by either typing in a number and confirming with the 'return'-key, or selecting from:
Auto-Exact: sets the boundary to exactly the max/min data point.
Auto-Near: sets the boundary near the max/min data point.
Auto-Far: sets the boundary to the next grid mark above/below the max/min data point.
 [23d] **User X/Y-Axis Scale:** switches the displays [23c] from 'Auto-' to numbers.
 [23e] **Cancel/OK:** abort/confirm chart reformatting.
- [24] **Structure, Absorption, ...:** tabs to switch from displaying the current data (like absorption) to other data (like spontaneous emission).

3.8 PL-Analyzer

The tool is activated through option 'Tools | Analyze Experimental PL', [2a].

This tool allows to make automated comparisons between theoretical and experimental PL-spectra to determine possible spectral shifts which usually indicate deviations between nominal and actual well-compositions and/or -widths. It also determines the inhomogeneous broadening present in the experiment, which gives information about the growth quality. A typical analysis takes less than ten seconds.

To test the features of this tool you can download a demo-GainDatabase and corresponding experimental data from our website at www.nlcstr.com/SimuLaseDemo.htm. The experimental data must be provided in two-column ASCII files with columns that are either space-, tab- or colon-separated. The first column has to give either the energy in electron Volts or the wavelength in nanometers in ascending order. The second column gives the PL. If data for several excitation densities is available, these can be loaded as several files, each containing data for one excitation density.

If experimental spectra to more than one excitation power are provided the excitation powers can be associated with theoretical carrier densities with high accuracy. For this, the experimental spectra have to be loaded in order of increasing excitation power. For more on this see [28].

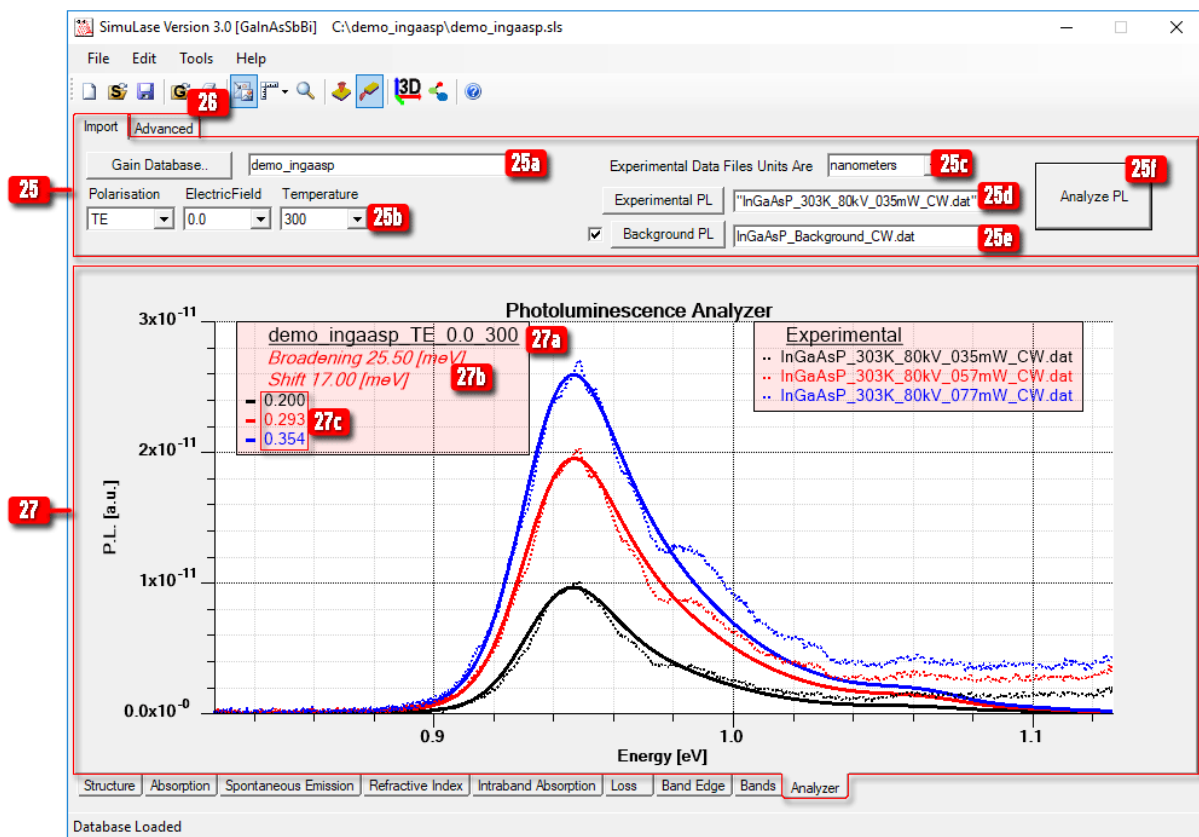


Figure 3.11: Main panel of the 'PL-Analyzer' tool.

Advanced options allow to try to improve the analysis result. E.g. 'Trim Left' and 'Trim Right' allow to exclude low- and high-energy tails in the experimental spectra from the analysis. Low energy tails are often covered by noise where the ideal spectra fall off below the bandgap.

On the high energy side experimental spectra often show enhancements of the PL beyond the ideal theoretical PL. This is usually due to non-thermal carriers in the experiment which arise in particular when using CW-excitation. These carriers have not relaxed toward the bottom of the wells - occupying higher subbands - and lead to an enhancement beyond the ideal thermal equilibrium situation assumed in the theory (see e.g. the features at 0.98 eV in Fig.3.11. These parts should be excluded from the analysis.

The Analysis should focus on the spectral region around the main peak that gives the best information about the inhomogeneous broadening and spectral shifts - starting where the PL reaches about 20% of the maximum to where the PL falls off again to about 50% of the peak value.

The PL-Analysis can fail if the experimental excitation powers are too far apart (about a factor ten or more). The only way to proceed then is to run the analysis for each spectrum individually.

A GainDatabase that is used for the PL-Analysis has to contain spectra to at least one more carrier density than the number of experimental excitation densities that shall be analyzed at the same time. Two theoretical densities are sufficient if only one experimental spectrum shall be analyzed. A typical set of densities would be: $\{0.05, 0.1, 0.2, 0.4, 0.8\} \times 10^{12}/\text{cm}^2$.

[25] Import Dialog: panel to load the theoretical and experimental PL-spectra.

[25a] Gain Database: opens a file manager through which the GainDatabase is selected (file '*.gdb') to which the experimental spectra shall be compared.

[25b] Polarization...: menu to select the files from the database that shall be used for the comparison, i.e., that best correspond to the situation in the experiment. Since the excitation level in PL-measurements are usually low, the data for the lowest sheet carrier densities will be used for the comparison. By default, the five lowest densities are used. This number can be adjusted on the 'Advanced' options panel, **[26i]**.

[25c] Experimental Data File Units Are: specify the units used for the x-axis in the experimental data file. Valid options are: wavelength in nanometers or energy in electron Volts.

[25d] Experimental PL: opens a file manager to select the file(s) containing the experimental data.

[25e] Background: opens a file manager to optionally load a file containing a background noise spectrum which will be subtracted from all the other experimental spectra before the PL is analyzed.

[25f] Analyze PL: starts the PL-Analysis.

[26] Advanced tab: tab to switch to a menu of additional options which can help to improve the PL-analysis. E.g., it allows to exclude parts of the experimental spectra that are no

[26a] FWHM Accuracy: accuracy in $[meV]$ with which the (FWHM of the) inhomogeneous broadening shall be determined. The calculation time for the analysis increases with this accuracy.

[26b] Apply Smoothing: if checked, the experimental spectra are going to be slightly broadened according to a Gaussian broadening before the analysis is performed. This can help to remove artificial noise-spikes in the experimental data that might prevent a good analysis. These spikes are particularly detrimental if they occur near the peak of the PL spectra which leads to wrong estimations for the overall amplitude and peak transition energy. The amount of broadening is given in terms of a percentage of the internally roughly estimated inhomogeneous broadening (FWHM) of the experimental spectra.

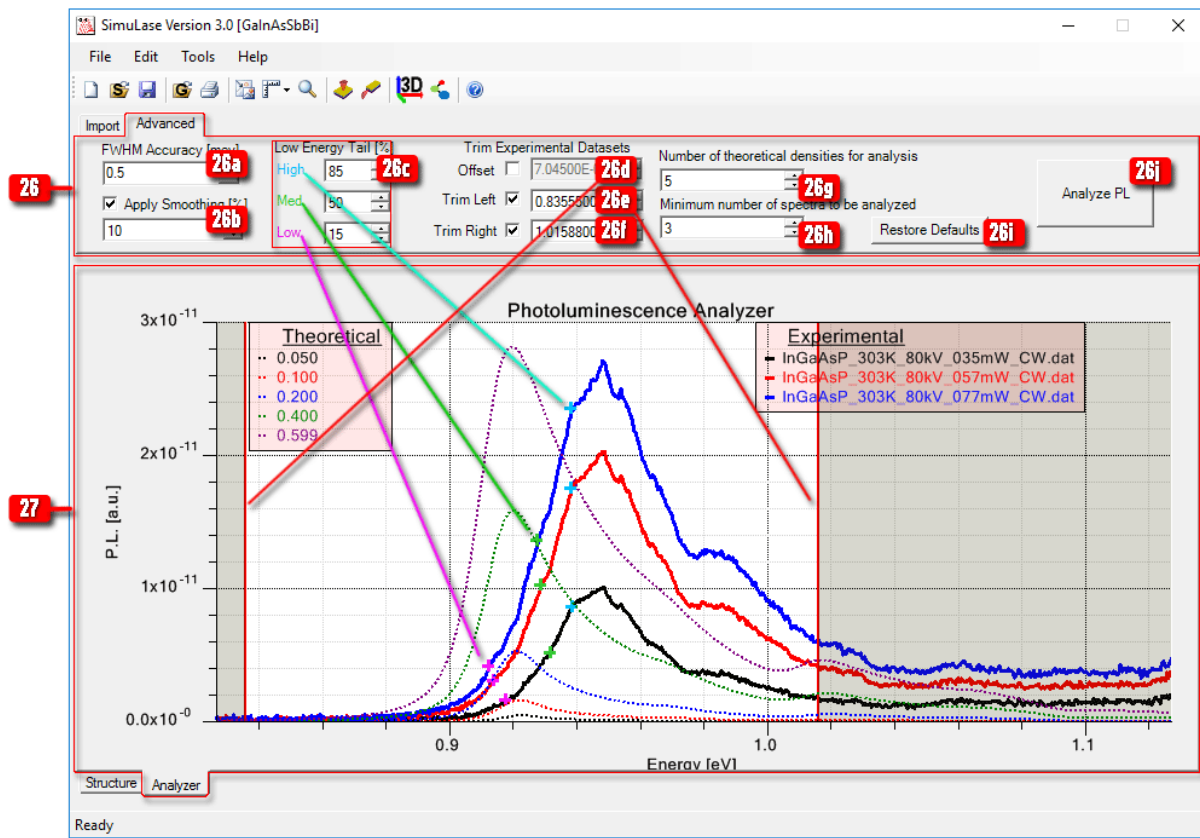


Figure 3.12: Advanced panel of the 'PL-Analyzer' tool.

- [26c] Low Energy Tail [%], High/Med/Low:** points on the low energy tail that will be used to determine the inhomogeneous broadening. The values are given in terms of percentage of the experimental PL amplitude. The resulting values are marked with colored crosses in the chart. These points should be moved if they fall on particularly noisy parts of the spectra. They should not be set too low where the influence of background noise is usually particularly high.
- [26d] Offset:** if checked, the specified value will be subtracted from all experimental spectra at all energies prior to performing the analysis. This simulates subtracting a constant background noise spectrum.
- [26e] Trim Left:** sets a transition energy below which all experimental data is not taken into account for the analysis. This can be used to cut off regions where the PL should have fallen off to zero and is covered by noise. The neglected spectral parts are shaded out in the chart window.
- [26f] Trim Right:** sets a transition energy above which all experimental data is not taken into account for the analysis. Especially when CW-pumping is used, typically not all carriers in the experiment are in thermal equilibrium. This leads to an enhancement of the high energy tail of the PL that is absent in the theory which assumes that all carriers have relaxed to the bottom of the well and are in thermal equilibrium. In the example shown here, this becomes apparent for energies above about 0.98 eV . The neglected spectral parts are shaded out in the chart window.
- [26g] Number of Theoretical Densities for Analysis:** specifies the number of theoretical spectra which are used for the analysis. The spectra to the lowest sheet carrier densities are used. Increasing this number prolongs the analysis. It usually does not

increase the accuracy.

[26h] Minimum Number of Spectra to be Analyzed: specifies the minimum number of provided experimental spectra for which a match with the theory shall be found in the analysis. If the given number is smaller than the number of provided spectra the analysis can disregard spectra it finds 'suspect' of being particularly noisy or that appear otherwise to not match the rest of the spectra.

[26i] Restore Defaults: resets all selections on the 'Advanced' panel, [26], to their default values.

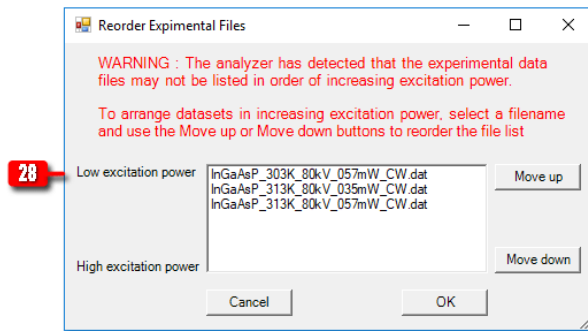
[26j] Analyze PL: starts the analysis.

[27] Photoluminescence Analyzer Chart: displays the comparisons between experimental and theoretical data. After the PL-analysis is done, the main results, [27a,b,c], are displayed in a chart box.

[27a] Broadening: the inhomogeneous broadening (FWHM) in [meV] the PL-analysis had to assume for the displayed comparison between experimental and theoretical data.

[27b] Shift : energetic shift in [meV] that had to be applied to all theoretical spectra for the displayed comparison between experimental and theoretical data.

[27c] The sheet carrier densities in units of [$10^{12}/cm^2$] for the theoretical spectra that are displayed.



[28] Reorder Experimental Files: if several experimental spectra are provided they have to be loaded in order of increasing excitation power. The program searches for maximum amplitudes to check if they are in this order. If it appears that this is not the case dialog [28] opens to allow for a reordering. If spectra have artificial spikes that can confuse the search for the peak amplitudes it might be better to leave these spectra out of the analysis. The difference between excitation powers should be chosen large enough that no question about their ordering can appear. Typically we suggest to increase the excitation powers by about a factor of two between neighboring spectra.

3.9 Shift and Broaden Database

The tool is activated through option 'Tools | Shift and Broaden Database', [2b].

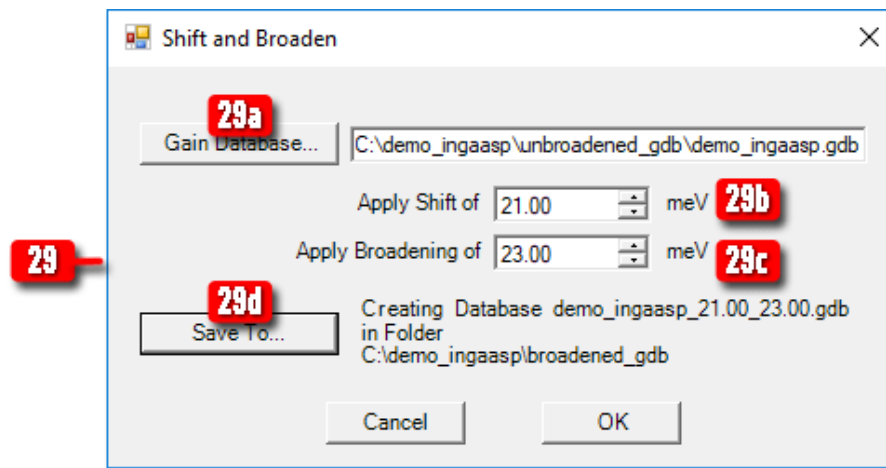
This tool allows to make copies of the originally calculated GainDatabases in which all spectra are shifted by a constant amount and/or broadened according to a Gaussian broadening. This corresponds to applying the spectral shift due to a mismatch between nominal and actual structural parameters (most commonly: the well composition) and applying an inhomogeneous broadening

as caused by local fluctuations of layer widths and/or compositions in real structures. The inhomogeneous broadening and spectral shift are usually determined using the 'PL-Analyzer'-tool, [2a], discussed in Sec.3.8.

The results will be written to a new GainDatabase with corresponding entries under the fields 'Shift' and 'Broadening'. The name of the new database is 'name_s.ss_b.bb.gdb' if 'name.gdb' is the name of the original database. 's.ss' is the shift and 'b.bb' the broadening with two digits accuracy.

The data files containing bandstructures, wavefunctions or carrier lifetimes are not influenced by this and simply copied from the original GainDatabase.

For a GainDatabase containing several hundred spectra this can take several minutes.



[29] **Shift and Broaden** Dialog: panel to create a copy of a GainDatabases in which all spectra are shifted by a global amount and/or inhomogeneously broadened.

[29a] **Gain Database:** opens a file manager to load the GainDatabase to which a spectral shift and/or inhomogeneous broadening shall be applied.

[29b] **Apply Shift of:** specifies the amount in [meV] by which all spectra shall be shifted.

[29c] **Apply Broadening of:** specifies the inhomogeneous broadening, (FWHM) in [meV] that shall be applied.

[29d] **Save to...:** opens a file manager to specify a directory into which the resulting GainDatabase is saved.

3.10 Current Calculator

To activate this tool one has to select the 'Edge Emitter Mode' either by clicking on the icon , [10], or through option 'Tools | Edge Emitter Mode', [2d].

This tool allows to calculate the loss current densities and related quantities for the structure that is currently in the 'Design Structure' window, based on the data contained in a corresponding GainDatabase. If, as usual, the database was set up for just one well, the data is scaled internally by the number of wells in the structure in the Design Structure window. The number of wells is determined by the number of times the 'Quantized Region' is found in the structure. For this, the compositions and widths of all well and barrier layers that are marked as 'quantized' are compared to all other sections of the structure. Only exact replicas are counted as wells.

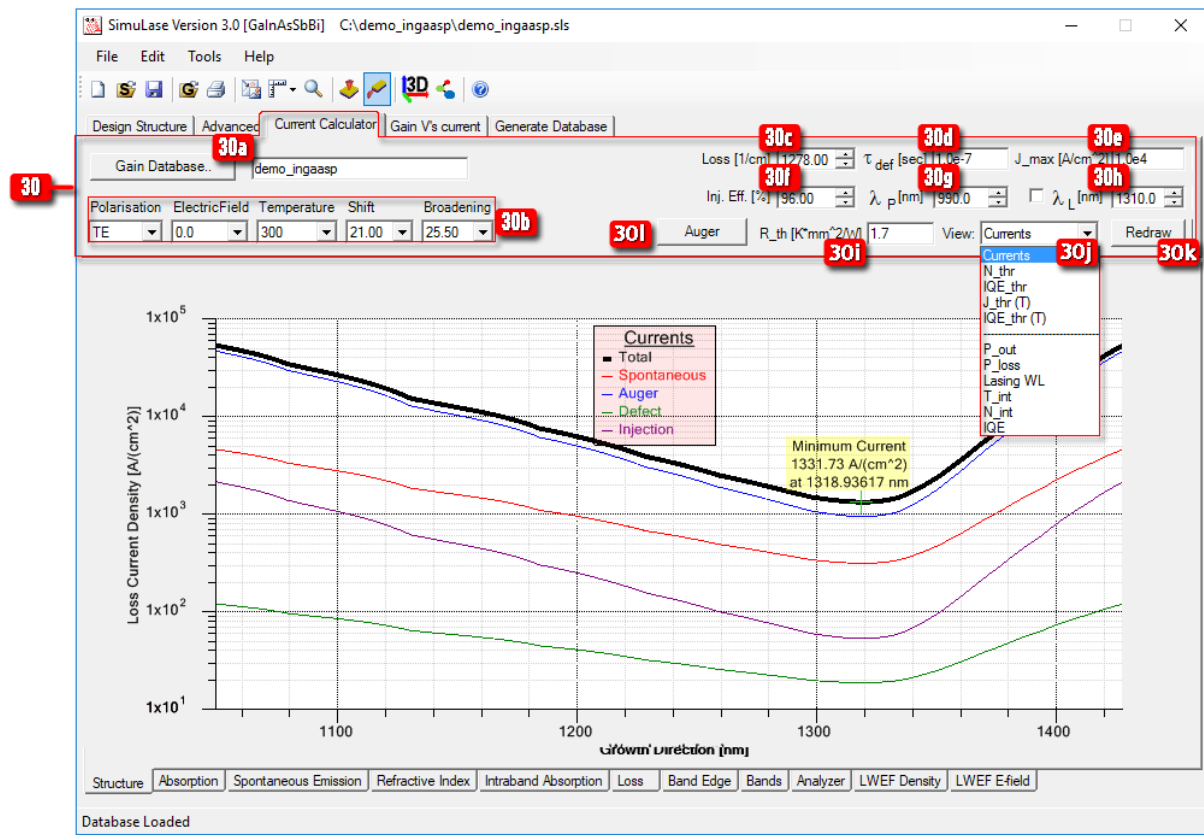


Figure 3.13: Options of the 'Current Calculator' tool.

As in the calculations of the databases itself, the underlying models here are one-dimensional in real space. No lateral profiles are taken into account and 2D current and power densities are calculated.

The tool has two modes of calculation:

- (1) One, calculating the threshold characteristics
- (2) One, calculating the input-output characteristics

Mode (1) is valid for electrical and optical pumping. However, here, internal heating is neglected. The internal temperature is assumed to be power independent and given by temperature selected from the gain database in [30b].

Mode (2) is strictly valid only for optical pumping. Here internal heating is taken into account. However, since **SimuLase**TM does not model the electrical injection problem, the corresponding heatings due to Joule and Peltier-Thomson heating are not known. Heating has to be modeled through the parameters for optical pumping, like the pump wavelength. Thus, for the case of electrical pumping this tool only serves as a 'toy' tool that allows to study general performance dependencies on various parameters, like the number of wells or thermal impedance. The heat sink temperature is given by the temperature for which the structure is set up ('Temperature' on the 'Advanced' panel).

The button 'Auger', [30i] opens and closes a sub-panel (see Fig.3.8) that allows to use either microscopically calculated Auger losses from the database (for this option and if the database does not include Auger losses, the Auger losses are assumed to be zero), use the CN^3 model, or the density-activated defect recombination (DADR) model. For more information on these

models see Sec.7.1.6.

3.10.1 Threshold Characteristics

The user has to specify the total material absorption losses in the field '**Loss**', [30c]. These are given by the sum of internal absorption and scattering losses plus the out-coupling loss. If these losses are known as modal losses for the total structure they have to be divided by the optical confinement factor for the total structure that can be calculated using the 'View | Transverse Mode' option on the 'Design Structure' panel. The wavelength and temperature for which the confinement factor is calculated are set on the 'Advanced' panel.

The user also has to specify the defect recombination loss time τ_{def} , [30d], and the injection efficiency ('Inj. Eff.'), [30f].

With just these settings the tool allows to determine the threshold characteristics assuming that there is no internal heating. The threshold current as well as the corresponding defect, radiative and Auger losses, the intrinsic carrier density (N_{thr}) and internal quantum efficiency ('IQE') are displayed by selecting the corresponding tabs from the 'View' pull-down menu, [30j]. The IQE is given by the ration between radiative losses and the total losses. These quantities are determined for the temperature as specified in the database selection menu, [30b]. No additional internal heating is considered. The program looks up from the database the carrier density that produces enough gain to overcome the total optical loss. Then, the defect, radiative and (if available) Auger carrier loss currents are looked up for this density and displayed together with the injection loss and the total loss current, i.e. the sum of all loss currents. The defect recombination loss current, J_d is calculated from the defect recombination time using:

$$J_d = eN_{thr}/\tau_{def}. \quad (3.1)$$

The loss currents and related data are displayed as function of the wavelength. In a device without wavelength selectivity, the minimum of the total loss current would give lasing wavelength at threshold. For a wavelength selective device like an edge emitter with wavelength selective grating, the total loss current at the specific wavelength gives the threshold current of this device. This fixed lasing wavelength can be set through the field ' λ_L ', [30h].

If the database contains more than one temperature the tool will also plot the threshold current and IQE at threshold as function of the temperature for all temperatures included in the database. The displayed current and IQE are the ones at the (temperature dependent) wavelength of minimum total current or, if checked, the fixed lasing wavelength λ_L . These plots are selected through the fields '**View | J_{thr} (T)**' and '**View | IQE (T)**'.

The plot of J_{thr} (T) includes an exponential fit according to:

$$J_{thr}(T) \propto \exp(T/T_0). \quad (3.2)$$

The plot of IQE (T) includes an exponential fit according to

$$IQE(T) \propto \exp(-T/T_1). \quad (3.3)$$

The characteristic temperatures T_0 and T_1 determined from the fit are displayed in labels in the corresponding plot windows.

3.10.2 Input-Output Characteristics

For these calculations the parameters J_{max} , R_{th} , and λ_P have to be specified in addition to the ones already mentioned for the calculation of the threshold characteristics. J_{max} is the maximum pump current density for which the output shall be calculated. R_{th} is the thermal impedance of the device. λ_P is the pump wavelength. For the case of electrical injection, this wavelength can be used to vary the amount of pump energy lost to heating. It replaces the effects of transport related heating mechanisms like Joule and Peltier-Thomson heating.

In this model the operating characteristics are calculated from the power balance:

$$P_p = P_{out} + P_{heat} + P_{rest}, \quad (3.4)$$

Where P_p is the pump power, P_{out} the output power, P_{heat} power converted to heat and P_{rest} power that is neither converted to heat nor to output power. P_{heat} is determined from the sum of power that goes to pump injected carriers that pass by the wells without being captured, P_{NA} , The excess energy (quantum defect) of carriers being captured into the wells, P_{QD} , Auger losses, P_{aug} , defect losses, P_d , and spontaneous emission from the wells that is re-absorbed in the device and converted to heat, P_{SE-H} :

$$\begin{aligned} P_{heat} &= P_{NA} + P_{QD} + P_{aug} + P_d + P_{SE-H} \\ &= \left(1 - \eta_{inj} \frac{\lambda_L}{\lambda_P}\right) P_p + W \left[\frac{1}{\tau_{def}} + \frac{1}{\tau_{aug}} + \frac{1 - \eta_{SE}}{\tau_{SE}} \right], \end{aligned} \quad (3.5)$$

$$P_{rest} = \frac{W \eta_{SE}}{\tau_{SE}}. \quad (3.6)$$

Here, $W = N n_w \hbar \omega_L$, where N is the sheet carrier density, n_w the number of wells and $\hbar \omega_L$ the lasing energy. η_{SE} is the fraction of spontaneous emission that is emitted from the wells without being reabsorbed and contributing to heating. η_{inj} is the injection efficiency. τ_{aug} and τ_{SE} are the Auger- and radiative lifetimes, respectively. η_{SE} is the fraction of spontaneous emission that is not contributing to heating. The results are usually only very weakly dependent on η_{SE} . We use here a fixed value of $\eta_{SE} = 0.5$ assuming that 50% of the spontaneous emission escapes through the surface of the device.

Once the input-output characteristic is calculated, it can be plotted using the option '**View | P.out**'. Side products from this calculation that can also be plotted are various power losses, 'P_loss', the lasing wavelength, 'Lasing WL', internal temperature, 'T_int', intrinsic carrier density, 'N_int' and the internal quantum efficiency, 'IQE'.

For a real live example of how to use this tool see Sec.5.1.4.

[30] Loss Currents Dialog: panel to specify for which data and which situations the loss current shall be calculated.

[30a] Gain Database: opens a file manager to load the GainDatabase which shall be used for the loss calculation and displays its name.

[30b] Polarization, . . . : fields to select the data corresponding to the situation for which the loss current shall be calculated.

[30c] Loss [1/cm]: the optical material loss due to and internal absorption (free carrier absorption) and scattering losses and out-coupling losses.

[30d] τ_{def} [sec]: defect recombination time.

[30e] J_{max} [A/cm²): maximum pump current density for which the input-output characteristic shall be calculated.

- [30f] **Inj. Eff.** [%]: injection efficiency.
- [30g] λ_P [nm]: pump wavelength.
- [30h] λ_L [nm]: if checked, this sets a fixed lasing wavelength. Otherwise the lasing wavelength is determined from the minimum of the loss current.
- [30i] **R_th** [mm²K/W]: thermal impedance.
- [30j] **View:** selects what data shall be displayed in the chart. Selections above the dashed line show data for the fixed temperature as selected from the entries in the database. Selections below the dashed line are calculated taking into account internal heating and assuming a heat sink temperature as given on the 'Advanced Panel'.
- '**Currents:**' loss currents at threshold.
- '**N_thr:**' intrinsic carrier density at threshold.
- '**IQE_thr**' internal quantum efficiency at threshold as given by the ratio of the radiative losses, '**Spontaneous**', over the total losses, '**Total**'.
- '**J_thr (T)**' threshold current for all temperatures in the database together with an exponential fit $\propto \exp(T/T_0)$.
- '**IQE (T)**' internal quantum efficiency at threshold for all temperatures in the database together with an exponential fit $\propto \exp(-T/T_1)$.

'**P_out:**' output power density.

'**P_loss:**' power lost to spontaneous emission, Auger, defect recombination, quantum defect and injection loss.

'**Lasing WL:**' lasing wavelength.

'**T_int:**' shows the intrinsic temperature.

'**N_int:**' shows the intrinsic carrier density.

'**IQE:**' internal quantum efficiency.

3.11 Gain V's Current

To activate this tool one has to select the '**Edge Emitter Mode**' either by clicking on the icon , [10], or through option '**Tools | Edge Emitter Mode**', [2d].

This tool calculates and displays the gain/absorption for a given pump current density. It allows, e.g., to study how the (peak-) gain varies in amplitude and wavelength with the temperature for a fixed pump current, or how the pump current has to be adjusted with temperature to obtain the same gain at a given wavelength.

For a specified '**Current**' the radiative and (if available) Auger losses are looked up from a GainDatabase and it is determined what carrier density leads to such a loss current. Then the gain for this carrier density is displayed.

Other loss mechanisms than radiative and Auger recombination processes, like defect recombination, are not included here. If these additional losses are known for a specific device and are relevant, the current has to be adjusted accordingly. Also, the internal carrier capture efficiency (injection efficiency) is assumed to be 100%. Reduced efficiencies can be accounted for by rescaling the current value by the actual capture efficiency.

Structures with multiple wells can be taken into account by specifying how many repeats of the active region ('well') for which the GainDatabase has been set up are supposed to be in the structure (field [31c]). See Sec. 3.10 for details about this scaling.

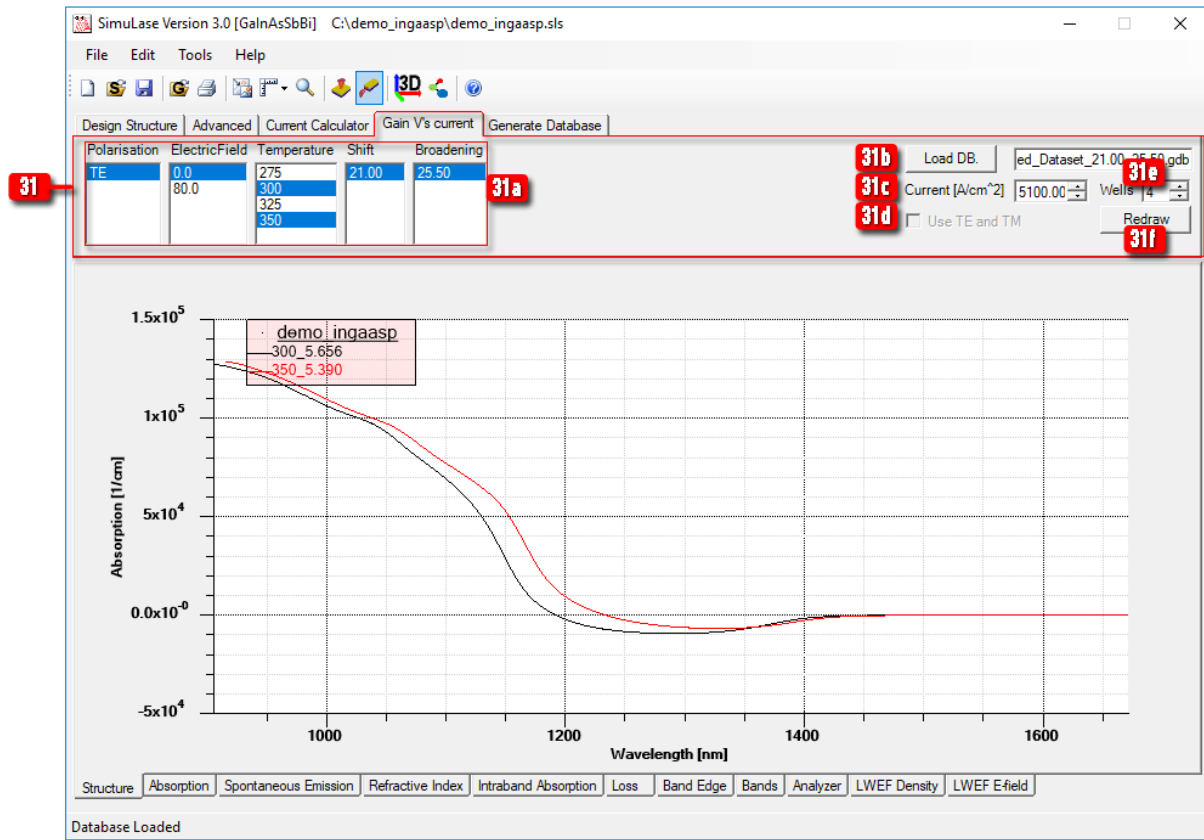


Figure 3.14: 'Gain V's Current'-tool window.

[31] **Gain V's Current** Dialog: panel to specify for which data and which situations the analysis shall be performed.

[31a] **Polarization,...**: fields to select the data from the GainDatabase.

[31b] **Load DB:** opens a file manager to select a GainDatabase.

[31c] **Current [A/cm²]:** Total loss current density in [A/cm²].

[31d] **Combine TE TM loss:** if checked, the radiative loss current is calculated by combining the TE and TM loss currents using $J_{rad} = 2/3 J_{TE,rad} + 1/3 J_{TM,rad}$. Otherwise, $J_{rad} = J_{TE,rad}$ and/or $J_{rad} = J_{TM,rad}$ is used depending on which polarization has been chosen through the selector field 'Polarization'.

[31e] **Number of Wells:** specifies the number of wells that are supposed to be in the structure. GainDatabases are typically set up for structures containing only one 'well' (one active region). If several (identical) wells (copies of the active region) are supposed to be in the structure the material gain as contained in the GainDatabase is scaled by the number specified here. Similarly, the radiative- and Auger-losses are multiplied by this number. The spectra displayed in the chart are the ones for the total assumed structure with possibly multiple wells.

[31f] **Redraw:** button to refresh the plot.

3.12 Potential and Band Structure Views

Once a gain database has been opened, these tools are part of the tabs on the bottom of the chart window. They allow displays of the confinement potentials, wavefunctions, levels and subbands for the cases included in the database.

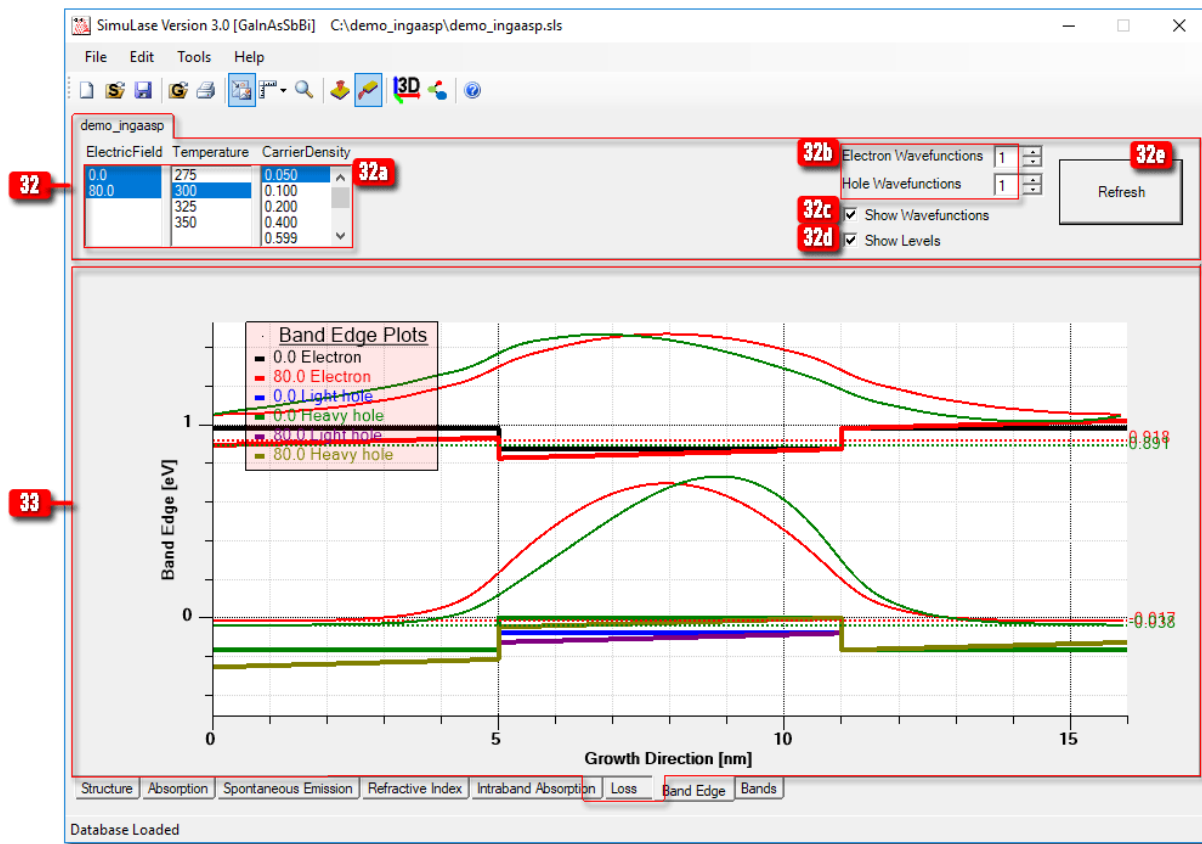


Figure 3.15: 'Band Edge'-display tool.

If the GainDatabase has been calculated without solving the quantum-mechanical Schrödinger-Poisson problem that determines density-dependent changes of the confinement potential due to potentials arising from local charge inhomogeneities, the data is identical for all densities. Since this data is independent of the optical polarization (TE or TM), there is no corresponding selector field.

- [32] **Band Edge Dialog:** panel to specify what data to display.
 - [32a] **Electric Field,...**: fields to select the data from the GainDatabase.
 - [32b] **Conduction Plots/Valence Plots:** specifies how many electron/hole subbands, wavefunctions and/or levels shall be displayed for each situation selected from the GainDatabase through [32a].
 - [32c] **Show Wavefunctions:** if checked, the wavefunctions are displayed. The confinement energies are the zeros for the wavefunction amplitudes.
 - [32d] **Show Levels:** if checked, the 'levels' are displayed. These are the confinement energies for zero in-plane momentum (bottom of the subbands).
 - [32e] **Refresh:** refreshes the plot windows [33] and [34].
- [33] **Band Edge Chart:** shows the confinement potentials for electrons, heavy- and light-holes and the electron and hole wavefunctions and levels.
- [34] **Subband Chart:** displays the subbands as function of the in-plane momentum. For conventional materials the dispersions are plotted as lines. For dilute materials the Bloch-character of the states is also displayed through circles with sizes proportional to the character. The density of the symbols and their size can be regulated through the options

'Symbol Density' and 'Symbol Scale'. The later two options are absent if the material does not contain dilute contributions.

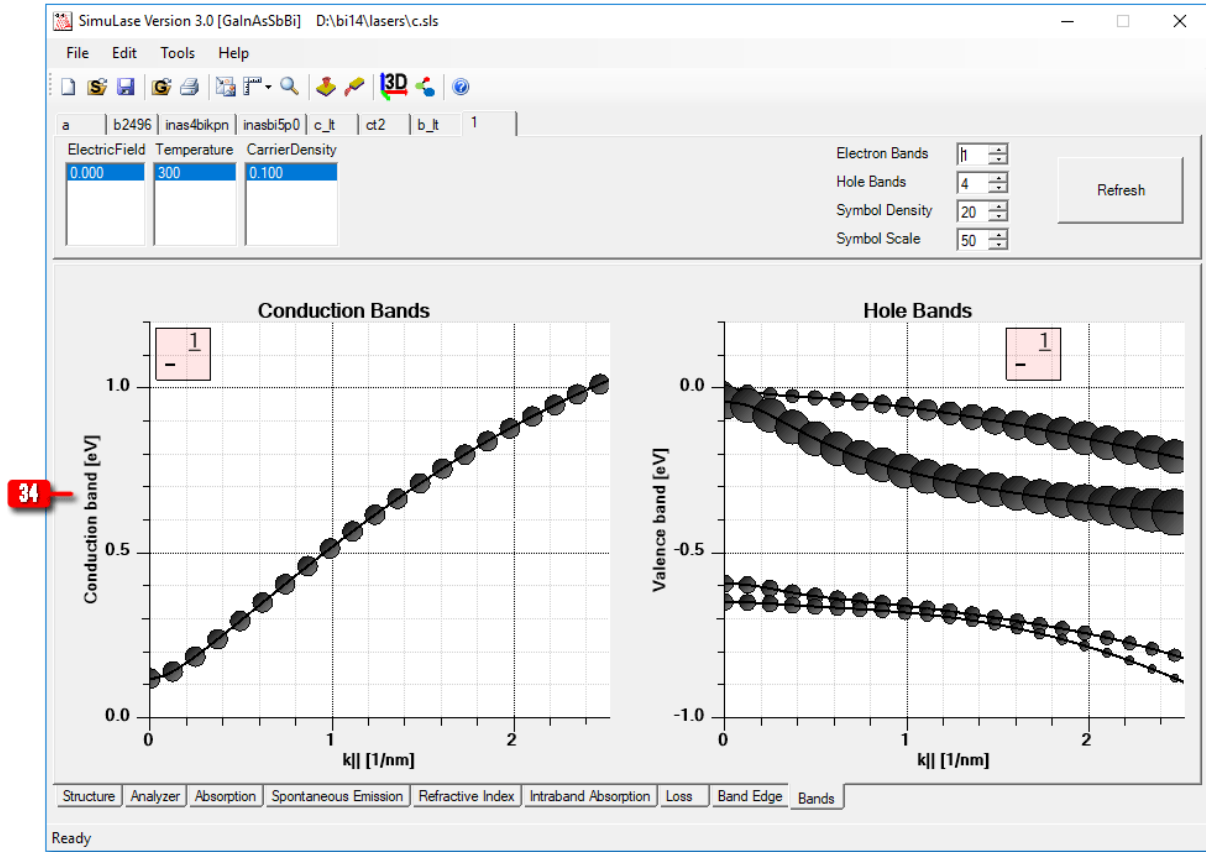


Figure 3.16: 'Subbands'-chart.

3.13 Linewidth Enhancement Factor

3.13.1 Linewidth Enhancement Factor | Carrier Density

Once a gain-database has been opened, this tool can be started through the 'Tools | Linewidth Enhancement Factor | Carrier Density'-option, [2f]. It allows to display the linewidth enhancement factor as function of the energy or wavelength for a specified carrier density. Multiple gain-databases can be opened at the same time in order to compare results for different densities.

[35] **Linewidth Enhancement Factor | Carrier Density** Dialog to specify what data to display.

[35a] **Polarization, Electric Field,...**: fields to select the data from the Gain-Database.

[35b] **Density** [$10^{12}/\text{cm}^2$]: Field to specify the sheet carrier density for which the linewidth enhancement factor shall be calculated/displayed.

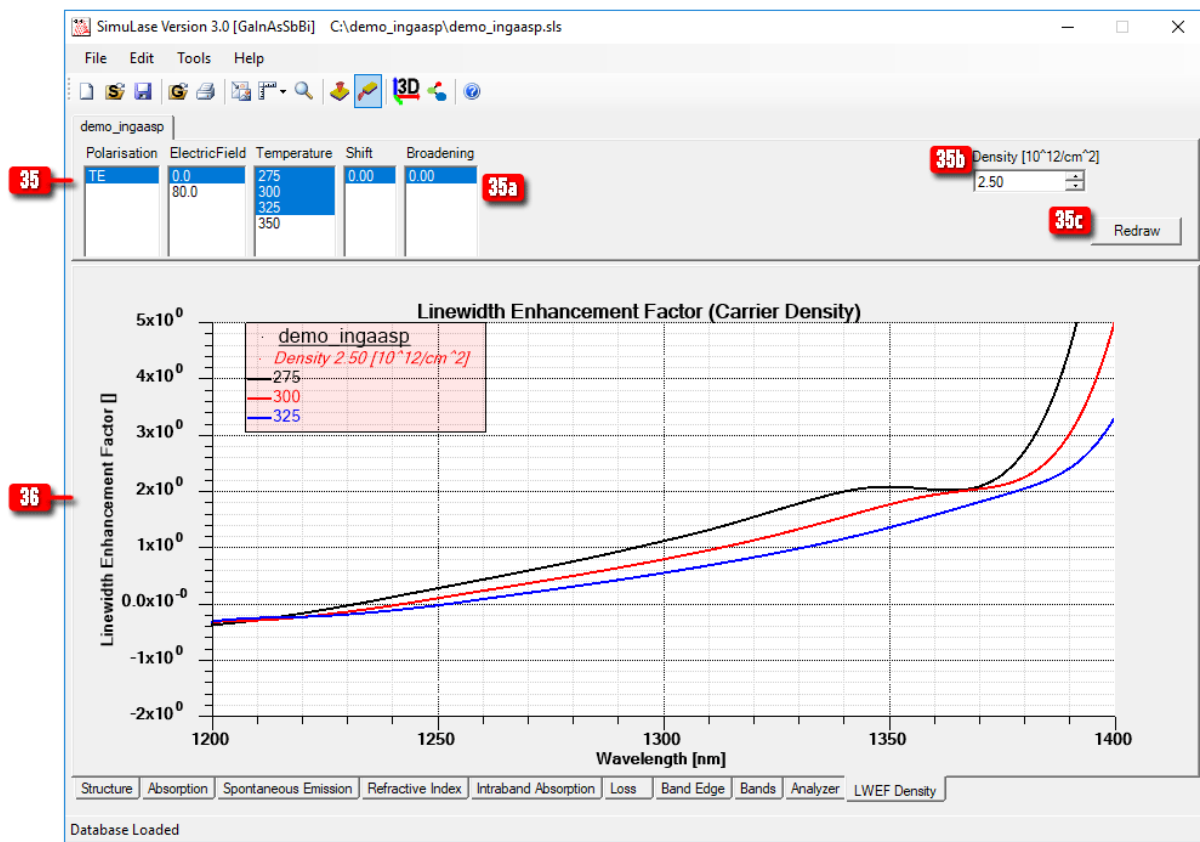


Figure 3.17: 'Linewidth Enhancement Factor' tool. LWEF for a given carrier density.

[35c] Redraw: refreshes the plot window [36].

[36] Linewidth Enhancement Factor | Carrier Density Chart: displays the results.

3.13.2 Linewidth Enhancement Factor | Electric Field

Once a gain-database has been opened, this tool can be started through the 'Tools | Linewidth Enhancement Factor | Electric Field'-option, [2f]. It allows to display the linewidth enhancement factor as function of the energy or wavelength as calculated for the difference between two electric field values (see Ref. [1]). Multiple gain-databases can be opened at the same time in order to compare results for different initial and/or final field values.

[37] Linewidth Enhancement Factor | Electric Field Dialog to specify what data to display.

[37a] Polarization, Electric Field,...: fields to select the data from the Gain-Database. Exactly two entries from the 'Electric Field' selection box have to be selected. The LWEF is calculated from the refractive index change and absorption change between these two electric fields. Multiple entries can be selected from all other selection boxes.

[37b] Redraw: refreshes the plot window [38].

[38] Linewidth Enhancement Factor | Electric Field Chart: displays the results.

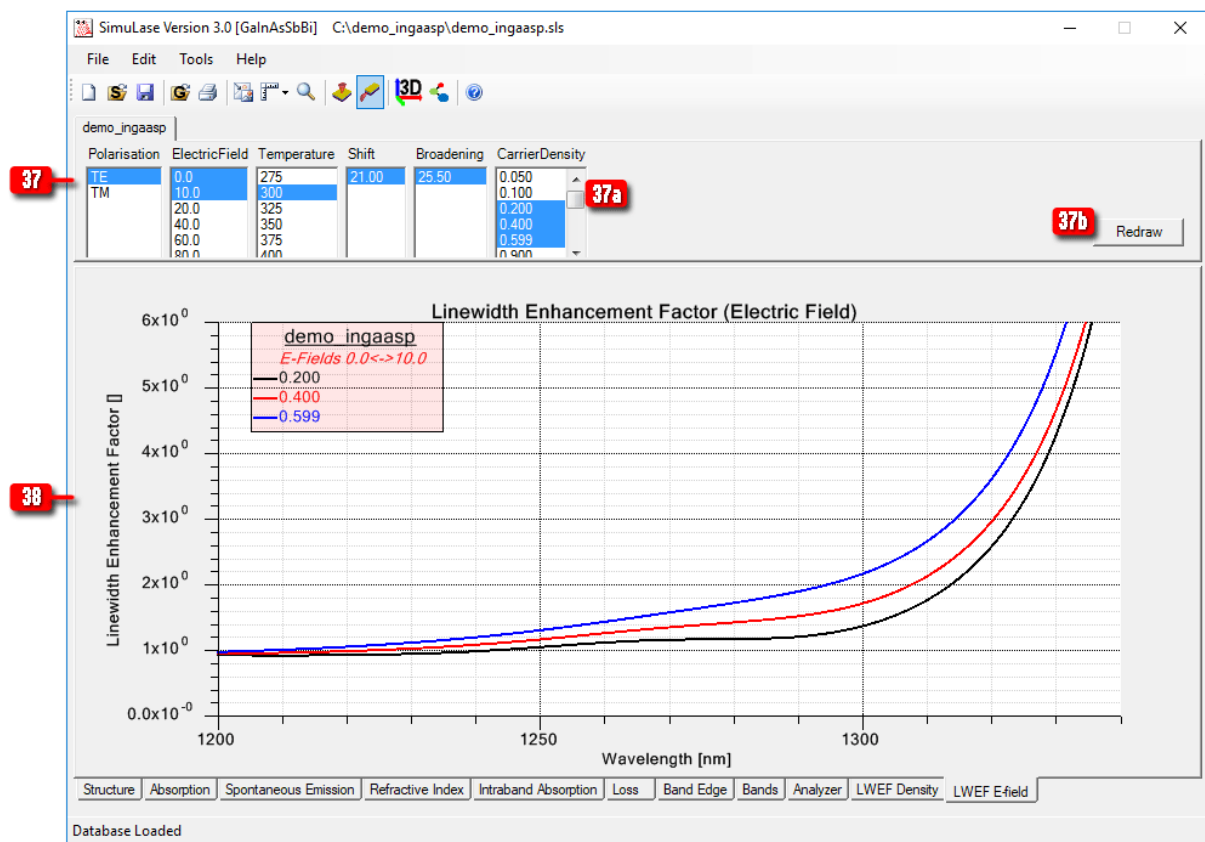


Figure 3.18: 'Linewidth Enhancement Factor' tool. LWEF for a change in electric field across the active region.

4 Data Format

SimuLaseTM creates a variety of files containing the data that comprises a GainDatabase like absorption/gain, PL and refractive index spectra, radiative losses, confinement potentials, bandstructures and wavefunctions. All Files are in ASCII-format in order to allow to investigate the data also outside the **SimuLase**TM environment. The following describes the labeling of the files and the formatting of the data.

The names of all files belonging to a GainDatabase start with a common string, which is set through the file manager that opens once the button '**Generate Database**', [17x], is clicked to start the calculation of a database. They are located in the directory as specified through the same file manager dialog.

In the following description of the files the abbreviation:

- “name” stands for the GainDatabase name.
- “PP” stands for the polarization (TE or TM).
- “F.FFF” stands for the external Voltage in Volts with per mille accuracy.
- “R.RRRe±RR” stands for the ratio between the hole density and the electron density in scientific notation.
- “TTT” stands for the temperature in Kelvin. An integer is used and all digits after the decimal point are dropped.
- “s.ss” stands for a spectral shift of the spectra in *meV* with percent accuracy.
- “b.bb” stands for the inhomogeneous broadening in *meV* (FWHM) with percent accuracy.
- “N.NNN” stands for the sheet carrier density in $10^{12}cm^{-2}$ with per mille accuracy.

The following files are created:



- **name_PP_F.FFF_R.RRRe±RR_TTT_im_s.ss_b.bb_N.NNN** : Material gain/ absorption spectra. The first column gives the energy in [eV]. The second column gives the material absorption, g , in [1/cm]. For information how to convert this into modal gain/absorption see Sec.7.1.2. $1/g$ is the length over which the intensity of the light is reduced by a factor $1/e$ if there is absorption, and increases by a factor of e if there is gain. The extinction coefficient (of the field amplitude), a , is derived from g by $a = g/2$. “im” in the file name stands for “IMaginary part of the optical susceptibility”.
- **name_PP_F.FFF_R.RRRe±RR_TTT_re_s.ss_b.bb_N.NNN** : Carrier induced refractive index spectra. The first column gives the energy in [eV]. The second column gives the carrier induced refractive index in [1/cm]. These units have been chosen such that the linewidth enhancement factor (α -factor) can be derived by simply dividing the difference between the refractive index for two carrier densities by the corresponding difference between the absorption/gain without need for rescaling. In order to get from the refractive index spectra in these units, $b(\omega)$, to the dimensionless electronic contribution to the refractive index, $\delta_n(\omega)$, one has to use the conversion: $\delta_n(\omega) = \frac{100c}{2\omega} b(\omega)$. The factor 100

arises from the conversion of $[1/cm]$ to $[1/m]$. c is the speed of light in vacuum in $[m/s]$ and ω is the angular frequency of the transition energy in $[1/s]$ ($\epsilon = \hbar\omega/e$, where ϵ is the energy in $[eV]$ as used in the file and e is the elementary charge).

In order to get to the total refractive index for a density N , one has to add $(\delta_n(N) - \delta_n(N_0))$ to the background refractive index which is contained in the files "...bgnr". Here, N_0 should be zero or the lowest density for which δ_n has been calculated.

"re" in the file name stands for "REal part of the optical susceptibility".

- **name_PP_F.FFF_R.RRRe±RR_TTT_pl_s.ss_b.bb_N.NNN** : Photo luminescence spectra (spontaneous emission). The first column gives the energy in $[eV]$. The second column gives the spontaneous emission in $[(eV\ s\ m^3)^{-1}]$. "pl" in the file names stands for "Photo-Luminescence".
- **name_PP_F.FFF_R.RRRe±RR_TTT_ie_s.ss_b.bb_N.NNN** : Electron free carrier (intraband) absorption spectra. The first column gives the energy in $[eV]$. The second column gives the material absorption in $[1/cm]$
- **name_PP_F.FFF_R.RRRe±RR_TTT_ih_s.ss_b.bb_N.NNN** : Hole free carrier (intraband) absorption spectra. The first column gives the energy in $[eV]$. The second column gives the material absorption in $[1/cm]$
- **name_PP_F.FFF_R.RRRe±RR_TTT_tsp** : Radiative carrier lifetimes. The first column gives the sheet carrier density in $[10^{12}cm^{-2}]$. The second gives the corresponding lifetime in $[sec]$.
- **name_F.FFF_R.RRRe±RR_TTT_taug** : Carrier lifetimes according to Auger recombinations. The first column gives the sheet carrier density in $[10^{12}cm^{-2}]$. The second gives the corresponding lifetime in $[sec]$.
- **name_F.FFF_R.RRRe±RR_TTT_c_N.NNN** : Electron subbands. For dilute Nitride or Bismide containing materials the first line contains the single symbol '#' to indicate that the file contains in addition to the energies also the Bloch-character of the states. The first column gives the in-plane momentum in $[1/nm]$. The $(n+1)$ 'st column gives the energy of the n 'th electron subband in $[eV]$. For dilute Bismide or Nitride containing materials the $(2n+1)$ 'st column contains the Bloch character of the state in the n 'th electron subband.
- **name_F.FFF_R.RRRe±RR_TTT_v_N.NNN** : Hole subbands. For dilute Nitride or Bismide containing materials the first line contains the single symbol '#' to indicate that the file contains in addition to the energies also the Bloch-character of the states. The first column gives the in-plane momentum in $[1/nm]$. The $(n+1)$ 'th column gives the energy of the n 'th hole subband in $[eV]$. For dilute Bismide or Nitride containing materials the $(2n+1)$ 'st column contains the Bloch character of the state in the n 'th hole subband.
- **name_F.FFF_R.RRRe±RR_TTT_ewaves_N.NNN** : Normalized electron wavefunctions. The first column gives the growth direction (z) in $[nm]$. The $(n+1)$ 'th column gives the n 'th electron confinement wavefunction (for zero in-plane momentum).
- **name_F.FFF_R.RRRe±RR_TTT_hwaves_N.NNN** : Normalized hole wavefunctions. The first column gives the growth direction (z) in $[nm]$. The $(n+1)$ 'th column gives the n 'th hole confinement wavefunction (for zero in-plane momentum).
- **name_F.FFF_R.RRRe±RR_TTT_edg_N.NNN** : Confinement potentials. The first column gives the growth direction (z) in $[nm]$. The second column gives the confinement potential for light holes in $[eV]$. The third column gives the confinement potential for heavy holes in $[eV]$. The fourth column gives the confinement potential for electrons in $[eV]$.

-
- **name.F.FFF_R.RRRe±RR_TTT_mus** : Chemical potentials. The first column gives the sheet carrier density in [$10^{12}cm^{-2}$]. The second column gives the electron chemical potential in [eV]. The third column gives the hole chemical potential in [eV]. The fourth column gives the interband chemical potential in [eV].
 - **name.F.FFF_R.RRRe±RR_TTT_bgnr** : Background refractive index. The first column gives the energy in [eV]. The second column gives the unitless background refractive index.
 - **name.F.FFF_R.RRRe±RR_TTT_strain** : Strain. The first column gives the growth direction (z) in [nm]. The second column gives the strain in [%].
 - **name.gdb** : This file contains information necessary to open the data with the GUI. When copying the data to another location, this file has to be in the same directory as all other files of this “GainDataBase” (“gdb”).
 - **name.sls** : (xml-formatted) File containing all information about the structure for which the database has been set up as specified through the ‘Design Structure’ window, [12]. This file is opened when an existing structure is loaded through the option **File | Open Structure**, or , and it is created once a GainDatabase is created or through the option **File | Save Structure** or corresponding icon . This file can also be read using Windows Excel.
 - **name.slm** : (xml-formatted) File containing all information about the parameters used for the GainDatabase as specified through the ‘Generate Database’ window. This file is used to check whether a GainDatabase with the current settings has already been created to avoid double calculation or overwriting of existing data.

5 Typical Examples

In this chapter we use two examples, an edge emitting laser and a vertical external cavity surface emitting laser (VECSEL), to demonstrate the usage and capabilities of **SimuLase™**. It is shown how the program settings are best used for efficient calculation and what information can be extracted from the created data.

5.1 Edge Emitting Laser

In this example a typical structure for an edge emitting laser is designed and analyzed using **SimuLase™**. The structure is an *InGaAsP/InP*-based device for operation around 1310 nm. Please note that this structure is for illustrative purposes and by no means an optimized device. Some of the results of this example have been published in Ref. [3].

The DVD containing the full **SimuLase™** program contains a directory '**demo_ingaasp**' that contains all data required to reproduce the example of an edge-emitting structure discussed in Sec. 5.1. '**demo_ingaasp**' contains the full structure. '**unbroadened_pl**' contains the GainDatabase for the PL-analysis. '**experimental_pl**' contains the experimentally measured PL spectra and '**broadened_gdb**' contains the GainDatabase for the current calculation. Please note that this example can only be run with the AllInGaPAs-version of **SimuLase™** and **SimuLase_Designer™**.

The structure from this example can be downloaded at:

www.nlcstr.com/Download_SimuLase_A/demo_ingaasp.sls

The database can be downloaded at:

www.nlcstr.com/Download_SimuLase_A/InGaAsP_DemoGDB.zip

The experimental PL can be downloaded at:

www.nlcstr.com/Download_SimuLase_A/UsersMeasuredPL.zip

5.1.1 STEP 1: Setting Up the Structure

When setting up the structure start by setting up the 'quantized region'. This is the sequence of layers containing one or more wells that is used for all microscopic calculations like calculating levels and wavefunctions in the 'Design Structure' window or to set up the gain database. There has to be one and only one connected block of layers that comprise the quantized region. Its layers are marked to be part of that region by checking the box 'Quantized', [12e].

Here, the full structure has four 6 nm wide $In_{0.9}Ga_{0.1}As_{0.53}P_{0.47}$ -well wells separated by 10 nm wide $In_{0.863}Ga_{0.137}As_{0.3}P_{0.7}$ -barriers. As detailed in Sec.6.5, the calculation effort increases dramatically - about cubically - with the number of wells. Thus, we suggest to only consider one well to be the 'quantized region' (layers 1, 2 and 3 in Fig.5.1) and make use of the fact that the microscopic calculations assume periodic boundary conditions. As long as the wells - or at

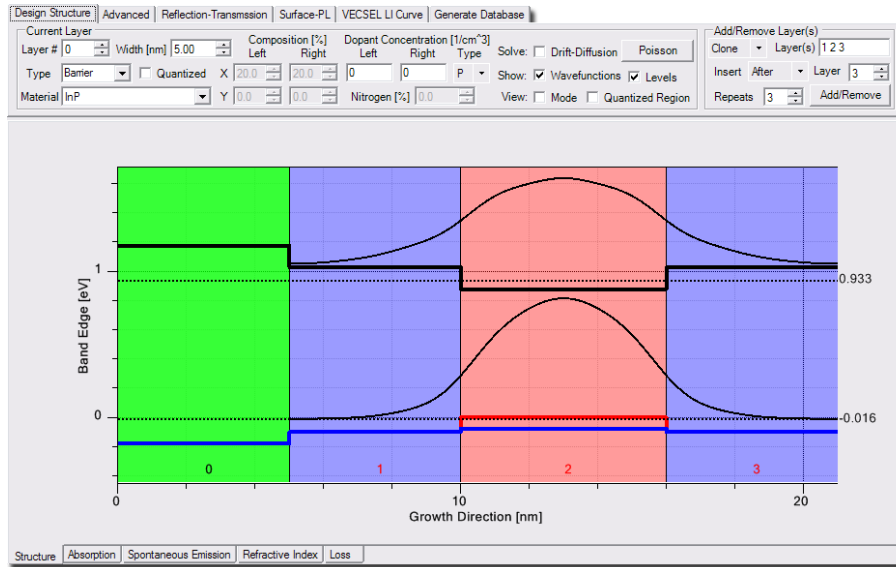


Figure 5.1: 'Quantized region' of the edge emitting laser (layers 1, 2, 3).

least the energetically lowest subbands that are most crucial for the optical properties - are not significantly electronically coupled and all wells are equally pumped, this approach will yield good results that can simply be rescaled by the total number of wells later. Note that for structures in which structurally different wells share a common chemical potential all wells have to be included in the quantized region in order to obtain correct results for a given pump situation.

The barrier layers 1 and 3 of the 'Quantized Region' should have only half the width of the total barrier width (5nm) since the periodic boundary conditions will lead to an effective width of twice the size. Also, this allows to set up the total active region of the device by simply adding copied of the initial well.

In order to see the influences of strain we temporarily added a layer of the substrate material, *InP*, as layer '0' that is not marked 'Quantized' before the first barrier.

Layers 1 and 3 are marked as 'Barrier' and layer 2 as 'Well' using the 'Type' selection [12b]. Layer 0 is marked as 'Cladding'. These labels are only relevant if the reflection, transmission or longitudinal (propagating) mode shall be calculated later taking into account data from Gain-Databases. Then the absorption/gain for the well/barrier layers is read from the GainDatabases and put in place locally according to these labels.

After setting up the first well and, thus, the 'quantized region', and checking that the electronic levels are at the expected energies, the other wells can be created as copies of the first one. The most efficient way is to use the 'Clone' option and create three clones of layers 1, 2 and 3 and inserting them after layer 3 using the settings for the options in the 'Add/Remove Layer(s)' sub-panel as shown in Fig.5.1. By using the 'Clone' option one can later change the layers of all wells consistently by simply applying the change to one of the clones. While the attributes 'well/barrier' will be transferred to the clones, the clones will not be part of the 'quantized region' unless they are manually marked to be part of it.

For this structure the well-region is followed on each side by 35 nm of undoped barrier material. The resulting structure so far is shown in Fig.5.2.

The structure is completed by adding n- and p-doped cladding layers of various dopant concentrations and/or material composition. Fig.5.3 shows the background refractive index profile and

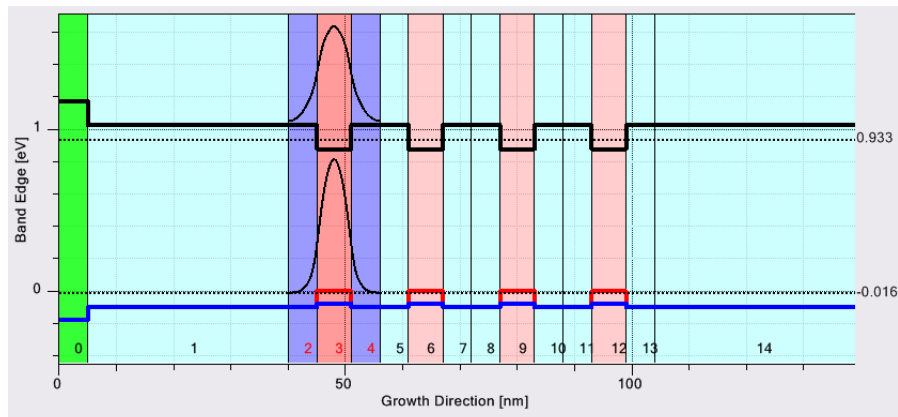


Figure 5.2: Undoped quantum well and cladding layers of the edge emitting device. The 'quantized region' (layers 1 2 3) is shown in darker blue and pink. The *InP*-layer '0' has been added temporarily to check for strain.

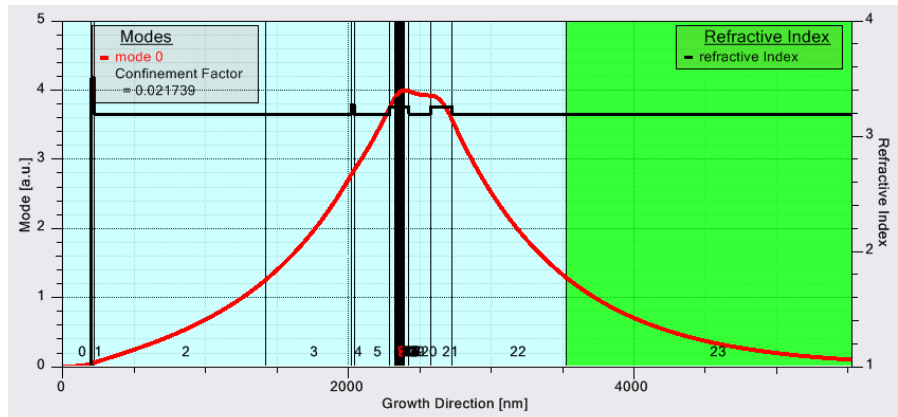


Figure 5.3: Refractive index profile and confined mode of the full edge emitting structure assuming an operating wavelength of 1310 nm . Layer '23' is the *InP* substrate.

the confined mode of the total structure. This view can be accessed by checking the 'View Mode' option, [121]. The desired operating wavelength for which the refractive index profile and mode are displayed has to be set on the 'Advanced'-options panel. In order to be able to calculate the optical mode and confinement factor correctly, we also added 200 nm of air (layer '0'), a 20 nm thick metalization layer (layer '1') and $2\text{ }\mu\text{m}$ of undoped *InP*-substrate.

At this point it is advisable to save the structure using the 'File | Save Structure' dialog. The structural information is saved in xlm-format in a *.sls file. This file can be read also using e.g., Windows Excel. This file can be downloaded from our web site at www.nlcstr.com/Download_SimuLase_A/dem

5.1.2 STEP 2: Analyzing Experimental PL

With the full structure set up, one can now go ahead and calculate GainDatabase data. If a structure according to this layout has already been grown, the next step should be to perform a PL-analysis. One should compare theoretical to experimentally measured PL-spectra to test the quality of the growth and possible deviations from the design.

The experimentally measured spectra for a PL-analysis should be taken under low but not too low excitation conditions. If the excitation is too weak the PL is dominantly coming from the

tail of energetically low defect states and not representing the actual well. Under too strong excitation the PL-lineshape and peak position change strongly with the excitation. Also, the PL can show several and/or poorly defined peaks. Finally, the PL under high excitation is strongly homogeneously broadened due to strong electron-electron scattering. This makes it hard to determine the inhomogeneous broadening that reflects the homogeneity of the growth. All of this makes a PL-analysis very difficult.

Under medium excitation, about 1-20% of threshold, the dominant effect of changes in the pump intensity is mostly a change in the PL-amplitude, the changes in the PL-lineshape are rather small and the PL is usually dominated by a single peak that clearly indicates the (excitonic) bandgap.

Often, the experimental PL is only known for one excitation density. Then, the comparison to the theoretical results can be somewhat inconclusive. While the inhomogeneous broadening and spectral mismatches between design and realization can still be determined with high accuracy, the determination of the intrinsic carrier density is not that conclusive. A more precise analysis can be performed if PL data has been measured for several excitation densities - typically increasing the excitation level by factors of about 1.5 to 3.0.

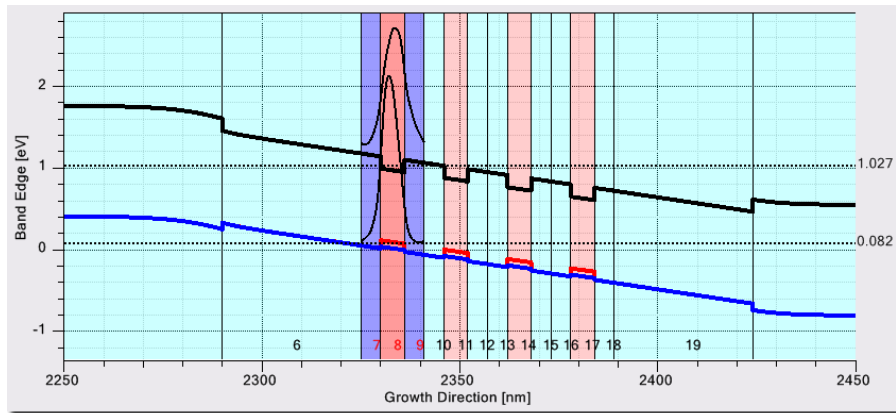


Figure 5.4: Confinement potential after solving the classical drift diffusion problem to determine the charge potentials due to ionized dopants.

Since the PL is usually measured under optical excitation and without an applied electric pump current and Voltage that compensate the fields from ionized dopants, the theoretical spectra have to take into account these fields. For that, one has to check on the 'Generate Database' panel the option 'Solve Drift-Diffusion', [17a]. To take into account also the possible screening of the dopant-related fields due to pump-created carriers one should also check the option 'Solve Poisson', [17b]. Then, the Poisson-Schrödinger problem will be solved for each carrier density.

Next, one has to specify the temperature as it was present in the experiment using field [17d]. If there is only one experimental spectrum (one excitation density), one only needs to set up spectra for two carrier densities, which is the minimum number of carrier densities that are required for a PL-analysis. Typical carrier densities would be 0.1 and $0.2 \times 10^{12}/\text{cm}^2$. If one has spectra to more excitation densities one needs to calculate spectra for at least one more carrier density than the number of experimental excitation densities. They should typically span the range between about 0.05 and $1.0 \times 10^{12}/\text{cm}^2$.

For a compressively strained structure as in the case here, the PL at low excitation powers will be dominated by TE-polarized light. Select calculating for that polarization using field [17c]. For other strains one might have to calculate also for TM-polarization.

All other fields of the 'Generate Database' panel can/should be left in their default settings. After hitting the 'Generate Database'-button, [17x], and selecting a name and directory for the database, the program returns a message about the estimated calculation time and required CPU memory. If these are extremely high (more than maybe 20 minutes per combination of density temperature and polarization) which could be the case for very wide and/or deep wells, one can try to speed up the calculation by resetting the number of subbands that shall be taken into account in the calculation using the options [17s]. Usually the low excitation PL is dominated by emission from the lowest confined subbands. Thus one usually obtains fair results if one only includes maybe 2 or 3 electron subbands and 2 to 5 hole subbands.

Once the database has been successfully created one can load it into the PL analyzer tool 'Tools | Analyze Experimental PL'. For a more detailed description of that tool and the required format for the experimental data see Sec.3.8.

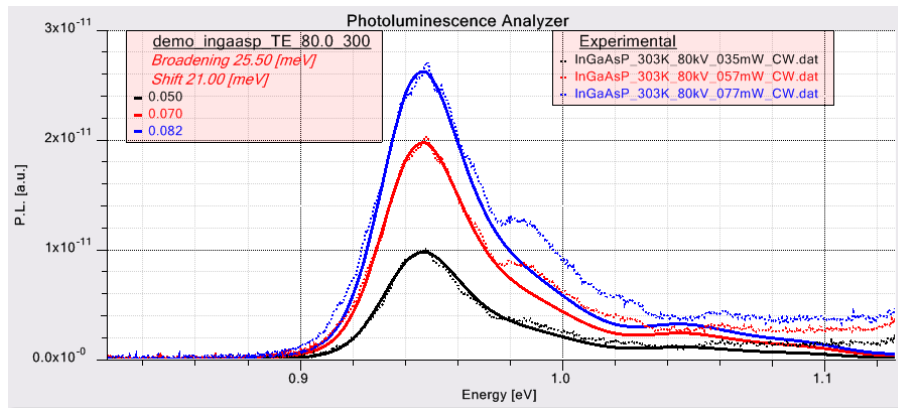


Figure 5.5: Comparison between measured and calculated PL-spectra using the PL-Analyzer tool.

After loading the experimental data and - since available - subtracting from it a measured background noise spectrum, we find for this structure the result shown in Fig.5.5. Here, the 'Advanced' options, [26] have been used to improve the quality of the agreement. The gain database and experimental spectra for this example can be downloaded from the web at www.nlcstr.com/SimuLaseDemo.htm.

The analysis reveals a spectral mismatch of about 21 *meV* between the theoretical and experimental spectra. This indicates a small mismatch between the nominal and realized material composition of the well. To a lesser extent this can be explained assuming a mismatch in the well width since typical well width fluctuations influence the transition energies not that strongly. To find out what might explain the mismatch one can vary the 'quantized' well in the 'Design Structure' window and monitor the level energies.

The analysis reveals an inhomogeneous broadening of about 25.5 *meV* (FWHM). This is the broadening due to local fluctuations in the material compositions and/or the layer widths. The microscopic calculations assume perfect crystals and initially only include the homogeneous broadening due to electron-electron and electron-phonon scattering. The additional broadening can be included by applying a Gaussian broadening to the only homogeneously broadened spectra. This can be done when setting up the initial data by entering one or more broadening values in field [17d]. The calculation will then create in addition to the only homogeneously broadened data copies with the specified inhomogeneous broadening. This has virtually no influence on the calculation time.

A copy of the original database including the determined spectral shift and inhomogeneous broadening can also be created later using 'Tools | Shift and Broaden Database', [29].

If the determined spectral shift is rather large (about 20 meV or more), one should adjust the parameters of the 'quantized region' and redo the calculation. If the shift is rather small, the only important influence of the deviation between actual and nominal structure is this overall spectral shift. Other results, like lineshapes, amplitudes as function of density and temperature or carrier losses will not be significantly influenced. Thus, one does not have to recalculate the whole database, but can simply apply the shift.

The analysis also shows that the experimental PL has stronger PL at energies above about 0.98 eV than the theory. The theory assumes that all carriers are in thermal equilibrium where they have relaxed to the bottom of the well and are in Fermi distributions. The deviations in the experiment come from the fact that CW-pumping was used under which not all carriers have relaxed to the bottom of the well but some emitted from states in higher subbands. This effect becomes more pronounced with increasing excitation power. It can be avoided by using pulsed excitation.

These energetically higher parts of the spectra should be excluded from the PL-analysis using the option 'Trim Right', [26f] from the 'Advanced' option panel.

In a case as here, where the experimental spectra are rather noisy, the analysis can be improved by applying a small broadening to the experimental data using the field [26b].

Finally, the analysis also reveals the intrinsic carrier densities that the pump excitation has created ([27c]). This association between carrier densities and pump excitation can only be performed with a high level of accuracy if experimental data to more than one excitation power is available.

5.1.3 STEP 3: Setting up a GainDatabase

In general, the database for PL-analysis only needs to be set up for a few densities and one temperature. On the other hand, the GainDatabase for studying the operating characteristics of a device needs to include a larger parameter set.

The carrier densities should cover the full range from low density absorption to the high density gain regime. The density steps also have to be kept small enough to allow for interpolation between them. A typical set of carrier densities for an edge emitting structure would be 0.05, 0.1, 0.2, 0.4, 0.6, 0.9, 1.3, 1.8, 2.4, 3.1, 4.0, 5.0, 7.0, 10.0 and $15.0 \times 10^{12}/\text{cm}$ if the 'quantized region' contains only one well. If it contains more wells, these densities should be multiplied by the number of wells. Note, that this is the number of wells for which the microscopic calculations are performed, not the number of wells in the structure.

The temperatures should cover the expected range of operating temperatures. A typical set would cover the range from 275 K to 375 K in steps of 25 K .

For highly compressively strained structures (compressive strain larger than about 0.5%) it is usually sufficient to consider only TE-polarized light. For other strains one might have to calculate for TE and TM polarization.

Since the database is for operating conditions where the pump Voltage and current compensate to a high degree dopant related fields, the calculation should be performed for the flat-band case, i.e. with the option 'Solve Drift-Diffusion', [17a], un-checked and the 'External Voltage' in [17d] left at the default value of zero.

For typical cases where the 'quantized region' has inversion symmetry, it is usually not necessary to include the potential changes due to free carriers (the option 'Solve Poisson', [17b]). This option should only be necessary if the well is asymmetric or if electrons and/or holes are not well confined due to very shallow electron and/or hole confinement potentials.

If the inhomogeneous broadening is known from a PL-analysis one should add this value to the list of broadenings in field [17d]. If it is not known one should add one typical broadening. The number of broadenings has no influence on the calculation time only on the memory size of the resulting database. Copies of the database for other broadenings and including overall spectral shifts can be created later using the 'Tools | Shift and Broaden Database'-tool.


All other options should usually be left in their default setting. However, for very wide wells or other situations where the default setting can lead to a situation that would require extraordinary amounts of calculation time, one can use the other settings to reduce the calculation effort - usually at the cost of reduced accuracy. The calculation requirements depend most crucially on the number of required subbands. These numbers are displayed in the message window that appears after hitting the 'Generate Database' button. One can check in the 'Design Structure' window whether all these subbands are really relevant or if some could be left off the calculation since they are energetically too far from the bandedge.

If one decides to set the number of subbands for the absorption/gain or the Auger calculation by hand, one should run a test first for the most extreme case - highest temperature and highest density - how the results change with a change in the number of subbands.

5.1.4 STEP 4: Determining Operating Characteristics

After having set up the database one can investigate the resulting gain/absorption, refractive index and PL spectra using the corresponding display panels. Besides this, **SimuLase**TM offers tools that allow to easily determine some of the most crucial device characteristics like the threshold current and lasing wavelength.

Threshold Characteristics

The threshold characteristics can be determined using the 'Current Calculator'-tool which can be accessed by clicking on the icon  in the top panel or by selecting 'Tools | Edge Emitter Mode'.

After the database has been set up one should first apply the spectral shift and inhomogeneous broadening as determined by the PL-analysis using the 'Shift and Broaden Database'-tool. Then one can load this database into the 'Current Calculator' and select the parameters (temperature, polarization,...) for which one wants to know the threshold current.

For this tool to work correctly, the structure has to be present in the 'Design Structure' window. The program determines from the structure the number of wells by counting how many **exact** copies of the quantized region are present in the structure. Since the database has been set up for just one well, the data contained in it will be scaled according to the number of wells as found. The best way to ensure that the intended number of wells is found, the additional wells should be created using the 'copy' or 'clone' option. Otherwise, small modifications of the well or barrier widths may not be transferred correctly to the other wells and they will not be identified as additional 'wells'.

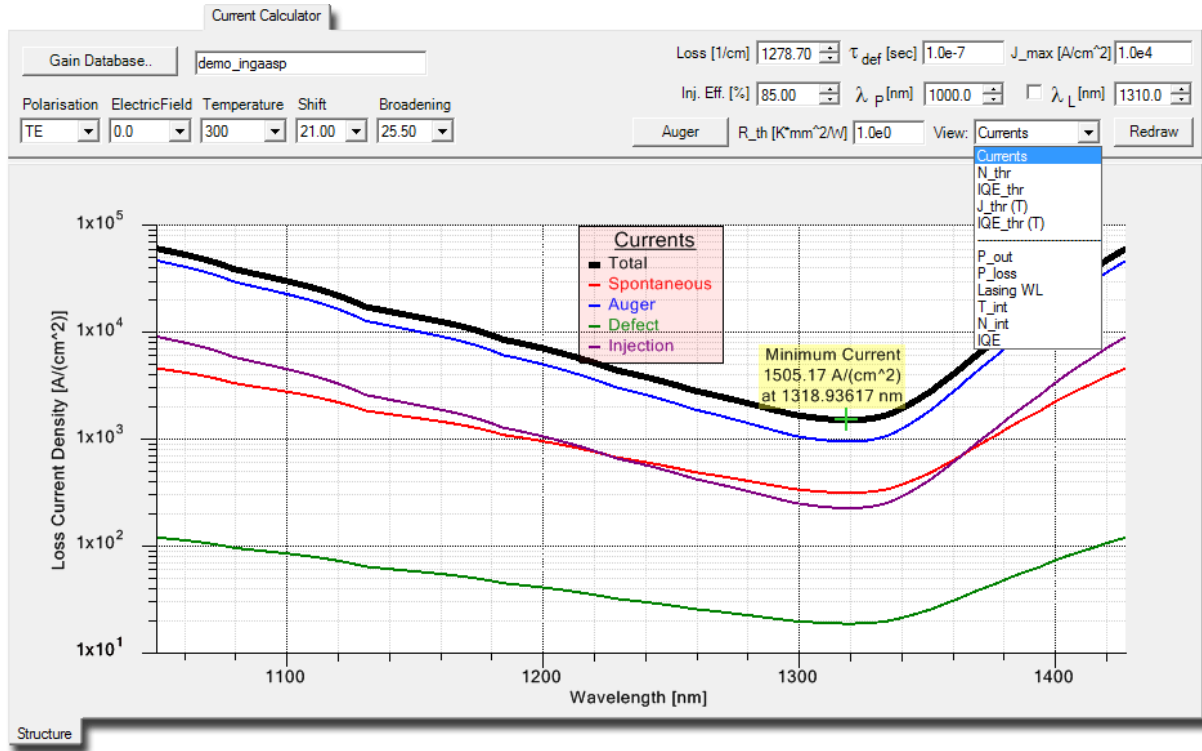


Figure 5.6: Determining the threshold current and lasing wavelength using the 'Current Calculator' tool.

Next, one has to set the material absorption loss in the field 'Loss'. This is the optical loss due to out-coupling and internal losses due to effects like scattering, absorption in un-pumped regions or intraband absorption. The out-coupling loss, α_{out} , can be calculated from the facet reflectivities, $R_{1,2}$, and the device length, L , using:

$$\alpha_{out} = \frac{1}{2L} \ln \left(\frac{1}{R_1 R_2} \right). \quad (5.1)$$

The internal loss, α_{int} , cannot be calculated. It can be measured through cut-back experiments using devices of different lengths. For a real device using the layout and wells as described here the total modal losses have been determined to be $27.8/cm$ with $\alpha_{out} = 17.2/cm$ and $\alpha_{int} = 10.6/cm$.

To convert the modal losses to the material loss units as used in the GainDatabase one has to divide them by the optical confinement factor that can be calculated using the 'View Mode' option within the 'Design Structure' panel (see. Fig.5.3). Here the confinement factor is 0.02174, resulting in a material loss of $1278.7/cm$.

One also has to specify the injection efficiency in the field 'Inj. Eff.'. This is the fraction of pump injected carriers that is actually captured into the wells. It can be measured using cut-back experiments. Since this number is not known for the structure here, we use it as an adjustable parameter.

The 'Current Calculator' looks up for each wavelength the gain spectra to find the carrier density that provides enough gain to overcome the material loss. For this density, N , the carrier loss current densities due to defect, radiative and - if available - Auger carrier recombinations,

$J_{def/rad/avg}$ are calculated from the corresponding recombination times $t_{def/rad/avg}$ using

$$J_{def/rad/avg} = \frac{e N n_w}{t_{def/rad/avg}}, \quad (5.2)$$

where n_w is the number of wells.

These loss currents are plotted together with the injection loss and the total loss for each wavelength.

In an edge emitter without wavelength selectivity, the device would lase at the minimum of the loss current since this is the wavelength where the smallest carrier density/pump current produces enough gain to overcome the optical losses. For the case that the device has wavelength selective gratings or other means to fix the lasing wavelength this wavelength can be specified by checking the box and setting the value in the field λ_L . For both cases, the threshold current and wavelength are marked with a label in the plot.

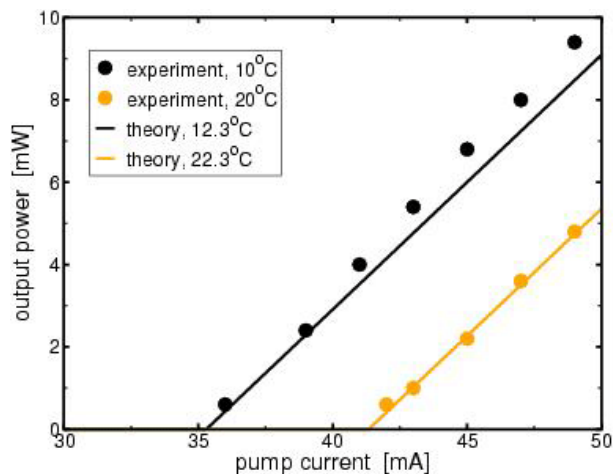


Figure 5.7: Comparison between experimental and theoretical L-I characteristics (from Ref. [3]).

For a ridge waveguide device based on this structure the threshold current densities were measured to be about 1.23 kA/cm^2 at 283 K and 1.45 kA/cm^2 at 293 K . Interpolating between the minimum threshold values for 275 K and 300 K , the analysis would predict threshold current densities of 1.22 kA/cm^2 and 1.44 kA/cm^2 for these temperatures, respectively, for an injection efficiency of 80%.

Typically, small difference between the theoretical and experimental values should be expected due to some spreading of the pump current in the device. Here we assumed the pumped quantum well area to be identical to the area of the top contact. Also, some internal heating should occur already at threshold. This could be accounted for by adjusting the injection efficiency. Similar agreement as found here could be achieved assuming an internal efficiency of 85% and a small additional heating of about 4K.

Please note that the results here differ somewhat from those in Ref. [3]. This is mostly due to the fact that in Ref. [3]) only spontaneous emission losses into TE-polarized light were included. Here we include losses into TE and TM modes assuming:

$$J_{rad} = \frac{2}{3} J_{TE,rad} + \frac{1}{3} J_{TM,rad}. \quad (5.3)$$

This leads in this case to a somewhat lower total radiative loss which is compensated for by assuming an injection efficiency that is 80% instead of 100% in Ref. [3].

The tool will always average the TE and TM losses using this formula if spontaneous emission losses for both polarizations are included in the database.

For devices with wavelength selective gratings the loss currents can be determined the same way. Only in this case the loss currents have to be looked up in the 'Current Calculator' at the wavelength determined through the grating and not at the wavelength of minimal losses.

The good agreement between theory and experiment is quite remarkable considering the very limited amount of adjustable parameters. The deviations from the nominal design (spectral detuning and inhomogeneous broadening) were obtained using simple, non-destructive low intensity surface-PL measurements. The only other parameters that needs to be known from the experiment is the internal loss and injection efficiency which can be obtained through cut-back experiments. These losses are usually rather insensitive to details of the structure or situational parameters, like carrier density or temperature. Thus, once they are known for one representative structure, they often can be transferred to investigations of various structures and physical situations without having to be re-measured. No other adjustments were done to all the parameters that are crucially sensitive to details of the structure and the physical situation, like, the gain, its density and spectral dependence or the radiative and Auger losses.

On the other hand, simpler models usually allow for additional fit-adjustments, like, usually, treating the Auger losses as an adjustable parameter. These adjustable parameters allow to **fit** rather featureless characteristics like the threshold. However, this requires the pre-existence of the experimental data and cannot **predict** any results correctly. It will also lead to wrong estimates for the underlying physics and, therefore, prohibit the model to be used to extrapolate to situations/structures that are not very similar to the one for which the experimental data already exists.

This found agreement also demonstrates the importance of correct material characteristics, like gain or Auger and radiative losses, for high quality device simulation. Without this correct input, simulations might wrongfully assume that deviations from the experiment are caused by processes that aren't really a dominant factor, like reduced carrier capture efficiencies or current spreading.

As shown in Fig.5.8, the tool also allows to display other threshold characteristics: the intrinsic carrier density, internal quantum efficiency, and the temperature dependent threshold current and internal quantum efficiency. The latter two are calculated for all temperatures that are included in the database (shown data is for 85% injection efficiency). Plotted together with them are exponential fits according to:

$$\begin{aligned} J_{thr}(T) &\propto \exp(T/T_0) \\ IQE_{thr}(T) &\propto \exp(-T/T_1). \end{aligned} \quad (5.4)$$

The internal quantum efficiency, IQE, at and below threshold is given by:

$$IQE = \frac{J_{rad}}{J_{total}}. \quad (5.5)$$

Input-Output Characteristics

For the calculation of the threshold characteristics as described above, internal heating is neglected. With this assumption the results are valid for optical and electrical pumping. For

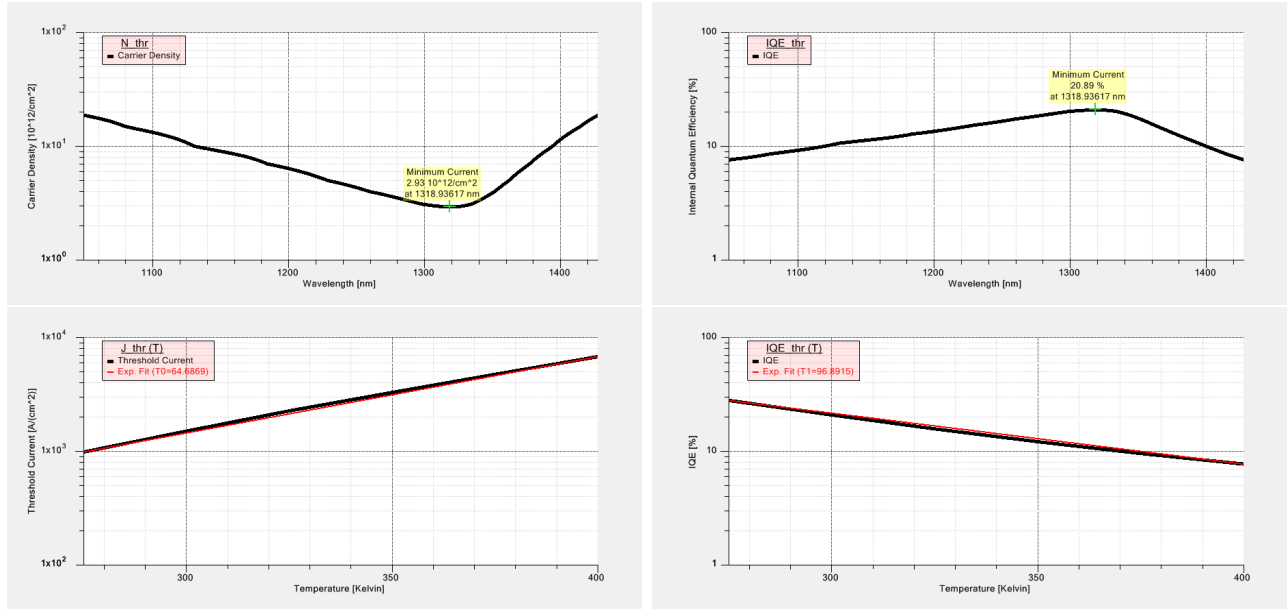


Figure 5.8: Threshold characteristics calculated using the 'Current Calculator' tool. Top left: intrinsic carrier density. Top right: internal quantum efficiency. Bottom left: threshold current as function of temperature. Bottom right: internal quantum efficiency as function of temperature.

operation above threshold the internal heating is crucially important since, e.g., it will lead to the eventual shut-off of the device.

Since **SimuLase**TM does not model the electrical pump-injection problem, various heating processes due to it, like Joule heating and Peltier-Thomson heating cannot be taken into account correctly. However, the current calculator tool allows to calculate the input-output characteristics, including the intrinsic heating, for the case of optical pumping. For electrical pumping, this tool can be used as a 'toy' model to study the tendencies of the dependence of the performance on various parameters, like the thermal impedance, number of wells or heat sink temperature.

Like the threshold model, this model requires input for the injection efficiency and optical loss. The model does not account for the temperature dependence of these quantities. Typically, the optical loss increases with increasing pump power and, thus, increasing internal temperature and carrier density. The injection efficiency decreases with pump power. Thus, if possible, these numbers should be adjusted depending on whether one is interested in characteristics near threshold or above threshold.

Besides the input required also for the threshold calculations described above - database, structure, optical loss, defect recombination time and injection efficiency (η_{inj}), the calculations of the input-output characteristics require some additional input to model the internal heating.

Here, the heat sink temperature is given by the temperature set on the 'Advanced' panel. A maximum pump current for which the data shall be calculated has to set in the field ' J_{max} '. The thermal impedance of the device has to be specified in the field ' R_{th} '. A pump wavelength has to be set in the field ' λ_p '.

In this model the operating characteristics are calculated from the power balance:

$$P_p = P_{out} + P_{heat} + P_{rest}, \quad (5.6)$$

Where P_p is the pump power, P_{out} the output power, P_{heat} power converted to heat and P_{rest}

power that is neither converted to heat nor to output power. P_{heat} is determined from the sum of power that goes to pump injected carriers that pass by the wells without being captured, P_{NA} , The excess energy (quantum defect) of carriers being captured into the wells, P_{qd} , Auger losses, P_{aug} , defect losses, P_{def} , and spontaneous emission from the wells that is re-absorbed in the device and converted to heat, $P_{\text{SE-H}}$:

$$P_{\text{heat}} = P_{\text{NA}} + P_{\text{qd}} + P_{\text{aug}} + P_{\text{def}} + P_{\text{SE-H}}$$

$$= \left(1 - \eta_{\text{inj}} \frac{\lambda_{\text{L}}}{\lambda_{\text{p}}}\right) P_{\text{p}} + W \left[\frac{1}{\tau_{\text{def}}} + \frac{1}{\tau_{\text{aug}}} + \frac{1 - \eta_{\text{SE}}}{\tau_{\text{SE}}} \right], \quad (5.7)$$

$$P_{\text{rest}} = \frac{W \eta_{\text{SE}}}{\tau_{\text{SE}}}. \quad (5.8)$$

Here, $W = N n_{\text{w}} \hbar \omega_{\text{L}}$, where N is the sheet carrier density, n_{w} the number of wells and $\hbar \omega_{\text{L}}$ the lasing energy. η_{SE} is the fraction of spontaneous emission that is emitted from the wells without being reabsorbed and contributing to heating. η_{inj} is the injection efficiency. τ_{aug} and τ_{SE} are the microscopically calculated Auger- and radiative lifetimes from the database, respectively. η_{SE} is the fraction of spontaneous emission that is not contributing to heating. The results are usually only very weakly dependent on η_{SE} . We use here a fixed value of $\eta_{\text{SE}} = 0.5$ assuming that 50% of the spontaneous emission escapes through the surface of the device.

The operating characteristics are determined directly from the balance of powers, $P_{\text{pump}} = P_{\text{out}} + P_{\text{heat}} + P_{\text{rest}}$, where P_{heat} is the amount of pump power that is converted to heat and P_{rest} is power lost to spontaneous emission that leaves the device without contributing to heating. For each temperature in the database the intrinsic carrier density at lasing is determined by looking for the density for which the gain is high enough to lead to enough gain to compensate for the optical losses as specified in 'Loss'. If a fixed lasing wavelength has been specified in the field λ_{L} , the gain has to be high enough at this wavelength. Otherwise, the gain maximum selects the lasing wavelength.

Then, the spontaneous emission, Auger and defect losses are calculated for this density. It is assumed that all these losses contribute to heating except for a fraction of the spontaneous emission that escapes the device. The results usually do not depend significantly on this fraction. We currently assume that 50% of the spontaneous emission escapes in all cases.

For each pump power, P_{pump} , additional heating losses are given by the amount of carriers that are not captured in the well, $P_{\text{pump}}(1 - \eta_{\text{inj}})$, and the quantum defect, P_{qd} , i.e. the difference between pump energy and lasing energy.

The intrinsic temperature increase due to this heating power, ΔT_{heat} is calculated using:

$$\Delta T_{\text{heat}} = P_{\text{heat}} R_{\text{th}}. \quad (5.9)$$

Finally, the operating point is determined by interpolating between the data for the fixed temperatures of the database in order to look up the temperature, T for which the heating losses lead to a temperature increase satisfying $T = T_{\text{HS}} + \Delta T_{\text{heat}}$. Here T_{HS} is the heat sink temperature. If such a temperature exists for a given pump power the device will lase with non-zero output power.

This model works for optically pumped devices. In electrically pumped devices there is of course no well defined pump wavelength. Carriers will also lose part of their energy to relaxation from the barrier into the wells, but the total energy loss depends on the positions of the Fermi levels, dopant levels and overall band bending due to space charges and applied Voltages - all of which

are pump current dependent. Joule heating and Thomson-Peltier heating are not taken into account. Thus, this model is not an exact tool for this situation. It should merely be seen as a help to estimate overall trends in the performance like their variation with optical losses, number of wells or heating as varied with the parameter λ_L .

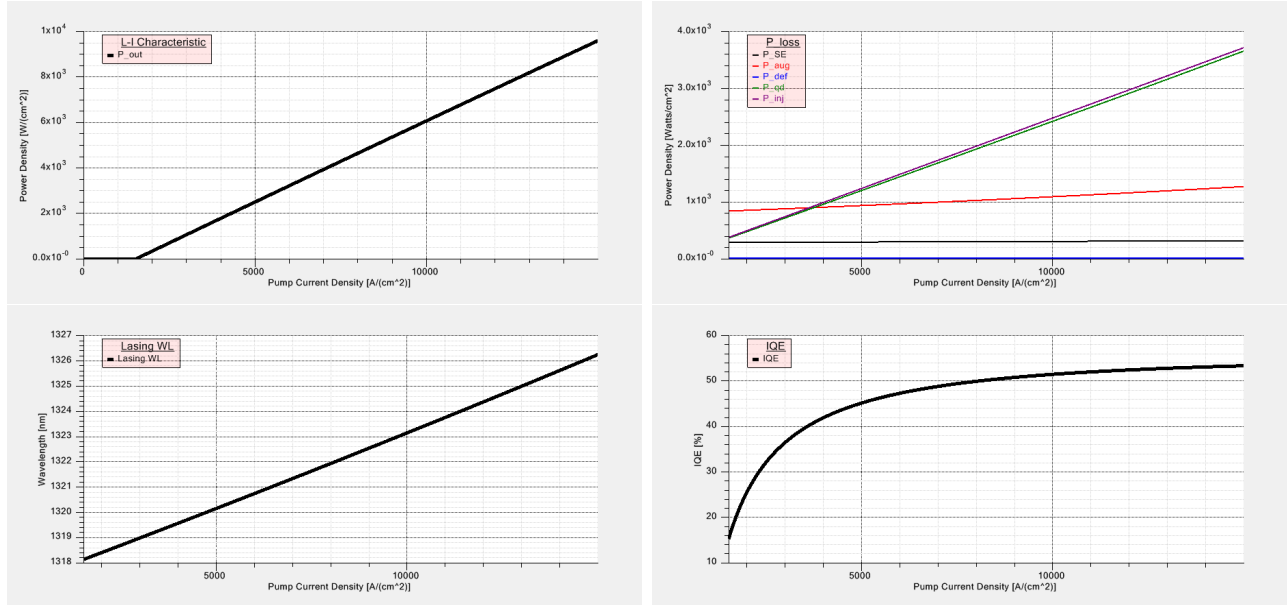


Figure 5.9: Operating characteristics calculated using the 'Current Calculator' tool assuming an injection efficiency of 80%, a thermal impedance of $0.3 \text{ mm}^2 \text{ K/W}$, a heat sink temperature of 293K and an optical loss of 1278/cm. Top left: output power. Top right: various power losses. Bottom left: lasing wavelength. Bottom right: internal quantum efficiency.

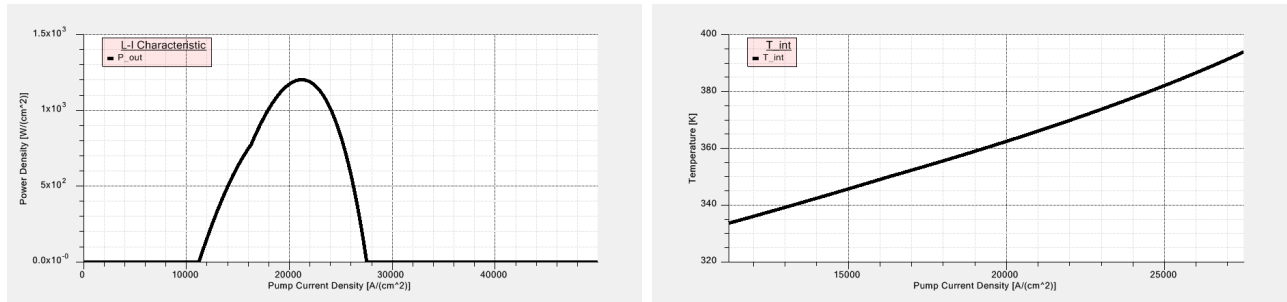


Figure 5.10: As Fig.5.9. Here, assuming an injection efficiency of 55% and an optical loss of 2100/cm. Left: output power. Right: intrinsic temperature.

For the structure investigated here, we find good agreement with the experiment for the threshold current and near-threshold slope efficiencies assuming a thermal impedance of $0.3 \text{ mm}^2 \text{ K/W}$, a pump lasing wavelength of 1000 nm, and the same injection efficiency (80%) and optical loss (1278/cm) as assumed in the threshold calculations. However, with these parameters the simulations do not show any device shut-off within a reasonable pump-current range. The output power is terminated only due to the numerics when the intrinsic temperature exceeds the temperature range for which the database was set up (400K).

This clearly indicates that the optical loss and injection efficiency degrade significantly at elevated pump levels. Shown in Fig.5.10 is an example where the output power is limited. Here, we

assumed an injection efficiency of only 55% and an optical loss of 2100/cm. Obviously, this leads to strong errors in the near-threshold characteristics.

For optically pumped devices the 'injection efficiency' takes on the place of the 'absorption efficiency'. As is explained in the example for an optically pumped VECSEL (Sec.5.2) this can be calculated rather easily from the calculated absorption spectra. Since in these devices no internal fields should be present, virtually all carriers that are absorbed in the active region will be captured into the wells if proper carrier confinement is provided through SCH or GRINSCH layers. The absorption efficiency varies usually negligibly with the intrinsic temperature or pump power.

Thus, for these cases, the 'injection/absorption efficiency' is no longer a rather free fit parameter. Also, the intrinsic losses usually vary not too much with pump power if the device is not doped - since this eliminates the free carrier absorption which is the main cause for the pump power dependence of the absorption loss. This should typically allow to use this tool very successfully for these situations with an accuracy as is demonstrated for the equivalent case of VECSELs in Sec.5.2.

5.1.5 STEP 5: How to Further Use the Data

The microscopically calculated data can also be imported into other simulation software like Crosslight Inc.'s **Lastip**TM or Synopsys Inc.'s **LaserMOD**TM for further evaluation of characteristics that go beyond the scope of **SimuLase**TM, like studies of electrical pump injection, far field broadening or other characteristics that require a model that takes into account in-plane inhomogeneities.

For interfacing **SimuLase**TM's data with Crosslight Inc.'s **Lastip**TM one has to export the GainDatabase into the format required by Lastip using the option '**File | Export Database as**'. **SimuLase**TM databases can be directly imported into Synopsys Inc.'s **LaserMOD**TM.

5.2 Vertical External Cavity Surface Emitting Laser (VECSEL)

VECSELs pose a very stringent test to the quality of a modeling tool. These devices are usually driven very hard which leads to internal heating to up to over 400 K at maximum output powers. The wavelength selectivity is provided by a DBR mirror and the resonant periodic gain region (RPG). With heating, the gain shifts spectrally due to the temperature dependence of the quantum well bandgaps. It also changes its lineshapes and amplitudes for a given carrier density due to the changes in the carrier distributions and the changes in the electron-electron and electron-phonon scattering. At the same time the resonance frequency of the RPG-region changes due to the temperature-induced refractive index changes. Ideally one would like to have the gain maximum to spectrally coincide with the resonance of the RPG region at the conditions of maximum output - i.e., at elevated temperatures and high carrier densities.

In order to be able to successfully model this system, the theory has to be able to predict the lineshape, amplitude and spectral position of the quantum well gain correctly for all temperatures and carrier densities. Since the measuring the PL is the best way to test whether the grown material has the desired wells, the theory also needs to be able to predict the PL and its spectral relation to the gain correctly. Carriers that do not contribute to the lasing but recombine due to Auger recombination or spontaneous emission contribute significantly to the heating of the device. Thus, the theory also needs to be able to predict these loss processes correctly.

Without models that can do all that, trying to develop a VECSEL for a given wavelength is destined to require many time and cost intensive iterations of designing, growing and processing, experimentally measuring, analyzing and re-designing. Even if an operating device is achieved, it will be unclear whether it is an optimized solution.

We at NLCSTR have been using the **SimuLase**TM software ourselves to design VECSELs very successfully. One example is the growth of a VECSEL for 1178 nm within a single design-growth iteration. Based on the design developed using the software the growers at NAsP III/V GmbH, Marburg, Germany, grew one wafer after the usual reactor calibration. Processed samples of this first wafer showed output powers up to 9 W . After intra-cavity frequency doubling the device showed powers of up to 5 W of 589 nm -yellow light emission (see Ref. [8] and our web-site for more information about this example).

Obviously, a complete VECSEL simulation requires modeling of more than the active region and the light propagation within the semiconductor material. It also involves modeling of the heat dissipation and light propagation in the full device - self-consistently with the carrier- and light-creation and losses. However, models for the heat dissipation and light propagation are rather insensitive to details of the active region and the quality of the results will always be far more crucially dependent on the correct microscopic input than the macroscopic modeling.

Here, we use the example of a (not fully optimized) VECSEL for high power operation at 1040 nm to show how **SimuLase**TM can be used to design and analyze such a device. Some of the results shown here can also be found in Ref. [9].

5.2.1 STEP 1: Setting Up the Structure

As in the case for the edge emitting structure, described in Sec.5.1, one should start setting up the structure with the 'quantized region', i.e. the layers for which the microscopic calculations of the gain/absorption and carrier losses, etc. are to be performed. Here, this region consists

of an 8 nm wide $In_{0.196}Ga_{0.894}As$ -well (layer 4) between 5 nm wide $GaAs$ -barriers (layers 3 and 5) and 5 nm wide $GaAs_{0.98}P_{0.02}$ -barriers (layer 2 and 6). A full period of the resonant periodic gain (RPG) region consists of this 'well' and 120.4 nm strain compensating $GaAs_{0.98}P_{0.02}$ -barrier (layer 1).

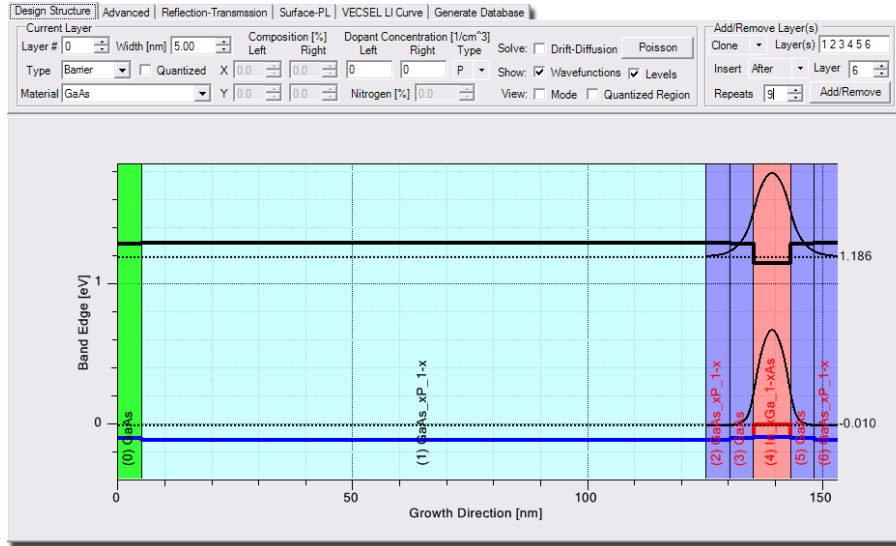


Figure 5.11: One repeat of the RPG-structure of the 1040 nm VECSEL (layers 1-6) including the 'quantized region' (layers 2-6).

Fig.5.11 shows the confinement potential of the first period of the RPG. Here, we also added temporarily a layer of $GaAs$ -substrate (layer 0) to see the influences of strain. Since the device shall be designed to have maximum output power at 1040 nm at an estimated internal temperature of about 375 K , one should set the 'Lattice Temperature' on the 'Advanced' options panel, [13a], to 375 K . Here, the well has been adjusted such that the lowest single particle transition energy at 375 K is at about 1040 nm .

We only include one well in the 'quantized region' for which the microscopic calculations will be performed and scale the results according to the actual number of wells afterwards. Also, we do not use the full RPG-period (layers 1-5) as the 'quantized region'. Instead, we reduced the thickness of the $GaAsP$ barrier layers by splitting them into one layer of 5 nm and another layer for the rest. As explained in Sec.6.5 and for the example of the edge emitter in Sec.5.1, this is one important way to reduce the calculation efforts without reducing the accuracy. To assign layers 2-6 to be the 'quantized region' one has to set the check-mark in field 'Quantized', [12e], for these layers.

Layer 4 contains the 'well'-material and has to be assigned the label 'Well' from the 'Type' selection, [12b]. Layers 1, 2, 3, 5 and 6 have to be assigned the 'Type' 'Barrier'. These labels are only used when the absorption/gain and carrier induced refractive index changes are assigned to 'well' and 'barrier' layers from the corresponding gain databases in the calculation of the longitudinal mode and the refraction and transmission spectra using the 'Reflection-Transmission' tool. The 'Type' 'Cladding' is for all layers that are not made of 'barrier' or 'well' material and cannot absorb at relevant wavelengths like $AlAs$ -layers in the DBR.

In order to make the full RPG region with 10 wells one should use the 'Clone'-option from the field [12p] and 'Insert' 'Layers 1 2 3 4 5 6' 'after' 'Layer 6' making 9 clones by selecting the number of 'Repeats', [12r], to be 9 (see the settings in Fig.5.11).

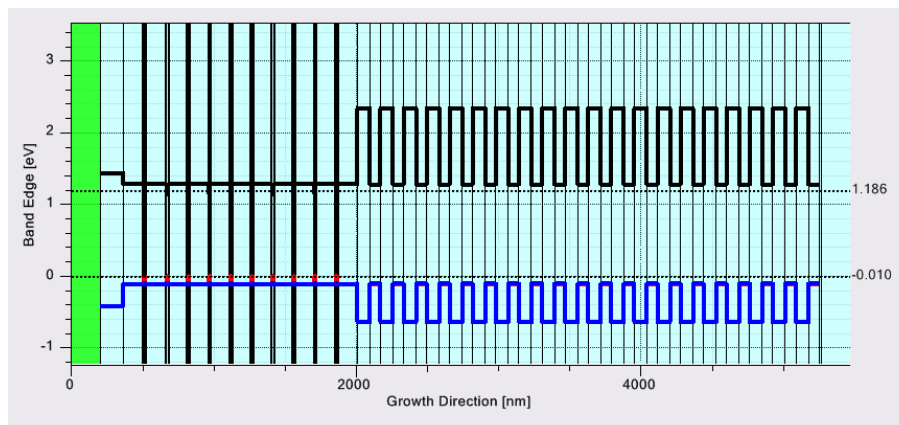


Figure 5.12: Confinement potential for the full 1040 *nm*-VECSEL structure.

Using the 'Clone' option rather than 'Copy' has the advantage that one can consistently change the material composition or width of layers in all clones by simply changing them in any one of them. This way, the RPG region can be easily modified in order to get, e.g., the cavity resonance at the desired spectral position.

After cloning the original RPG period, the 'Type's 'Well' and 'Barrier' are copied to the new layers. However, the 'Quantized'-mark is not. Thus, layers 2, 3, 4, 5 and 6 remain the only layers of the 'quantized region'.

After adding some carrier confinement and spacing layers (using the 'Copy' option), the DBR is added. Here again one should start with one period of the DBR and then use the 'Clone'-feature to create the other repeats. Then all periods of the DBR can easily be adjusted simultaneously in order to get, e.g., the stop band in the correct spectral position.

Fig.5.12 shows the confinement potential of the full structure. Layer 0 is made of air and we added metal layers behind the DBR. Air and metal layers are assigned the 'Type' 'Cladding'. Here, the DBR-repeats are made of *GaAs* and *AlAs* layers. The layer 'Type' for the *AlAs*-layers is 'Cladding' and the 'Type' of the *GaAs*-layers is 'Barrier' since the *GaAs*-layers are able to absorb the 808 *nm* pump light that is used in the experiment. All pump absorbing layers should be labeled either 'well' or 'barrier' in order to achieve the correct reflectivity.

At this point it is advisable to save the structure using the 'File | Save Structure' dialog. The structural information is saved in xlm-format in a *.sls file. This file can be read also using e.g., Windows Excel.

5.2.2 STEP 2: Setting up GainDatabases

The next step would be to investigate the longitudinal (propagating) mode and the reflection and transmission of the structure to see whether the nodes and anti-nodes are at the desired positions - like anti-nodes at the positions of the wells - and whether the DBR-stop-band covers the desired spectral region and the cavity resonance is at the correct position.

While one can do that right away, one should set up GainDatabases for the absorption/gain in the wells and the absorption in the barriers first. Without these, one can only study the unexcited case without pump carriers present. The pump carriers and the induced absorption/gain in the wells and barriers lead to changes in the refractive indices of these layers that shift and

modify the cavity resonance and longitudinal mode. For an accurate design of the device at the desired high power operation these changes should be included.

The main GainDatabase is the one for the wells, i.e., the 'quantized region' as it has been defined at the start of setting up the structure (layers 2, 3 4, 5 and 6 in Fig.5.11). The absorption/gain and carrier induced refractive index changes for this quantized region will be added to the background refractive index in all layers marked as 'Well' through the option 'Type' once the database is loaded into the 'Reflection-Transmission'-tool.

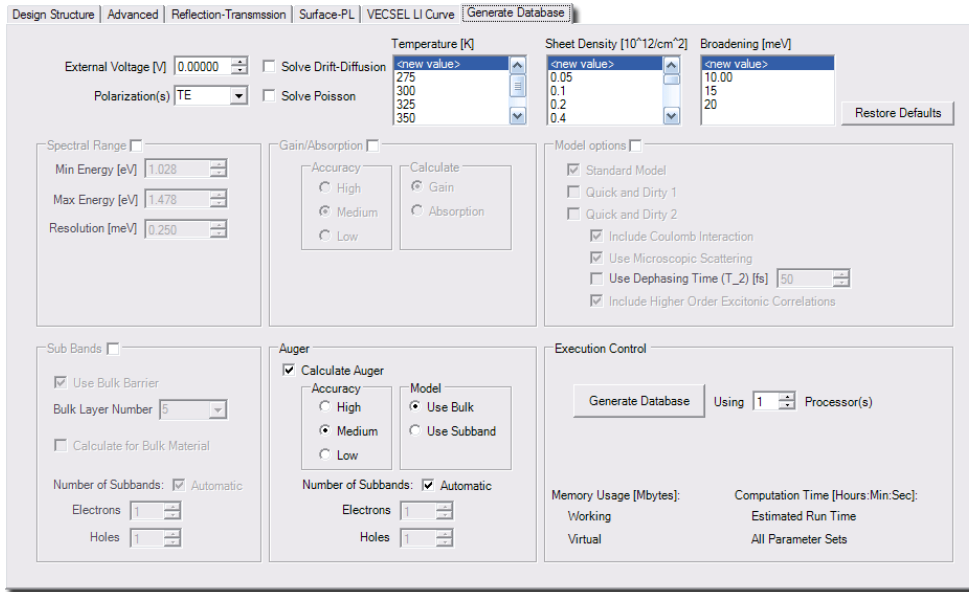


Figure 5.13: 'Generate Database'-panel with the settings for the calculation of the GainDatabase for the well-layers of the 1040 nm-VECSEL structure.

The database can be created with the full structure or just the partial structure as shown in Fig.5.11 in the 'Design Structure' window since both were set up to contain the same 'quantized region'.

Here, all options in the 'Generate Database' window that are not mentioned below can/should be left in their default configurations. Since Auger losses are important at this wavelength one should check the option 'Calculate Auger'. The only other fields that have to be specified are the values for 'Temperature', 'Sheet Density' and inhomogeneous 'Broadening'. For the purpose of this database we would suggest to calculate for temperatures of 275, 300, 325, 350, 375, and 400 K. A typical set of carrier densities would be 0.05, 0.1, 0.2, 0.4, 0.6, 0.9, 1.3, 1.8, 2.4, 3.1, 4.0, 5.0, 7.0, 10.0 and $14.0 \times 10^{12}/cm^2$.

Due to the large compressive strain in this structure the absorption/gain and PL near the bandedge is dominated by contributions from TE-polarization. Thus, and for simplicity of this example, we only set up the well database for this polarization.

The GainDatabase is set up taking into account the homogeneous broadening due to electron-electron and electron-phonon scatterings. The 'Broadening' as specified here is the additional inhomogeneous broadening due to growth fluctuations (see Sec.7.1.5 for details). The number of broadenings as specified here does not influence the calculation time significantly. To cover the typical range of growth conditions one might want to set the database up for broadenings of 10, 15 and 20 meV. Copies of the database for additional broadenings can also be created quickly afterwards using 'Tools | Shift and Broaden Database'.

For this set of parameters and this quantized region the calculation time on a typical laptop computer with one CPU takes about 15 hours.

One might not need that many temperatures and densities to just design the device for high power operation. For that purpose two temperatures near the expected high power operating temperature would be sufficient (two in order to allow for interpolations between them) and one would only need densities in the high gain region which is typically above about $3 \times 10^{12}/\text{cm}^2$. Additionally one low density is required (typically we use $0.05 \times 10^{12}/\text{cm}^2$) in order to be able to determine the change in the carrier induced refractive index. The latter is always calculated by the difference between the values for a given density and the lowest density contained in the database.

Setting up the more comprehensive database is usually worth while. One can then use the database also to analyze low density photo luminescence or to study the device characteristics over the full temperature and excitation range. It also limits possible errors due to interpolations between the datasets.

One often finds afterwards that one would like a database for a slightly different quantized region. This might be due to the fact that the gain maximum at high power operation is found to be not exactly at the desired lasing wavelength. One might also find from experimental measurements of, e.g., the low excitation PL, that the grown device differs slightly from the design. Usually, these changes only amount to small changes in the quantized region like a change in the (Indium-) composition in the quantum well by one or two percent. These deviations usually only amount to a shift of the bandedge transition energy. Other characteristics, like gain amplitudes as function of density or gain lineshapes are virtually un-affected by this. In this cases one does not have to set up a completely new database, but one can simply apply the determined spectral shift to the spectra in the existing database using 'Tools | Shift and Broaden Database'. The 'Reflection-Transmission'-tool includes an option to specify such a shift. Typically, if the required shift exceeds about 15 meV one should consider a re-calculation.

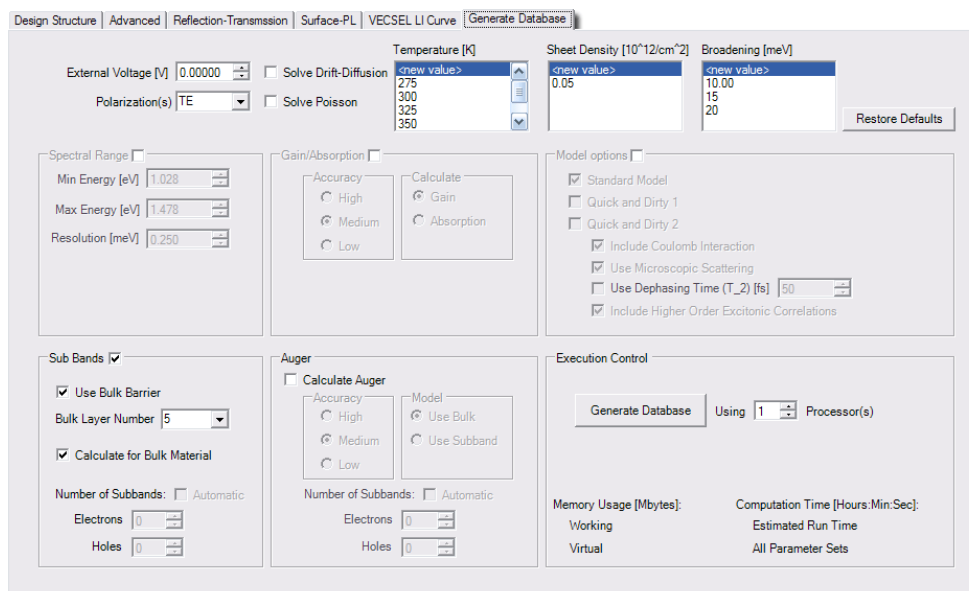


Figure 5.14: 'Generate Database'-panel with the settings for the calculation of the GainDatabase for the barrier-layers of the 1040 nm -VECSEL structure.

One might also want to set up an additional GainDatabase for the absorption in the barrier

layers. While this absorption usually has no significant influence on the characteristics at lasing wavelengths, it can influence the transmission and reflection near the high energy end of the DBR stop-band especially in the case of rather shallow wells. It can also be used to estimate the amount of pump-light that is absorbed in the RPG region.

This database is included in the 'Reflection-Transmission'-calculations through the option 'Use Pre-Computed Database for Barrier Material'. If it is included, the absorption is added to the imaginary part of the refractive index for all layers that are marked to be of 'Type' 'Barrier'.

Fig.5.14 shows the settings one should use for creating this database.

It is assumed that the carrier density in the barriers is negligible due to the large widths of these layers. Thus, this database only needs to be set up for one low density (we use typically $0.05 \times 10^{12}/\text{cm}^2$). It should be set up for the same temperatures as the database for the wells.

Since the carrier density of the barriers is assumed to be low, one can neglect Auger losses for this database.

Due to the width of the layers, the barrier material can be described best as bulk material. For this one has to check the options 'Use Bulk Barrier' and 'Calculate for Bulk Material'. In this structure the barrier is made of two materials, *GaAs* and *GaAs_{0.98}P_{0.02}*. Since the *GaAsP*-layers are much wider than the *GaAs*-layers we decided here to calculate for bulk-*GaAs_{0.98}P_{0.02}* by selecting a layer of the quantized region made of this material (layer 2 or 6 of the structure shown in Fig.5.11) through the field 'Bulk Layer Number'. Since the material properties like the bandgap are very similar for both kinds of materials, we designate this absorption also to the *GaAs*-layers when calculating reflection, transmission or modes. Since the device is pumped optically above the bandgap of both materials, we also use this absorption for both kinds of layers when estimating the pump absorption.

Setting up this GainDatabase only takes about 30 minutes on a single CPU.

5.2.3 STEP 3: Fine-Tuning the Structure

The 'Reflection-Transmission'-tool can be used for some fine-tuning of essential characteristics. For optimum operation one wants to check that the quantum wells are exactly at the anti-nodes of the longitudinal mode and that the mode has nodes or anti-nodes at some other interfaces. The stop-band of the DBR should cover the desired wavelength range and the cavity resonance of the RPG-region should be at the expected lasing wavelength.

Since the device is intended for high power operation these characteristics should be tested at the expected operating temperature and carrier densities. Thus, one should first load a GainDatabase that includes the data for the properties of the well material under the expected conditions. The absorption/gain is then added to the imaginary part of the refractive index in all layers labeled 'Well' by the option 'Type' on the 'Design Structure' window. The carrier induced refractive index change is added to the real part of the refractive index.

Fig.5.16 shows reflection and transmission spectra for the 1040 nm-VECSEL structure. If one calculates these spectra without taking into account the absorption/gain in the well layers one finds a flat stop-band with a small cavity resonance dip at the desired wavelength of 1040 nm (about 1.192 eV). This shows that the separation of the wells has been chosen correctly. The DBR stop band is at the correct position and wide enough to support operation over the whole expected range of conditions. Also, the reflection is high enough to avoid a noticeable optical loss.

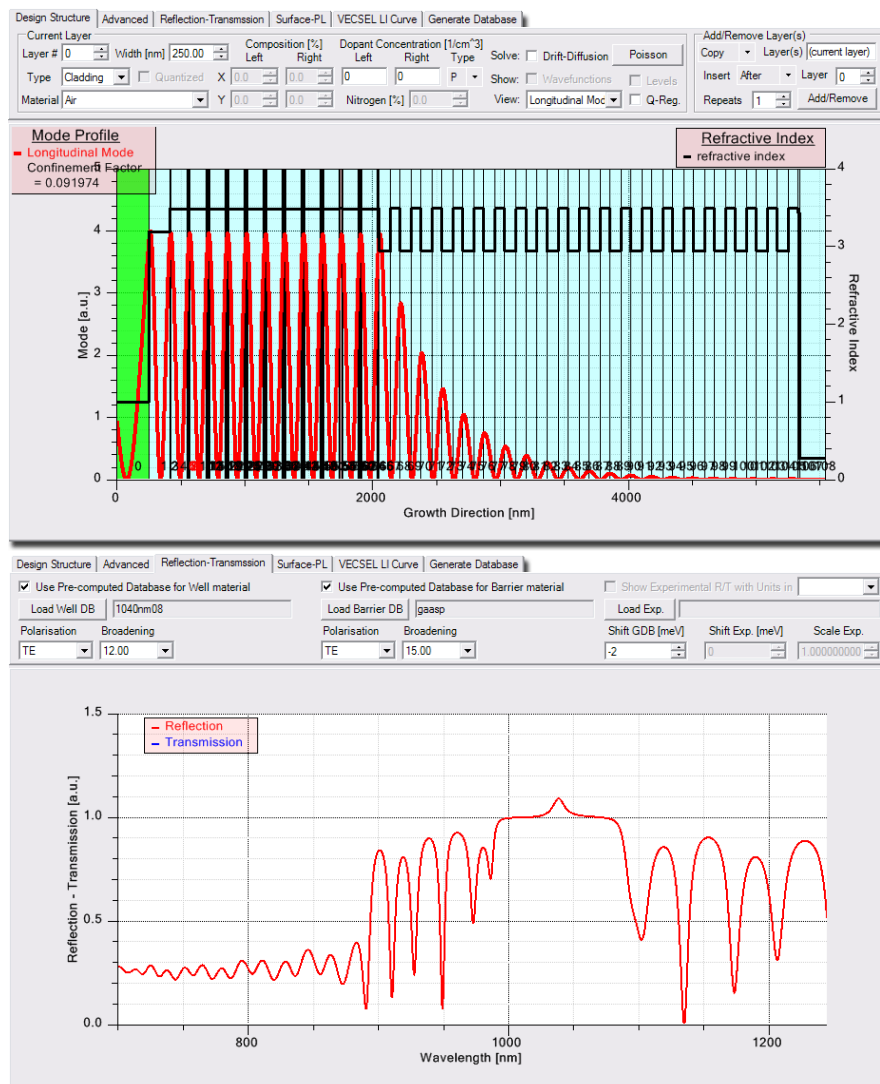


Figure 5.15: Top: Refractive index profile and longitudinal (propagating) mode for the full 1040 nm-VECSEL structure at 375 K, 1040 nm and a density of $5 \times 10^{12}/\text{cm}^2$. Bottom, reflection for the same conditions.

Including the database for the wells leads to a reduction or enhancement of the reflection at wavelengths where the well material has absorption or gain, respectively. In the low density limit the absorption spectra of the well show a well defined excitonic peak at the bandedge. This leads to a dip in the reflection at the excitonic transition energy - here, at about 1.229 eV (1009 nm) at 300 K. With increasing temperature the absorption bandedge shifts toward lower energies and eventually coincides with the cavity resonance. This leads to a strong enhancement of the cavity resonance and the absorption dip and cavity resonance are no longer distinguishable.

Once the density is increased (using the corresponding switch on the 'Advanced' panel) and gain occurs at the position of the cavity resonance the reflection at this wavelength becomes larger than one and light at this wavelength will be amplified. The peak of the reflection determines the lasing wavelength.

The enhancement of the reflection is the highest if the gain peak coincides with the cavity resonance. To see whether this is the case one can use the option 'Shift GDB' to shift the

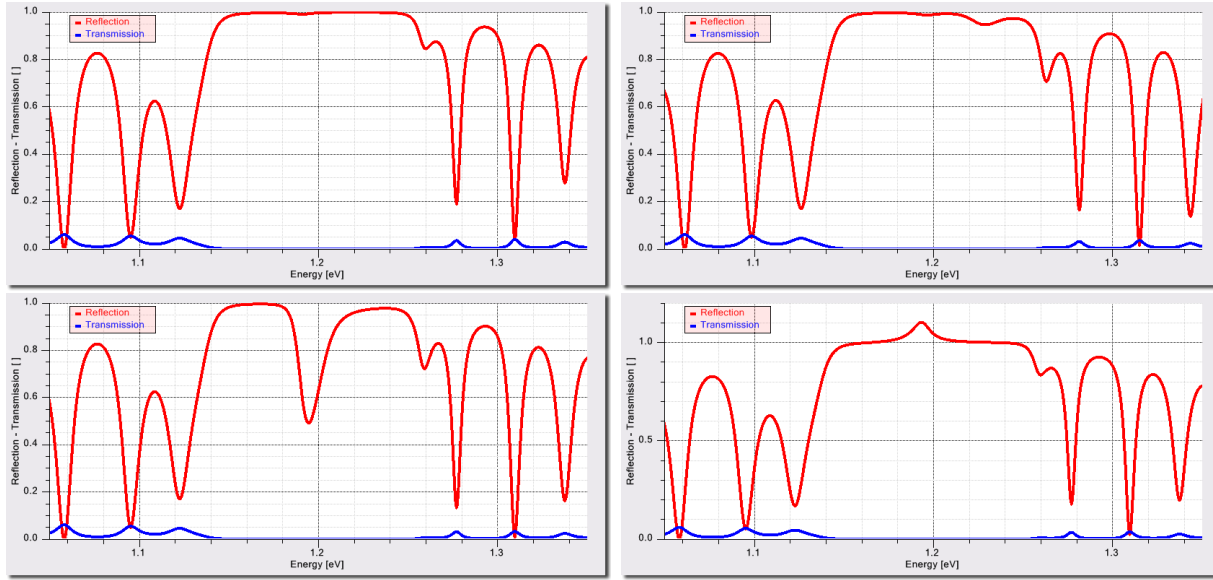


Figure 5.16: Reflection and transmission spectra of the 1040 *nm*-VECSEL. Top left: 375 *K*, without a database for the well. Top right: 300 *K*, with well-database and zero carrier density. Bottom left: 375 *K*, with well-database and zero density. Bottom right: 375 *K*, with well-database and a density of $5 \times 10^{12}/\text{cm}^2$.

absorption/gain spectra by a certain amount while checking whether the reflection peak increases or decreases.

Here, an out-coupling mirror with 94% reflectivity was used and the internal (surface scattering) loss is estimated to be 1%. Thus, for optimum high power operation one has to find the spectral shift for which the peak in the reflectivity reaches 1.07 at 375 *K* for the lowest carrier density. We find that a shift of the original database by about 15 *meV* would be required. The results shown in Fig.5.16 are for data that has been shifted by that amount. To realize this shift the Indium-composition in the well layers would have to be changed from 19.6% to 18.2%.

5.2.4 STEP 4: Comparison to the Experiment

While a complete modeling of characteristics of a VECSEL like the input-output power relation requires a model that combines the light propagation/amplification self consistently with the heat- and carrier dynamics (see e.g. Ref. [10]), many important characteristics can be evaluated just using the GainDatabases and the tools within **SimuLase**TM.

VECSEL devices with the structural layout as discussed here were grown at the Phillips University, Marburg, Germany, and processed and examined at the University of Arizona and by NLCSTR. The design of these devices did not include the additional shift of about 15 *meV* that has been found to be optimal in the reflectivity analysis discussed in Sec.5.2.3. Fig.5.17 shows the experimentally measured performance characteristics for one of these devices.

The first task when evaluating a grown device should be to determine how close the growth has met the design specifications. For a VECSEL the main characteristics that determine the final performance are the spectral position of the cavity resonance, the DBR stop band and the emission wavelength of the quantum wells. The first is given by the distance of the wells, the second by the thickness of the DBR layers and the last by the thickness and composition of the

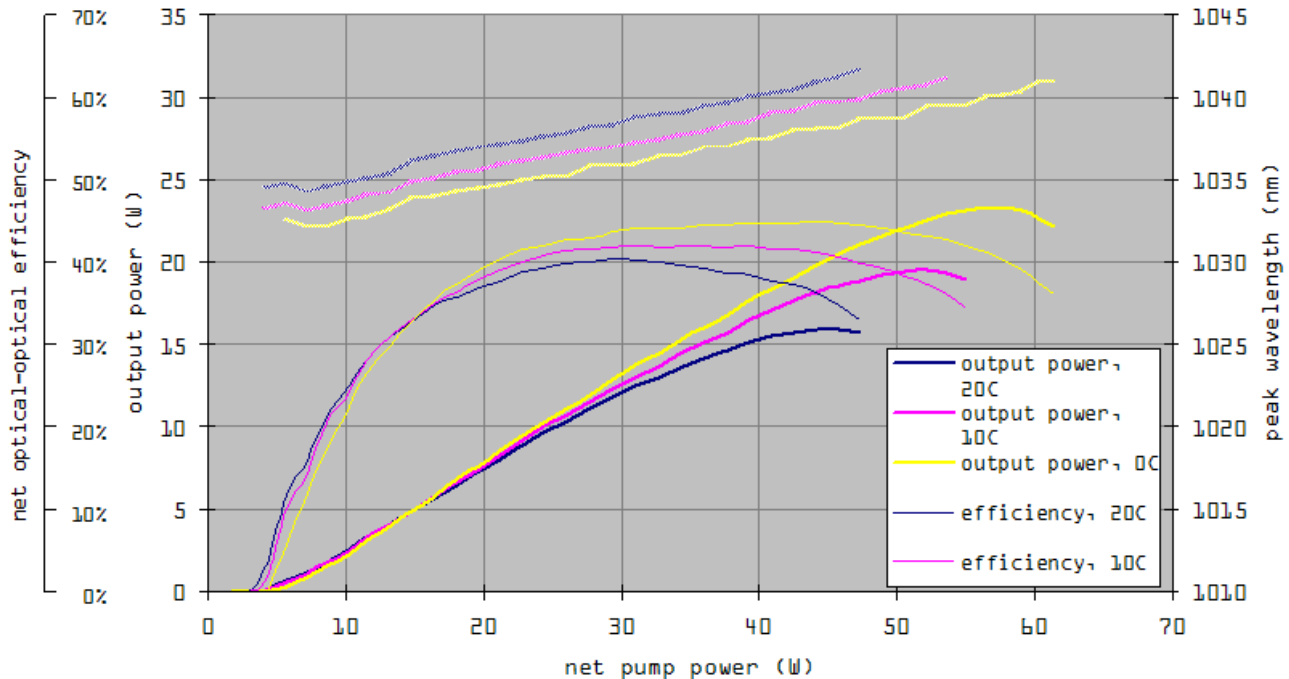


Figure 5.17: Experimentally measured output power, lasing wavelength and efficiency as function of the net pump power for the 1040 nm VECSEL. Here, an output coupling mirror with 94% reflectivity was used and a pump spot with a diameter of $550\mu\text{m}$.

wells.

Two rather easy measurements can be used to determine how close to the design these characteristics are in the grown device. One is to measure reflectivity spectra, the other is to measure surface PL. **SimuLaseTM**'s '**Reflection-Transmission**'- and '**Surface-PL**'-tool are designed to allow for an easy analysis of these characteristics.

Reflection Spectra

Fig.5.18 shows a comparison between measured and calculated reflection spectra for the 1040nm-VECSEL. The reflection was calculated including a GainDatabase for the quantum well absorption and one for the barrier absorption. Note that the reflection is calculated for the structure that is currently set up in the 'Design Structure' window and for the carrier density and temperature as set in the 'Advanced'-options panel.

The barrier absorption leads to the drop of the reflectivity and transmission for wavelengths shorter than about 870nm . The remaining reflection at shorter wavelengths comes from the surface reflection at the air interface.

Outside the DBR stop band of high reflection the agreement between theory and experiment is not very good. This is could in part be due to some calibration issues in the experiment which also leads to the deviations at the edges of the stop band. In general this is also caused by the fact that modes at wavelengths outside the stop band are not localized in the active region like the lasing modes shown e.g. in Fig.5.15. They are delocalized throughout the structure and influenced by all layers, from the top cap layer to the bottom metallization layers. Since these modes are not essential for the lasing operation we do not try to improve the agreement for these wavelengths by fine tuning all layers of the structure.

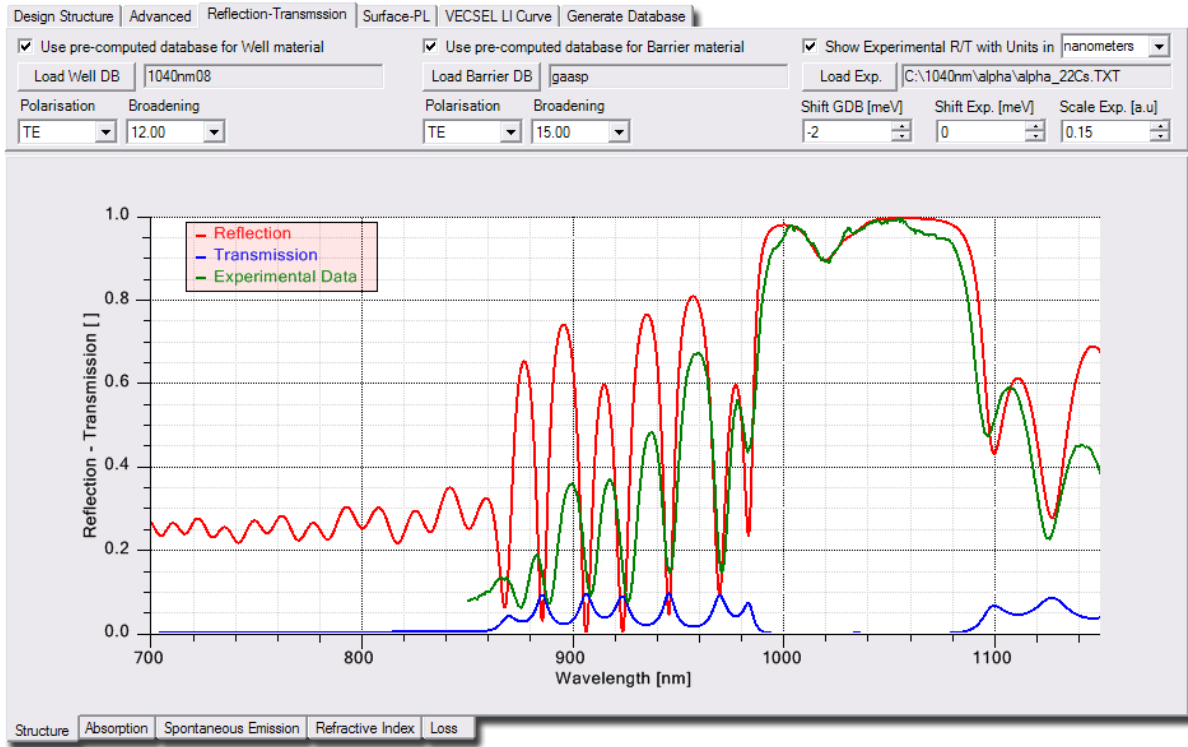


Figure 5.18: Comparison between experimentally measured and calculated reflectivity spectra for the 1040 nm VECSEL at 22°C and very weak excitation using **SimuLase**TM's 'Reflection-Transmission'-tool.

In order to get the agreement for the reflectivity as shown in Fig.5.19 we had to shift the DBR stop band by about 5 nm to longer wavelengths by increasing the thickness of the DBR layers by about 0.5%. The cavity resonance appears to be at the designed wavelength, about 1034 nm for this temperature, indicating that the well-separation as in the design. Finally, we had to shift the quantum well absorption spectra of the GainDatabase by -2 meV. This indicates a slightly lower indium-composition in the wells. Overall, the growth is found in very good agreement with the design.

As can be seen in Fig.5.19, the reflection analysis is very sensitive to details of the structure. Despite a rather low quality experimental spectrum, the location of cavity resonance and absorption bandedge can be precisely determined and even small deviations, like the 2 meV deviation from the calculated absorption can be easily determined.

Since the dip in the DBR stop band is due to a combination of the well absorption and the (empty) cavity resonance, it is neither at the wavelength of the absorption nor at the wavelength of the cavity resonance. This would make it almost impossible to determine the absorption or cavity resonance without knowing the material absorption precisely.

Surface-PL

Measuring PL-spectra from the surface of the device is one of the most commonly used tools to analyze semiconductor devices. In structures without strong cavity effects, like typical edge-emitting devices (see Sec.5.1.2), the surface PL is essentially identical to the pure material PL of the quantum wells that is calculated when setting up a GainDatabase. Here, a direct

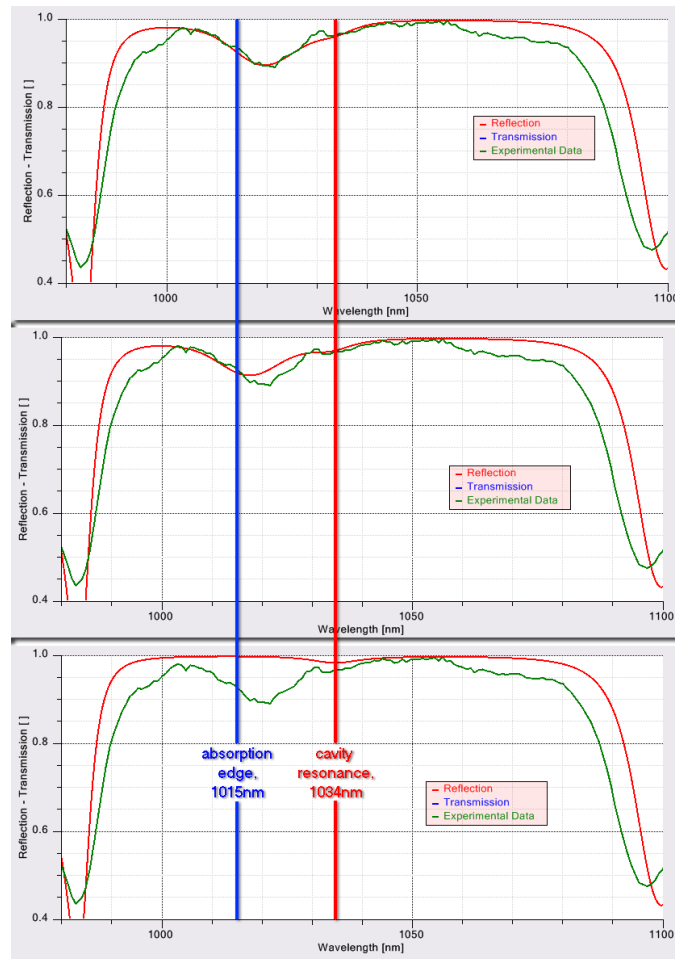


Figure 5.19: Comparison between measured and calculated reflectivity spectra. Top: After shifting the absorption in the GainDatabases by -2 meV . Middle: For original Gain-Database data. Bottom: Without quantum well absorption. The vertical red line marks the empty cavity wavelength, the blue line marks the excitonic absorption bandedge.

comparison between the calculated material PL and the PL measured from the surface gives valuable information about the quantum wells.

In structures with strong cavity effects, like V(E)CSELs, the PL is strongly modified on its way from the quantum wells to the surface by reflections at various interfaces and subsequent interferences. This can be seen for the example of the 1040 nm -VECSEL in Fig.5.20. Here, the cavity effects completely change the lineshape of the PL spectrum. The measured surface-PL has multiple maxima, none of them are at the position of the maximum of the material PL and the lineshape and width of the surface-PL peaks significantly differs from the one of the material PL.

To account for the cavity effects **SimuLase**TM uses the so-called 'Filter-Function Approach' (see Ref. [2]). Here the surface PL is given by the product of the pure material PL of the wells and a filter function that describes the modifications due to cavity effects. Please note that the filter function is calculated for the structure that is currently set up in the 'Design Structure'-window and for the temperature as set on the 'Advanced'-panel. The filter function is independent of the carrier density.

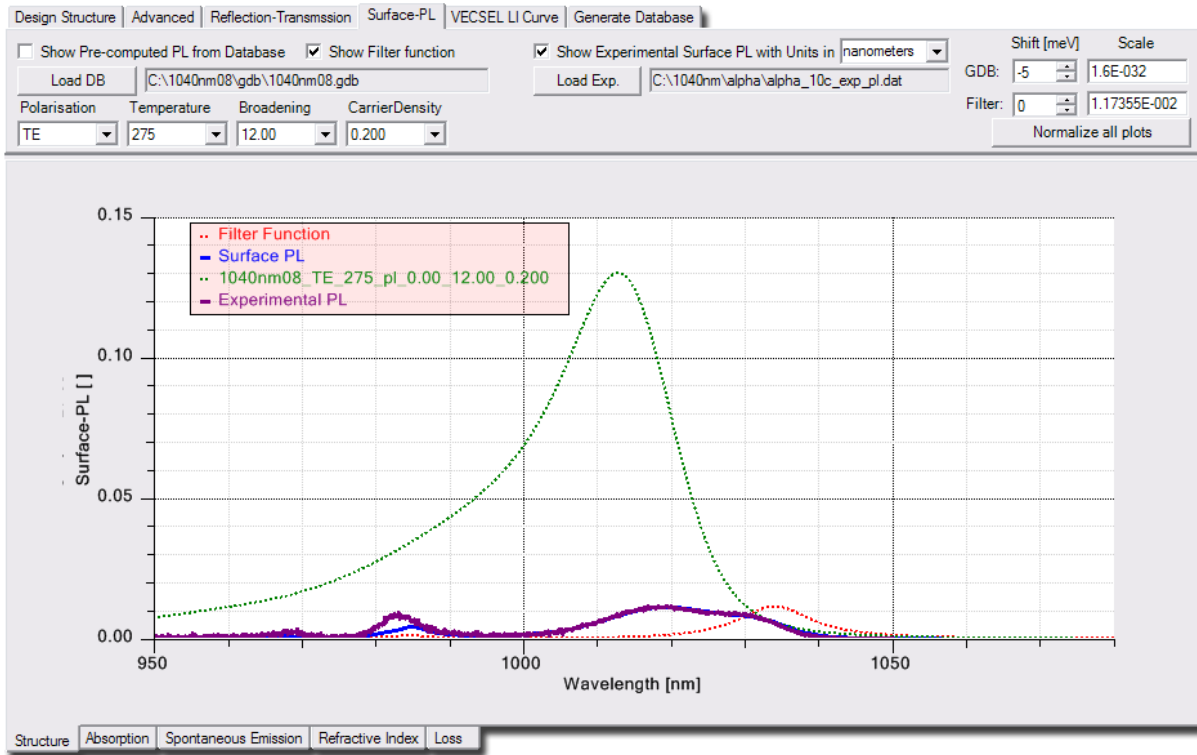


Figure 5.20: Comparison between experimental and calculated surface-PL spectra for the 1040 nm VECSEL at 10°C using **SimuLase**TM 's 'Surface-PL'-tool.

For the comparisons shown in Fig.5.21 the structure was modified according to the deviations between design and actual growth found through the reflectivity analysis. Especially, the same spectral shift has been applied to the pure material PL as the one already determined from the analysis of the reflection spectra. Since the GainDatabase was not set up for the same temperature as in the experiment we used instead the next closest temperature and applied an additional shift to the PL spectra to compensate for the temperature induced bandgap change. From the comparison we conclude an inhomogeneous broadening of the material PL of about 12 meV (FWHM). This indicates good growth quality with only small local fluctuations in the well width and composition.

The calculated surface-PL agrees very well with the measured one for wavelengths inside the DBR stop band and close to it. As has been seen for the reflectivity, for wavelengths outside this range (shorter than about 980 nm) the agreement is less accurate since the modes there are delocalized throughout the structure and we did not attempt to describe them with ultimate accuracy.

For 10°C, where material PL and cavity resonance are fairly detuned the lineshape of the surface-PL is rather complicated with a double-peak structure inside the stop band and a side peak at the short wavelength side of the DBR stop band. Neither peak is exactly at the position of the maximum of the material PL or the cavity resonance. This shows that an analysis of the surface PL will be quite inconclusive if the correct material PL is not known precisely. Especially, the result depends greatly on details of low and high energy tails of the material PL. Simplified models for calculating the PL will lead to strong errors in these details.

At higher temperatures the material PL and filter function are more resonant. Here the surface-PL is dominated by a single peak at the wavelength of the cavity resonance.

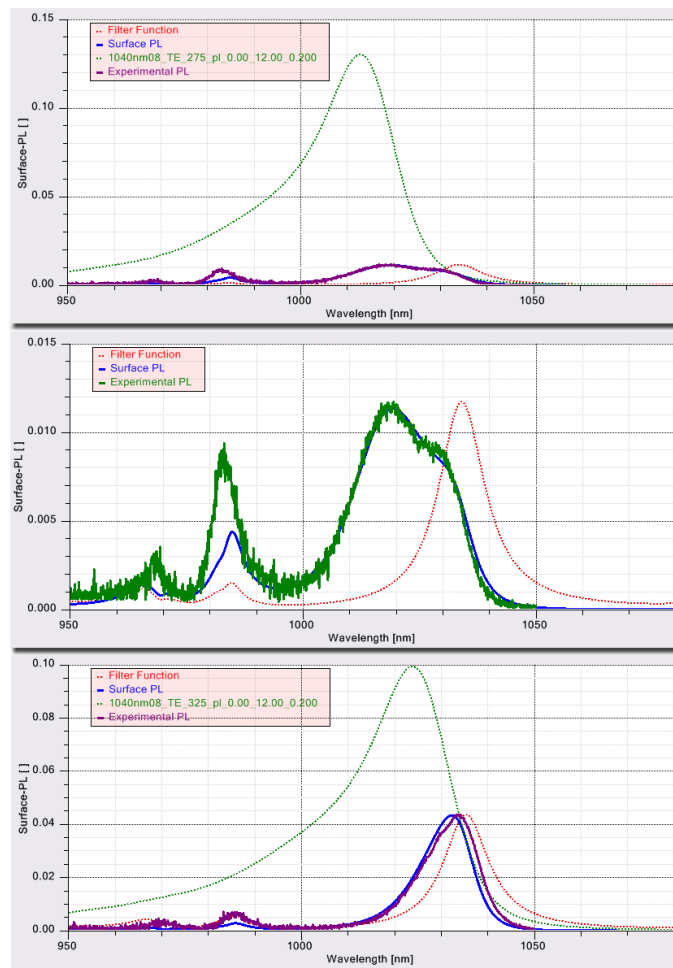


Figure 5.21: Experimental and calculated surface-PL spectra for the 1040 nm VECSEL. Top: At 10°C. Middle, as top, here without showing the material PL. Bottom: At 40°C.

It is noteworthy that the agreement for the surface-PL is achieved for the same deviations between design and actual growth as determined from the reflectivity analysis. As can be seen from the examples shown here, the surface-PL is very sensitive to exact lineshapes and spectral positions of the cavity resonance, the material PL and the DBR stop band. Thus the 'Surface-PL'-tool allows for a very accurate characterization of the device.

For the following results we applied this spectral shift and the determined inhomogeneous broadening to the database using 'Tools | Shift and Broaden Database'.

Lasing Wavelength

Fig.5.22 shows the calculated reflectivity peaks at various temperatures. In the experiment an out-coupling mirror was used that had a reflectivity of 94% (out-coupling loss $L_{out} = 0.06$) and the internal (surface scattering) loss, L_i , was estimated to be about 1%. Thus, for threshold the carrier density has to be high enough to give a maximum reflectivity of about 1.075 to fulfill the threshold condition $L \times R = 1.0$, where L is the total loss, $1 - L_i - L_{out}$, and R is the reflectivity of the chip. The results in Fig.5.22 are for these threshold carrier densities.

The lasing wavelength at threshold is given by the wavelength of the reflectivity peak. Here it is

at 1031.7 nm for 2°C , 1033.2 nm for 27°C and 1034.7 nm at 52°C . For the temperature that we expect at maximum operating powers, about 100°C , the lasing wavelength is about 1 nm below the desired wavelength of 1040 nm .

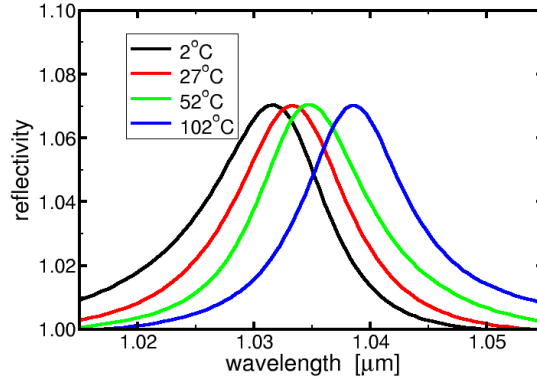


Figure 5.22: Calculated reflectivity at threshold carrier density for the 1040 nm VECSEL at various temperatures. (Data calculated with and exported from **SimuLaseTM** .)

In the measurement the lasing wavelength at threshold is found to be about 1033 nm for a heat sink temperature of 0°C and 1034.5 nm for 20°C (see Fig.5.17). Comparing these results to the theoretical numbers one finds agreement if one assumes that the internal temperature at threshold is about 25°C above the heat sink temperature. Using the GainDatabase in the frame of the comprehensive VECSEL model described in Ref. [10] we find indeed a heating at threshold of just about such an amount.

In the experiment the lasing wavelength at maximum power is found to be just above 1040 nm (see Fig.5.17) indicating that the active region of the device reaches temperatures of slightly above 100°C for these conditions.

Threshold Power

The threshold power, P_{thr} , can be estimated using the simple formula:

$$P_{thr} = \frac{N_{thr} N_w A_p \hbar \omega_p}{\eta_{abs} \tau_{tot}}, \quad (5.10)$$

where N_{thr} is the sheet carrier density per well at threshold, N_w the number of wells, A_p the pumped area, $\hbar \omega_p$ the energy of the pump light, η_{abs} the pump absorption efficiency and the total carrier lifetime τ_{tot} is connected to the lifetime due to defect-, radiative- and Auger-recombinations via:

$$\frac{1}{\tau_{tot}} = \frac{1}{\tau_{defect}} + \frac{1}{\tau_{rad}} + \frac{1}{\tau_{aug}}. \quad (5.11)$$

In the experiment the total loss due to out-coupling and surface scattering is about 7%. Thus, the threshold carrier density is determined by using the 'Reflectivity-Transmission'-tool to search for the carrier density that leads to a peak in the reflectivity spectrum of about 1.075. For the resulting threshold power one can look up the carrier lifetimes due to radiative and Auger losses,

τ_{rad} and τ_{aug} from the well-database on the 'Loss'-panel. Due to the good growth quality in these devices the defect recombination, $1/\tau_{defect}$, is negligible for densities near or above threshold.

The absorption efficiency is determined from the formula:

$$\eta_{abs} = 1 - \exp(-\alpha(\hbar\omega_p) w_{active}), \quad (5.12)$$

where w_{active} is the width of the active region (wells plus barriers) that can absorb the pump light. For $\alpha(\hbar\omega_p)$ we look up the absorption spectra from the database that we have set up for the barrier material. Here we find $\eta_{abs} = 0.796$ at $0^\circ C$ and it increases to $\eta_{abs} = 0.838$ at $100^\circ C$.

The threshold power can also be obtained using 'Tools | Current Calculator'. Here one has to load the GainDatabase that has been shifted by the -2 meV determined from the reflection analysis described above and inhomogeneously broadened by the amount of 12 meV determined through the PI-analysis. The correct value for 'Material Loss' can be looked up in the 'Absorption Window'. Here one has to search for the gain at the wavelength of the reflection peak (lasing wavelength) at threshold density. Since the GainDatabase has been set up for just one well, the value has to be multiplied by the number of wells in the structure. The 'Number of Wells' has to be set to the number of repeats of the 'quantized region' in the structure. Then, the threshold current density is displayed for various wavelengths.

This threshold current density, J_{thr} , is related to the threshold power, P_{thr} , through:

$$P_{thr} = J_{thr} \frac{A_p \hbar\omega_p}{e \eta_{abs}}, \quad (5.13)$$

For this conversion one can export the current density data using 'File | Export Dataset'.

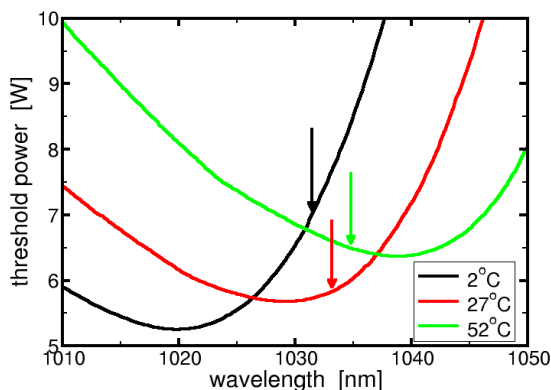


Figure 5.23: Threshold power for the 1040 nm-VECSEL as function of the lasing wavelength. Arrows indicate the actual lasing wavelengths. Data calculated using 'Tools | Current Calculator' and rescaled according to Eq.(5.13).

Fig.5.23 shows the resulting threshold powers for the 1040 nm-VECSEL. Within the scattering of the experiment the theory agrees very well with the experimental threshold values if one assumes the same internal heating above the heat sink temperature by about $25^\circ C$ that has been determined in the analysis of the lasing wavelengths. Assuming this heating the threshold power is about 5.9 W for a heat sink temperature of $0^\circ C$ and increases to about 6.5 W for a heat sink temperature of $20^\circ C$. Without this heating the threshold power would show the wrong

temperature dependence and wrong absolute numbers, decreasing from about 7.3 W at 0°C to about 6.2 W at 20°C .

The experimental pump powers at threshold are slightly smaller than in the calculation (see Fig.5.17). This is probably due to inhomogeneous pump absorption at these rather low pump levels. Wells closer to the surface absorb more carriers and reach threshold carrier density earlier than those further away. Effectively this means that the device reaches threshold operating with less than all wells. As can be seen from Eq.(5.10), such a reduced effective N_w leads to a reduced threshold power. It could also be that at threshold only parts of the pumped area are contributing to lasing. Thus, the effective A_p would be smaller.

At higher pump powers the pump absorption and carrier distribution over the active region become more homogeneous leading to a better agreement between theory and experiment.

In Sec.5.2.3 we found that the operating characteristics at maximum powers should be better if the design of the wells would be changed such that the absorption/gain is shifted to higher energies by about $10 - 15\text{ meV}$ (to shorter wavelengths by about $11 - 17\text{ nm}$). This corresponds to shifting the threshold power curves in Fig.5.23 by this amount while the lasing wavelength (arrows) stay at the same wavelength or leaving the curves at the same position while shifting the arrows to longer wavelengths. Obviously, this would lead to a strong increase of the threshold power. However, above threshold the increase of the internal temperature with pump power should be decreased which should lead to higher slope efficiency and allow to go to higher pump and output powers before thermal roll over.

Operating Characteristics

Finally, the operating characteristics can be calculated using the 'VECSEL LI-Curve' tool.

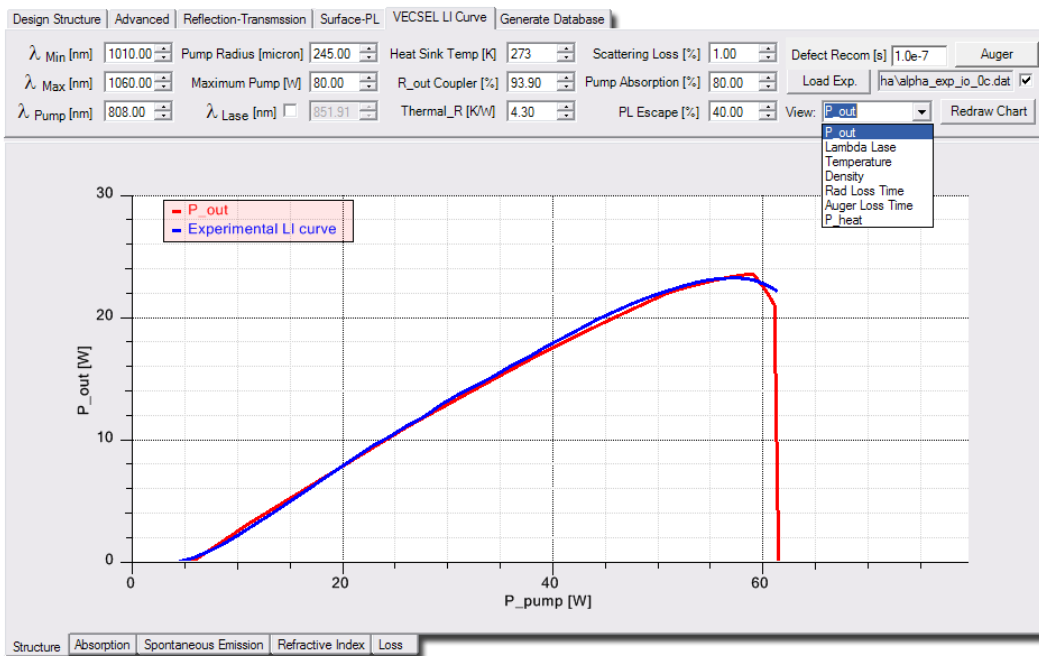


Figure 5.24: Input-output power characteristic for the 1040nm-VECSEL for a heat sink temperature of 273K. Red: calculated; Blue: imported experimental data.

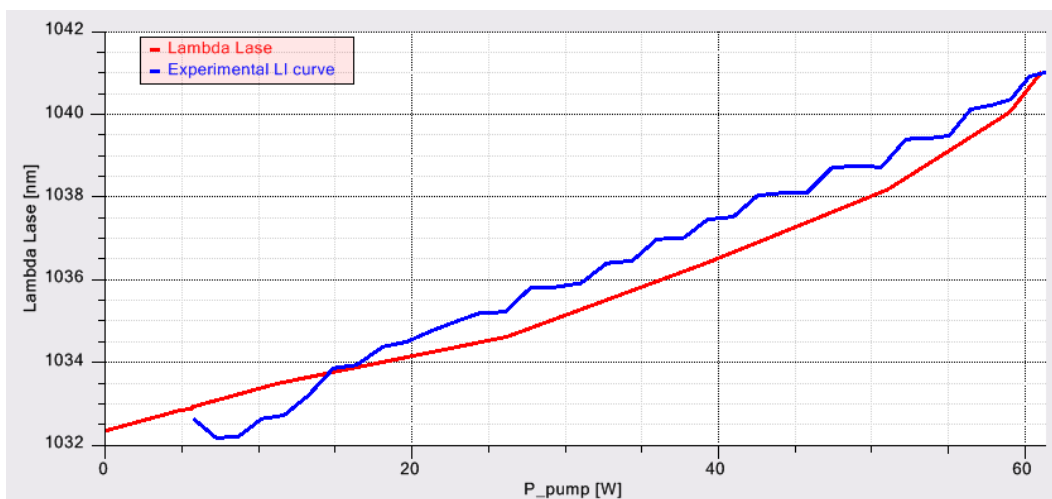


Figure 5.25: Lasing wavelength as function of the pump power for the 1040nm-VECSEL for a heat sink temperature of 273K. Red: calculated; Blue: imported experimental data.

Here, the characteristics are calculated for the structure currently set up in the '**Design Structure**' and using the GainDatabase for the wells as loaded through the '**Load Well DB**' option on the '**Reflection-Transmission**' panel. The polarization and inhomogeneous broadening, as well as the spectral shift of the well database are also taken over from the corresponding options ('**Polarization**', '**Broadening**' and '**Shift GDB**') on that panel.

The calculations are based on the rather simple one dimensional rate equation model as described in Ref. [10]. I.e., a (circular) top hat profile for the pump spot is assumed and the lasing mode is assumed to have the same shape and size. This simple model is most suitable for situations as here, where the pump spot size is rather large and high power operation is investigated. Then, lateral effects like carrier and heat diffusion from the pump spot into the un-pumped areas are rather negligible. Some deviations between theory and experiment usually occur near threshold with the experimental thresholds usually being lower than the experimental ones. This is caused by lateral and vertical pump inhomogenities. Some wells close to the surface will be pumped stronger than others leading to a situation that resembles one that has less wells. Also, unlike in the assumed top hat pump profile, real pump profiles have areas of higher pump intensity. Near threshold this can lead to lasing from a smaller area than the nominal total pump spot. At higher pump powers and correspondingly higher intrinsic temperatures the carriers become more evenly distributed over all wells due to higher carrier scattering rates and mobilities. Also, at powers high above threshold deviations from the average pump intensity become less significant and the pump profile can be better described by a top hat. An interpolation of the experimental characteristic from high powers down shows good agreement with the theoretical results and demonstrates the amount of deviations from the homogeneous situation in the real system.

Apart from the obvious parameters like pump radius, pump wavelength (' λ_{Pump} '), thermal impedance ('ThermalR'), pump absorption (η_{abs} in Eq.(5.12)), scattering loss (L_i in the discussion of the lasing wavelength), the out-coupling mirror reflectivity ('R_out Coupler', L_{out}), defect recombination time ('Defect Recomb', τ_{defect} in Eq.(5.11)) and the heat sink temperature the program also allows to specify the fraction of spontaneous emission that escapes the system versus the one that is re-absorbed in un-pumped areas outside the pump-spot ('PL Escape'). The number set here is the percentage of spontaneous emission (PL) that escapes the system. It is assumed that the re-absorbed fraction of the PL contributes to heating. This fraction can be calculated using ray-tracing software. For the example investigated here we found that about

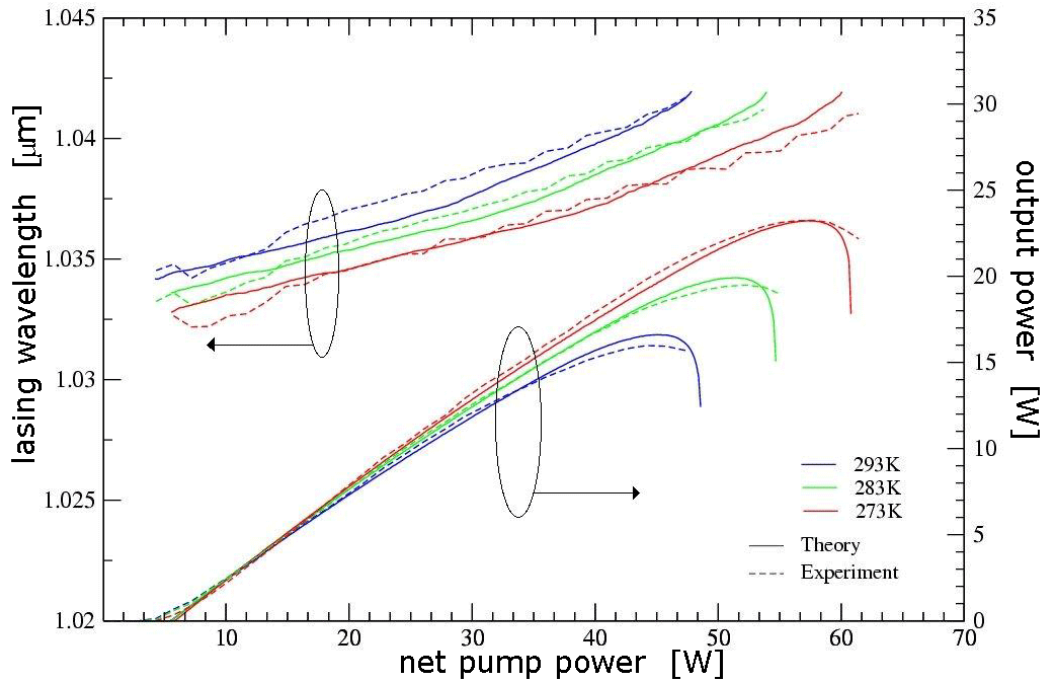


Figure 5.26: Comparison of theoretical and experimental output powers and wavelength shifts for the 1040 nm-VECSEL. Theoretical data calculated with and exported from **SimuLase**TM.

40% of the PL escapes the system. The results are not very critically dependent on this fraction. In our example, the maximum out-put power changes by about 10% when varying the fraction over the whole possible range. The influence on the threshold is even smaller.

The calculation time is only a few seconds. It can be reduced even further by limiting the spectral range that is taken into account in the calculation using the options $\lambda_{\text{Min/Max}}$. By default, the spectral range is set according to the spectral range for which the GainDatabase has been set up. Reducing the range typically speeds up the calculation by about a factor of two. Setting the range one has to make sure that it includes all lasing wavelengths for all possible pump powers. Otherwise the correct solution will not be found.

As shown in Fig.5.26, theory and experiment agree remarkably well for absolute numbers and temperature dependence of all operating characteristics.

For the agreement shown here it was important to include the correct barrier absorption. Only about 80% of the pump light that enters the device is absorbed in the active region and contributes to pumping the wells. The rest enters the DBR layers which are in this case absorbing the pump light. This leads to a reduced efficiency. The pump light that is lost into the DBR acts as a heat source there which further degrades the performance. Overall, the loss of pump light into the barrier reduces the maximum achievable power by about 50%.

The theoretical results are extremely sensitive to many aspects like the correct spectral position of the well-absorption/gain, the correct prediction of the gain amplitude at the lasing wavelength and the correct prediction of the density that is required to overcome the losses (threshold density) as well as the temperature dependence of all these quantities. Errors in the threshold density will be even further amplified if the models for the radiative and Auger losses are incorrect since these quantities depend even stronger on the carrier density than the gain.

As will be shown in more detail in Secs.5.3 and 7.2, less sophisticated models than the fully microscopic models implemented in **SimuLaseTM** usually result in uncontrolled errors of factors of two or more for quantities like threshold density or radiative and Auger losses and assume wrong dependencies for their density and temperature dependence. In order to compensate for these errors simplified models introduce fit parameters like loss constants for radiative and Auger losses and their dependencies.

SimuLaseTM does not require or allow any such adjustable fit parameters which makes its results truly predictive and an theory-experiment agreement as shown here truly remarkable.

5.3 Summary

Using the tools in **SimuLase**TM allows to design and analyze semiconductor devices effectively and with high accuracy. For the example of a 1040 nm-VECSEL we showed how they can be used, e.g., to:

- Design RPG and DBR regions for specific wavelength applications;
- Determine the optimal detuning between cavity resonance and absorption edge;
- Determine growth inhomogeneities using PL-analysis;
- Determine deviations from the nominal layer thicknesses and compositions using reflection- and PL-analysis;
- Predict the correct operating characteristics like output-power or the lasing wavelength;
- Show reliably how to optimize devices and
- how close an existing device is to an optimum solution.

Thanks to the predictive quality of the microscopic calculations all these results can be obtained with unprecedented accuracy and without introducing additional fit parameters like radiative or Auger recombination coefficients.

Predicting a quantity like the threshold power and its temperature dependence correct requires all ingredients of the model to be extremely accurate.

If the gain model fails to predict the threshold density correct the resulting radiative and Auger losses will be off even more. Since these losses increase stronger with the density than the gain, an error of just 20% in the threshold density will result in an error in the threshold power by about 50% or more. As is demonstrated in Sec.7.2, models for the gain that do not calculate the electron-electron and electron-phonon scattering processes on a microscopic level can easily lead to an error in the threshold density by a factor of two.

Using a simplified model for the spontaneous emission (PL) like the Kubo Martin Schwinger relation usually results in an error for the radiative loss at a given density of the order of a factor of two (see Sec.7.2). It also leads to errors in the lineshape that make a PL-analysis less conclusive. The latter is especially significant in a surface-PL analysis as shown for the VECSEL in Sec.5.2.4 where the measured PL is dominated by the high and low energy tails of the material PL.

The density and temperature dependencies that are assumed in simple models for the radiative and Auger losses, like the classical power law $J = AN + BN^2 + CN^3$, are far from reality (see e.g. Sec.7.2 and Refs. [5,6]). The density dependence for the radiative losses in the high carrier density regime in which VECSELs are usually operated tends to be closer to be linear than the quadratic BN^2 law. The density dependence for Auger losses in this regime is also lower than the cubic assumption CN^3 and typically only quadratic.

Since such simplified models cannot predict the operating characteristics correctly one has to introduce additional fit parameters in order to be able to reproduce experimental results. Such parameters include the loss constants B and C as well as additional parameters for their temperature dependence. Other models include, e.g., lineshape broadenings for the gain and PL. Even if one is able to reproduce experimental results using such parameters, the underlying physics will be described incorrectly.

Even if a fit to some existing experimental data was successful with a simplified model one usually cannot use the determined parameters to extrapolate to other situations than the ones

in the experiment. E.g., since the density and temperature dependencies are wrong in these models one cannot reliably use them to determine high power characteristics from a low power measurement. Since the underlying physical processes are usually very sensitive to structural details like well and barrier compositions or widths, one also cannot use the simplified models to evaluate reliably changes of characteristics due to changes in the structural design.

SimuLaseTM is the only commercially available software that includes all the microscopic models that are required for such a highly accurate, quantitatively predictive design and analysis as demonstrated here. For further studies that include e.g. investigations of details like carrier/current- and heat diffusion, **SimuLaseTM** allows to easily implement the GainDatabase results into other commercially available software packages using the option File | Export Database as. A ready to use interface with Crosslight Inc.'s software **LastipTM** already exists.

Current models for those macroscopic properties that determine characteristics like far field broadening, current filamentation or thermal lensing are usually very reliable and accurate. Thus, the overall error of such simulations is usually dominated by the errors that are introduced by using simplified models for the underlying microscopic properties. Therefore, **SimuLaseTM**'s GainDatabases offer the ideal - if not required - starting point for such investigations.

6 Important Tips for Optimal Usage

6.1 System Requirements

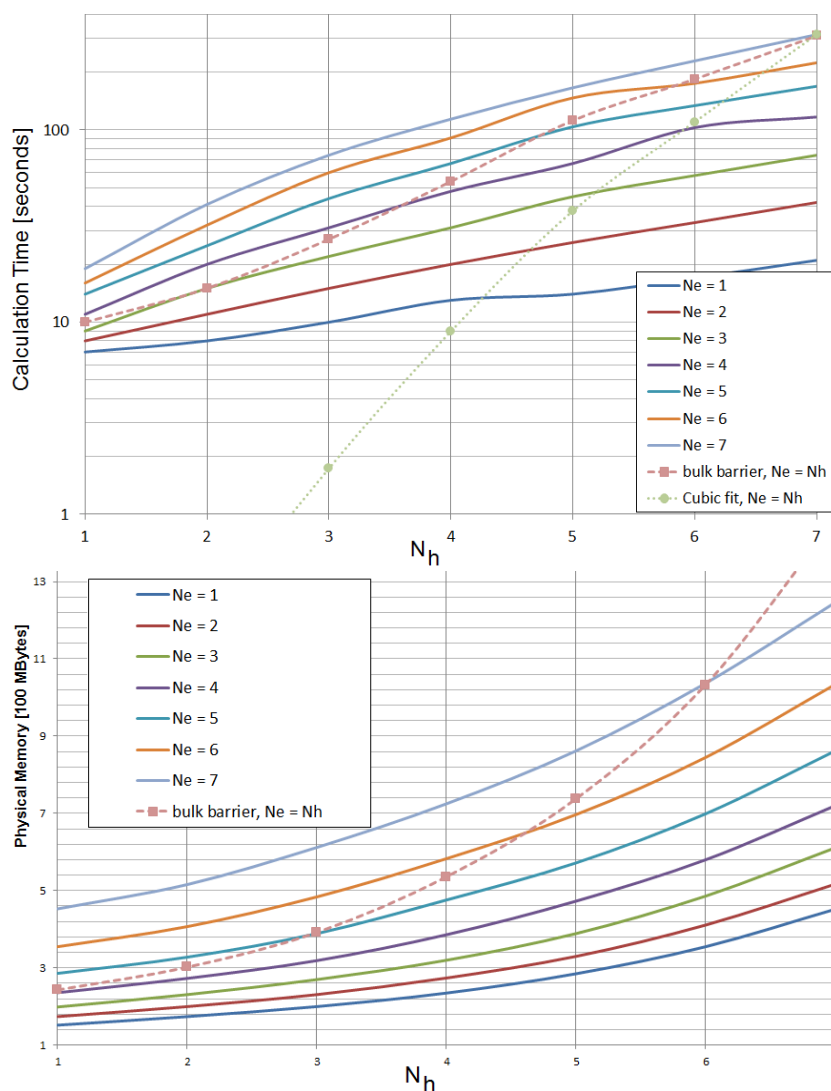


Figure 6.1: Time and memory required to calculate GainDatabase-data for one temperature and carrier density using 'Medium' accuracy, the 'Gain' and 'Standard Model' and varying numbers of electron and hole subbands (N_e and N_h). Solid lines: not using the 'Bulk Barrier Model'. Red symbols: using the 'Bulk Barrier Model' and $N_e = N_h$.

The system requirements for **SimuLase**TM are minimal except for setting up GainDatabases. The program itself, as well as all included tools for displaying and analyzing data or setting up

structures return results virtually instantaneously and require minimal CPU memory. They can be run on any laptop computer or workstation.

However, the microscopic calculations that have to be performed to set up GainDatabases can require substantial CPU time and memory and both increase dramatically with the number of included subbands. Fig.6.1 shows calculation times and memory requirements on a 2013 Intel Xion E5-2690 with 2.9 GHz processor speed running Windows 7 (last evaluation: 2014). These results are for calculating GainDatabase-data without Auger or intraband absorption calculation for one combination of entries in the field selecting polarizations, densities, temperatures,... Here, the model options '**Medium**' accuracy, '**Gain**', and '**Standard Model**' were used. Calculations were performed on one core and without the use of GPUs.

The calculation time increases by about a factor of five when the '**Accuracy**'-level for the '**Absorption/Gain**'-calculation is increased. The calculation time increases by about a factor of three when switching from the '**Gain**'-model to the '**Absorption**'-model.

The Auger calculation generally takes only a few tens of percents of the total calculation time if the same '**Accuracy**'-levels are used.

Intraband absorption calculations can be comparable in calculation time to the absorption/gain calculations. For more time intensive situations, time spent on the intraband absorption becomes less relevant.

The internal variables with by far the biggest influence on the system requirements are the number of electron and hole subbands, N_e and N_h . All other variables, like the variables defining the spectral resolution, typically change the required memory and calculation time only by less than a factor of two.

As shown in Fig.6.1, the calculation time rises almost with the third power of the number of subbands. In the limit of high numbers of subbands (here, $N_e = N_h \geq 4$) a cubic fit to the calculation time coincides almost perfectly with the calculation times for $N_e = N_h$.

The calculation time also increases with decreasing temperature. At lower temperatures more internal grid points have to be used in order to resolve the energetically sharper features like more step-like distribution functions. Typically, a calculation at 200K takes three times as long as a calculation at 300K. For temperatures above 300K the calculation time becomes nearly temperature independent.

The required memory increases by almost one order of magnitude when switching from '**Low**' to '**Medium**' '**Accuracy**'. When switching from '**Medium**' to '**High**' '**Accuracy**' the required memory typically increases by a factor of the order of two to three.

For very high numbers of subbands the required memory can reach the GigaByte level and it scales about with the third power of the number of subbands. If the '**Bulk Barrier Model**' is used (see [17p] and Sec.6.7.4) one electron and three hole bulk bands are considered in the calculation in addition to the confined subbands. This increases the system requirements somewhat. However, using this model usually reduces the number of subbands required to resolve the desired spectral range considerably, leading to overall strongly reduced calculation times and memory requirements for a given structure.

The required memory also increases with decreasing temperature due to the same reasons as mentioned above for the calculation time. As for the calculation time, the required memory about triples when going from 300K to 200K and becomes about temperature independent above 300K.

As shown in Fig.6.1, the system requirements are drastically reduced if the models '**Quick and Dirty**' 1 or 2 are used instead of the '**Standard Model**'. However, we strongly recommend

to use these models only for 'Quick' and 'Dirty' estimates, not for calculations intended for serious applications.

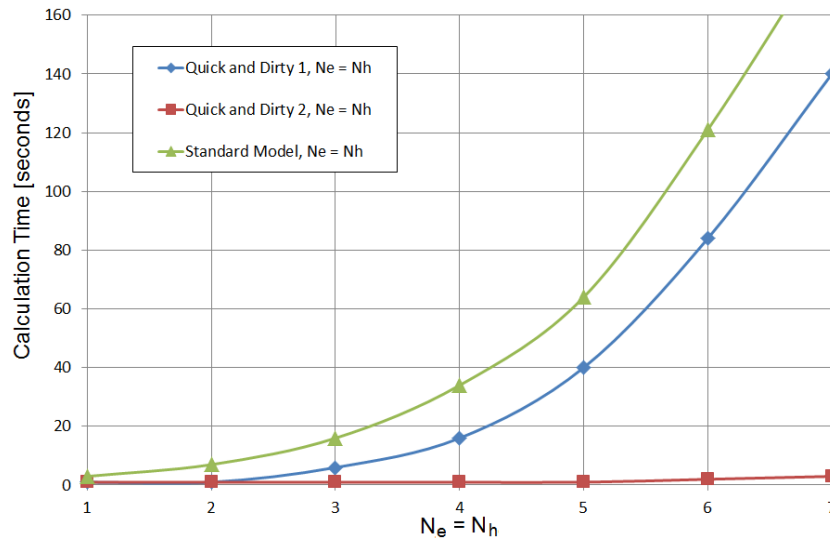


Figure 6.2: Time and memory to calculate GainDatabase-data for one temperature and one carrier density as function of the number of subbands using the models 'Quick and Dirty 1' and '2' as compared to the 'Standard' model. Here, the 'Bulk Barrier Model' was not used.

Storage space for GainDatabases is fairly minor for today's typical storage capacities. The GainDatabase data for one temperature and carrier density usually amounts to less than a hundred kilo-bytes. For a complete GainDatabase, including about ten densities, five temperatures and TE and TM polarization this can amount to maybe a few ten mega-bytes. Even if calculations are done for several structures and several shifted and broadened copies of the data are created the total amount rarely exceeds a few hundred mega-bytes for all possible variations one might be interested in for a particular structure.

Even for such large amounts of data, investigating all this data with the tools included in **SimuLase**TM hardly ever leads to noticeable slow-downs of the program.

6.2 Use of GPUs

SimuLaseTM Version 2.0 and later offers the option to use graphical processor units (GPUs). These allow to highly parallelize certain time-consuming functions in the code. In Version 2.0, the functions that have been implemented on GPUs are the Coulomb sums in the calculation of the optical and photon-assisted polarizations (Eqs. (7.2)-(7.4)). These are the dominant time-consuming functions in the limit of large numbers of subbands.

The implementation on GPUs allows to speed these functions up by about a factor of ten. The speed-up through the use of GPUs depends on the required number of subbands (see Fig.6.3). At low numbers of subbands, the resulting overall speed-up for these cases is typically a few tens of percents. For high numbers of subbands the use of GPUs reduces the calculation times by more than a factor of two when using the 'Absorption' model and more than a factor of four when the 'Gain' model is used.

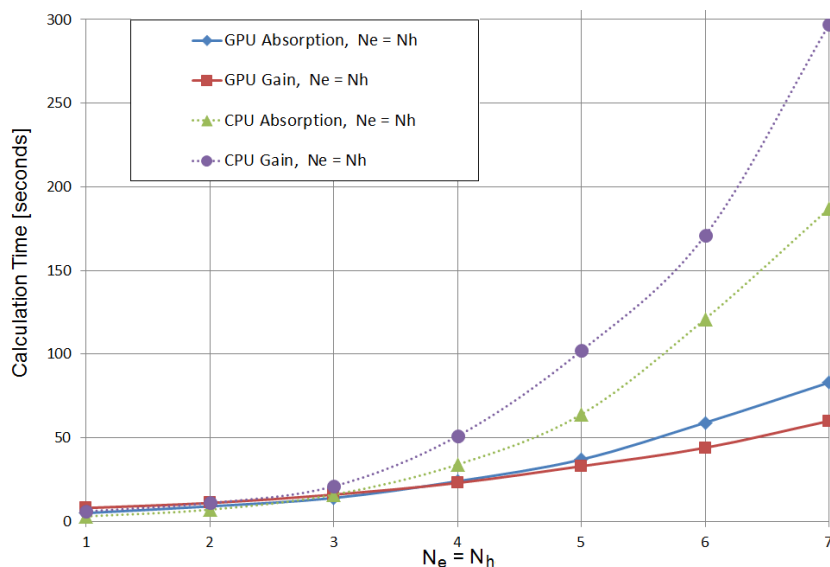


Figure 6.3: Comparison of calculation times for equal numbers of electron and hole subbands, with and without using GPUs. Here, 'Medium' accuracy and the 'Standard' model were used and the 'Bulk Barrier' model was not used.

SimuLase™ determines automatically the amount of available GPU hardware. It allows to select one or multiple of the GPUs before a gain database is set up and automatically distributes the calculation effort for optimized load sharing. **SimuLase™** automatically switches back to the CPU-optimized version if the GPUs cannot handle the calculation effort.

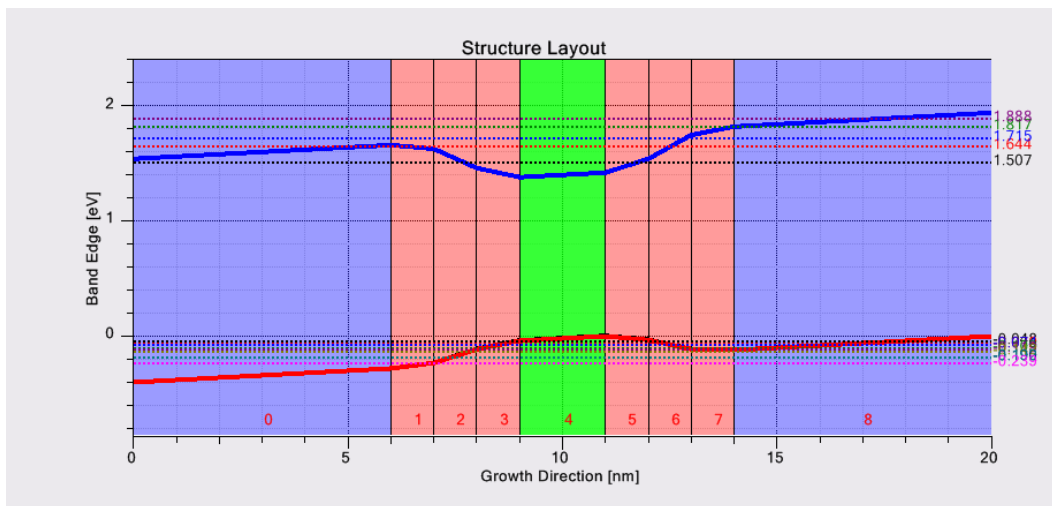
6.3 Selecting the Number of Subbands, [17s]

As discussed in Sec.6.1, calculation time and CPU-memory requirements for setting up Gain-Databases can be quite significant and depend crucially on the number of subbands. **SimuLase™** can automatically set these. However, if the 'Automatic' option(s) are used the program will use numbers that are on the cautious side and it may be possible to get sufficient accuracy with smaller numbers - thus reducing the calculation effort.

The number of subbands that **SimuLase™** will use for the calculation is displayed in the dialog ([17ab]) after the 'Generate Database' button has been clicked to start the calculation of a GainDatabase and a directory and name for the database have been selected. You can use this to find out the number of subbands for the case where the 'Automatic'-option has been chosen. If the 'Automatic'-option has not been used, **SimuLase™** will use the numbers of subbands as specified in field [17s].

After you find out the information you can cancel the actual calculation by selecting 'cancel' on the dialog [17ab].

For Auger calculations we generally recommend to use the 'Use Bulk'-model ([17v]) whenever possible and let the program determine the number of required subbands. The program automatically determines whether the 'Use Bulk'-model can be used. The only time the 'Number of Subbands' for Auger calculations should be set by hand using [17w] is if the program determines that an accurate calculation would require too many subbands for solution within



wells. If a field - external or due to dopants - is present, all states are included that are not completely de-localized but have to tunnel through a barrier potential to escape the well. Also included are all levels with lower energy, whether they are localized in a well or de-localized in the barrier.

Three more electron and hole subbands are added to include the barriers. If electric fields are present, the additional states are needed in order to be able to screen the fields with fair accuracy if a carrier density is present and the Schrödinger-Poisson problem is solved (option [17b]). For this, more than three de-localized states will lead to higher accuracy. However, one might want to sacrifice some accuracy for compute time.

Here, 'well' is defined as a sequence of consecutive layers labeled as 'well' through the option 'Type', [12b]. For the example shown in Fig.6.4, the 'well' consists of layers '1' through '7'. Here, the program would look for electron levels below the energy of the electron confinement potential in the barrier layer '0' at the interface to layer '1' and hole levels with energies just below the energy of the hole confinement potential energy in layer '8' at the interface to layer '7'. For the example shown in Fig.6.4, this leads to 5 electron and nine hole subbands.

If more than one 'well' is in the quantized region, the program looks for the number of subbands such that the above described criteria is fulfilled for all wells.

Since the calculation time rises with the fourth power of the number of subbands (see Sec.6.1), calculations including external or dopant related electric fields can be extremely time consuming. Check Secs.6.5 and 6.10 for ways to deal with this problem.

Calculating for Bulk Material

If box [17r] is checked, SimuLaseTM calculates for pure bulk material where the material is given by the material of the layer specified through the field 'Bulk Layer Number', [17q]. In this case a 3D-bandstructure model is used, no subbands are taken into account and the option to set the number of subbands, [17s], is de-activated.

In this case, the Auger calculation is also done for pure bulk. The model options for describing the final states, [17v], 'Use Bulk' or 'Use Subbands', are disabled and the 'Number of Subbands', [17w], are set to zero.

6.4 Min/Max Energy, Resolution, [17f]

The fields 'Min Energy', 'Max Energy' and 'Resolution', [17f], control the spectral range and resolution for the calculated spectra. They have no influence on the Auger calculation. They influence the calculation time and memory requirements only indirectly. If a wider spectral range shall be resolved, usually the number of in-plane momentum grid points has to be increased to keep the accuracy the same.

In order to resolve the desired spectral range the semiconductor-Bloch, and semiconductor-luminescence equations have to be solved for a test-pulse of a correspondingly short temporal pulse width (see Sec. 7). The wider the spectral range, the shorter the pulse has to be. Thus, the time-steps for solving these equations have to be adjusted to be able to resolve the short exciting pulse correctly. This changes the time required to solve these equations somewhat.

By default, the upper spectral boundary, 'Max Energy', is set to 0.25 eV above the highest bandgap energy (local energetic distance between the electron confinement potential and the

higher of the light- and heavy-hole confinement potentials) within the quantized region. The minimum energy is set by default to 150 meV below the lowest bandgap energy in the quantized region. The default spectral resolution is 0.25 meV .

6.5 Defining the 'Quantized Region'

As discussed in Sec.6.1, creating GainDatabases can take significant compute time and CPU memory. Both scale roughly with the third power of the number of subbands and number of in-plane momentum grid points. The memory even increases with the fourth power of the number of subbands. A structure that requires more than about a dozen electron or hole subbands can exceed the memory available on many machines and take several hours to complete - and that is for just one combination of carrier density and temperature. Thus, it is important to follow a few guidelines which help to keep the computational requirements within reason while not influencing the accuracy of the results. The following is a list of the most important guidelines.

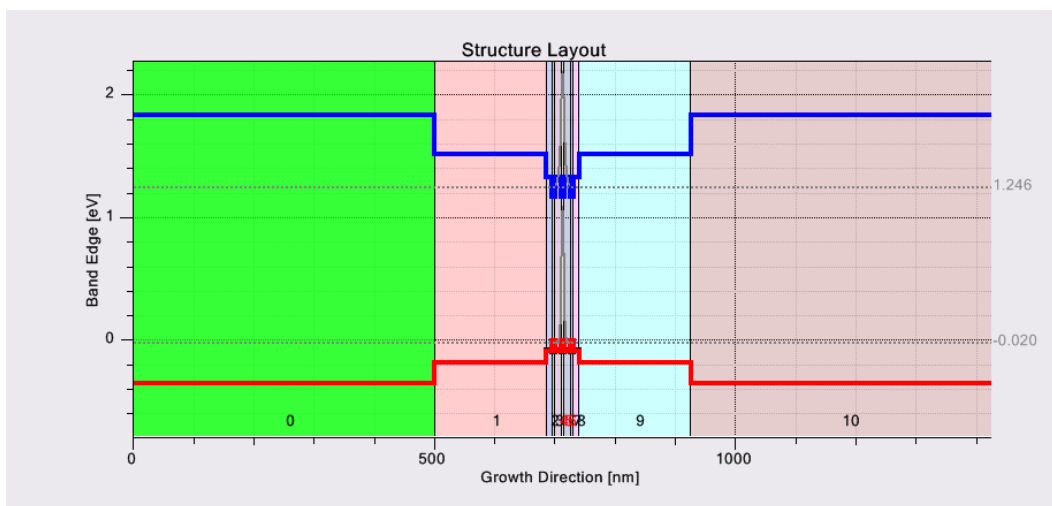


Figure 6.5: Schematics of a laser structure.

Typical semiconductor optical devices consist of many layers, most of which are required for purposes like pump absorption, carrier injection or mode confinement, but do not directly influence the generation, absorption or amplification of light, like layers 0, 1, 9 and 10 in the schematic shown in Fig.6.5.

SimuLaseTM performs microscopic calculations only for what is typically referred to as the 'optically active' region of the device. This is the region where light is absorbed, generated and/or amplified by certain amounts depending on the presence of carriers. Usually this region consists of layers which are only a few (tens of) nanometers thin and therefore require a quantum mechanical treatment of the quasi-particle interactions in terms of confinement wavefunctions, quantized states and subbands. Therefore, these layers are referred to as '**Quantized**' in **SimuLaseTM**. **SimuLaseTM** has to resolve the quantized region in real space and in energy space. This is done by resolving the confinement potential along the growth direction z using an equidistant grid, Fourier transforming it into k_z -space and using a matrix inversion to find the eigenvalues (subbands) and eigenfunctions (confinement wavefunctions).

In order to be able to resolve the quantized region with enough z -grid-points and subbands, the 'Quantized Region' (layers marked as 'Quantized' through option [12e]) should not contain any layers that are not essential for solving for the optical response (layers 0, 1, 9 and 10 in Fig.6.5). The following gives some additional tips on how the quantized region can/should be further simplified. These guidelines apply also to the calculation of Auger losses.

6.5.1 Use Short Barriers

The width of the barrier layers, layers 0 and 2 in Fig.6.6, should be kept as short as possible.

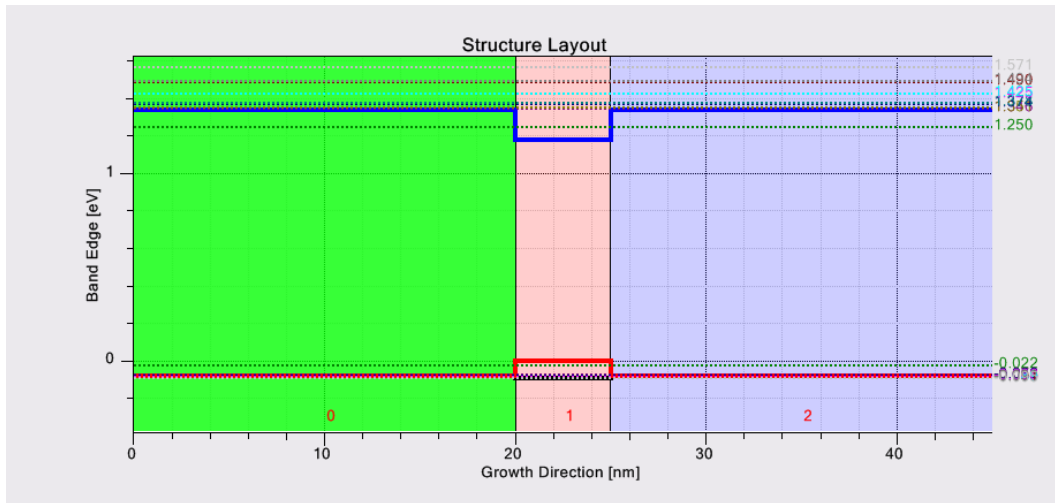


Figure 6.6: Structure with too wide barrier layers and ten lowest electron and hole levels.

This reduces the number of z -points required to resolve the quantized region. Also, this leads to higher subband separation for barrier states which allows to resolve the barrier to higher energies.

If your barrier layers are very wide you should split these layers in two and make only one part of the quantized region.

If the 'Bulk Barrier Model' is used the results should be unaffected by the width of the barrier layers as long as they are chosen thick enough such that the states that are confined in the well cannot tunnel through the barriers (fall off to zero before reaching the end of the quantized region). Usually a barrier thickness of 10 nm is sufficient to ensure that this is the case. Even shorter barriers can be sufficient.

6.5.2 Calculate for Only One Well

If a structure contains several identical wells the quantized region should only include one of the wells. If the barriers are thick enough such that there is negligible electronic coupling between the wells (no 'superlattice'), the optical response for the whole structure can usually be very well approximated by calculating for just one well and then multiplying the results by the number of wells. This is usually justified if the barriers between wells are at least about 10 nm thick. Since the number of subbands that is required to describe a structure scales about linearly with the number of wells (N) and the computing time and memory scale with the third and fourth power

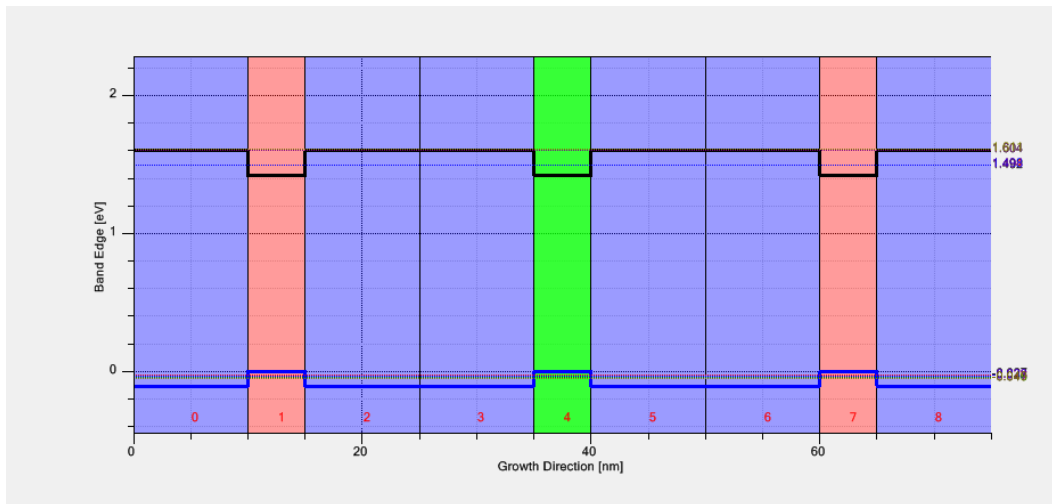


Figure 6.7: Multi-Well structure with the six lowest electron and hole levels.

of the number of bands, respectively, calculating for just one well reduces the numerical effort by at least a factor N^3 . Quantized regions with multiple wells also lead to the same problems as structures with too wide barriers discussed above.

For the structure shown in Fig.6.7, the quantized region should only contain one well (layer no. 4) and the barriers 3 and 5.

6.5.3 Fields Across the Quantized Region

The selection of what to include in the quantized region can be particularly crucial if a dopant-

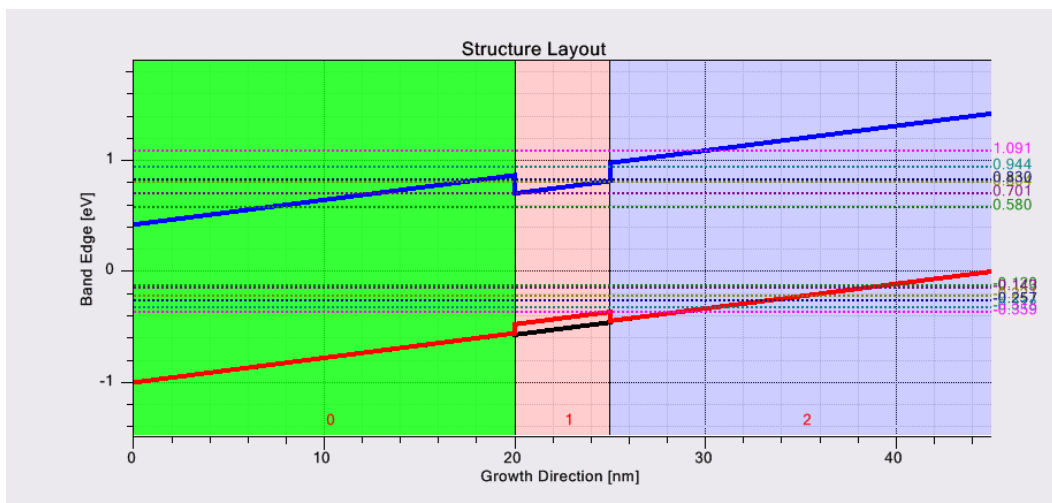


Figure 6.8: Structure with an applied electric field and six lowest electron and hole levels.

related or external electric field is taken into account (solving '**Drift-Diffusion**' or applying an '**External Voltage**'). Then the '**Bulk Barrier Model**' cannot be used and the barrier has to be resolved in terms of confined states. In this case, the quantized region has to be short in order to ensure that the states that are confined in the well(s) are taken into account.

In Fig.6.8, all shown hole levels would be energetically above the well and confined in the barrier if the current barrier width would be used. While the states with the lowest intraband energies are included, the ones that have the lowest interband-transition energies - those that are at least partially confined in the wells - are missing for the holes. Of course, the states with the lowest interband transition energies are the most important ones for optical processes.

For the example shown in Fig.6.8, if the barrier-width is reduced to about one half, the same amount of subbands would be sufficient to also include the states confined in the wells.

If the '**Automatic**' option is used to determine the number of required subbands, the program makes sure that it includes all states that are at least in part localized in the wells (see Sec.6.3). This can lead to impractically large numbers of subbands if the barriers are chosen too wide.

6.6 Absorption/Gain-Model, [17h]

The '**Gain**'-model is usually about a factor of three faster than the '**Absorption**'-model. In the

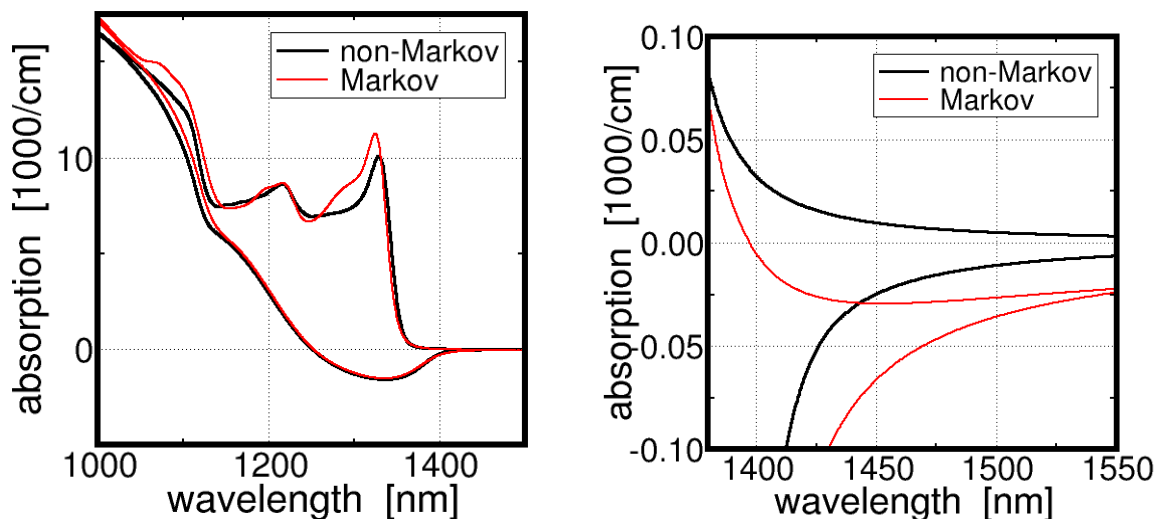


Figure 6.9: Absorption and gain spectrum for an *InGaAsP*-based quantum well. Red: calculated using the Markov approximation for electron-phonon scattering. Black: calculated by solving the equations of motion for the phonon-assisted polarizations. Right: zoom into left picture.

'**Gain**'-model the electron-phonon scattering is solved using the Markov-approximation whereas in the '**Absorption**'-model this scattering is solved by calculating the equations of motion for the phonon assisted polarizations.

As shown in Fig.6.9, both approaches give the same results within the typical uncertainties of the experiment for in-band absorption and gain for materials operating at wavelengths of about 800nm or longer. However, the '**Gain**'-model usually leads to errors in the below bandgap absorption as it is needed, e.g., for the modeling of electro-absorption modulators.

The electron-phonon scattering becomes increasingly stronger with larger bandgap. For materials operating at wavelengths shorter than about 800nm the '**Gain**'-model can lead to substantial

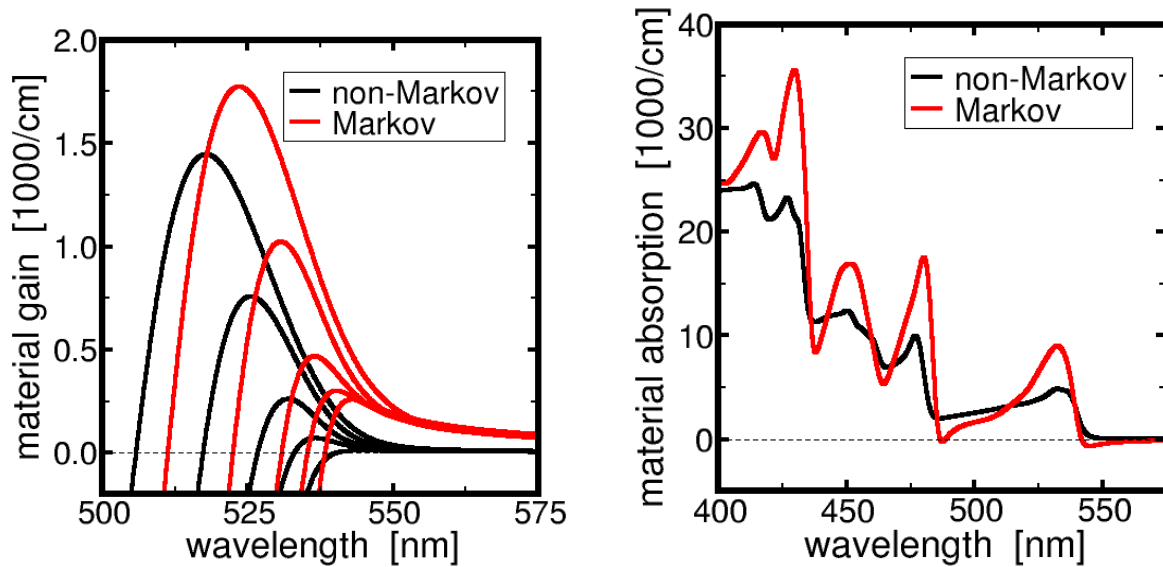


Figure 6.10: As Fig. 6.9, here for an *InGaN/GaN*-quantum well. Left: gain at five different densities. Right: absorption for zero density.

errors like significant unphysical gain at zero carrier density (see Fig.6.10). for these materials the '**Absorption**'-model should be used.

The model '**Accuracy**', [17g], determines the accuracy of the internal grids used for the real-space, in-plane momentum and z-momentum. The calculation time increases by about a factor of five when going to a higher '**Accuracy**'-level. By default we suggest to use '**Medium**'-accuracy.

6.7 Model Options

While NLCSTR advises to use the '**Standard Model**' whenever calculating a GainDatabase that is intended to be used for realistic modeling, testing or optimization of devices, it sometimes may be helpful to get quick estimates based on simplified models that require much less calculation time. As demonstrated by the results shown in Fig.6.11, these simplified models have serious shortcomings and one has to be careful in their use. The following gives a brief overview over these models.

The '**Bulk Barrier Model**' approximates the barrier material as infinite bulk material. In many cases this approximation is very good. It replaces all the subbands that would otherwise be required to describe the states in the barrier region by just one electron, one heavy hole, one light hole and one split-off hole bulk band which typically leads to a dramatic reduction in the required calculation effort.

The option to describe the barrier material using bulk material is set for the gain/ absorption/ PL calculation through '**Bulk Barrier Model**', [17p], (see Sec.6.7.4). A similar option exists for the Auger calculation, [17v].

If the calculation is for pure bulk material through option '**Calculate for Bulk-Material**', [17r], this is also applied to the gain/absorption/PL calculation and the Auger calculation and all other related options are automatically set correspondingly.

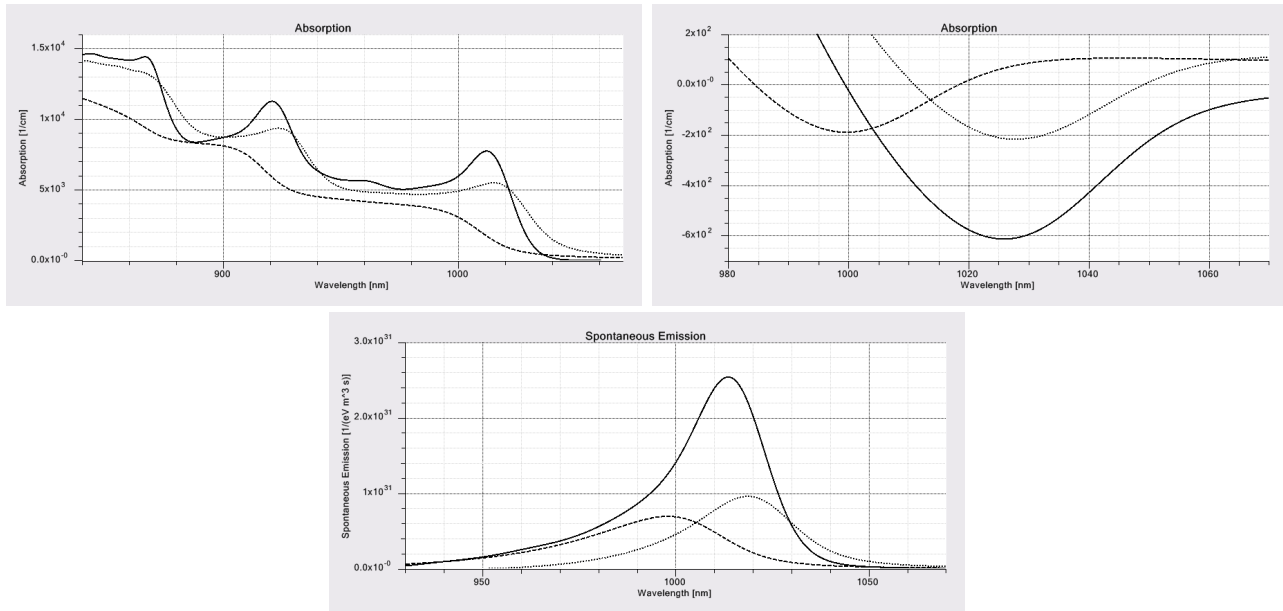


Figure 6.11: Spectra calculated for the same structure and grids, using the '**Standard Model**' (solid lines), the '**Quick and Dirty 1**' model (dotted lines) and the '**Quick and Dirty 2**' model (dashed lines). Top left: Absorption calculated for a density of $0.05 \times 10^{12}/\text{cm}^2$. Top right: Absorption (negative gain) calculated for a density of $2.4 \times 10^{12}/\text{cm}^2$. Bottom: PL calculated for a density of $0.05 \times 10^{12}/\text{cm}^2$.

6.7.1 Standard Model, [17i]

The '**Standard Model**' (option [17i]) is the model NLCSTR suggests to use for setting up all GainDatabases. It includes all the important microscopic many-body effects like Coulomb corrections to the absorption (Excitons, bandgap renormalization,...), electron-electron and electron-phonon scattering and higher excitonic correlations for the spontaneous emission (see the description of the theoretical model, Sec.7, for details).

6.7.2 Quick and Dirty 1, [17j]

If the '**Quick and Dirty 1**'-model is used (option [17j]) the model still includes all Coulomb effects that the '**Standard Model**' includes, like excitons, bandgap renormalization, Coulomb enhancement of the absorption and screening effects. However, it neglects electron-electron and electron-phonon scatterings and higher excitonic correlations. The model is reduced from what we usually describe as a 'fully microscopic many-body' model to what is still often revered to in the literature as a 'microscopic many-body' model - although the only remaining many-body interaction is the coherent effect of the Coulomb interaction that leads to the effects mentioned above.

Here, only processes that are linear in the Coulomb interaction are taken into account. The neglected effects are of second order in the Coulomb interaction. Thus, the latter include highly multi-dimensional in-plane momentum integrations and many iterated subband summations (see Sec.7) which significantly increases the calculation effort. Neglecting the higher order effects reduces the calculation time typically by more than one order of magnitude (see Sec.6.1).

As shown in Fig.6.11, using this simplified model leads to significant errors in the results. Since

the scatterings that lead to the dephasing of the optical polarization and, thus, the homogeneous broadening of the spectra, are not taken into account, one has to use a phenomenological dephasing time, T_2 , [17n], instead. For the gain this leads to unphysical absorption below the bandgap as well as wrong density-gain amplitude relations, errors in the spectral positions and lineshapes. This reflects the fact that the scatterings do not only influence the lineshapes but also the amplitudes and spectral positions (see also Sec.7.2).

Other lineshape broadenings than the Lorentzian lineshapes resulting from using a dephasing time have been discussed in the literature, including fairly sophisticated ones based on 'memory effects', etc.. While some of these can get rid of the unphysical absorption below the bandgap, they cannot overcome problems like the wrong relation between density and gain amplitude or errors in the spectral positions and density-dependent shifts. The latter are results of the complex nature of the scatterings that lead to density and spectrally dependent couplings. Thus, no phenomenological description replacing the explicit calculation of the scatterings can realistically describe the underlying processes and their impact on the spectra. 'Improvements' through 'sophisticated' schemes are merely cosmetics.

The higher excitonic correlations are source terms for the spontaneous emission (PL). As shown in Fig.6.11, neglecting these source terms leads to a significant underestimation of the PL-amplitude. In turn, this means that the radiative carrier lifetime that is given by the integral over the PL-spectrum will be calculated as too long if these correlations are not taken into account. Typically, this leads to an underestimation of the radiative loss current for a given density by a factor of two or more. The error becomes particularly dramatic for materials with wider bandgaps (wavelength less than one micron), which usually have particularly strong Coulomb interaction.

6.7.3 Quick and Dirty 2, [17k]

If the 'Quick and Dirty 2'-model is used, all many-body interactions are neglected. In addition to the electron-electron and electron-phonon scatterings and the higher excitonic correlations that are already neglected in the 'Quick and Dirty 1'-model, here also all coherent Coulomb effects are neglected like excitonic resonances, Coulomb enhancement of the absorption or density-dependent bandgap renormalizations. This simplifies the model to a pure single-particle model.

Here, the calculation time is almost exclusively given by the time required to calculate the bandstructure and single particle wavefunctions. Typical calculation times within this model are only a few seconds for one temperature and carrier density.

Besides the errors arising from the neglect of scatterings and higher excitonic correlations discussed above for the 'Quick and Dirty 1'-model, the complete neglect of all Coulomb effects leads to significant errors in the spectral positions, an underestimation of the continuum absorption and the absence of excitonic resonances at the bandedge.

PL-lineshapes at low carrier densities are usually dominated by excitonic effects. Thus, neglecting these effects leads to completely wrong PL-spectra that will render a PL-Analysis as useless.

6.7.4 Using the Bulk Barrier Model, [17p]

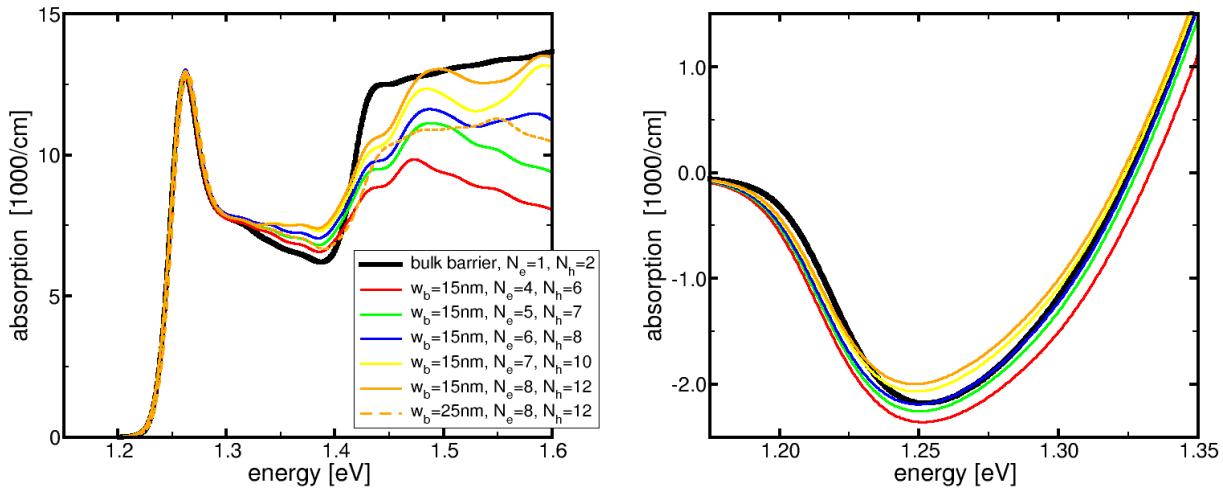


Figure 6.12: Absorption spectra using the **Bulk Barrier Model** (black) and using various numbers of electron/hole subbands, $N_{e/h}$ to describe the barrier assuming a barrier width w_b of 15 nm or 25 nm. Left: Absorption for a carrier density of $10^{10}/\text{cm}^2$. Right: for a density of $5 \times 10^{12}/\text{cm}^2$.

The '**Bulk Barrier Model**', [17p] can significantly reduce the calculation time and CPU memory requirements. If it is used, the barrier material is described as ideal bulk material using an 8×8 - $\mathbf{k} \cdot \mathbf{p}$ -bulk bandstructure model. If it is not used, the barrier has to be described by subbands. Since the barriers are usually fairly wide as compared to the wells, the energetic subband separation is much smaller than in the wells. Thus, usually a very high number of subbands will be required if one tries to resolve the barrier absorption and other barrier effects correctly to energies high above the well.

Replacing the barrier material by bulk is usually a good approximation as long as the total width of the barriers (i.e. the combined width of all barrier layers in the total active region - not just the 'Quantized Region') is more than about 25 nm. Then the subband separation is usually small enough such that the effective density of states is virtually bulk-like. A correct description of the barrier density of states is particularly important if the wells are rather shallow and a significant portion of carriers occupies not only states in the well, but also in the barriers. Although for the case of fairly short total barrier width the correct barrier absorption may still show remnants of the finite barrier width that get lost if the bulk barrier model is used, this usually has negligible impact on the quantities that are most interesting like the gain, bandedge absorption and PL near the bandedge.

As discussed in Sec.6.5, it is numerically highly advantageous to reduce the total width of the quantized region by reducing the width of the barrier layers or calculating for just one well in a multi quantum well structure. In these cases, the actual barriers are much wider than what is taken into account. Thus, using the barrier model might be even more appropriate than if one would resolve the barriers in quantized subbands, especially since in the later case the quantization energies (subband levels) would be calculated for the wrong barrier width.

In a multi-quantum well structure, the barrier levels for each period are electronically coupled in the real structure. This leads to broad minibands rather than the sharp levels one obtains if one calculates for just one period. The program assumes periodic boundary conditions. However, no electronic coupling between neighboring periods is taken into account. Thus, the barrier of the real structure resembles much more bulk than what one might assume by calculating for just one period.

Fig.6.12 demonstrates the differences between the two approaches. With increasing number of subbands the barrier absorption becomes closer to the one in the bulk barrier model while some remnants of the discrete nature of the subband bandstructure remain if a finite barrier width is assumed. Just below the barrier edge the well absorption is slightly enhanced in the subband model. This is due to some Coulomb induced subband coupling between barrier states and well states. For wider barriers, where the overlap between well and barrier states is reduced this effect is reduced. In the bulk-barrier model Coulomb coupling between well and barrier states is neglected.

At higher densities the Coulomb interaction is almost completely screened. Thus, in the gain region the coupling between well and barrier states is no longer an issue.

There are some small differences between the gain amplitudes and peak wavelengths even in the limit of very high numbers of subbands. This is due to the finite barrier width assumed here. In the limit of wider barriers this would disappear.

6.8 Including the Poisson Drift-Diffusion Problem

If the Poisson '**Drift Diffusion**'-model is solved, by checking [17a], the electric fields due to ionized dopants are included in the calculation. The '**Drift Diffusion**' model should be included if one uses optical pumping on doped structures. This situation most commonly occurs if PL is measured on doped and un-processed structures in order to check the growth quality, i.e., if one creates a Gain Database for the PL-Analysis (using the tool described in Secs.3.8 and 2.3.1). As discussed in Sec.6.5.3 for the case for an applied '**External Voltage**', one then has to be careful not to use too wide barriers for the microscopic calculation since the '**Bulk Barrier Model**' cannot be used and wide barriers would require high numbers of subbands.

If one considers the situation of an electronically pumped device under operating conditions one should usually not include the '**Drift Diffusion**' problem, leaving [17a] un-checked. In this situation the external pump voltage strongly compensates dopant-related internal fields leading to a virtual flat-band situation across the quantized region. Neglecting the internal fields completely usually leads to very good results for this case and saves greatly CPU-time and memory.

6.9 Including the Schrödinger Poisson Problem

The Schrödinger Poisson problem ('**Solve Poisson**', [17b]) should be included if a structure with an active region without inversion symmetry is considered. E.g., this can be due to an applied external Voltage, internal electric fields due to ionized dopants, asymmetric wells, or when the active region contains different wells that share a common chemical potential. In these cases, the local charge distribution for electrons and holes are different. This leads to internal potentials that modify the confinement potential and the resulting wavefunctions and energies.

The required number of subbands, and, thus, calculation time and memory usually increase if this problem is included. If '**Automatic**' is selected for the '**Number of Subbands**' and the '**Bulk Barrier**'-model is not used, the program will include three electron and hole subbands in addition to what would be included without that problem. This is to make sure that the charge distribution can be spatially resolved with sufficient accuracy.

If no internal fields are present and one has just one symmetric well or several identical wells, the influence of charge inhomogeneities from free carriers are usually negligible. We recommend to not include the Schrödinger Poisson problem in these cases.

6.10 Possible Speed-Ups

Some of the most effective methods to reduce calculation times and memory requirements have already been discussed in Secs.6.5, 6.7, 6.8 and 6.9:

- Using the 'Bulk Barrier' model, [17p].
- Using short barriers, especially if an external Voltage is considered or the Poisson drift diffusion problem is included.
- Calculating for only one well in case of a multi-well structure with identical wells.
- Including the Poisson drift diffusion problem ([17a]) only if really necessary - not when calculating for operating conditions where the pump voltage compensates dopant related fields or no dopants are present.
- Including the Schrödinger-Poisson problem ([17b]) only if really necessary - not for symmetric potentials or very low densities.

Generally, one should keep in mind that it generally makes no sense to try to calculate with higher accuracy than what can be experimentally measured. Therefore one should also check the results including an inhomogeneous broadening that is typical for the real device. The broadening tends to mask deviations due to otherwise insufficient grid resolution. Thus, results tend to converge much faster including this broadening.

The following discusses three common examples for which the calculation effort can often be further reduced:

6.10.1 Setting up a Database for PL-Analysis

Experimental PL is usually measured under low excitation conditions. Thus, a GainDatabase for a PL-Analysis also only needs to be set up for low carrier densities that are usually only a few tens of percents of the transparency density, i.e., usually only densities below $1 \times 10^{12}/\text{cm}^2$ are relevant.

If only one experimental spectrum is available the analysis cannot precisely determine the intrinsic carrier density. For the later experimental spectra for several (three or more) excitation densities are required. In the low density regime, the spectral shapes do not vary much with excitation density, but only the amplitudes and to a small extend the spectral positions.

Thus, **if there is only one experimental spectrum, one can use only two theoretical spectra to perform the PL-analysis** and the choice for the carrier densities is not very important. For that case we suggest to set up only a minimal Database with typical density values for low excitation conditions: $0.1 \times 10^{12}/\text{cm}^2$ and $0.2 \times 10^{12}/\text{cm}^2$.

The minimum number of theoretical densities a Database has to include for a PL-Analysis is given by the number of experimental excitation densities that are to be analyzed simultaneously, plus one. Since the carrier densities in PL experiments are usually low, also the screening of dopant-related electric fields is negligible. It leads to small changes in the spectral positions that

- based on a single experimental spectrum - cannot be distinguished from shifts due to small deviations between nominal and actual material compositions or layer widths. Thus, one has to include the Poisson drift diffusion problem for doped structures ([17a]), but does not need to include the more time intensive Schrödinger-Poisson problem ([17b]).

Finally, since the PL originates predominantly from the states close to the bandgap, one can often reduce the number of subbands to only a few (two to four) that are close enough to the bandgap to have significant numbers of carriers occupying them. One should check that using the 'Automatic' option for the number of subbands does not lead to the inclusion of unnecessary high numbers of subbands and, if so, set the numbers of subbands by hand.

6.10.2 Setting up a Database for Operating Conditions

Usually, when investigating characteristics for an operating/lasing device, one is only interested in the carrier density regime close to transparency density and a few times above that. Thus, when setting up a GainDatabase to investigate e.g. the threshold of a device, one does not need to include carrier densities that are much lower or higher than that.

In order to estimate the required density range one should first set up a Database for a few densities using the '**Quick and Dirty**'-models for typical densities between $10^{12}/cm^2$ and $10^{13}/cm^2$ with the density change between neighboring densities being about a factor 1.5.

From this data one obtains a rough estimate for the transparency density. One should reduce this value by about a factor of two or three to account for the possible errors of the simplified model. This density should be used for the low end of the density range. For the high end of the density range one should use the transparency-value determined from the simple model, multiply it by two or three for the possible errors in that model and then multiply it by as many times of the transparency density as one expects to be relevant. In most cases, carrier densities do not exceed $2 \times 10^{13}/cm^2$ even under extreme excitation and high temperatures. Set up the Database using the '**standard Model**' for densities in the resulting range using an increase-factor of about 1.5 between neighboring densities.

6.10.3 Structures with Very Deep Wells

If one is not interested in the barrier absorption but only the spectral range close to the bandgap that contain the PL and gain and if the wells are fairly deep (more than about 100 meV deep) one does not have to describe the barrier regime with high accuracy. Then it is usually sufficient to include only the subbands that are confined in the well and not using the '**Bulk Barrier Model**', [17p].

In this case one can also often further reduce the number of subbands to those with a bandedge less than about 100 meV above the lowest subband. For that one has to turn off the 'Automatic' option for the number of subbands. The subbands levels can be checked in the '**Design Structure**'-window where the number of subbands is set on the '**Advanced**'-options panel.

7 Theoretical Background

SimuLaseTM uses state of the art microscopic many-body models to calculate the crucial electro-optical properties of semiconductor heterostructures. These models that have been developed over the last two decades differ fundamentally - in accuracy and predictability - from simpler approaches that are still commonly used today. **SimuLaseTM** is the first software product that allows to take full advantage of all the improvements made by modern semiconductor theory.

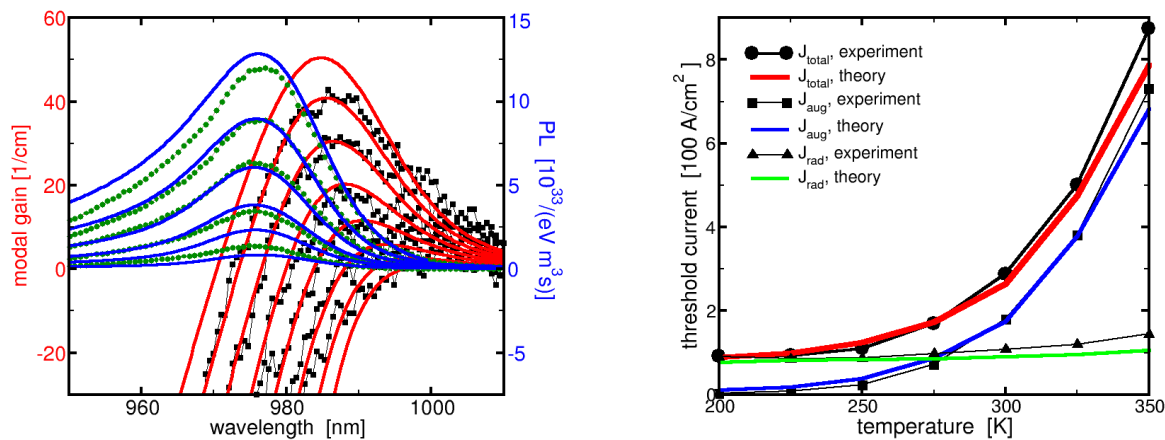


Figure 7.1: Examples of comparisons of results of the fully microscopic many-body models and experimental data. Left: comparison of experimental PL (green) and calculated PL (blue) and for predicted gain (red) and measured gain (black) at several excitation densities in an *InGaAsP*-based device [11]. Right: theoretical and experimental threshold currents and contributions due to radiative and Auger losses in an *InGaAsP*-based device [7]. More examples can be found at our web site [12].

The fundamental difference between these models and what is usually done to describe these properties is that they explicitly calculate the many-body interactions, like electron-electron and electron-phonon scattering, rather than replacing the underlying mechanisms by phenomenological parameters like dephasing times or broadening parameters. This eliminates all these fit parameters for which one would need experimental input that is strongly situation dependent. These parameters - i.e. the underlying physical processes they represent - are strongly dependent on the carrier density, the temperature and the spectral position as well as the structure, its material composition and layer widths. E.g., the spectral broadening due to electron-electron scattering obviously depends on how many carriers are present (the density) as well as at what energies they are located. If all states are filled or empty no initial or final states are available for carriers to be scattered to or from. This leads to a strong spectral dependence of the scattering and its effect on the spectra that cannot be described by a single dephasing or broadening parameter.

The second crucial shortcoming of the simpler approaches besides requiring experimental feedback is the fact that the simple parameters usually describe the underlying physics incorrect.

One prominent example for that is the failure of the commonly used *ABC*-power law for the density dependence of the loss current, $J = AN + BN^2 + CN^3$. As has been demonstrated in Ref. [5], the quadratic and cubic dependencies for radiative and Auger losses, BN^2 and CN^3 , respectively, completely break down for carrier densities in the regime interesting for laser operation (see Fig.7.2). Here, the radiative losses have been shown to become more like linear in the density and the dependence for the Auger losses is reduced to only quadratic or less. Similarly, the usually assumed temperature dependencies for the losses have been shown to be generally very wrong for all densities [6]. If a model requires fit parameters it cannot predict

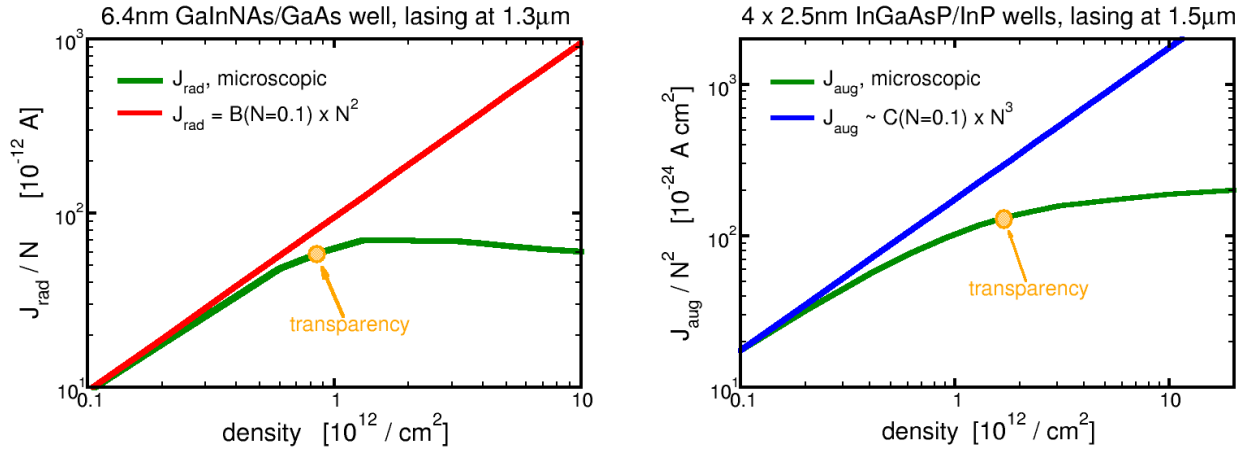


Figure 7.2: Left (Right): Fully microscopically calculated loss currents due to radiative (Auger) recombination processes as function of the carrier density versus the classically assumed density dependency, $J_{rad} = B N^2$ ($J_{aug} = C N^3$) [5].

results for situations (temperatures, densities, well widths, well compositions, barrier heights, etc.) away from the one at which the fit parameters were obtained. In contrast, since the fully microscopic models do not require any such parameters their results can easily be applied to a wide variety of situations and materials without any loss of accuracy. Since the results of the microscopic models have been shown to be quantitatively correct, usually within the scattering of any experimental data, the microscopic models can truly be called quantitatively predictive.

The following briefly reviews the models used in **SimuLase**TM and discusses shortcomings of simpler models.

7.1 Implemented Models

7.1.1 Bandstructure and Wavefunctions

SimuLaseTM uses an $8 \times 8 - \mathbf{k} \cdot \mathbf{p}$ -model to calculate the single particle wavefunctions and energies (subbands). For zincblende materials the details of this model can be found in Ref. [13] and for wurtzite structures in Ref. [14]. For dilute nitride containing materials the zincblende model is extended to a $10 \times 10 - \mathbf{k} \cdot \mathbf{p}$ -model that includes the conduction band anti-crossing [15]. Strain between heterostructure layers is treated as described in Ref. [16]. The microscopic Schrödinger-Poisson problem of potential modifications due to local charge inhomogenities is solved as described in Ref. [17] if the corresponding option, '**Solve Poisson**', [17b], is selected.

The classical Poisson drift diffusion problem is solved according to Ref. [18] if the option '**Solve Drift-Diffusion**', [17a], is selected. In the current version we assume that all affinities are negligible. If this option is selected or a non-zero '**External Voltage**' is applied ([17d]) the '**Bulk Barrier**' model ([17p]) cannot be used since the bulk model has to assume a constant confinement potential. This usually leads to a strong increase in CPU-time and memory requirement. Since under operating conditions the pump fields usually compensate the fields due to ionized dopants, we suggest to only include the Poisson drift diffusion problem to calculate low density PL to compare it to measured data obtained under optical pumping conditions. For operating conditions, the external voltages and fields due to the Poisson drift-diffusion problem should be considered to be compensated (see also Sec.6.8).

The single particle Schrödinger equation is solved using the 'Ultimate Concept' as described in Ref. [19]. Here the problem is Fourier-transformed from z - into k_z -space and solved by matrix inversion.

The wavefunctions that are written into the corresponding files of the GainDatabase are the dominant spinor components at zero in-plane momentum. For calculating the material properties like gain/absorption the full 8-component spinors are used.

This method implicitly assumes periodic boundary conditions. For multi-quantum well structures with identical wells this is a natural fit. One only calculates for one well and scales the results according to the number of wells. However, the model does not include electronic coupling between the individual periods. For states that are unconfined in the barrier this coupling leads to the formation of broad and overlapping minibands instead of degenerate subbands. The real density of states resembles much more bulk than the individual levels obtained for single periods. To solve this problem **SimuLase**TM has the option to describe the barrier states by a bulk model instead of using subbands ([17p], see also Sec.6.7.4).

For a given sheet carrier density the carrier distributions for electrons/holes, $f^{e/h}$, are determined by filling the carriers into the subbands assuming thermal equilibrium and using Fermi distribution functions. While the general approach also allows to consider non-equilibrium situations and distributions, we currently restrict the program to this well defined situation that is very accurate for most applications.

7.1.2 Gain/Absorption, Refractive Index

The wavefunctions and subbands are used to set up the matrix elements that enter the semiconductor-Bloch equations [20, 21] that are used to calculate the gain/absorption and carrier induced refractive index changes:

$$\frac{d}{dt}p_{j_1 i_1, \mathbf{k}} = \frac{1}{i\hbar} \left\{ \sum_{i_2, j_2} [\mathcal{E}_{j_1 j_2, \mathbf{k}}^h \delta_{i_1 i_2} + \mathcal{E}_{i_1 i_2, \mathbf{k}}^e \delta_{j_1 j_2}] p_{j_2 i_2, \mathbf{k}} + [1 - f_{i_1, \mathbf{k}}^e - f_{j_1, \mathbf{k}}^h] \mathcal{U}_{i_1, j_1, \mathbf{k}} \right\} + \left. \frac{d}{dt} p_{j_1 i_1, \mathbf{k}} \right|_{corr}, \quad (7.1)$$

where

$$\mathcal{E}_{i_1 i_2, \mathbf{k}}^e = \varepsilon_{i_1, \mathbf{k}}^e \delta_{i_1 i_2} - \sum_{i_3, \mathbf{q}} V_{\mathbf{k}-\mathbf{q}}^{i_1 i_3 i_2 i_3} f_{i_3, \mathbf{q}}^e, \quad (7.2)$$

$$\mathcal{E}_{j_1 j_2, \mathbf{k}}^h = \varepsilon_{j_1, \mathbf{k}}^h \delta_{j_1 j_2} - \sum_{j_3, \mathbf{q}} V_{\mathbf{k}-\mathbf{q}}^{j_2 j_3 j_1 j_3} f_{j_3, \mathbf{q}}^h, \quad (7.3)$$

$$\mathcal{U}_{i_1 j_1, \mathbf{k}} = -\mu_{i_1 j_1, \mathbf{k}} E(t) - \sum_{i_2, j_2, \mathbf{q}} V_{\mathbf{k}-\mathbf{q}}^{i_1 j_2 j_1 i_2} p_{j_2 i_2, \mathbf{q}}. \quad (7.4)$$

Here, \mathcal{E} are the density dependent renormalized energies that lead to the bandgap renormalization. \mathcal{U} is the renormalized field that leads to the creation of excitonic resonances and Coulomb-enhancement of the absorption. $i(j)$ are the subband indices for electrons (holes), \mathbf{k}, \mathbf{q} are in-plane wave-vectors, ε are subband energies, μ are the interband dipole matrix elements. V are the Coulomb matrix elements for which we include the terms that represent the Coulomb induced intersubband coupling which is essential in order to be able to describe the transition from an ideal two-dimensionally confined system to the bulk limit [22].

The last term in Eq.(7.1) describes the dephasing of the polarizations due to electron-electron and electron-phonon scattering. In contrast to simpler models, in the fully microscopic model (if 'Use Microscopic Scattering', [17m], is checked) these terms are calculated explicitly. The importance of this is discussed in Sec.7.2.1. The explicit form of the scattering terms can be found in Ref. [23].

Implemented in **SimuLase**TM are two different models for the calculation of the electron-phonon scattering. If the '**Gain**'-model is used, the electron-phonon scattering is calculated using the second Born and the Markov approximation as described in Ref. [23]. This model has been found to be highly accurate for the calculation of in-band absorption and gain in materials operating at wavelengths of about 800nm or longer. However, it tends to lead to an overestimation of the absorption tail below the bandgap and it tends to lead to general errors in materials at wavelengths shorter than about 800nm in which the electron-phonon interaction generally is stronger than in materials at longer wavelengths.

If one is interested in absorption below the bandgap, as, e.g., typically for applications as electro-absorption modulators, or for materials operating at wavelengths shorter than about 800nm one should use the '**Absorption**'-model. In this model the Markov approximation is not used and memory effects are taken into account by solving the equations of motion for the phonon-assisted polarizations. Calculations with this model usually are about a factor three slower than when using the '**Gain**'-model.

To calculate the linear absorption/gain, the equations of motion for the microscopic polarizations, p , Eq.(7.1), are solved for a test pulse, E , of arbitrarily small amplitude. Fourier transforming the macroscopic polarization, P ,

$$P(t) = \frac{2}{w} \sum_{i,j,\mathbf{k}} p_{ji,\mathbf{k}} \mu_{ij,\mathbf{k}}^* \quad (7.5)$$

from time to frequency space yields the absorption/gain, α , via:

$$\alpha(\omega) = \frac{\omega}{\varepsilon_0 n_r(\omega) c E(\omega)} \mathcal{I}m\{P(\omega)\}. \quad (7.6)$$

The refractive index change is obtained the same way from the real part of P . Here, ε_0 is the permittivity and c is the vacuum speed of light. n_r is the background refractive index.

Eqs.(7.6) and (7.5) yield the material gain/absorption for the field intensity. w is the well width, i.e. the combined width of all layers marked 'well' within the quantized region.

If the bulk model is used to describe barrier states or to calculate for pure bulk material the same equations as above have to be solved. Only the indices no longer refer to subbands but bulk bands and the momentum vectors become three-dimensional.

To obtain the modal gain the material gain has to be multiplied by the optical confinement factor that can be calculated through the 'View Mode'-tool, [121]. Here, one has to specify the operating wavelength through the field 'Wavelength' on the 'Advanced' structure set-up panel, [13d].

The confinement factor is then calculated by the overlap of the optical mode for this wavelength with the all layers of the total structure marked as 'well'.

A more detailed description of the semiconductor-Bloch equations approach can be found in Refs. [21, 24].

7.1.3 Spontaneous Emission (PL), Radiative Carrier Losses

To calculate the spontaneous emission (photo luminescence) and the resulting radiative carrier lifetimes the semiconductor luminescence equations (SLE) are solved. These are explained in detail in Ref. [25]. As shown in Ref. [26], for situations that are typical for opto-electronic device operation (e.g., no ultra low temperatures) the SLE take a form very similar to the semiconductor Bloch equations discussed in Sec.7.1.2. Here, the equations are not for the microscopic polarizations but for photon-assisted polarizations. The SLE also contain effects like bandgap renormalization, Coulomb enhancement and incoherent contributions due to electron-electron and electron-scatterings. As for the gain/absorption calculation, treating these scatterings explicitly is crucial for the accuracy of the results.

In addition, the SLE contain higher order excitonic correlations which act as source terms for the spontaneous emission. Neglecting these leads to significant errors in the amplitudes and lineshapes. Typically, one overestimates the resulting carrier lifetime by a factor of more than two if these additional source terms are neglected (see Sec.7.2.2). The error generally becomes more dramatic the larger the bandgap since the Coulomb interaction becomes stronger with increased bandgap. In wide bandgap Nitrides the error can be close to one order of magnitude.

Since these additional source terms do not appear in the semiconductor Bloch equations, their impact is not taken into account in any approach that determines the PL from the absorption spectra using a conversion approach like the Kubo-Martin Schwinger relation - no matter how sophisticated the underlying model for the absorption is. **SimuLase**TM is the only commercially available software that includes these important effects.

The surface-PL is calculated using the so-called 'Filter-Function' approach [2]. Here, the modifications of the PL due to reflections at layer interfaces on its way from the quantum wells to the surface of the device are taken into account by the filter function and the surface-PL is given by the product of the pure material PL and the filter function.

From the photo luminescence spectra for TE/TM-polarization, $PL^{TE/TM}(\omega)$, the spontaneous emission rate, $w_{rad}^{TE/TM}$, can be determined through the relation:

$$w_{rad}^{TE/TM} = \int_0^{\infty} d\omega \tilde{P}L^{TE/TM}(\omega). \quad (7.7)$$

$\tilde{P}L$ is the modal analogous to PL , i.e. it is obtained as PL , but in the calculation of the macroscopic PL from the microscopic photon-assisted polarizations similarly to Eq.(7.5) the scaling factor $1/\sqrt{w_i w_j}$ is omitted.

This rate is related to the radiative carrier lifetime, $\tau_{rad}^{TE/TM}$ through:

$$\tau_{rad}^{TE/TM} = \frac{N_{2D}}{w_{rad}^{TE/TM}}. \quad (7.8)$$

Here, N_{2D} is the sheet carrier density per well. The total radiative carrier lifetime is given by:

$$\tau_{rad} = \left(\frac{2}{3\tau_{rad}^{TE}} + \frac{1}{3\tau_{rad}^{TM}} \right)^{-1}. \quad (7.9)$$

Finally, the loss current density due spontaneous emission, J_{rad} is given by:

$$J_{rad} = \frac{e n N_{2D}}{\tau_{sp}}, \quad (7.10)$$

where n is the number of wells and e is the elementary charge.

7.1.4 Intraband (Free Carrier) Absorption

The intraband absorption is calculated by solving the equations of motions for the intraband polarizations:

$$\frac{d}{dt} f_{i_1 i_2, \mathbf{k}} = \frac{1}{i\hbar} \left\{ [\varepsilon_{i_1, \mathbf{k}} - \varepsilon_{i_2, \mathbf{k}}] f_{i_1 i_2, \mathbf{k}} - [f_{i_1, \mathbf{k}} - f_{i_2, \mathbf{k}}] \mu_{i_1 i_2, \mathbf{k}} E(t) \right\} + \frac{d}{dt} f_{i_1 i_2, \mathbf{k}} \Big|_{corr}. \quad (7.11)$$

Unlike in the semiconductor Bloch equations for the interband polarizations (7.1), Coulomb renormalizations are neglected here and the unrenormalized field (E) and energies (ε) are used. This is possible here, since the Coulomb interaction between carriers with very similar effective masses (parallel bands) is negligible. We tested that this approximation leads to insignificant errors.

The last term on the right hand side of Eq. (7.11) describes the dephasing of the polarizations. While this is calculated explicitly from the corresponding electron-electron and electron-phonon scattering terms for the interband polarizations, a dephasing time is used instead for the intraband polarizations. This is a fair approximation here due to the weak Coulomb interaction for these polarizations and because the resulting spectra have rather limited spectral variation which is not altered significantly by the scatterings/dephasing.

The macroscopic intraband polarization and resulting absorption are calculated using the same formulas as for the interband polarization and absorption, Eqs. (7.5), (7.6).

The same controls for 'Accuracy', 'Model' and 'Number of Subbands' are used for the intraband absorption as for the Auger calculations. Please see Sec.7.1.6 for a description of the functionality of these controls.

7.1.5 Inhomogeneous Broadening

It is assumed that the inhomogeneous broadening is caused either by local fluctuations in the material compositions or by fluctuations in the layer thicknesses. Both effects are simulated through a Gaussian distribution of the bandedge energies. The spectra that are inhomogeneously broadened according to a broadening, Δ (FWHM), $S(\hbar\omega, \Delta)$ are obtained from the homogeneously broadened spectra $S(\hbar\omega, 0)$ through the conversion:

$$S(\epsilon, \Delta_0) = \frac{2}{\Delta_0 \sqrt{\pi}} \int d\epsilon' S(\epsilon', 0) \exp \left[-\frac{(\epsilon - \epsilon')^2}{\Delta_0^2} \right], \quad (7.12)$$

where $\Delta_0 = 0.5 \ln(2) \Delta$.

7.1.6 Auger Losses

SimuLaseTM uses the basic quantum-Boltzmann scattering equations as derived by Beattie and Landsberg fifty years ago [27] to calculate carrier losses due to Auger recombinations. Mostly due to numerical limitations, approaches to solve these Auger equations in the past employed uncontrolled approximations like averaging over spin- or momentum indices or simplifications to the Coulomb matrix elements. Using any of these approximations leads to uncontrolled errors that are generally order(s) of magnitude.

Using the most crude approximations leads to the most simple - yet still commonly used - approximation for the Auger loss current, $J_{aug}(N) = C N^3$, i.e. a cubic dependence on the intrinsic carrier density N . Here, C is obtained from fits to experimental data. One important approximation used to derive this simple law is the use of Boltzmann distributions instead of Fermi-distributions. This is only valid for the low density regime. Consequently, this simple law breaks down dramatically for densities that are relevant for laser operation, near or above transparency/threshold (see Fig.7.2. Here phase-space filling becomes important and Boltzmann distributions fail to describe the carrier distributions.

The fully microscopic Auger calculation implemented in **SimuLase**TM uses no such approximations. This has been shown to reduce the uncertainty of the results to an unprecedented regime of less than about twenty percent [7].

The microscopic model has been tested successfully against the experiment for various materials for wavelengths of around 800nm and longer (see www.nlcstr.com/examples0.htm or the literature list at www.nlcstr.com/publications.htm for examples). However, for wide bandgap Nitrides, the Auger losses as calculated with this model cannot match the non-radiative losses at elevated densities. Especially in InGaN-based LEDs and lasers for the blue-green wavelength regime, such losses lead to a significant decline of the internal quantum efficiency with increased pump power - the so-called 'efficiency droop'.

To date, the origin of these losses is not clear. It is argued that indirect Auger processes, like phonon-assisted Auger processes dominate in this material system over the direct ones that are calculated within **SimuLase**TM. However, calculations of these require first principle band-structure calculations beyond the $\mathbf{k} \cdot \mathbf{p}$ model used here and involve processes that are orders of magnitude more complex than the already numerically expensive processes calculated in **SimuLase**TM. No first principle calculations including all the relevant processes, like higher order phonon-Coulomb couplings and memory effects have ever been performed. Simpler models have been used, but the neglect of the additional terms/processes leaves the accuracy of the results questionable. The losses calculated with these models are too small to explain experimental observations, sometimes have unphysical dependencies - like wrong temperature dependencies and no direct comparison to experimental data has ever been demonstrated.

In the simplest form, the losses at higher densities are modeled using the classical CN^3 loss where the parameter C , as well as its temperature and density dependence are used to fit experimental data. The large room for the fit-parameters, especially if also radiative losses are modeled using the equally simple BN^2 law, allows to find good agreement with any experimental data. However, this of course does not mean that Auger processes are actually the culprit of the droop.

An alternative model for the IQE droop was proposed in Refs. [28, 29]. Here, it is assumed that the material contains two types of defect recombination centers. The first ones are distributed throughout the material and lead to the usual Shockley-Reed-Hall defect recombination loss that scales linearly with the density. In the tools of **SimuLase**TM, this is modeled using a defect recombination time. A second type of defect recombination centers has a much faster

recombination time. However, the centers are surrounded by some potential barriers which prevents carriers to reach the centers at low densities. At elevated densities, increased electron-electron scattering allows carriers to overcome the barriers, resulting on a strong additional, density-activated defect recombination (DADR) loss above a certain threshold density. Since the loss is mediated by carrier-carrier scattering, the density dependence of this loss scales like the scattering quadratically with the density.

Like the CN^3 -model, the parameters for the DADR model are not calculated from first principle. Since it is dependent on the material quality, which cannot be predicted theoretically, this is not possible. Thus, the parameters of this model can also only be determined through comparison with existing experimental data. However, as shown in Ref. [29], the involved parameters and their density and temperature dependence have more realistic behaviors than the ones of the CN^3 model.

For AlInGaAsP, AlInGaAsSb and dilute Nitride materials we strongly suggest to calculate the Auger losses with the microscopic model. For AlInGaAN, we implemented both, the CN^3 and the DADR model in the tools calculating operating characteristics for edge- and surface emitters.

Microscopic Auger Model

The details of the fully microscopic Auger model are described in Ref. [7]. Just like the models for gain/absorption and spontaneous emission, the Auger model does not require/allow any fit parameters. The only input are again basic bulk material parameters that can be found in the standard literature (see Sec.8).

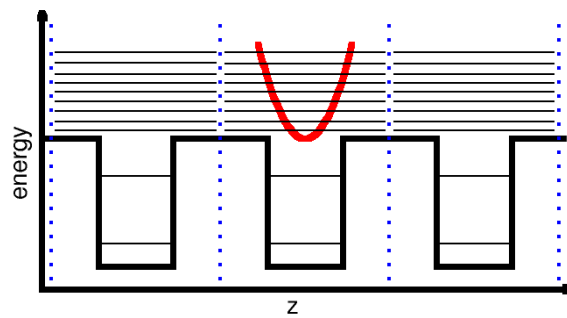


Figure 7.3: Schematics of the energy levels in a multi-well structure. In 'Use Subbands' is chosen to describe the final states of the Auger scatterings, all states are described by subbands ($\mathbf{k}_{\parallel} = \mathbf{0}$) subband edges are indicated by black horizontal lines. If 'Use Bulk' is chosen, only the states confined in the layers marked as 'well' are treated in terms of subbands. The final states are described by a bulk model (red dispersion for $k_z \neq 0$, $\mathbf{k}_{\parallel} = \mathbf{0}$).

SimuLaseTM offers three levels of numerical accuracy, 'Low', 'Medium' and 'High' through option [17u]. The calculation time increases with the accuracy. Calculations with 'High' accuracy take about ten times as long as calculations with 'Medium' accuracy which take about ten times as long as calculations with 'Low' accuracy.

According to the chosen accuracy level the numerical grids are chosen more or less refined. The numerical error is typically around 30% – 50% for 'Low' accuracy, around 10% for 'Medium'

accuracy and around 5% for 'High' accuracy. The numerical error is generally larger for low carrier densities and low temperatures.

SimuLaseTM offers two models to describe the final states high above the well bandgap into which the carriers are scattered that take on the energy of the recombining electron-hole pair. If 'Use Bulk' is selected from option [17v], these final states are described using a bulk model. The material that shall be assumed for all final states is chosen through the 'Bulk Layer Number'-option. Here, the same general guidelines as for choosing 'Use Bulk Barrier', [17p] for the absorption/gain/PL calculation (see Secs.6.3 and 6.7.4 for more details).

In this model, only the states that are confined in the 'well' are described by subbands. The electron/hole that takes on the excess energy of the recombining electron-hole pair will be scattered into a state that is energetically at least one bandgap above the fundamental bandgap. In general, these final states are energetically high above the barrier. For structures with wide barriers (about 20 nm) or wider, these final states are well described by the bulk approximation. Keep in mind that in multi-quantum well structures the relevant barrier width is not the one of a single barrier/well repeat, but the total combined width of all barrier layers.

We recommend to use this model whenever possible. However, this model cannot be used if an electric field is present across the quantized region, i.e. if the field due to ionized dopants is taken into account by solving the drift-diffusion problem ([17a]) or an external voltage is applied through [17d].

If 'Use Subbands' is chosen, all states are described in terms of quantized subbands. This option has to be chosen if electric fields are present across the quantized region. It should also be used if the relevant barrier regions are composed of not just one material but of various layers with different materials (like, e.g., in digital alloy structures).

In general we recommend to include just one well/barrier repeat of a multi quantum well structure in the 'quantized region' which is used for the actual calculation and then scale the results by the number of identical wells. The program assumes periodic boundary conditions which seems particularly appropriate for multi-quantum well structures. However, the program neglects the electronic coupling between well/barrier units. In reality, the electronic coupling of the levels leads to the formation of energetically broad mini-bands and a density of (barrier-) states that is much more bulk-like instead of sharp levels.

In the results for the Auger loss rates the artificially sharp barrier levels lead to artificial enhancements or suppressions depending on whether or not there is a final level energetically close to the desired energy about one gap energy above the well gap. Thus, the results can change fairly strongly with the barrier width (see Fig.7.4).

In both models the initial states energetically close to the bandgap, i.e. the states that are at least partially filled with carriers in thermal equilibrium, are described in terms of quantized subbands. If the 'Automatic'-option is selected for the number of subbands [17w], the number of initial states is determined internally by the program. In some cases, like, e.g., very wide and/or deep wells, the ideal number of initial subband-states might become too large for calculation within reasonable CPU-time and/or memory. Then the number of initial subbands should be reduced and set by hand in field [17w].

The numbers set through field [17w] do not influence the number of subbands used for the final states in case 'Use Subbands' is chosen. If the barriers of the quantized region are very wide, many subbands are required to resolve the final states which can lead to long calculation times and large memory requirements. Thus, one should keep the total width of the active region fairly short (typically < 30 nm). As mentioned above, for wide barriers, the bulk-model might be more appropriate anyways.

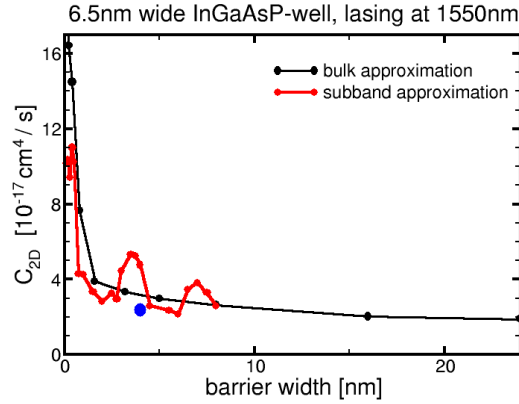


Figure 7.4: Auger loss coefficient $C = J_{aug}/N^3$ as function of the barrier width for a structure with a 6.5 nm wide *InGaAsP*-well lasing at 1.55 μm , at 293 K and a density of $N = 5 \times 10^{12}/\text{cm}^2$. Black: using the bulk approximation for the final states. Red: using subbands to describe the final states.

The bandstructure as written into the corresponding files contained in the final GainDatabase is the one as used for the gain/ absorption calculation. The one for the Auger calculation usually is calculated to higher k_{\parallel} -values. Also, the subbands and wavefunctions in the GainDatabase are the ones from the gain/ absorption/ PL calculation not the ones from the Auger calculation which usually requires many more subbands.

CN^3 Model

As discussed above, and shown in more detail in Sec.7.2.3, the classical CN^3 model for Auger losses generally fails to represent the true density and temperature dependence of the Auger losses. In addition, it requires to have preexisting experimental data for operating characteristics in order to fit the otherwise unknown Auger coefficient C . The transferability of the C -coefficient to other structures is generally limited since the Auger losses strongly depend on structural details as well as operating parameters like temperature and current/carrier density. The transferability is extended within **SimuLase**TM thanks to the exact knowledge of the radiative losses which would otherwise be free fit parameters as well.

In the absence of accurate microscopic Auger models for wide bandgap Nitride materials the CN^3 can be used to obtain insights into the internal carrier losses. Therefore, we implemented this model into the 'Current Calculator' tool for operating characteristics of edge-emitters and the 'VECSEL LI' tool for surface emitters.

Within this model the Auger loss current is assumed to scale cubically with the carrier density, N :

$$J_{aug} = CN^3. \quad (7.13)$$

Here, C is a fit parameter. For some guidance on the density and temperature dependence of this parameter please see Sec.7.2.3 and References there.

DADR Model

Alternatively to the CN^3 model, the density-activated defect recombination (DADR) model can be used to simulate the non-radiative losses that are known to lead to the efficiency droop in AlInGaN based devices. The model is explained in detail in Refs. [28,29]. As the CN^3 model, the DADR model is implemented within the 'Current Calculator' tool for operating characteristics of edge-emitters and the 'VECSEL LI' tool for surface emitters.

In this model the loss current is given by:

$$J_{DADR} = \begin{cases} 0, & \text{for } N < N_0 \\ \frac{en_w}{\tau_{DADR}} \frac{(N-N_0)^2}{2N_0}, & \text{for } N > N_0 \end{cases} \quad (7.14)$$

Here, n_w is the number of wells and N and N_0 are sheet carrier densities per well. The recombination time, τ_{DADR} , and N_0 are determined by fits to experimental data. A Gaussian broadening is used to model the statistical distribution of heights of the barriers surrounding the strong recombination centers:

$$J(N) = \frac{1}{\sqrt{2\pi\Delta_N^2}} \int_0^\infty d\tilde{N} J(\tilde{N}(\tilde{N}, N)) e^{-\frac{(N-\tilde{N})^2}{2\Delta_N^2}}, \quad (7.15)$$

with

$$\tilde{N}(\tilde{N}, N) = \tilde{N} N \left(\frac{1}{\sqrt{2\pi\Delta_N^2}} \int_0^\infty dN' N' e^{-\frac{(N-N')^2}{2\Delta_N^2}} \right)^{-1}. \quad (7.16)$$

The broadening δ_N , the DADR recombination time τ_{DADR} and the threshold density N_0 are fit parameters. The broadening is only applied to J_{DADR} since these barrier fluctuations should not affect the radiative and conventional defect recombination of the predominant number of carriers occupying areas of low defect recombination.

7.1.7 V(E)CSEL Operating Characteristics

The calculation of the operating characteristics of optically pumped V(E)CSELs are based on the rather simple one dimensional rate equation model as described in Ref. [10]. A (circular) top hat profile for the pump spot is assumed and the lasing mode is assumed to have the same shape and size. This simple model is most suitable for situations where the pump spot size is rather large and high power operation is investigated. Then, lateral effects like carrier and heat diffusion from the pump spot into the un-pumped areas are rather negligible. Some deviations between theory and experiment usually occur near threshold with the experimental thresholds usually being lower than the experimental ones. This is caused by lateral and vertical pump inhomogeneities. Some wells close to the surface will be pumped stronger than others leading to a situation that resembles one that has less wells. Also, unlike in the assumed top hat pump profile, real pump profiles have areas of higher pump intensity. Near threshold this can lead to lasing from a smaller area than the nominal total pump spot. At higher pump powers and correspondingly higher intrinsic temperatures the carriers become more evenly distributed over all wells due to higher carrier scattering rates and mobilities. Also, at powers high above threshold deviations from the average pump intensity become less significant and the pump profile can be better described by a top hat. An interpolation of the experimental characteristic

from high powers down shows good agreement with the theoretical results and demonstrates the amount of deviations from the homogeneous situation in the real system.

Beyond the model described in Ref. [10], the model implemented in **SimuLase**TM allows to also take into account imperfect pump absorption and partial escape/re-absorption of spontaneous emission (PL) from the pumped area. For the fraction of spontaneous emission that escapes the system versus the one that is re-absorbed in un-pumped areas outside the pump-spot ('PL Escape'). The number set here is the percentage of spontaneous emission (PL) that escapes the system. It is assumed that the re-absorbed fraction of the PL contributes to heating. This fraction can be calculated using ray-tracing software. For the example investigated here we found that about 40% of the PL escapes the system. The results are not very critically dependent on this fraction. In our example, the maximum out-put power changes by about 10% when varying the fraction over the whole possible range. The influence on the threshold is even smaller.

7.1.8 Edge Emitter Operating Characteristics

Two models are implemented in **SimuLase**TM to determine the operating characteristics of edge emitting devices. One determines the threshold characteristics. One determines input-output characteristics. The first one neglects internal heating and is appropriate for electrical and optical pumping. The second one takes into account internal heating, but with a simple model that is primarily designed for optical excitation. For electrical injection, the model can be used to examine the performance near threshold or near shut-off by adjusting the parameters to fit these specific points. However, it will generally not be able to describe the whole input-output characteristic correct with one set of input parameters. The shortcomings of this model are due to the fact that **SimuLase**TM does not solve the current injection problem and the resulting heating due to processes like Joule heating or Peltier-Thomson heating. Thus, also the temperature dependence of the intrinsic loss and injection efficiency are not taken into account. Setting these parameters by hand for various temperatures allows to study the characteristics at these points though.

The models are described in detail in Sec.5.1.4 where their functionality is demonstrated for a real-live example. The model for the threshold characteristics simply looks up from the database the carrier density that produces enough gain to overcome the user specified optical losses due out-coupling and intrinsic losses. It then calculates the losses due to spontaneous emission, Auger recombination and defect recombination for this density. The total loss current is given by the sum of these losses plus the injection loss. This is done for all wavelengths for which gain is found in the database at the specified temperature. The threshold wavelength is then given by the wavelength where the total current is minimal. If a fixed operating wavelength is specified, the threshold current is given by the total loss at this wavelength.

For the case of optical excitation, the only difference is that the absorption efficiency (fraction of pump injected light that is absorbed in the active region and leading to carriers captured into the wells) takes the place of the injection efficiency and has to be specified through this parameter.

The model for the input-output characteristics is very similar to the one used for the operating characteristics of optically pumped VECSELs described in Sec.7.1.7. The only difference is that here the spectral dependence of the optical confinement factor is neglected. In VECSELs, the DBR and RPG regions lead to significant changes of the mode spectrum which leads to a significant modification of the gain spectrum. This leads to strong gain enhancement and the modal gain maximum can be at significantly different wavelengths than the material gain

maximum. In edge emitting devices usually no such strong cavity effects are present. The optical confinement factor only has a very weak spectral dependence and the modal gain maximum is at the same wavelength as the material gain maximum.

Internal heating and its effects for the performance are taken into account just like in the VECSEL-LI tool. The latter tool has been tested extensively and very successfully against various experimental cases. Thus, this tool should work very accurately for cases of optically pumped devices.

For electrically pumped devices the heating is described using the same model. Current and Voltage induced heatings have to be modeled by adjusting the pump wavelength.

While these models are quite simple and can only be used on a level of a toy model for electrical injection, especially the threshold characteristics and the operating characteristics for optical injection should have a high level of accuracy thanks to that of the underlying gaindatabases. Many other software tools can describe the current injection problem with high accuracy. However, they rely on much simpler models for gain/absorption, spontaneous emission, etc. and treat Auger losses with what equates to a free fitting procedure. Some of the main shortcomings of these models is described in Sec.7.2.

In order to take full advantage of both, the accuracy of **SimuLase**TM databases and the modeling capabilities of more phenomenological software, the both should be combined by importing **SimuLase**TM databases into such software. Several commonly used software packages allow to directly use **SimuLase**TM gaindatabases, like Crosslight Inc.'s **Lastip**TM and Rsoft Inc.'s **LaserMOD**TM. Please contact them or NLCSTR for information about these interfaces.

7.2 Shortcomings of Simpler Models

7.2.1 Absorption/Gain

The important distinction between the fully microscopic approach and simpler models for the absorption/gain is the way the last term of Eq.(7.1), $\frac{d}{dt}p_{ji,k}|_{corr}$ is treated. This term describes the dephasing of the polarizations due to higher many-body correlations like electron-electron and electron-phonon scattering. Simpler models often replace this term by a simple dephasing time term $p_{ji,k}/T_2$. This gives rise to a transition energy independent Lorentzian broadening of the absorption/gain. As shown in Fig.7.5, this does not only lead to incorrect lineshapes, but also unphysical absorption energetically below the gain as well as incorrect spectral positions and amplitudes. In particular, the relation between gain amplitude and carrier density is wrong, leading e.g. to errors threshold and transparency density that can easily reach a factor of two. If one the uses the wrong threshold carrier densities to calculate the threshold loss currents, these will be off even more since the losses generally scale super-linearly with the density (see Fig.7.5).

Eq.(7.1) can also be solved by Fourier transformation into frequency space where the expression for the absorption/gain essentially becomes Fermi's golden rule. Here one can introduce other broadening schemes than the Lorentzian in order to replace the explicit calculation of the scatterings. Some of these schemes get rid of the unphysical absorption below the gain. However, this is not much more than cosmetics. The errors in the spectral positions, amplitudes and generally in the lineshapes remain. As mentioned in Sec.7.1.2, the Markov approximation for the electron-phonon scattering that is used in the ('Gain'-model) tends to fail to describe the below-bandgap absorption correctly. Here, the absorption values often do not converge correctly to zero, but to values of a few tens per centimeter (see Figs.7.6,7.7). To resolve this problem,

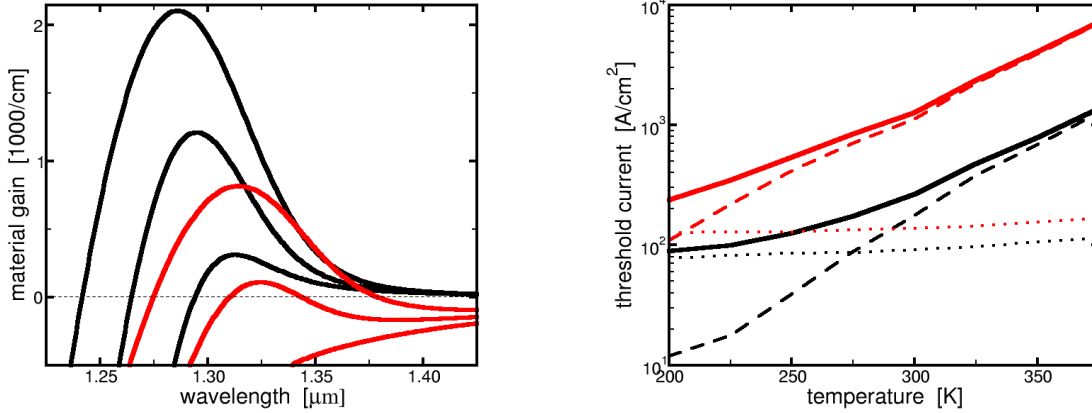


Figure 7.5: Left: Gain spectra for a *GaInNAs*-based structure at carrier densities of 0.9 , 1.3 and $1.8 \times 10^{12}/\text{cm}^2$. Black: fully microscopic model. Red: everything as in the full model, but using a dephasing time, $T_2 = 50 \text{ fs}$, instead of calculating the underlying scatterings explicitly. Right: Threshold current for this structure using threshold carrier densities as obtained from the fully microscopic model (black) and from the dephasing time model (red). Solid/dashed/dotted: total/Auger/radiative loss. The microscopically calculated results agree very well with the experiment [7].

the '**Absorption**'-model can be used in which the equations of motion for the phonon-assisted polarizations are solved explicitly. While this typically increases the calculation time by a factor of the order of three, it leads to far higher accuracy for the below-bandgap absorption.

The '**Absorption**'-model also has to be used for materials operating at wavelengths shorter than about 800nm like wide-bandgap nitrides. In these materials the electron-phonon coupling is much stronger than in materials at longer wavelengths. As shown in Fig.7.6, the Markov approximation can lead to strong errors in these materials. It can produce unphysical gain at densities for which there is no inversion. It also leads to strong errors in the overall absorption and gain lineshapes and amplitudes.

7.2.2 Spontaneous Emission, Radiative Carrier Losses

SimuLaseTM uses the fully microscopic semiconductor luminescence equations to calculate the spontaneous emission (PL) and the corresponding radiative carrier lifetimes. Simpler approaches usually use the so-called Kubo Martin Schwinger (KMS) relation to derive the spontaneous emission from the absorption/gain spectra. This is a simple integral conversion which effectively costs no computer resources once the absorption/gain is known. However, this approach leads to fairly uncontrolled errors in the PL-lineshapes as well as in the resulting lifetimes (see Fig.7.8). It is only strictly true in the absence of any broadenings. However, as pointed out in Sec.7.2.1, for the correct calculation of the gain/absorption one has to include the homogeneous broadening due to electron-electron and electron-phonon scattering.

The KMS approach also usually neglects the higher excitonic source terms. Thus, even if the absorption/gain is calculated correctly, including the microscopic scatterings, the KMS will underestimate the spontaneous emission amplitude and overestimate the radiative carrier lifetimes.

The error due to neglecting the higher excitonic correlations is typically a factor of the order of two or higher for typical III-V materials. However, it depends on the strength of excitonic inter-

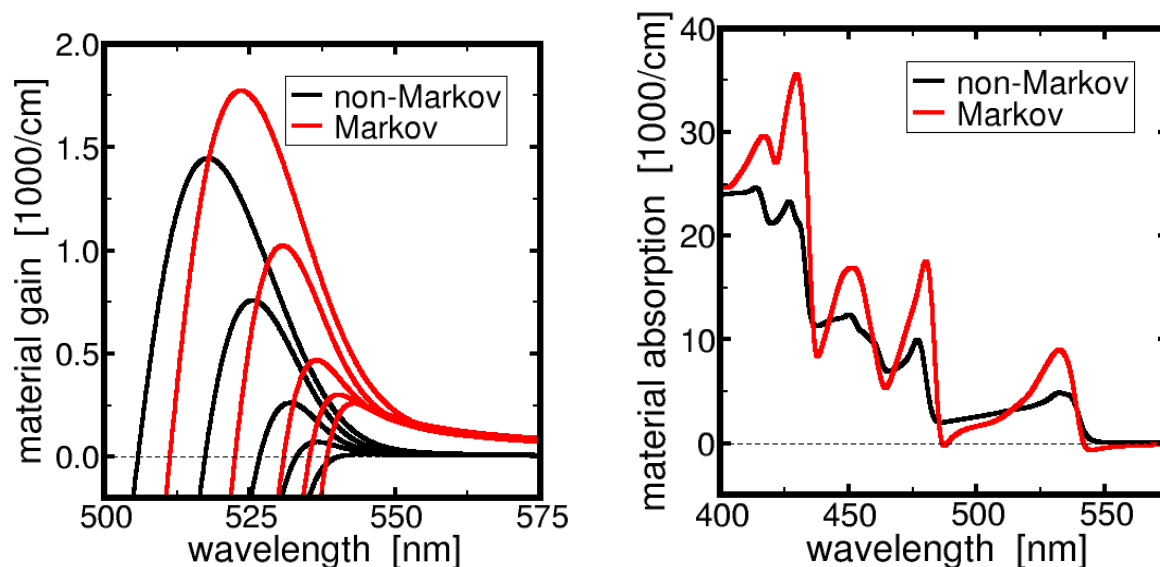


Figure 7.6: Left/Right: Gain/(zero-density) Absorption spectra for an *InGaN/GaN*-quantum well calculated using the Markov approximation for electron-phonon scattering (red) and not using the Markov approximation but solving the equations of motion for the phonon-assisted polarizations instead (black).

actions and can become significantly larger for materials with very strong Coulomb interaction like wide bandgap Nitride-based materials. Here it can be close to one order of magnitude.

As shown in Fig.7.8, the error due to the use of the KMS relation is particularly strong for carrier densities near transparency. The conversion formula has a pole at the position of the chemical potential. In the gain regime, this pole is compensated by the effect that the spectra change from gain to absorption at the chemical potential and, thus, the spectra have a zero at the position of the pole. For densities below transparency the chemical potential is below the bandgap. In the case for which the KMS-relation holds, without broadenings, the pole is in a region of zero absorption and leads to no issues. Here however, the homogeneous broadening leads to an absorption tail below the bandgap which leads to an artificial enhancement of the resulting PL and disturbs the PL-lineshapes.

For a comparison of spontaneous emission spectra calculated with and without electron-electron and electron-phonon scattering see Fig.6.11. For an other example of how the excitonic source terms and the electron-electron, electron-phonon scattering and other effects influence the radiative carrier lifetime see Ref. [6].

The simplest approach to estimate the carrier loss currents is to use semi-empirical power laws, $J_{rad} = B N^2$ for the radiative losses and $J_{aug} = C N^3$ for Auger losses. As shown in Fig.7.2, these laws completely break down in the density regime that is relevant for laser operation, near transparency and above. Similar break downs have been demonstrated for the temperature dependencies for these losses (see Ref. [6]).

Fig.7.9 shows the temperature dependence of the radiative loss current for various carrier densities for a *InGaAsP*-structure lasing around $1.3 \mu m$. The classical estimate for the temperature dependence is $J_{rad} = B_0 / T$, with a density independent proportionality constant B_0 . for low densities where the assumptions that go into the derivation of the $1/T$ -dependence should hold best, the microscopic calculations resemble more $1/T^3$. Obviously, the temperature dependence

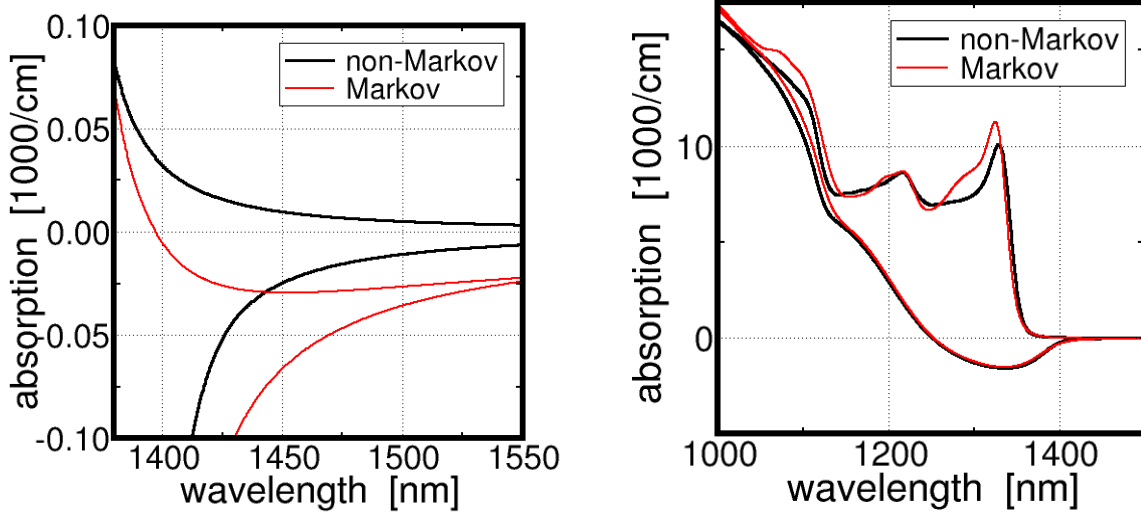


Figure 7.7: As Fig.7.6, here for an *InGaAsP*-based quantum well.

is strongly density dependent and the temperature and density dependencies cannot be decoupled. For more discussion of the temperature dependence see Ref. [6].

7.2.3 Auger Losses

As mentioned in Sec.7.1.6, the numerical difficulties in solving the quantum-Boltzmann type scattering equations that describe Auger losses have led to the use of many approximations in order to solve these equations. All of these approximations lead to uncontrolled errors that can easily be on order of magnitude or more.

Equally important, these approximations do not only lead to wrong absolute numbers for the losses, they also lead to wrong dependencies. Generally they also introduce phenomenological fit parameters for which one needs numbers from the experiment. These experiments are very involved and have only been performed for a very limited set of structures/devices and situations so far. However, the underlying Auger processes are strongly dependent on structural details like, e.g. the barrier height, as well as situational parameters like the temperature. This prohibits the use of literature values for the fit parameters in almost all cases and renders the simple approximations even more useless. These sensitivities and errors are demonstrated in Figs.7.10 and 7.11.

In the simplest approximation, the Auger loss current J_{aug} is approximated by:

$$J_{aug}(N, T) = C_0 \exp(-E_a/k_B T) N^3, \quad (7.17)$$

with a T - and N -independent fit constant C_0 and an empirical activation energy E_a . As shown in Fig.7.10, the microscopically calculated loss current (that agrees with the experiment within the uncertainties of the experiment) deviates strongly from the simple cubic density dependence. Even though here, the exact Auger constant C is known from the fit at low densities, the cubic power law gives an error of about three already near transparency. For higher densities the error can quickly become a factor of ten or more.

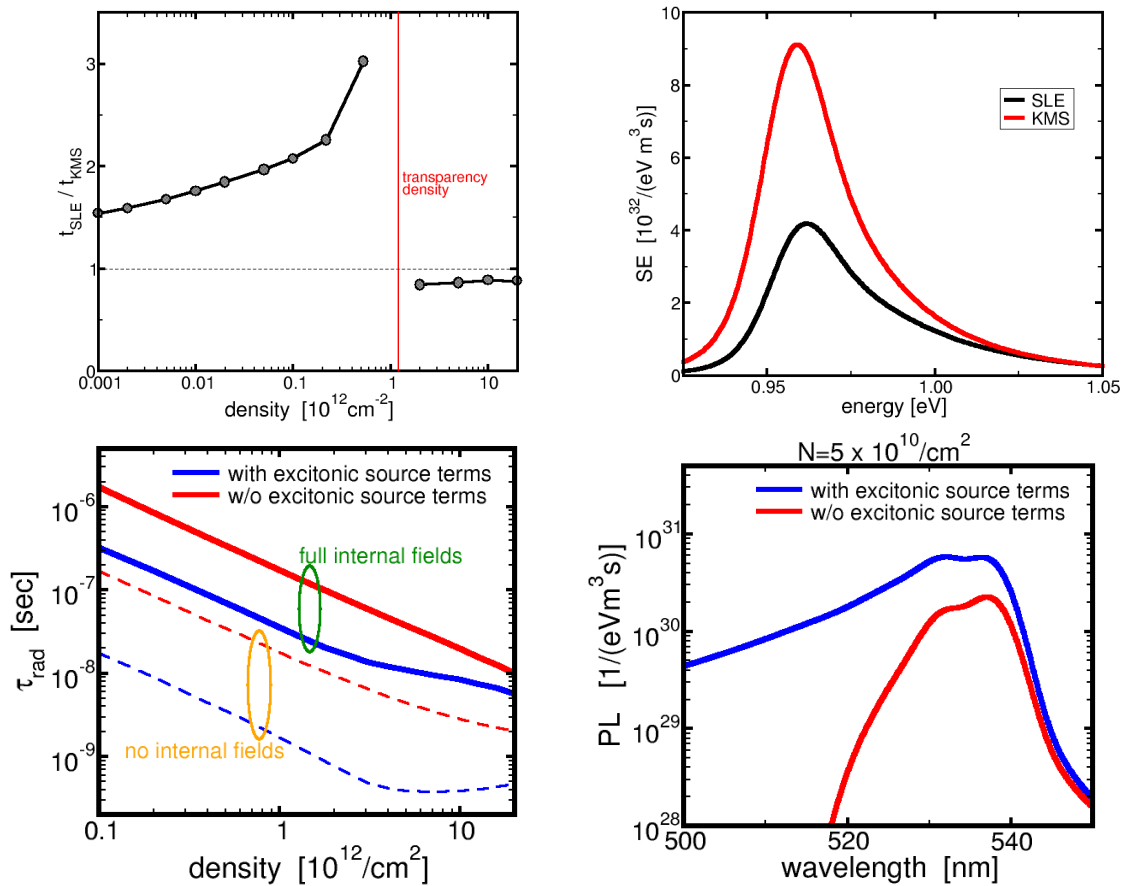


Figure 7.8: Top left: Ratio between radiative carrier lifetimes calculated with the SLE and KMS-relation [30]. Top right: PL spectra calculated with the SLE and KMS. Bottom left: radiative carrier lifetime as function of the carrier density for a 535nm *InGaN/GaN* structure calculated with/without (blue/red) higher excitonic source terms and with/without (solid/dashed) internal piezoelectric and spontaneous polarization fields. Bottom right: PL for the same structure as bottom left with/without (blue/red) higher excitonic source terms.

Fig.7.11 shows the temperature dependence of the loss currents for two similar structures at various carrier densities. Obviously the assumption of a density-independent temperature dependence is generally wrong. For limited temperature ranges the temperature dependence can be described using the exponential activation energy law. However, the activation energy depends strongly on the density. Moreover, a fit with an activation energy can require the unphysical assumption of negative activation energy.

The activation energy required to fit the results also strongly depends on the structural details. Both structures have the same well width and material. They only differ in the height of the barriers. This demonstrates that literature values for the fit parameters C and E_a usually cannot be taken from literature except for the rare case of truly identical structures.

For more examples of the shortcomings of simplified models see our website, [http:// www.nlcstr.com/theory2.htm](http://www.nlcstr.com/theory2.htm).

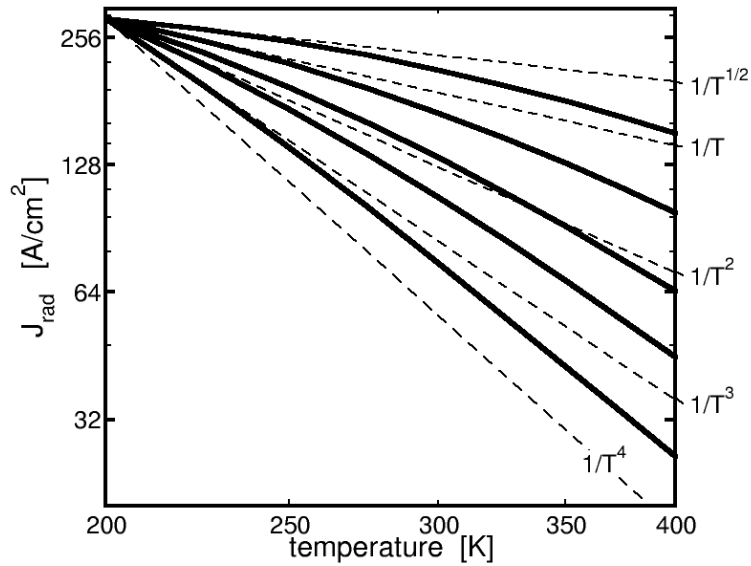


Figure 7.9: Solid: $J_{rad}(T)$ at sheet carrier densities of $0.05, 0.9, 1.8, 4.0$ and $10.0 \times 10^{12}/cm^2$ (bottom to top). Currents for $0.05, 0.9, 1.8,$ and $4.0 \times 10^{12}/cm^2$ have been scaled by factors of $1160.1, 8.82, 4.06$ and 2.00 , respectively. Dashed lines: Fits according to dependencies of $1/\sqrt{T}, 1/T, 1/T^2, 1/T^3$ and $1/T^4$ (top to bottom). (From Ref. [6]).

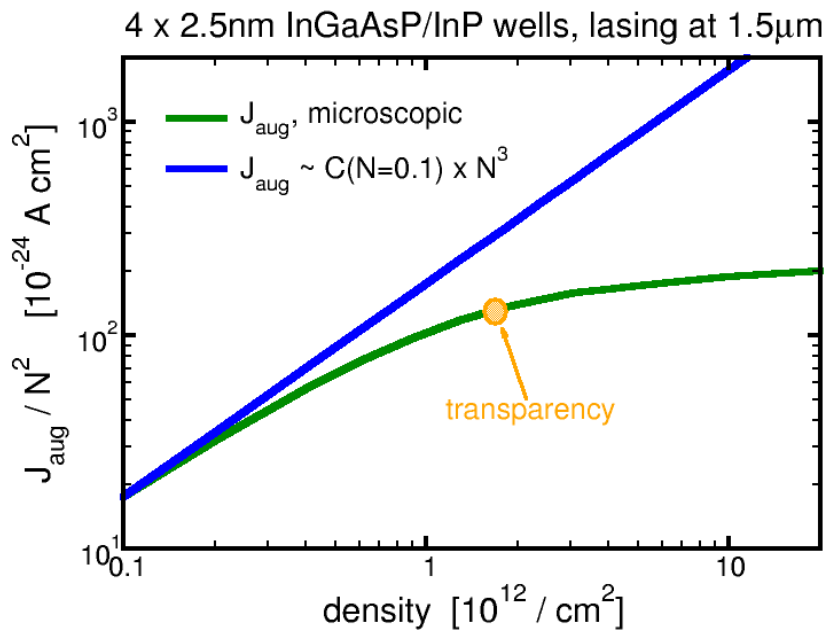


Figure 7.10: Fully microscopically calculated loss currents due to Auger recombination processes as function of the carrier density versus the classically assumed density dependency, $J_{aug} = C N^3$. From Ref. [5].

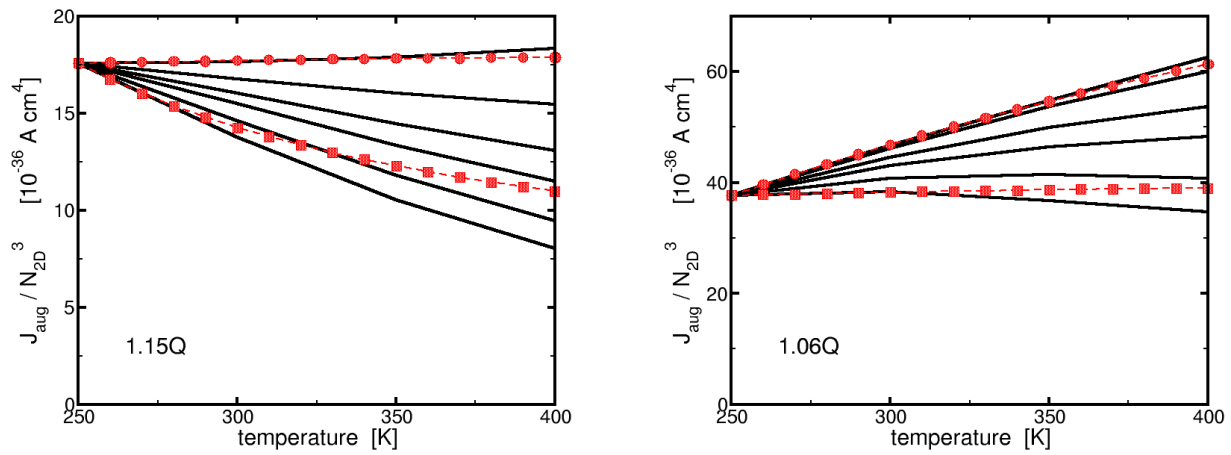


Figure 7.11: Solid lines: $C = J_{aug}(T)/N_{2D}^3$ for carrier densities of 0.05, 0.4, 1.3, 2.4, 5.0 and $10.0 \times 10^{12}/cm^2$ (bottom to top). Circles (squares): Fit using an activation-energy of $E_a = 1 meV$ ($-27 meV$) (left), and $E_a = 28 meV$ ($2 meV$) (right). *InGaAsP*-well lasing at $1.3 \mu m$ with shallo/high barriers (left/right). Results have been scaled to coincide at 250 K. For the exact scaling see Ref. [6].

8 Material Parameters

The following is a list of all material parameter values used in this version of **SimuLase™**. Unless stated explicitly, linear interpolation is used to derive the parameter values for ternary materials from the values for the binaries. Please contact us if you would like to have somewhat different parameters implemented for your version of **SimuLase™**.

8.1 AllInGaAsP-Material Family

The *AllInGaAsP-Material Family* contains the following materials:

- $AlAs$, $InAs$, $GaAs$, AlP , InP , GaP ,
- $Al_xGa_{1-x}As$, $In_xGa_{1-x}As$, $In_xAl_{1-x}As$, $In_xGa_{1-x}P$, $Al_xGa_{1-x}P$, $GaAs_xP_{1-x}$, $InAs_xP_{1-x}$,
- $Al_xGa_yIn_{1-x-y}As$, $In_xGa_{1-x}As_yP_{1-y}$, $Al_xGa_{1-x}As_yP_{1-y}$, $In_{1-x}(Al_yGa_{1-y})_xP$,

for all x and y between 0 and 1.

For the temperature dependence of the Γ -point bandgap in GaP we use [33]:

$$E_g(GaP, T) = 2.886 + 0.1081 [1 - coth(164/T)]. \quad (8.1)$$

For all other materials the temperature dependence of the bandgap is calculated using the corresponding Varshni-parameters. For the composition dependence of ternary and quaternary materials we use the following formulas:

$$E_g(Al_xGa_{1-x}As) = E_g(GaAs) + 1.519x + x(1-x)(0.127 - 1.310x) + 0.075x^3, \quad (8.2)$$

$$E_g(Al_xGa_{1-x}P) = E_g(AlP)x + E_g(GaP)(1-x), \quad (8.3)$$

$$E_g(In_xGa_{1-x}As) = E_g(InAs) + 0.518(1-x) + 0.549(1-x)^2, \quad (8.4)$$

$$E_g(In_xGa_{1-x}P) = E_g(InAs)x + E_g(GaP)(1-x) - 0.77x(1-x), \quad (8.5)$$

$$E_g(GaAs_xP_{1-x}) = E_g(GaP) - 1.544x + 0.190x^2, \quad (8.6)$$

$$E_g(InAs_xP_{1-x}) = E_g(InP) - 1.110x + 0.113x^2, \quad (8.7)$$

$$E_g(In_xAl_{1-x}As) = E_g(InAs)x + E_g(AlAs)(1-x) - 0.70x(1-x), \quad (8.8)$$

$$E_g(Al_xGa_yIn_{1-x-y}As) = E_g(InAs) + 2.093x + 0.629y + 0.568x^2 + 0.438y^2 \\ + 1.013xy - 2.0xy(1-x-y), \quad (8.9)$$

$$E_g(In_xGa_{1-x}As_yP_{1-y}) = E_g(InP) + 0.643(1-x) - 1.110y + 0.786(1-x)^2 + 0.113y^2 \\ - 0.159(1-x)y - 0.304(1-x)^2y + 0.101(1-x)y^2, \quad (8.10)$$

$$E_g(Al_xGa_{1-x}As_yP_{1-y}) = E_g(Al_xGa_{1-x}As)y + E_g(AlP)x(1-y) \\ + E_g(GaP)(1-x)(1-y), \quad (8.11)$$

$$E_g(In_{1-x}(Al_yGa_{1-y})_xP) = E_g(InP)(1-x) + E_g(AlP)xy + E_g(GaP)x(1-y) \\ - 0.18x(1-x) + 0.48x(1-x)y - 0.77x(1-x)(1-y), \quad (8.12)$$

	GaAs		AlAs		InAs		GaP		AlP		InP	
E_g	1.423	[31]	3.017	[31]	0.356	[32]	2.777	[33]	3.553	[33]	1.353	[33]
Δ_0	0.341	[32]	0.275	[32]	0.410	[32]	0.080	[33]	0.070	[33]	0.108	[33]
m_e	0.0665	[32]	0.124	[32]	0.026	[33]	0.130	[33]	0.220	[33]	0.079	[32]
γ_1	6.85	[32]	3.25	[32]	19.67	[32]	4.20	[32]	3.47	[32]	6.28	[32]
γ_2	2.10	[32]	0.64	[32]	8.37	[32]	0.98	[32]	0.06	[32]	2.08	[32]
γ_3	2.90	[32]	1.21	[32]	9.29	[32]	1.66	[32]	1.15	[32]	2.76	[32]
a_0	5.653	[32]	5.660	[32]	6.058	[33]	5.451	[33]	5.467	[33]	5.869	[33]
E_P	28.8	[33]	21.1	[32]	21.5	[33]	22.2	[32]	17.7	[33]	20.7	[33]
a	-7.17	[33]	-5.64	[33]	-5.08	[33]	-8.20	[33]	-5.70	[33]	-6.35	[32]
b	-1.7	[32]	-1.5	[31]	-1.8	[32]	-1.6	[33]	-1.5	[33]	-2.0	[31]
C_{11}	11.81	[32]	12.02	[31]	8.329	[33]	14.12	[32]	13.20	[32]	10.11	[32]
C_{12}	5.32	[32]	5.70	[31]	4.526	[33]	6.253	[32]	6.30	[33]	5.61	[32]
ϵ_0	12.91	[32]	10.06	[32]	15.15	[32]	11.11	[32]	9.8	[32]	12.61	[32]
ϵ_∞	10.9	[32]	8.16	[32]	12.25	[32]	9.11	[32]	7.54	[32]	9.61	[32]
$\hbar\omega_{LO}$	35.4	[32]	50.0	[32]	29.6	[32]	46.0	[32]	62.5	[32]	42.6	[32]
α	0.5408	[32]	0.885	[33]	0.276	[33]			0.5771	[33]	0.363	[33]
β	204	[32]	530	[33]	93	[33]			372	[33]	163	[33]

Table 8.1: Material parameters for the AlInGaAsP-material family at 300 K. E_g is the fundamental bandgap in [eV]. Δ_0 is the spin-orbit splitting in [eV]. m_e is the effective electron mass in bare electron masses. $\gamma_{1,2,3}$ are Luttinger parameters. a_0 is the lattice constant in [\AA]. E_P is the bulk dipole energy in [eV]. a and b are deformation potentials in [eV]. c_{11} and c_{12} are strain constants in [10^{11} dyn/cm^2]. ϵ_0 and ϵ_∞ are dielectric constants. $\hbar\omega_{LO}$ is the LO-phonon energy in [meV]. α is a Varshni coefficient in [meV/K]. β is a Varshni coefficient in [K].

The x -dependence for the bandgap in $Al_xGa_{1-x}As$ is taken from Ref. [31] and corrected by the last cubic term to obtain agreement with the gap for $AlAs$ as listed in Table 8.1. The dependence for $Al_xGa_{1-x}P$ is from Ref. [33]. The dependence for $In_xGa_{1-x}As$ is from Ref. [31] with minor adjustments to obtain agreement with the formulas for other materials. The dependence for $In_xGa_{1-x}P$ is from Ref. [33] with minor adjustments to obtain better agreement with Ref. [31]. The formula for $In_xAl_{1-x}As$ is according to Ref. [33]. The formulas for $GaAs_xP_{1-x}$, $InAs_xP_{1-x}$, $Al_xGa_yIn_{1-x-y}As$ and $In_xGa_{1-x}As_yP_{1-y}$ are from Ref. [34] with small adjustments. The formula for $In_{1-x}(Al_yGa_{1-y})_xP$ is according to Ref. [33].

In all cases the temperature dependence of the bandgap is calculated by linear interpolation between the variations of the constituting binary materials.

For heterostructures we use the band-offset ratios as listed in Ref. [33].

Values for the background refractive index, $n_r(\omega)$, are interpolated from data published at Ref. [35] and Refs. [36] and [37].

For the electron/hole mobilities, $\mu_{n/p}$, we use the values as given in Ref. [38]. For the temperature dependence of the mobilities we use the relation [18]:

$$\mu(T) = \mu(300 \text{ K}) \cdot \left(\frac{300 \text{ K}}{T} \right)^\alpha, \quad (8.13)$$

with $\alpha = 2.1$.

8.2 AllnGaAsSb-Material Family

The *AllnGaAsSb-Material Family* contains the following materials:

- *AlAs, InAs, GaAs, AlSb, InSb, GaSb,*
- *Al_xGa_{1-x}As, In_xGa_{1-x}As, In_xAl_{1-x}As, Al_xGa_{1-x}Sb, In_xGa_{1-x}Sb, Al_xIn_{1-x}Sb, GaSb_xAs_{1-x}, InSb_xAs_{1-x},*
- *Al_xGa_yIn_{1-x-y}As, Al_xGa_{1-x}As_ySb_{1-y}, In_xGa_{1-x}As_ySb_{1-y}, Al_xGa_yIn_{1-x-y}Sb*

for all x and y between 0 and 1.

	GaAs		AlAs		InAs		GaSb		AlSb		InSb	
E_g	1.423	[31]	3.017	[31]	0.356	[32]	0.727	[33]	2.300	[33]	0.174	[33]
Δ_0	0.341	[32]	0.275	[32]	0.410	[32]	0.760	[33]	0.676	[33]	0.810	[33]
m_e	0.0665	[32]	0.124	[32]	0.026	[33]	0.042	[33]	0.140	[33]	0.0135	[33]
γ_1	6.85	[32]	3.25	[32]	19.67	[32]	13.3	[33]	5.18	[33]	34.8	[33]
γ_2	2.10	[32]	0.64	[32]	8.37	[32]	4.4	[33]	1.19	[33]	15.5	[33]
γ_3	2.90	[32]	1.21	[32]	9.29	[32]	5.7	[33]	1.97	[33]	16.5	[33]
a_0	5.653	[32]	5.660	[32]	6.058	[33]	6.096	[33]	6.136	[33]	6.479	[33]
E_P	28.8	[33]	21.1	[32]	21.5	[33]	22.4	[32]	18.7	[33]	23.3	[33]
a	-7.17	[33]	-5.64	[33]	-5.08	[33]	-7.5	[33]	-4.50	[33]	-6.94	[33]
b	-1.7	[32]	-1.5	[31]	-1.8	[32]	-2.0	[33]	-1.35	[33]	-2.0	[33]
C_{11}	11.81	[32]	12.02	[31]	8.329	[33]	8.839	[32]	8.769	[33]	6.847	[33]
C_{12}	5.32	[32]	5.70	[31]	4.526	[33]	4.033	[32]	4.341	[33]	3.735	[33]
ϵ_0	12.91	[32]	10.06	[32]	15.15	[32]	15.69	[32]	12.04	[32]	16.8	[32]
ϵ_∞	10.9	[32]	8.16	[32]	12.25	[32]	14.44	[32]	10.24	[32]	15.68	[32]
$\hbar\omega_{LO}$	35.4	[32]	50.0	[32]	29.6	[32]	25.4	[32]	36.0	[32]	24.4	[32]
α	0.5408	[32]	0.885	[33]	0.276	[33]	0.417	[33]	0.42	[33]	0.32	[33]
β	204	[32]	530	[33]	93	[33]	140	[33]	140	[33]	170	[33]

Table 8.2: Material parameters for the AllnGaAsSb-material family used in this version of **SimuLaseTM** for 300 K (at the Γ -point of the Brioullin zone). All symbols and units are as in Table 8.1.

For the composition dependence of ternary and quaternary materials containing Antimonide we use the formulas given in Ref. [33]. For materials not containing Antimonide we use the formulas given in Sec.8.1.

In all cases the temperature dependence of the bandgap is calculated by linear interpolation between the variations of the constituting binary materials.

For heterostructures we use the conduction band-offset ratios, $\Delta E_c/\Delta E_g$, as listed in Ref. [33].

Values for the background refractive index, $n_r(\omega)$, are interpolated from data published at Ref. [35] and Refs. [36] and [37].

For the electron/hole mobilities, $\mu_{n/p}$, we use the values as given in Ref. [38]. For the temperature dependence of the mobilities we use Eq.(8.13).

8.3 Dilute AllnGaAsSbBi-Material Family

The *Dilute AllnGaAsSbBi-Material Family* contains the following materials:

- $GaAs, InAs, GaSb, InSb,$
- $In_xGa_{1-x}As, In_xGa_{1-x}Sb, GaSb_xAs_{1-x}, InSb_xAs_{1-x}, Al_xGa_{1-x}As_ySb_{1-y},$
 $Al_xIn_yGa_{1-x-y}As_wSb_{1-w},$
- $GaAs_{1-z}Bi_z, InAs_{1-z}Bi_z, GaSb_{1-z}Bi_z, InSb_{1-z}Bi_z, In_xGa_{1-x}As_{1-z}Bi_z,$
 $In_xGa_{1-x}Sb_{1-z}Bi_z, GaSb_xAs_{1-x-z}Bi_z, InSb_xAs_{1-x-z}Bi_z, In_xGa_{1-x}As_{y-z}Sb_{1-y}Bi_z.$

for all w, x and y between 0 and 1 and z between 0 and 0.2.

For materials without dilute Bi, we use the material parameters and bandgap formulas as listed in Secs.8.2. For materials containing dilute Bi, the extended band anti-crossing (EBAC) model as described in Ref. [39] is used. EBAC parameters for InAsBi and GaAsBi are as stated in Ref. [39]. For other Bi-containing materials the EBAC parameters were derived using first principle DFT calculations. NLCSTR holds the resulting parameters proprietary.

In the absence of better knowledge, we use for the background refractive index $n_r(\omega)$ in dilute Bi-containing materials the data for the corresponding Bi-free compounds and shift them spectrally according to the Bi-induced heavy-hole bandgap reduction.

For the electron/hole mobilities, $\mu_{n/p}$, we neglect the influence of Bi and use the values for the corresponding Bi-free materials as listed in Sec.8.2.

The values for the background refractive indices and mobilities as derived using the procedures described above are probably somewhat erroneous. However, the resulting errors should typically be minor since the Bi-content is rather small and, usually, the layers containing dilute Bismuth are fairly short compared to the overall structure thicknesses - especially those responsible for mode confinement and pump-injection.

8.4 AllnGaN-Material Family

The *AllnGaN-Material Family* contains the following materials:

- $AlN, InN, GaN,$
- $Al_xGa_{1-x}N, In_xGa_{1-x}N, Al_xGa_{1-x}N,$
- $Al_xGa_yIn_{1-x-y}N$

for all x and y between 0 and 1. Wurtzite crystal structure is assumed.

For all bandstructure parameters we use the values from Ref. [40].

In all cases the temperature dependence of the bandgap is calculated by linear interpolation between the variations of the constituting binary materials.

For heterostructures we use the conduction band-offset ratios, $\Delta E_c/\Delta E_g$, as given in Ref. [40].

Values for the background refractive index, $n_r(\omega)$, are interpolated from data published at Ref. [35] and Refs. [41–43] with temperature dependencies fitted to data in Refs. [32, 44, 45].

For the electron/hole mobilities, $\mu_{n/p}$, we use the values as given in Refs. [46–49]. For the temperature dependence of the mobilities we use Eq.(8.13).

8.5 Dilute AllnGaNAs-Material Family

The *Dilute AllnGaNAs-Material Family* contains the following materials:

- *AlAs, InAs, GaAs*
- $Al_xGa_{1-x}As, In_xGa_{1-x}As, In_xAl_{1-x}As, GaN_zAs_{1-z}$
- $Al_xGa_yIn_{1-x-y}As, In_xGa_{1-x}N_zAs_{1-z}$

for all x and y between 0 and 1 and z between 0 and 0.2.

For materials without dilute Nitrogen we use the material parameters and bandgap formulas as listed in Sec. 8.1. The bandgaps, eigenstates and energies in the presence of dilute Nitrogen are calculated using the 10-band $\mathbf{k} \cdot \mathbf{p}$ -band anti-crossing model described in Ref. [15]. For the band anti-crossing in $In_xGa_{1-x}N_zAs_{1-z}$ we use the following parameters:

$$V_{NM}(x, z, T) = \left((1-x)V_{NM}(GaAs, 300K) + xV_{NM}(InAs, 300K) + x(1-x)1.07 - \left[0.2 - (0.00112)\frac{T^2}{T+204} \right] \right) \sqrt{z}, \quad (8.14)$$

$$E_N(x, z, T) = \left((1-x)E_N(GaAs, 300K) + xE_N(InAs, 300K) - x(1-x)0.72 + \left[0.04 - (2.24 \times 10^{-4})\frac{T^2}{T+204} \right] \right), \quad (8.15)$$

$$\Delta E_0^N(x, z, T) = -2.33z \quad (8.16)$$

with $V_{NM}(GaAs, 300K) = -2.4 eV$, $V_{NM}(InAs, 300K) = -1.6 eV$, $E_N(GaAs, 300K) = 1.62 eV$ and $E_N(InAs, 300K) = 1.05 eV$. ΔE_0^N is the reduction of the bandgap due to lattice relaxation in the presence of dilute Nitrogen.

For the lattice constant of *GaN* we use a value of $0.450 nm$. For the lattice constant of *InN* we use $0.498 nm$.

For heterostructures we use the conduction band-offset ratios $\Delta E_c/\Delta E_g$ as listed in Ref. [33] for materials that do not contain Nitrogen. For materials containing dilute Nitrogen, we use the band anti-crossing formula:

$$\Delta E = \frac{E_n + E_0 + \Delta E_0^N - \sqrt{(E_n - E_0 - \Delta E_0^N)^2 + 4V_{NM}^2}}{2}, \quad (8.17)$$

to estimate the bandgap reduction due to the anti-crossing, ΔE , and add 25% of the reduction to the valence band edge. Here, E_0 is the bandgap in the absence of Nitrogen.

Values for the background refractive index, $n_r(\omega)$, are interpolated from data published at Ref. [35] and Refs. [36] and [37]. In the absence of better knowledge, for materials containing dilute Nitrogen we use the spectra for the materials without the Nitrogen and shift them spectrally according to the anti-crossing shift ΔE .

For the electron/hole mobilities, $\mu_{n/p}$, we use the values as described in Sec.8.1. Here, the presence of dilute Nitrogen is neglected.

The values for the background refractive indices and mobilities as derived using the procedure described above are probably somewhat erroneous. However, the resulting errors should typically

be minor since usually the layers containing dilute Nitrogen are fairly short compared to the overall structure thicknesses - especially those responsible for mode confinement and pump-injection.

8.6 Metals

Metals are only included in the calculations of the optical modes. Thus, the only relevant material parameters are the real and imaginary parts of the refractive indices, n and k .

Currently implemented metals are: Gold, Titanium and Chromium. The material parameters are taken from Ref. [50].

8.7 Dielectric Coatings

Like metal layers, dielectric coatings are only included in the calculations of the optical modes. Thus, the only relevant material parameters are the real and imaginary parts of the refractive indices, n and k .

We use for non-crystalline Si_3N_4 a fit to experimental data:

$$\begin{aligned} n(\epsilon) &= 1.7735 + 5.5 \times 10^{-5} \epsilon + 5.0 \times 10^{-3} \epsilon^2 + 8.3 \times 10^{-7} \epsilon^7 \\ k(\epsilon) &= 2.7 \times 10^{-6} (\exp(1.73 \epsilon) - 72), \quad \text{if } \epsilon \geq 2.472 \text{ eV} \\ k(\epsilon) &= 0, \quad \text{if } \epsilon < 2.472 \text{ eV}, \end{aligned} \tag{8.18}$$

where ϵ is the energy in eV.

Experimental values for $n(\epsilon)$ and $k(\epsilon)$ for Al_2O_3 , SiO_2 , Ta_2O_5 , TiO_2 and Y_2O_3 have been provided by Alexander Hein, Ulm University, Institute of Optoelectronics, Albert-Einstein-Allee 45, 89081 Ulm, Germany. The implemented values are based on analytical fits to that experimental data.

8.8 Air

Air is only included in the calculation of the optical mode. Its refractive index is 1.0.

Bibliography

- [1] N. Suzuki, Y. Hirayama, IEEE Photon. Technol. Lett. **7**, 1007 (1995).
- [2] M. Schafer, W. Hoyer, M. Kira, S.W. Koch, and J.V. Moloney, J. Opt. Soc. Am. B, **25**, 187 (2008).
- [3] J. Hader, J.V. Moloney, M. Fallahi, L. Fan, and S.W. Koch, Optics Lett. **31**, 3300 (2006).
- [4] L.A. Coldren, and S.W. Corzine, *Diode Lasers and Photonic Integrated Circuits*, (Wiley, NY 1995).
- [5] J. Hader, J.V. Moloney, and S.W. Koch, Appl. Phys. Lett. **87**, 201112 (2005).
- [6] J. Hader, J.V. Moloney, and S.W. Koch, IEEE J. Quantum Electron. **44**, 185 (2008).
- [7] J. Hader, J.V. Moloney, and S.W. Koch, IEEE J. Quantum Electron. **41**, 1217 (2005).
- [8] M. Fallahi, L. Fan, Y. Kaneda, C. Hessenius, J. Hader, H. Li, J.V. Moloney, B. Kunert, W. Stolz, S.W. Koch, J. Murray, and R. Bedford, IEEE Photon. Technol. Lett. **20**, 1700 (2008).
- [9] J. Hader, G. Hardesty, T.-L. Wang, M.J. Yarborough, Y. Kaneda, J.V. Moloney, B. Kunert, W. Stolz, and S.W. Koch, IEEE J. Quantum Electron., **46**, 810 (2010).
- [10] A.R. Zakharian, J. Hader, J.V. Moloney, S.W. Koch, P. Brick, and S. Lutgen, Appl. Phys. Lett. **83**, 1313 (2003).
- [11] J. Hader, et al., IEEE Photon. Technol. Lett. **14**, 762 (2002).
- [12] <http://www.nlcstr.com/examples.htm>.
- [13] J. Hader, N. Linder, and G.H. Döhler, Phys. Rev. B **55**, 6960 (1997).
- [14] J. Hader, J.V. Moloney, and S.W. Koch, *Numerical Simulation of Wide Bandgap Nitride Materials*, ed. by J. Piprek (2007).
- [15] J. Hader, S.W. Koch, J.V. Moloney, and E.P. O'Reilly, Appl. Phys. Lett. **76**, 3685 (2000).
- [16] S.L. Chuang, Phys. Rev. B **43**, 9649 (1991).
- [17] D. Ahn, S.L. Chuang, J. Appl. Phys. **64**, 6143 (1988).
- [18] S. Selberherr, *Analysis and simulation of semiconductor devices*, Springer-Verlag, Wien, New York (1984).
- [19] R. Winkler and U. Rössler, Surf. Sci. **305**, 295 (1994).
- [20] M. Lindberg and S.W. Koch, Phys. Rev. B **38**, 3342 (1988).
- [21] H. Haug and S.W. Koch, *Quantum Theory of the Optical and Electronic Properties of Semiconductors*, 4th ed., World Scientific Publ., Singapore (2004).
- [22] J. Hader, J.V. Moloney and S.W. Koch, IEEE J. Quantum Elect. **35**, 1878 (1999).
- [23] J. Hader, J.V. Moloney, and S.W. Koch, Sol. Stat. Electron. **47**, 513 (2003).

- [24] W.W. Chow and S.W. Koch, *Semiconductor Laser Fundamentals*, Springer Verlag, Berlin.
- [25] M. Kira, and S.W. Koch, *Prog. Quantum Electron.* **30**, 155 (2006).
- [26] W. Hoyer, M. Kira, et al., *J. Opt. Soc. Am. B* **24**, 1344 (2007).
- [27] A.R. Beattie, and P.T. Landsberg, *Proc. Royal Soc. London A* **249**, 16 (1958).
- [28] J. Hader, J.V. Moloney, and S.W. Koch, *Appl. Phys. Lett.* **96**, 221106 (2010).
- [29] J. Hader, J.V. Moloney, and S.W. Koch, *Appl. Phys. Lett.* **99**, 181127 (2011).
- [30] J. Hader, J.V. Moloney, and S.W. Koch, *Proc. SPIE*, **6115**, 61151T, (2006).
- [31] E.H. Li, *Physica E* **5**, 215 (2000).
- [32] Landoldt-Börnstein, *New Series III*, 22a, ed. O. Madelung (1987).
- [33] I. Vurgaftman, J.R. Meyer, and L.R. Ram-Mohan, *J. Appl. Phys.* **89**, 5815 (2001).
- [34] J. Minch, S.H. Park, T. Keating, and S.L. Chuang, *IEEE J. Quantum Electron.* **35**, 771 (1999).
- [35] <http://www.ioffe.ru/SVA/NSM/nk/>.
- [36] S. Adachi, et al., *J. Appl. Phys.* **66**, 6030 (1989).
- [37] M. Schubert, et al., *J. Appl. Phys.* **77**, 3416 (1995).
- [38] M.E Levinshtein, S. Rumyantsev, and M. Suhr, *Handbook series on semiconductor parameters*, World Scientific, Singapore, New Jersey (1996).
- [39] J. Hader, S.C. Badescu, L.C. Bannow, J.V. Moloney, S.R. Johnson, and S.W. Koch, *Appl. Phys. Lett.* **112**, 062103 (2018).
- [40] I. Vurgaftman, and J.R. Meyer, *J. Appl. Phys* **94**, 3675 (2003).
- [41] D. Brunner, H. Angerer, E. Bustarret, F. Freudenberg, R. Höppler, R. Dimitrov, O. Ambacher, and M. Stutzmann, *J. Appl. Phys.* **82**, 5090 (1997).
- [42] M.M.Y. Leung, A.B. Djuricic, and E.H. Li, *J. Appl. Phys.* **84**, 6312 (1998).
- [43] J. Piprek, *Optoelectronic Devices - Advanced Simulation and Analysis*, Springer Verlag, New York (2005).
- [44] N. Watanabe, T. Kimoto, and J. Suda, *J. Appl. Phys.* **104**, 106101 (2008).
- [45] H.P. Zhou, and W.Z. Shen, *J. Appl. Phys.* **96**, 3199 (2004).
- [46] M.E Levinshtein, S.L. Rumyantsev, and M.S Suhr, *Properties of Advanced Semiconductor Materials: GaN, AlN, InN, BN, SiC, SiGe*, John Wiley and Sons, New York (2001).
- [47] R. Gaska, J.W. Yang, A. Osinsky, Q. Chen, M. Asif Khan, A.O. Orlov, G.L. Snider, and M.S. Shur, *Appl. Phys. Lett.*, **72**, 707 (1998).
- [48] H.J. Hovel, and J.J. Cuomo, *Appl. Phys. Lett.* **20**, 71 (1972)
- [49] F. Chen, et al., *Appl. Phys. Lett.* **87**, 212104 (2005).
- [50] K.H. Hellwege, and O. Madelung, *Landoldt-Bornstein Tables, New Series III, 15b*, Springer, New York (1985).